

Elements of the wave-particle duality of light

Borys Jagielski



Thesis submitted for the degree of

Master of Science

in Physics

University of Oslo

May 2009

Abstract

The following Master's thesis is concerned with several aspects of the wave-particle duality of light. It is loosely divided in three parts. In the first part we consider historical, theoretical and experimental aspects of the duality problem. We explain how the notion of duality has developed through the last 400 years. We discuss theoretical underpinnings of the duality embodied by Maxwell's electromagnetic theory, quantization of electromagnetic modes, Fock's states and coherent states. We critically review several experiments which serve to demonstrate the corpuscular or undulatory behaviour of light and matter; in particular we present how the photoelectric effect and the Compton effect can be explained using the undulatory model, and we critically review Grangier, Roger and Aspect correlation experiment.

In the second part we describe two illustrative experiments on the duality of light conducted at Quantum Optics Laboratory at University of Oslo. The results of the experiment allow us to discuss how coincidence measurements can be used to exhibit the corpuscular behaviour of light, and how Mach-Zender interferometry performed at very low intensity can be used to exhibit the undulatory behaviour at the (assumed) single-photon level. In addition, in the second part we review elements of theories closely associated with the experiment and the experimental setup: optical coherence, photocount and photon statistics, beam splitter models and Gaussian beams. A proposition for extending the semiclassical model is given, and shortcomings of the present beam splitter models are discussed.

In the third part of the thesis we consider first Afshar's experiment and some of the critical response that it has been met with. Then we discuss how the wave-particle duality is to be understood in the standard interpretation of quantum mechanics, and how it could possibly be explained using either an alternative model for light or an alternative interpretation of quantum mechanics, and what difficulties such explanations present.

The thesis has been written in L^AT_EX using the graphical program L_yX. The figures not reproduced from original sources have been generated using Matlab or drawn using Dia.

Contents

Acknowledgments	iii
Introduction	v
1 The historical development of the wave-particle duality concept	1
1.1 The 1600s and the birth of modern optics	2
1.2 1800s and the triumph of the wave theory of light	7
1.3 The early 1900s and the rise of quantum mechanics	11
2 The classical and the quantum descriptions of light	17
2.1 Maxwell's electromagnetic theory	17
2.2 The review of the quantum harmonic oscillator formalism	20
2.3 Quantization of the electromagnetic modes	22
2.3.1 The electromagnetic potentials	22
2.3.2 Expansion in electromagnetic modes	24
2.3.3 The photon number states	25
2.3.4 Some problematic aspects of the quantized theory	27
2.4 The coherent states	29
3 Experimental considerations of the wave-particle duality	31
3.1 The black-body radiation	32
3.2 Interference (Michelson interferometry)	33
3.3 The photoelectric effect	40
3.4 The Compton effect	46
3.5 The photon anticoincidence effect	51
4 Classical description of optical coherence and correlations	57
4.1 The complex analytic signal	57
4.2 Describing optical coherence	60
4.3 Quantifying optical coherence	67
4.4 Application to interferometry	74
5 The main elements of the experimental setup: theoretical review	77
5.1 Photodetector	78
5.1.1 Types of photodetectors	78
5.1.2 The semiclassical model	79
5.1.3 The corpuscular model	83
5.1.4 Concluding remarks	87
5.2 Beam splitter	89
5.2.1 The classical description	89
5.2.2 The quantum model	92
5.2.3 Shortcomings of the beam splitter model	95
5.3 The shape of the laser beam	98
5.3.1 The paraxial Helmholtz equation	99
5.3.2 The Gaussian beam	100
5.3.3 The ABCD law	103
6 The main elements of the experimental setup: specifications and preliminary measurements	105
6.1 Modelling the laser beam shape	105
6.2 Measuring the coherence length	109
6.3 Specifications of the beam splitter model	111

6.4	The single-photon counting module	112
6.5	Measuring the photocount statistics	116
7	An experimental illustration of wave-particle duality	119
7.1	The coincidence measurements	120
7.1.1	Description	120
7.1.2	Setup and discussion of photocount rates	120
7.1.3	Results	123
7.1.4	Analysis and comparison with numerical simulations	123
7.1.5	Conclusion	126
7.2	The Mach-Zender interferometry	129
7.2.1	Description	129
7.2.2	Setup	129
7.2.3	Results and analysis	130
7.2.4	Conclusion	133
8	The Afshar experiment	135
8.1	Description and results	135
8.2	Criticism of the experiment	138
8.3	Concluding remarks	139
9	Explaining the wave-particle duality	143
9.1	The “photon clump” model	143
9.1.1	Basic assumptions	143
9.1.2	Quantitative considerations	145
9.1.3	Concluding remarks	147
9.2	Complementarity of the Copenhagen interpretation	148
9.3	The Bohmian interpretation of quantum mechanics	151
9.3.1	Reformulating the Schrödinger equation	152
9.3.2	The nature of the quantum field	156
9.3.3	Interpretation of electromagnetic field	158
9.3.4	Concluding remarks	159
10	Conclusion	161
10.1	Summary and outlooks	161
10.2	Closing words	164
A	The formalism of quantum mechanics	167
B	Demonstration of properties of the coherent states	173
B.1	The minimal uncertainty	173
B.2	The time evolution of a coherent state	174
B.3	The coherent states as a basis	175
C	Matter waves	179
D	Numerical routines	183
D.1	Simulation of thermal emission	183
D.2	Simulation of coincidence measurements	184
	References	189

Acknowledgments

First and foremost I would like to thank my thesis advisor, **Arnt Inge Vistnes**. His critical remarks regarding the wave-particle duality inspired me to dedicate my thesis to this highly interesting and problematic subject; and then, during the writing process, his patient help, both with theoretical questions and practical difficulties encountered at the laboratory, was truly invaluable. Thank you, Arnt Inge.

Furthermore, I wish to thank Arnt Inge Vistnes, **Joakim Bergli**, **Håkon Brox**, **Johanne Lein** and **Eimund Smestad** for our informal discussions regarding Afshar's experiment, coincidence measurements and quantum mechanics in general.

I want also to thank **Stanislaw Krawczyk**, **Michal Klosowski** and **Bartosz Porebski** for reading some chapters of the thesis prior to the publication and providing apt comments regarding both the content and the lingual side. Of course, any remaining mistakes and obscurities are solely due to my negligence.

My thanks go to **Efim Brondz** who had constructed several electronic and photodetecting devices that I employed when conducting my measurements.

Finally, I thank **Joar Bølstad** for introducing me to the program LyX with which the thesis was written. Working with LyX is definitely much more fun than using L^AT_EX in plain-text format.

Introduction

I remember quite well my first exposure to quantum mechanics. It occurred during the early high school years through a Polish edition of the book *The Large, the Small and the Human Mind* written by Roger Penrose [1]. In accordance with the title, Penrose dedicated the middle part of his rather short book to the issues concerning the microscopic world. It was a fascinating reading but not a very easy one, despite the book being labeled as popular science. If I could today advise my younger self, probably I would propose another, more accessible introduction to the quantum branch of science. On the other hand... maybe I would not, because getting thrown into intellectual deep water sometimes may act stimulating, and, after all, Penrose's book did not subdue my interest for physics.

One often hears that the quantum phenomena are against our common sense and stand in sharp contradiction to our day-to-day perception of the world. However, this opinion is usually uttered by professionals in the field who have had enough time to grow accustomed to different aspects of quantum mechanics. Even on me, after barely six years of studying physics, the paradoxes and the strange ontology of the microscopic realm do not make as huge an impression as they once did. But when I was reading *The Large, the Small and the Human Mind*, my reactions were very different indeed. The superposition principle as applied to the quantum states, saying that an object may possess two mutually exclusive properties, struck me with amazement. The wave-particle duality, illustrated in a standard way by the double-slit experiment, seemed hard to grasp. And after reading the chapter about quantum entanglement and the EPR paradox I naively assumed that the author had meant in fact something else and that I did not understand correctly what he had been saying. It was simply too weird.

The wave-particle duality is one of the central concepts of quantum mechanics, but the discussion on the nature of light is much older than the physical discipline initiated by Max Planck's famous lecture in December 1900. Let us briefly notice that the general notion of duality (or dualism) alone has also a long and interesting history, and has always stood for crucial philosophical contrasts and problems. The relationship between matter and mind is arguably the most famous of these, and René Descartes was the first philosopher who considered it in depth. Descartes maintained that mind ought to be viewed as a non-physical substance. This so-called Cartesian dualism initiated modern philosophy of mind which up to the present day ponders the problem of the interactions between mind and body. Among other dualisms, there is the famous concept due to Plato who postulated that our mundane world is accompanied by the world of eternal ideas; and Immanuel Kant's distinction between the empirical knowledge and the noumena that are independent of the senses [2].

The duality that will concern us here, the wave-particle duality, evolved from the dispute over the nature

of visible light that had started already in the times of Isaac Newton when the modern physics was being born. However, it was quantum mechanics that radically changed the character of the debate by saying that the structure of matter is exactly as ambiguous as that of light, and then by claiming that the way out of the wave-or-particle stalemate is to take the dualistic stance – light and matter behave sometimes like particles, and sometimes like waves, depending on (experimental) circumstances. Such a solution still causes unrest among some physicists, but the general majority of the scientific society just take for granted the following short definition of the wave-particle duality given by dictionaries:

“[t]he phenomenon where electromagnetic radiation and particles can exhibit either wave-like or particle-like behaviour, but not both.” [3]

The famous double-slit experiment, different versions of which we will come back to in the course of the thesis, serves as the canonical illustration of the wave-particle duality. Let us here present its simplified description: A light beam emerges from a source, propagates through two very small slits and impinges on a screen. We can reduce the intensity of the beam in such a way that according to a standard concept of quantum mechanics there will be only one quantum of light (photon) present in the apparatus at any given time. If we now place a detector behind each slit, we will see that they do not respond simultaneously, and thus we will be led to the conclusion that the photons behave like tiny corpuscles moving through either the first or the second slit. However, if we choose not to disturb the light with measurement before it reaches the screen, an interference pattern will emerge on it. This pattern is most easily predicted and explained by claiming that light is in fact an electromagnetic wave. The double-slit experiment can be also conducted with electrons (or other material particles) instead of light, and the same conclusions would be reached. In the words of Richard Feynman, this extraordinary phenomenon “is impossible, absolutely impossible, to explain in any classical way, and (...) has in it the heart of quantum mechanics. In reality, it contains the only mystery” [4]. Thus, claimed Feynman, the wave-particle duality problem is one of the central features of quantum mechanics.

Even though the problem of the wave-particle duality is in principle as much about light as about matter, in practice an asymmetry sneaks in and a tendency to favour light often occurs. The main reason is a technological one – it is easier to probe the properties of light and to make it exhibit undulatory or corpuscular behaviour, than to conduct experiments where matter behaves in a wavelike fashion. The double-slit experiment with electrons remained a thought experiment through the large part of the 20th century, and it was performed in a precise way in a laboratory as late as in 1989 [5]. On the other hand, the invention of laser in the early 1960s [6] invited the scientists to explore the fundamental properties of light and paved the way for a new branch of physical science: quantum optics.

The author has chosen to accept this asymmetry fully and dedicate the thesis to the wave-particle duality *of light*. This is partly due to the fact that his experiments conducted at Quantum Optics Laboratory at University of Oslo are concerned with light, and partly due to the fact that (in his opinion) the wave-particle duality of light seems more interesting than the duality of matter. However, since a complete exclusion of the duality of matter from the treatment would be inappropriate, it has been succinctly described in Appendix C.

Two important remarks must be made at this point. In the whole thesis the word “light” will serve as a synonym for “electromagnetic radiation” although in literature “light” means usually the visible part of the

electromagnetic spectrum lying approximately between 400 and 800 nm. We will rather use the explicit term “visible light” every time we want to refer to the latter. On the other hand we should notice that almost any discussion of corpuscular properties of light is *in practice* restricted to the region lying around the visible part of the spectrum and below it (in the sense of even shorter wavelengths), even though the idea of photon should *principally* apply to the whole spectrum. We will follow this somewhat problematic practice in the course of our thesis, but we will comment on it in Section 2.3.4.

Secondly, we want to keep apart the photonic hypothesis (saying that the electromagnetic field consists of corpuscular entities called photons) and the quantization hypothesis (saying that at the microscopic level many properties of physical systems change discretely with energy being probably the most important one). The concept of photon will be critically analyzed in the thesis, but the general quantization hypothesis will never be challenged. The difference between these two will be also examined closer in Section 2.3.4.

After these remarks, we are now ready to present the goal of the thesis: **to describe, examine and critically analyze several aspects of the wave-particle duality of light**. More specifically we intend to:

- present the wave-particle duality from the historical, the theoretical and the experimental point of view. Particularly, in the latter case, we aim at giving a *critical* review of some experiments commonly associated with the corpuscular nature of light.
- describe different photodetection models in connection with experiments conducted by the author at Quantum Optics Laboratory. These experiments will serve as an illustration of the wave-particle duality of light, and their analysis will reveal that it is in fact easier to unambiguously demonstrate the undulatory properties of light than the corpuscular properties.
- discuss whether and how the wave-particle duality could be possibly explained in the context of Afshar’s experiment, an alternative model of light and an alternative interpretation of quantum mechanics.

There can be no doubt that the totality of the wave-particle duality problem is a very complex and rich subject, in the sense that one may consider it from many different angles and initiate an in-depth discussion of any single aspect of it. Unfortunately, there is no room for all that in a Master’s thesis, and this is why the title of the work begins with “Elements of” – some elements were included, but then other elements had to be left out. Particularly:

- We will avoid any considerations of quantum electrodynamics (QED). This may seem as a very large omission, but we will see that a lot of interesting issues related to the wave-particle duality may be consistently discussed outside the framework of QED. The author does not doubt that through careful analysis of quantum electrodynamics many important insights would be gained, but entering the realm of quantum field theories in addition to everything else would be simply too big a task.
- We will refrain from relating the wave-particle duality explicitly to the measurement problem of quantum mechanics and to the collapse of the wave function, although this issue will be briefly touched upon in Chapter 9.2 when discussing the standard interpretation of quantum mechanics. However, in our discussion we will omit altogether decoherence phenomena, quantum nonlocality and Bell’s theorem.

- In our discussion of nonclassical states of light in Chapters 4 and 5.1 we examine both antibunched light and sub-Poissonian light, but the third main instance of nonclassical light, so-called squeezed states, is left out.

We believe that despite any necessary omissions we will still manage to give a coherent – although definitely not exhausting – treatise on the subject of the wave-particle duality of light.

The thesis is loosely divided into three parts which correspond to our aforementioned intentions. The first part describes the fundamental historical, theoretical and experimental ingredients of the wave-particle duality of light. Chapter 1 is strictly historical, and follows in a non-mathematical fashion the development of the wave-or-particle question from the 17th till the 20th century. The “real” physics does not begin until Chapter 2, where we depict two standard, but very different physical models of light, the classical electromagnetic one postulating light waves, and the quantum-mechanical one postulating photons (to be understood either as light corpuscles or as quanta of radiative energy). These contradictory models represent the theoretical essence of the wave-particle duality in the case of electromagnetic radiation. The first part of the thesis ends with Chapter 3 where we inspect critically what the empirical side of physics has to say on the dual nature of light and matter. We describe interferometry experiments suggesting that radiation possesses a wave nature, and we review experiments which seem to ascribe corpuscular properties to light.

The second part of the thesis describes an experiment performed on laser light at Quantum Optics Laboratory (QOL) at the University of Oslo. Utilizing two different experimental setups, one with single-photon detectors measuring a split beam in coincidence, and another employing a Mach-Zender interferometer, we try to give an experimental illustration of the duality of light, and we carefully discuss the results. All this does not come before Chapter 7, with Chapters 4, 5 and 6 preparing grounds for the experiment. In Chapter 4 we review the theory of coherence, in Chapter 5 we present theoretical elements of photodetection and beam-splitting processes together with a mathematical model for examining the shape of laser beam, and in Chapter 6 we perform preliminary measurements which are necessary because all the laboratory equipment we work with is new and its specifications have not yet been verified. In Chapter 5 we also deliberate on a possible extension of the semiclassical model of photodetection, and we discuss shortcomings of the present beam splitter models. The results of the main experiments and their analysis are finally presented in Chapter 7.

In the third and last part of the thesis we discuss whether and how the wave-particle duality could be explained. In Chapter 8 we review the controversial, but highly innovative Afshar experiment which in recent years has helped to revive the scientific interest in the wave-particle duality of light. We will see what are the conclusions of the authors, on which basis they have been criticized and what meaning the results of the experiment can have for the duality problem. In Chapter 9 we present two possibilities for a direct explanation of the wave-particle duality. First of these is a new model for light which unites the corpuscular and the undulatory aspect in a rather simple manner. The model is very speculative, but its consequences are experimentally verifiable which makes it valuable from the scientific point of view. The second possibility for explaining the duality is an alternative interpretation of quantum mechanics (“alternative” in the sense of being opposed to the standard, or Copenhagen, interpretation, presentation of which will also be given). We will see what exactly happens with the dual nature of light (and matter) in this interpretation, and we will debate on more general grounds whether the interpretation should be considered seriously. In Chapter

10 we conclude the thesis and present some outlooks, but also we share with the reader some of our general thoughts concerning the wave-particle duality problem in the framework of physics as such.

The science of physics constantly evolves, sometimes gradually, sometimes in sudden leaps. We should never ignore the possibility that some well-established part of physics can unexpectedly get expanded or re-interpreted by new discoveries or theories. The scientific arrogance of this sort was severely punished at least once, in the end of the 19th century, when a common belief spread among the contemporary physicists that physics was quickly approaching its end. However, during the next 25 years the advent of the relativity theories and quantum mechanics revolutionized our view of the world. Today the wave-particle duality remains a small, but noteworthy part of the scientific puzzle. Whatever the outcome of the future research might be, it is the author's hope that the following work will help in a slightly better understanding of the phenomenon by bringing together and consistently presenting some of its different aspects and subtleties which usually are to be found in many different books, anthologies, articles and publications.

1 The historical development of the wave-particle duality concept

Although the wave-particle duality is one of the conceptual cornerstones of quantum mechanics, the wave-or-particle dilemma limited to light only is at least 250 years older than the quantum branch of physics. The question of the nature of light has been an important scientific issue since the 17th century, the same time when modern optics was born. One can easily discern three different stages in the evolution of this problem, and to each of these stages we can attach names of several famous physicists who contributed to our understanding of light. Their discussions and different explanations demonstrate how baffling the nature of light has seemed from the beginning, and how rich is the current of thoughts and ideas that it has stimulated. Only in the last century, thanks to the quantum theory, did the duality problem unexpectedly expand to embrace matter as well.

The first modern scientific inquiries into the realm of optics date back to ca. 1650. Isaac Newton stated that light was composed of particles emitted in all directions from a source, and it was this corpuscular view that became dominant in the 1700s (Ch. 1.1). The second of the aforementioned stages started in the early 19th century when Thomas Young conducted his famous slit experiment which unambiguously proved that light rays interfered just like water waves. Shortly afterwards Augustin-Jean Fresnel presented the wave theory of light grounded firmly within a mathematical framework, and in the 1870s James Clerk Maxwell explained light as propagation of electromagnetic waves (Ch. 1.2). However, in 1905 Albert Einstein, motivated by Max Planck's scheme of energy quantization, put forward an idea that that light itself propagated in space and interacted with matter as discrete particles (light quanta). Twenty years later Louis de Broglie advanced a hypothesis that all matter manifests a wavelike nature, even if under many experimental circumstances it also behaves as if it were consisted of particles. Quantum mechanics employed this conceptual breakthrough in order to united the wave and the particle views: Light and matter show both wavelike and particlelike properties, although not at the same time (Ch. 1.3).

In the following sections we will examine the development of the wave-particle duality concept in more detail, but still rather succinctly. We omit or relegate to later chapters the more detailed quantitative treatments of the presented phenomena, because right now our goal is only to look upon the *historical* evolution of the concept. Hence we can better appreciate the colossal amount of scientific research hidden behind and beneath it.

1.1 The 1600s and the birth of modern optics

Given the extraordinary importance of light in everyday life, it should not seem peculiar that already the ancient scholars studied its properties and tried to understand its essence. The first known scientific (or quasi-scientific) theories on light developed in India between 7th and 5th century BC. The Indian theories were heavily influenced by Hinduistic and Buddhistic mysticism, but the local schools of thought differed as to their view upon the character of light – some assumed that light is a continuous element, some postulated its atomicity or discreteness [7].

The European pioneer in the field of optics was the Greek mathematician Euclid who lived around 300 BC. In *Optica* he studied the properties of light employing rigid geometrical formalism. Euclid’s most important result was the formulation of the law of reflection (angle of incidence equals angle of reflection). He pragmatically considered light as rays, i.e. something propagating through space in straight lines, without giving any thought to whether light was continuous waves or discrete corpuscles [8].

At this point one could also mention the Greek atomists, like Democritus (ca. 460-370 BC) or Lucretius (ca. 99-55 BC). In their view everything consisted of minute indivisible atoms. However, they did not examine light in particular (they talked rather about “all matter”), and they based their beliefs on philosophical considerations without making use either of mathematics or of experiments. Thus we can hardly call their theories physical in the modern sense of the word [9].

The scientific legacy of the ancient Greeks was carried on by medieval Muslim scientists who did perform real experiments. Bin Al-Hath (965-1040) dealt with i.a. rainbow, colours, camera obscura, eclipses and shadows, but, more importantly in our context, he explained light rays as streams of small energy particles which traveled with finite speed [10]. Another great Muslim scholar from that period, Ibn Seena (ca. 980-1037) commonly known in English as Avicenna, shared al-Haytham’s opinion and proposed that “the perception of light is due to the emission of some sort of particles by a luminous source” [11].

The wave-particle dichotomy did not become more apparent until the 1600s when the modern studies of light began in Europe. Their starting point was the phenomenon of refraction which occurs when a light ray propagates from one medium to another. Johannes Kepler (1571-1630), Willebrord Snell van Royen (1591-1626), René Descartes (1596-1650) and Pierre Fermat (1601-1666) all tried to explain it quantitatively and dress it up in an appropriate mathematical formula. Kepler failed and the other three succeeded, but they approached the solution along different paths. Snell derived the formula empirically utilizing experimental results, while Descartes and Fermat used theoretical considerations. Fermat’s justification of the refraction law was much more elegant, since it followed directly from his principle of least time.

However, it was not Fermat but Descartes who, in order to deduce the proper relation, asked himself how one could perceive light. The French scholar assumed that the propagation of light is similar to the movement of a projectile, like a tennis ball. By decomposing the motion of a light ray into two parts, a parallel and a normal one (relatively to the boundary between the two media, see Fig. 1), and assuming that only the normal part is influenced when the light ray leaves the first medium and enters the second one (with another density), Descartes arrived quite close to the correct formula which today we write as:

$$n_1 \sin \theta_1 = n_2 \sin \theta_2,$$

where n_i are the refractive indices of the media and θ_1 and θ_2 are, respectively, the angle of incidence and the angle of refraction [12]. The result itself is not important here. What is of significance is the fact that

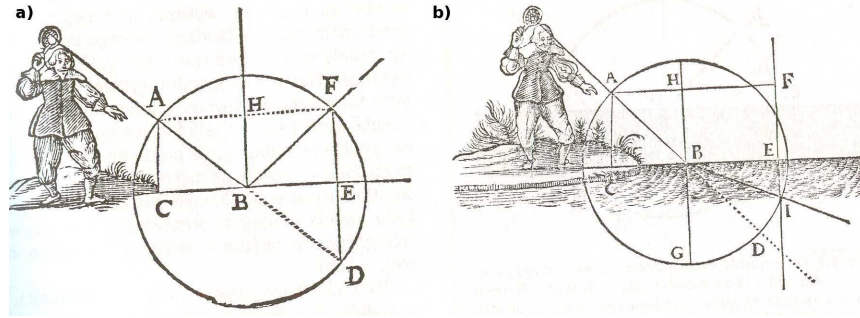


Figure 1: A drawing from Descartes' *La dioptrique* illustrating the phenomenon of **a)** light reflection and **b)** refraction. Descartes used an analogy with a tennis ball in order to give a quantitative description of these phenomena. Using the modern language of vector algebra we would say that he decomposed the velocity of the light ray into a normal and a parallel component, but in his original treatise he relied solely on geometrical considerations. Note that in **b)** the refraction angle in water, GBI, is larger than the incidence angle in air, ABH, while for a light ray it should be the other way around. Descartes was aware of that. Later on in *La dioptrique* he examined the behaviour of real light rays (and not merely tennis balls) and presented appropriate figures.

Descartes, by ascribing light some form – in this specific case the corpuscular form – tried to deduce a correct physical relation. Efforts to fathom the nature of light were no longer only a philosophical issue. From now on they would result in quantitative descriptions of the properties of light and of the light-matter interactions.

We have to stress, however, that Descartes did not really regard light as such as a stream of corpuscles. The above analogy with tennis ball was used by him merely as an illustration and an intellectual shortcut, even if it made Descartes succeed in the end. The philosopher held rather that light was a disturbance of *plenum*, a continuous substance permeating the entire Universe. According to him this disturbance was of a wavelike character; it transmitted through *plenum* in a form of a pressure wave propagating from light sources to eyes [13].

The phenomenon of light diffraction, crucial as the argument for the wave nature of light, was discovered in the second half of the 17th century by Francesco Maria Grimaldi (1618-1663). He described it in his work *Physico-mathesis de lumine, coloribus et iride* (*Physical science of light, colours and rainbow*) published in 1665. The experimentalist Grimaldi observed fringes which developed when a narrow beam of light illuminated a screen after the beam had passed a sharp boundary of an obstacle (Fig. 2). These observations proved unambiguously that sometimes light rays do not propagate in straight lines, but are (slightly) deflected instead. Thus Grimaldi concluded that light had to be treated as a fluid possessing wave nature, since fluids also showed such a diffractive behaviour. The Italian physicist assumed that different colours resulted from different types of light undulations, and that therefore light was a phenomenon comparable to sound [14].

Unfortunately, Grimaldi's discovery was not acknowledged with enthusiasm by his contemporaries. Many claimed that the observed diffraction was due to some experimental errors, and nothing to be really concerned about. Edmé Mariotte (1620-1684) wrote for instance:

“(…) when one conducts very precise experiments, one always confirms the hypothesis of rectilinear propagation of light, without any diffraction. That I have checked in many accurate observations together with very intelligent persons.” [15]



Figure 2: Grimaldi's drawing from *Physico-mathesis de lumine, coloribus et iride* showing diffraction fringes.

Even though diffraction was not given proper attention in the 1600s, and 150 years had to pass before Thomas Young conducted his epoch-making interference experiments (see Ch. 1.2), other scientists from that period did not ignore the possibility that light could have a wave nature. Robert Hooke (1635-1703) and Christiaan Huygens (1629-1695) can be considered the two main advocates of the wave view in the late 17th century.

Huygens formulated his wave theory of light in *Traite de la lumiaere* (*Treatise on light*) published in 1690. He proposed that light was emitted from its source as a series of waves propagating in a medium called “luminiferous ether” which was nothing else than another name for Descartes’ *plenum*. The particles which the light source consisted of in this view would move rapidly and would strike the surrounding (and much smaller) ether particles, which again would agitate another layer of ether particles and so on, so the light would propagate outwards from the light source in a wavelike fashion. Huygens wrote:

“And I do not believe that this movement can be better explained than by supposing that all those of the luminous bodies which are liquid, such as flames, and apparently the sun and the stars, are composed of particles which float in a much more subtle medium which agitates them with great rapidity, and makes them strike against the particles of the ether which surrounds them, and which are much smaller than they. (...) Now if one examines what this matter may be in which the movement coming from the luminous body is propagated, which I call Ethereal matter, one will see that it is not the same that serves for the propagation of Sound. (...) When one takes a number of spheres of equal size, made of some very hard substance, and arranges them in a straight line, so that they touch one another, one finds, on striking with a similar sphere against the first of these spheres, that the motion passes as in an instant to the last of them. (...) And it must be known that although the particles of the ether are not ranged thus in straight lines, as in our row of spheres, but confusedly, so that one of them touches several others, this does not hinder them from transmitting their movement and from spreading it always forward.”

[16]

Huygens topped his proposition with an important principle, later called after him and also after Augustin-Jean Fresnel who over one hundred years later supplemented it mathematically (see Ch 1.2). The Huygens-Fresnel principle says that each point of an advancing wave front can be regarded as a source of a new train of waves, and that the totality of the advancing wave is in fact a sum of all these secondary wavelets. This

view would allow to explain diffraction easily, but in fact Huygens did not pay much attention to interference phenomena and did not use them as the main argument for the wave nature of light.

It was the corpuscular view that was about to gain upper hand for the whole 18th century. The person responsible, Isaac Newton (1643-1727), who was committed to several different branches of science and had great achievements in each of them, summarized his results in optics in his second major book on physical science, *Opticks*, published in 1704. However, the treatise *New Theory of Light and Colours* presented to the world in 1672 already contained many important and ground-breaking conclusions regarding colours and the method for extracting them from a sunbeam with the use of a prism.

With this treatise a strife between Newton and another Fellow of the Royal Society, namely Robert Hooke, began. Newton maintained that light could be explained as a stream of tiny particles propagating in ether in straight lines from an object to the human eye. Different types of these light particles corresponded to different primary colours, and by mixing them one could attain other colours as well. Robert Hooke opposed Newton's opinion. Hooke was a supporter of the wave hypothesis, which he had employed in order to explain colours of thin films observed personally under a microscope. Hooke challenged Newton to explain this phenomenon using the corpuscular hypothesis.

The answer he got was a carefully thought-out compromise where Isaac Newton tried to unite the corpuscular and the wave aspects of the light theory. He still maintained that light was a stream of corpuscles, but he proposed that these corpuscles in a natural way, like stones thrown into water, created ripples in the ethereal medium permeating all space. The ether undulations could then be responsible for phenomena like the colours of thin films, claimed Newton; phenomena where the corpuscular view alone was not sufficient.

“The hypothesis of light's being a body, had I propounded it, has a much greater affinity with the objector's own [wave] hypothesis, than he seems to be aware of; the vibrations of the aether being as useful and necessary in this as in his. For, assuming the rays of light to be small bodies emitted every way from shining substances, those, when they impinge on any refracting or reflecting superficies, must as necessarily excite vibrations in the aether, as stones do in water when thrown into it. And, supposing these vibrations to be of several depths or thicknesses, accordingly as they are excited by the said corpuscular rays of various sizes and velocities; of what use they will be for explicating the manner of reflection or refraction; the production of heat by the sun-beams; the emission of light from burning, putrifying, or other substances, whose parts are vehemently agitated; the phaenomena of the transparent plates, and bubbles, and of all natural bodies; the manner of vision, and the difference of colours; as also their harmony and discord; I shall leave to their consideration, who may think it worth their endeavour to apply this hypothesis to the solution of phaenomena.” [17]

He pointed out that light could not possibly be only a wave of some kind, because waves have a tendency towards a spherical propagation, while light rays propagate through space in straight lines which clearly suggests a corpuscular form. In his reply to Hooke, Newton also stressed that he only wanted to develop a quantitative theory of colours and their refraction, and that he was not that much concerned about the more fundamental question of the nature of light [18].

However, during the next few years Newton was drawn into a polemic regarding this very question. A circle of his critics broadened. Hooke was joined by Huygens, Jesuits Franciscus Linus and Ignace Pardies,

and others. The opponents admittedly appreciated Newton's theoretical and experimental efforts. They claimed, however, that if one considered different colours to be different types of light particles (and not different types of undulations), then it would be difficult to explain how this variety of light particles was created in the first place. Newton replied reluctantly and unconvincingly, because he just did not understand how someone could not agree with his "self-evident" theory [14].

Isaac Newton elaborated on his corpuscular view in *Hypothesis of light* presented to the secretary of the Royal Society in December 1675. There he again put forward the conciliatory hypothesis where both the corpuscular and the wave assumption were utilized. Light sources emit light particles, and the light particles make ether vibrate. He stressed that light is neither ether nor its undulatory motion, but something else that propagates from the luminous bodies [19].

The discussion about the nature of light reached a stalemate. The publication of Huygens' *Traite de la lumiaere* in 1690 did not make Newton change his mind. Admittedly they both agreed that ether is necessary for the propagation of light. However, Huygens' believed that light *is* the movement (or oscillations) of the ether particles, while Newton maintained that light corresponds to some other type of particles which only *travel through* ether (possibly interacting with the ether substance as well).

Robert Hooke died in 1703. In November the same year Newton was elected a new president of the Royal Society (after the former president, Lord Somers, had died). Newton ruled the English science with an iron hand till his death in 1727, and used the distinguished position to ruthlessly fight his scientific opponents. No one dared to contradict his corpuscular view on the nature of light any longer, and Newton himself made this view very clear in his canonical work *Opticks* where in the very first definition he stated that

“*Defn. I.* By the Rays of Light I understand its least Parts, and those as well Successive in the same Lines, as Contemporary in several Lines. For it is manifest that Light consists of Parts, both Successive and Contemporary; because in the same place you may stop that which comes one moment, and let pass that which comes presently after; and in the same time you may stop it in any one place, and let it pass in any other. For that part of Light which is stopp'd cannot be the same with that which is let pass. The least Light or part of Light, which may be stopp'd alone without the rest of the Light, or propagated alone, or do or suffer any thing alone, which the rest of the Light doth not or suffers not, I call a Ray of Light.” [20]

Thus the corpuscular view dominated the scientific stage for around 100 years. The research progress in optics in the 18th century was small. Instead, analytical mechanics, thermodynamics, electricity and magnetism were being developed. The theory of Huygens was forgotten and even Leonhard Euler (1707-1783), who argued in *Nova theoria lucis et colorum* (1746) that diffraction could be explained more easily by the wave hypothesis, did not refer to it. One had to wait 50 more years before another prominent English scientist set out to change the optical paradigm. But even after the wave view had finally triumphed over the corpuscular view in the 19th century, Newton's ideas about the nature of light were still treated with a great deal of respect.

“So great, however, was Newton's fame among men of science that a number of writers on optics, especially among the British, took care to inform their readers that Newton's corpuscular

theory, while clearly incorrect, was nevertheless a very ingenious creation and had been fully able to explain all of the facts about light known in Newton's day. In other words, this theory was not wholly relegated to the realms of the antique and the curious but was rather presented to the reader with an apology and a discussion of the 17th-century situation in physics." [21]

1.2 1800s and the triumph of the wave theory of light

The polymath Thomas Young (1773-1829), later called "the last man who knew everything", contributed to the scientific understanding of physics, physiology and Egyptology. When he was still a student, he presented a treatise on the structure and accommodation of the eye, becoming the founder of physiological optics. Then he got interested in the nature of light, and after a series of experiments he tried to revive the almost forgotten wave theory of light.

In two lectures given to the Royal Society in 1800 and 1801 Young carefully reminded his colleagues of the possibility that light might be perceived as a wave propagating in ether. He was well aware of the dominant position of the corpuscular view supported by the late Newton's enormous authority. Therefore he reminded his listeners that Newton himself had not completely rejected the wave view, and then advanced following postulates:

1. That a luminiferous ether, rare and elastic in a high degree, pervades the whole universe.
2. That undulations are excited in this ether whenever a body becomes luminous. And,
3. That the sensation of different colours depends on the frequency of vibrations excited by light in the retina." [22]

Young presented a number of propositions describing these ether undulations qualitatively. In the last of them he claimed that

"[w]hen two undulations from different origins coincide either perfectly or very nearly, in direction, their joint effect is a combination of the motions belonging to each. (...) This last Proposition may be considered as the general result of the whole investigation." [22]

Thomas Young elaborated on the interference phenomena in his later treatises. He never based his reasoning on pure theoretical assumptions, but performed actual interference experiments, both with water and light, in order to emphasize the wave analogy. Thus very soon he could find a hard experimental proof for light diffraction, and presented it to the Royal Society in November 1803.

"In making some experiments on the fringes of colours accompanying shadows, I have found so simple and so demonstrative a proof of the general law of the interference of two portions of

light, which I have already endeavoured to establish (...) Exper. 1: I made a small hole in a window-shutter, and covered it with a piece of thick paper, which I perforated with a fine needle. For greater convenience of observation, I placed a small looking glass without the window-shutter, in such a position as to reflect the sun's light, in a direction nearly horizontal, upon the opposite wall, and to cause the cone of diverging light to pass over a table, on which were several little screens of card-paper. I brought into the sunbeam a slip of card, about one-thirtieth of an inch in breadth, and observed its shadow either on the wall, or on other cards held at different distances. Besides the fringes of colours on each side of the shadow, the shadow itself was divided by similar parallel fringes, of smaller dimensions, differing in number, according to the distance at which the shadow was observed, but leaving the middle of the shadow always white. Now these fringes were the joint effect of the portions of light passing on each side of the slip of card and inflected, or rather diffracted, into the shadow." [23]

Young conducted several other experiments and gathered a solid amount of evidence that light interfered. Thus his results strongly suggested that light had a wave nature. Unfortunately, many other scientists mercilessly criticized Young's methods and conclusions. The authority of Newton was still strong, and his corpuscular view was too respected to allow one juvenile scientist to establish a completely new theory, especially when this theory was qualitative rather than mathematical. Young got discouraged and abandoned his optical research for some years.

On the other side of the English Channel, however, progress in optics was still being made by French physicists. Étienne-Louis Malus (1775-1812) discovered polarization of light by reflection in 1809 and explained double refraction of light in crystals in 1810. Pierre-Simon Laplace (1749-1827) and Jean-Baptiste Biot (1774-1862) worked out a mathematical theory describing propagation of light in crystals. Unfortunately, all these scientists still employed the corpuscular view, and in order to explain the phenomenon of polarization Malus assumed that the light corpuscles are not rotationally symmetrical, but somewhat elongated. The angle between the direction of their propagation and their, say, major axes, were supposed to correspond to a given polarization.

It was another French scientist, Augustin Fresnel (1788-1827), who not only approved of Young's wave theory, but got inspired by it and extended it considerably. Fresnel synthesized the wave ideas of Young as well as Christiaan Huygens' using a rigid mathematical apparatus, and showed how one could apply them in order to explain quantitatively a large class of optical phenomena. The predictive powers of Fresnel's work were in fact so great that they gave rise to one of the best known anecdotes in the annals of the history of science.

Fresnel submitted his work to a competition held by Académie des Sciences in 1819 where the best theory on diffraction was to be awarded. At first the work was met with scepticism by the prominent members of the committee – Dominique Arago, Siméon Poisson, Laplace and Biot among the others – because Fresnel's model discarded the corpuscular view. Poisson, though, liked mathematics very much (even though he disagreed with the physical interpretation) and pushed the original calculations of the author even further. In the end he predicted that, according to Fresnel's theory, the shadow of a circular disc was supposed to have a small bright spot in its centre. No one had observed such a thing before, so it seemed that the model was erroneous. Arago proposed to put it to a decisive experimental test. The committee expected that no bright spot would appear, and that the model could then be rejected on the grounds of its absence. Surprisingly,

Arago ended up with discovering the spot (from now on called Arago spot), so the accuracy of Fresnel's model was established and he could receive the main prize in the competition [24].

In the meantime Young and Fresnel corresponded with each other, and, of course, the English scientist approved very much of the results of his French colleague. It seemed that the wave theory of optics could overturn the corpuscular view after all. Paradoxically, the polarization of light presented the largest problem, because in the beginning Young and Fresnel had assumed that the ether undulations were longitudinal, in analogy with sound waves, so the polarizational degree of freedom was missing. However, soon an intellectual step forward was made and Thomas Young proposed in 1817 to provide the undulations with a transverse component. Four years later Fresnel proved that polarization could be explained only if there was no longitudinal component at all, just the transverse one. It took some time before other physicists fully accepted this revelation [14].

Thanks to the mathematical framework developed by Fresnel, the wave theory of light gained a broad acceptance in the following years. New developments helped to establish it further. For instance, Christian Doppler (1805-1853) utilized it to explain the effect (later called by his name) that caused shifts in the stellar frequency spectra (though probably the same effect could be explained using the corpuscular view). However, Doppler's result had to pale into insignificance in comparison with a great breakthrough that was soon about to happen: the discovery that not only electricity and magnetism are intimately connected, but also that the realm of optics lies *de facto* inside the realm of electromagnetism.

We are not going to present even a short summary of the history of electromagnetism since such a digression would not have anything to do with the development of the notion of wave-particle duality. Thus, let us rudely ignore the achievements of Gilbert, Coulomb, Volta, Oersted, Ampère, Faraday and many others, and proceed directly to Maxwell's synthesis of the electromagnetic laws and its repercussions for the understanding of the nature of light.

James Clerk Maxwell (1831-1879) created the classical theory of electromagnetism by incorporating the results of several other physicists into a coherent mathematical framework. In order to achieve this consistency he had to somewhat change the nomenclature used by his colleagues, and fill all gaps with a thorough qualitative discussion of the electromagnetic phenomena. Possibly the most important conclusion of the electromagnetic theory was that the electromagnetic phenomena propagated in an undulatory fashion through ether. Thus Maxwell could predict, on purely theoretical grounds, the existence of electromagnetic waves¹. *A Treatise on Electricity and Magnetism* published by him in 1873 became a physical milestone – but it did not happen immediately, because for some time the rival electrodynamic theory of Wilhelm Weber was dominant, especially in Germany.

Maxwell understood that the electromagnetic theory could be used to explain the phenomenon of light; moreover, he pondered if light could not in fact *be* some kind of electromagnetic propagation. Let us quote an important fragment of the treatise:

“781. In several parts of this treatise an attempt has been made to explain electromagnetic phenomena by means of mechanical action transmitted from one body to another by means of a medium occupying the space between them. The undulatory theory of light also assumes the

¹One should be reminded that Maxwell did not write down the equations called after him the way they are known to physicists today. The Scotch scientist was using the quaternion notation instead of the vectorial one. It was Oliver Heaviside (1850-1925) who put the equations in their modern form.

existence of a medium. We have now to shew that the properties of the electromagnetic medium are identical with those of the luminiferous medium.

To fill all space with a new medium whenever any new phenomenon is to be explained is by no means philosophical, but if the study of two different branches of science has independently suggested the idea of a medium, and if the properties which must be attributed to the medium in order to account for electromagnetic phenomena are of the same kind as those which we attribute to the luminiferous medium in order to account for the phenomena of light, the evidence for the physical existence of the medium will be considerably strengthened.

But the properties of bodies are capable of quantitative measurement. We therefore obtain the numerical value of some property of the medium, such as the velocity with which a disturbance is propagated through it, which can be calculated from electromagnetic experiments, and also observed directly in the case of light. If it should be found that the velocity of propagation of electromagnetic disturbances is the same as the velocity, and this not only in air, but in other transparent media, we shall have strong reasons for believing that light is an electromagnetic phenomenon, and the combination of the optical with the electrical evidence will produce a conviction of the reality of the medium similar to that which we obtain, in the case of other kinds of matter, from the combined evidence of the senses.” [25]

To recapitulate: From the two assertions, that the electromagnetic phenomena propagate through ether as waves, and that light also propagates through ether as waves, Maxwell reached a rather obvious conclusion that light is an electromagnetic phenomenon. But this reasoning was not only qualitative. On the contrary: Maxwell noticed a remarkable correspondence between some electromagnetic quantities and the speed of light. Using today’s physical symbols, we would say that he discovered that

$$\sqrt{\epsilon\mu} \approx c^{-1}$$

where ϵ is the electric permittivity, μ is the magnetic permeability and c is the speed of light. However, Maxwell expressed his conclusions quite carefully:

“It is manifest that the velocity of light and the ratio of the units are quantities of the same order of magnitude. Neither of them can be said to be determined as yet with such a degree of accuracy as to enable us to assert that the one is greater or less than the other. It is to be hoped that, by further experiment, the relation between the magnitudes of the two quantities may be more accurately determined.” [25]

The scientific community did not have to wait long for an experimental confirmation of the electromagnetic waves postulated by Maxwell. Heinrich Hertz (1857-1894) demonstrated propagation of these waves in air in the second half of the 1880s. In Hertz’s experiment one observed how electromagnetic undulations, excited in the primary conductor using Ruhmkorff coil, were wirelessly transmitted to a secondary conductor placed several meters away. Thereafter Hertz showed how these waves reflected from walls of a room (effectively creating standing waves). In a similar fashion one could examine their refraction and interference.

It seemed that the wave theory of light achieved its ultimate victory. In less than 100 years, thanks to the efforts of physicists like Young, Fresnel, Maxwell and Hertz, the corpuscular theory of Newton had been knocked down from the pedestal. Admittedly the falsification was indirect, since instead of finding erroneous conclusions of the corpuscular view, the scientists had rather showed how the wave view could be used to explain many natural phenomena in a strictly mathematical way. The wave theory of light seemed completely consistent as well, and the conclusion was very elegant: Visible light is only one type of electromagnetic undulations which propagates transversely and with different oscillation frequencies through ether.

Two problems remained. Albert Abraham Michelson (1852-1931) and Edward Morley (1838-1923), using a special kind of interferometer, tried to measure the speed of Earth relatively to ether – and failed completely. Their results led to the astounding conclusion that ether, which scientists had taken for granted at least since 1600s, in fact did not exist. This discovery had colossal implications for classical mechanics, and inspired Albert Einstein to propose his special theory of relativity in 1905. But for optics it did not really mean that much. After all, one could just move on to the assumption that the electromagnetic waves propagate in vacuum, and although such a statement was difficult to accept from the then-valid philosophical point of view, it did not matter for the quantitative part of the theory.

The second problem was much more grave: The electromagnetic theory was not able to fully explain either the black-body radiation or the photoelectric effect. However, no one suspected that a new paradigm would be needed in order to resolve these discrepancies. On the contrary – the common belief in that time was that theoretical physics was completed. “The grand underlying principles have been firmly established (...) further truths of physics are to be looked for in the sixth place of decimals”, claimed Michelson in 1894 [26].

Only six years after this proud statement, the quantum mechanics was born. Our picture of light soon had to be reshaped once again.

1.3 The early 1900s and the rise of quantum mechanics

The recovery of the corpuscular view is directly connected to the origin of quantum mechanics, with Max Planck (1858-1947) traditionally considered to be its father. In 1890s Planck investigated the theoretical frontier between the well-established classical mechanics and the relatively new sciences of electrodynamics and thermodynamics. Specifically, he wanted to show how the second law of thermodynamics could be derived from some fundamental model for heat oscillators, a model firmly rooted in the principles of classical mechanics and electrodynamics. However, his scheme met huge difficulties, largely because Planck opposed atomistic view and did not want to accept the statistical interpretation of the second law given by Ludwig Boltzmann (1844-1906). His attitude to Boltzmann’s theory gradually changed to become more positive, and in the last years of the decade Planck started to work on another, related issue – the spectral distribution of the black-body radiation.

The black-body spectral density (the radiation energy density per unit frequency) had been described by an empirical law proposed by Wilhelm Wien (1864-1928) in 1886. Planck set out to find a rigorous theoretical derivation of Wien’s law. In the meantime, very precise measurements on the black-body radiation, conducted

in 1899 in Berlin by Otto Lummer and Ernst Pringsheim [27], showed that Wien's formula was not completely valid, because it broke down at low frequencies. Planck was not only able to improve the formula, but also, using his superior insights gained previously from the study of the second law of thermodynamics, to show how the formula followed from the first principles. However, in order to succeed, Planck had to introduce two novel ideas. He postulated a new constant of nature, h (later called by his name); and he claimed that the energy involved in the radiation process was divided into minute, but finite portions. Max Planck announced his final results² to the scientific community in a famous lecture given in Berlin on December 14, 1900. His formula, later called Planck's law (see Ch. 3.1), was in perfect accordance with the experimental results, and the derivation seemed elegant and faultless [28].

The date of Planck's lecture is today commonly recognized as the day the quantum mechanics was born. However, it should be stressed that Planck himself considered the quantization of energy merely as a mathematical trick, "a purely formal assumption" [29]. Most of his colleagues apparently shared this view; in any case, they were not aware that a revolution in physics was just happening. Although Planck probably understood that a possible physical interpretation of this "mathematical trick" was discrete absorption and emission of light by matter, he believed the whole quantization scheme to be only a temporary feature of the model, something to be removed by further improvements. But the foundations for the quantum mechanics had already been laid, and the first big step towards the "new" corpuscular view of light had been made.

It was Albert Einstein (1879-1955) who first really appreciated the idea of Planck and extended it in order to explain the photoelectric effect. The photoelectric effect was discovered by Hertz in 1887 and clarified by Philipp von Lenard in 1902. The effect is a phenomenon where electrons are emitted from a material illuminated by electromagnetic radiation with high enough frequency (see Ch. 3.3). From Maxwell's theory one would expect that the radiation intensity alone should decide if the electrons got emitted, but the experimental reality showed that the radiation frequency was an even more important factor [30].

Einstein presented an innovative solution to the problem in 1905, but his convictions about the nature of light related to the photoelectric effect mattered more than the formulas reproducing the experimental results.

"In fact, it seems to me that the observations on "black-body radiation", photoluminescence, the production of cathode rays by ultraviolet light and other phenomena involving the emission or conversion of light can be better understood on the assumption that the energy of light is distributed discontinuously in space. According to the assumption considered here, when a light ray starting from a point is propagated, the energy is not continuously distributed over an ever increasing volume, but it consists of a finite number of energy quanta, localised in space, which move without being divided and which can be absorbed or emitted only as a whole." [31]

Thus Einstein went much further in his argumentation than Planck. He assumed that not only the absorption

² Many popular accounts claim erroneously that Planck aimed to resolve the so-called "ultraviolet catastrophe", i.e. the paradox where classical physics predicted an infinite amount of energy emitted by a black body at high frequencies. This is emphatically not true, because the "catastrophe" was first expressed through the Rayleigh-Jeans formula proposed as late as in 1905; and the term "ultraviolet catastrophe" was coined by Paul Ehrenfest only in 1911. In other words, the paradox did never really had time to become a problem, because Planck's law had solved it before it was explicitly formulated [28].

and emission of radiation occurs in a discrete fashion, but also that the propagation of light in space is of a quantum character. Most other physicists were against such a radical hypothesis, not only because of its far-reaching consequences and (at least partial) negation of the wave view, but also because the explanation of the photoelectric effect turned out in the end to be possible by means of the classical electromagnetic theory. This had been achieved by several persons: J. J. Thomson in 1910, Arnold Sommerfeld and Peter Debye in 1911, and, most notably, by Owen Richardson in 1912 (see Ch. 3.3) [32].

During the next years Albert Einstein has become a highly respected scientist, largely due to his special and general theory of relativity. However, many scientists still did not regard the corpuscular idea seriously, because the wave view, being firmly grounded in Maxwell's theory, was so much appealing as an explanation of the physical reality of light. As always, in order to convince the skeptics, one needed an unambiguous experiment. Such an experiment was conducted in 1922 by Arthur Compton (1892-1962) who examined X-ray scattering. Compton noticed that the problematic experimental results could be easily explained if one adapted the corpuscular view of the radiation. It was, however, not easy for him to embrace this idea, and he employed it only as the last resort. First he had tried to explain his data by assuming large size of the electron (i.e. larger than the measurements of Ernest Rutherford had indicated) and by aid of the Doppler effect. In the end Compton had to admit that the corpuscular hypothesis offered the easiest explanation, because it implied that the radiation and the electrons exchanged momentum like minute particles, just like Compton's experiments had suggested (see Ch 3.4).

Einstein's corpuscular considerations backed up by Compton's results propelled anew the interest in the nature of light. On the one hand, the corpuscularity of light seemed at least partly confirmed; on the other hand, the "old" interference phenomena were still taking place, and in order to explain them the wave view seemed to be necessary. Physicists started to look for a way to avoid the apparent paradox. Fortunately, the intellectual atmosphere of that period encouraged new and bold ideas – after all Niels Bohr (1885-1962) had just proposed a new atomic model, and many scientists had understood that another revolution in physics, based on quantum mechanical ideas, was imminent.

John Slater (1900-1976) advanced the notion of "virtual oscillators" which could be used to unite the classical theory of electromagnetic field with the quantum theory of light. Bohr, Slater and Hendrik Kramers extended this notion and created a new theory of radiation, so-called BKS theory [34]. However, it had one large disadvantage: It implied that the energy and momentum exchange in microscopical physical processes were of a statistical nature, so the energy and momentum conservation principle were no longer valid. Such a suggestion sounded like a heresy to the scientific community, and was soon experimentally refuted [35].

It was Louis de Broglie (1892-1987) who in his doctoral thesis in 1924 put forward the extraordinary idea which in some sense solved the problem of the dualistic nature of light by extending it to the rest of the world, i.e. to all matter. De Broglie assumed that, just as light sometimes showed corpuscular and sometimes undulatory behaviour, the atomic matter possessed in addition a wave nature (see Appendix C) [36]. Even though the idea might have sounded like a bad joke in the beginning, the laboratory proofs confirming de Broglie's hypothesis had already existed, but the connection had not been noticed immediately. In 1921 Clinton Davisson and Charles Kunsman published the results of their experiments in which electron beams were undergoing dispersion and reflection from crystals. The angular distribution of the reflected electrons suggested in fact a possibility of their wave nature. The controversial proposal of de Broglie encouraged the scientific community to examine the matter more closely, and in 1927 the hypothesis had been ultimately confirmed. Davisson and Lester Germer, by firing electrons at a crystalline nickel target obtained a diffractive

pattern which matched exactly the theoretical predictions of de Broglie [37]. Three years later, in 1930, Otto Stern and Immanuel Estermann observed a similar diffraction of much larger helium atoms and hydrogen molecules [38].

The wave-particle duality problem fully emerged. No one could deny that in the macroscopic world matter has entirely corpuscular properties, but in the same breath no one could ignore the results of the Davisson-Germer experiment neither; the experiment which had clearly demonstrated that on microscopic level the matter – or at least its smallest constituents – showed an undulatory behaviour and was able to interfere. One was thus unwillingly forced to admit that the matter, in a difficult to perceive sense, is *both* particles and waves. This effectively eliminated the old wave-or-particle dilemma with regard to light: Since the physical situation in the realm of light was completely analogous, i.e. some experiments and models emphasized the corpuscular nature of light and other experiments and models the undulatory nature, one could apply a similar conclusion here and claim that light is *both* particle and wave at the same time.

Niels Bohr tried to explain the highly philosophical problem of the wave-particle duality using so-called complementarity. A whole school of thought has been built around this concept, and we relegate the discussion of the principle to Chapter 9.2. Here suffice it to say that complementarity, instead of answering the central question “Are matter and light particles or waves?”, effectively claimed that this question is meaningless and presented an exhaustive justification for such a claim. On the quantitative side complementarity was supported by the uncertainty principle advanced by Werner Heisenberg (1901-1976) in 1927 which implied that it was fundamentally impossible to simultaneously measure the position and the momentum of a physical object with an arbitrary high precision (see Appendix A).

After the discovery of the uncertainty principle, neither new experimental breakthroughs nor fully successful theoretical models have considerably changed the shape of the wave-particle duality problem. Several new physical ideas were proposed in order to resolve it, but they did not gain broad acceptance since they had not been supported strongly enough by empirical data. Arguably the most noteworthy among them was the Bohmian interpretation of quantum mechanics developed by David Bohm (1917-1992) in the early 1950s [39]. Bohm built on the ideas of Louis de Broglie and postulated that every material particle is accompanied by a field which guides the motion of the particle. This field (called the pilot wave by de Broglie and the quantum field by Bohm) evolves according to the Schrödinger equation of quantum mechanics and is responsible for the undulatory behaviour of matter (see Ch. 9.3).

Another interesting (but tentative) theory related to the wave-particle duality problem was put forward by Edwin Jaynes (1922-1998), a proposer of the neoclassical model of radiation [40]. Jaynes aimed to modify quantum electrodynamics by eliminating its inherent need for quantization of electromagnetic field. Thus Jaynes wanted to create a physical model as successful as quantum electrodynamics, but where only the interactions between light and matter were quantized, not light itself. Discrepancies with experimental results eventually extinguished the interest of the physical community for the neoclassical model.

Quantum mechanics has not managed to radically change our way of perceiving the wave-particle duality after the 1930s, but the problem kept on receiving attention in the second half of the last century. It was largely due to three discoveries that took place around 1960 and completely refreshed the science of optics. In 1955 Robert Hanbury Brown and Richard Twiss constructed a new type of stellar interferometer which did not measure the correlations of the electric and magnetic field *strengths*, but the correlations between *intensities* [41]. Such a new angle of approach immediately raised several new and interesting questions about light interference. The effects discovered by Hanbury Brown and Twiss were soon explained by themselves

as correlations of the fluctuations in the electromagnetic field. However, it was demonstrated by others that such effects could be also directly related to the corpuscular view of light, and understood as bunching of photons (i.e. phenomenon where photons occur in bunches) [42].

The interferometry experiment due to Hanbury Brown-Twiss is often considered to be the experimental confirmation of classical theory of optical correlations (see Ch. 4). Roy Glauber showed in 1963 [43] how one can translate the notion of optical coherence to quantum terms [43] and obtain new predictions not accounted for by the classical theory (see Ch. 4.4). These predictions were later confirmed by experiments with nonclassical states of light (see Sect. 5.1.4).

Between Hanbury Brown-Twiss' experiment and Glauber's paper, Theodore Maiman demonstrated in 1960 the first working laser [6]. While industry embraced the new invention and used it to produce several devices that changed our everyday world (CD players being arguably the most prominent example), scientists could use the laser as a new tool for exploring the corpuscular and undulatory properties of light. Thanks to the efforts of Hanbury Brown, Twiss, Maiman, Glauber and others, a new branch of physics – quantum optics – became firmly established in the early 1960s, and other scientists could start following a new scientific path.

The aforementioned events stimulated the interest in the general properties of light, but several experiments conducted quite recently touched directly upon the problem of the wave-particle duality. In 1989 the team of Akira Tonomura conducted for the first time the famous double-slit experiment with electrons in carefully controlled laboratory conditions (see Appendix C) [5]. In 1999 Anton Zeilinger and his colleagues performed another experiment of the same kind, but with fullerene molecules instead of electrons [44]. The interference pattern was again obtained, confirming that also particles much larger than electrons are able to behave in accordance with de Broglie relations.

The somewhat controversial Afshar experiment was one of the most recent words uttered on the matter of the wave-particle duality of light [45]. It was first conceived and carried out by Shahriar Afshar in 2005 (but later repeated in an improved form). The experiment is assumed by some to demonstrate a paradox of the wave-particle duality, because it seemingly allows to observe both the corpuscular and the undulatory behaviour of light at once [46]. However, a consensus has not been yet reached. The Afshar experiment and its possible implications will be analyzed in Chapter 8.

Thus we have followed, in a rather abridged way, the historical development of the wave-particle duality notion. We have seen how it evolved from an either-or question concerning solely light to a much deeper problem regarding the dual nature of the totality of radiation and matter. Although today the paradox is phrased in the same way as it was in the 1930s, in the meantime the progress of science, especially in the framework of quantum optics, has highlighted some novel features of the duality (as, for instance, photon bunching and antibunching).

The author would like to make one final remark. The wave-particle duality is a beautiful illustration of applied Hegelian dialectic. This philosophical doctrine formulated by Heinrich Chalybäus (and not by Georg Hegel, as the name suggests) states that in the development of new ideas we can (usually) distinguish three phases: the initial *thesis*, the contradictory *antithesis* and the final *synthesis* which resolves the tension between the first two and offers a compromise solution. As we have seen in the above chapter, the wave theory of light was used to negate the corpuscular statements of Isaac Newton, and then quantum mechanics united both views through the wave-particle duality paradox. But in the Hegelian dialectic the synthesis is by no means the final word in the whole story, because usually it gives rise to a new thesis and the scheme

repeats itself. It remains to be seen if the wave-particle duality of de Broglie and Bohr will be challenged by another explanation of the quantum-mechanical phenomena, and if the discussion about the nature of light and matter will be reincarnated in some other form.

2 The classical and the quantum descriptions of light

After having discussed the historical development of the wave-particle duality notion, we are now ready to consider the strictly physical aspects of the problem. In the following chapters we will review, compare and comment chosen elements of the classical and quantum-mechanical theories regarding either the undulatory or the corpuscular nature of radiation.

We start by giving a short presentation of Maxwell's electromagnetic theory embedded into Maxwell's equations which unanimously declare light to be an electromagnetic wave (Ch 2.1). Another approach to radiation based on quantum harmonic oscillator (Ch. 2.2) and quantization of electromagnetic modes (Sects. 2.3.1-2.3.2) is possible as well. In this way we introduce the photon number states (Sects. 2.3.3-2.3.4) and suppress the wave aspect of radiation. Furthermore, one can also employ the coherent state formalism which represents "classical" states of light (Ch. 2.4).

Before we proceed, we have to stress that what follows is in fact a strongly abridged review of the basic elements of the essential theories. Although we try to keep the consistency level high, move from one stage to another in a smooth fashion (that is, highlighting the links between the stages) and delve into the relevance the different theories have for the wave view or for the corpuscular view, it is by no means possible to deal with the chosen theories exhaustively. For instance, dedicating only three pages to a section called "Maxwell's electromagnetic theory" may seem as an insult to the theory; or, while exploring the possibility for quantizing the electromagnetic modes, we deliberately ignore the fact that the huge domain of quantum field theory is right behind the corner.

2.1 Maxwell's electromagnetical theory

The electromagnetic field is described classically by two vectorial quantities: the electric field \mathbf{E} and the magnetic field \mathbf{B} . Generally these vector fields are not constant, but position- and time-dependent, so we should rather write $\mathbf{E} = \mathbf{E}(\mathbf{r}, t)$, $\mathbf{B} = \mathbf{B}(\mathbf{r}, t)$. More importantly, they also depend on each other, and the

way they are linked together in the physical space is quantified by Maxwell's equations³:

$$\nabla \times \mathbf{B} = \mu \mathbf{J} + \mu \epsilon \frac{\partial \mathbf{E}}{\partial t} \quad (1)$$

$$\nabla \times \mathbf{E} = -\frac{\partial \mathbf{B}}{\partial t} \quad (2)$$

$$\nabla \cdot \mathbf{B} = 0 \quad (3)$$

$$\nabla \cdot \mathbf{E} = \frac{\rho}{\epsilon} \quad (4)$$

The meaning of the symbols should be evident, but for the sake of completeness let us quickly define them. \mathbf{J} and ρ are, respectively, total current density and total charge density (total meaning both free and bound currents / charges are to be considered); ϵ is the electric permittivity which describes how the electric field affects and is affected by the actual medium; and μ is the magnetic permeability which describes how the magnetic field affects and is affected by the actual medium. In vacuum the values of the permittivity and the permeability are written ϵ_0 and μ_0 , respectively, with the values ⁴:

$$\epsilon_0 \equiv 8.85 \times 10^{-12} \text{ F/m}$$

$$\mu_0 \equiv 4\pi \times 10^{-7} \text{ H/m.}$$

Thus in free space Maxwell's equations reduce to:

$$\nabla \times \mathbf{B} = \mu_0 \epsilon_0 \frac{\partial \mathbf{E}}{\partial t} \quad (5)$$

$$\nabla \times \mathbf{E} = -\frac{\partial \mathbf{B}}{\partial t} \quad (6)$$

$$\nabla \cdot \mathbf{B} = 0 \quad (7)$$

$$\nabla \cdot \mathbf{E} = 0 \quad (8)$$

Maxwell's equations have to be supplemented by the Lorentz force law governing the motion of a point charge in an electromagnetic field:

$$\mathbf{F} = q(\mathbf{E} + [\mathbf{v} \times \mathbf{B}]). \quad (9)$$

Here \mathbf{F} is the force working on the particle, q is the charge of the particle and \mathbf{v} is its velocity.

A great variety of electrostatic and electrodynamic phenomena can be quantitatively described using these five simple equations. Undoubtedly their most important prediction is that of the electromagnetic waves which paves the way to the realm of electrodynamics. More precisely, from Maxwell's equations one can deduce the wave equation which suggests existence of some kind of electromagnetic waves. To derive the wave equation in free space we will need one of the vector identities:

$$\nabla \times (\nabla \times \mathbf{Z}) = \nabla(\nabla \cdot \mathbf{Z}) - \nabla^2 \mathbf{Z}$$

³We present Maxwell's equation in the differential form, but they can equivalently be written in the integral form. See, for instance, Rao [47].

⁴The modern convention is to define both ϵ_0 and μ_0 in such a way that $\epsilon_0 \mu_0 = c^{-2}$ where c is the speed of light. However, it does not mean that Eq. (12) (see below) should be considered trivial. Historically speaking, both the permittivity and the permeability were initially measured, and the scientists did not know about their connection with c . It was Maxwell who discovered the relation given by Eq. (12), and only afterwards it was used to motivate the definition.

which is valid for any vector field \mathbf{Z} . Now, let us apply the curl operator to Eq. (6), make use of the vector identity above and then simplify the resulting expression using Eq. (5) and Eq. (8):

$$\begin{aligned}
\nabla \times (\nabla \times \mathbf{E}) &= \nabla \times \left(-\frac{\partial \mathbf{B}}{\partial t} \right) \\
\nabla(\nabla \cdot \mathbf{E}) - \nabla^2 \mathbf{E} &= -\frac{\partial(\nabla \times \mathbf{B})}{\partial t} \\
-\nabla^2 \mathbf{E} &= -\mu_0 \epsilon_0 \frac{\partial^2 \mathbf{E}}{\partial t^2} \\
\nabla^2 \mathbf{E} - \mu_0 \epsilon_0 \frac{\partial^2 \mathbf{E}}{\partial t^2} &= 0.
\end{aligned} \tag{10}$$

An identical equation can be derived for \mathbf{B} . Thus all components of the electric and the magnetic field satisfy the wave equation which, for some scalar quantity u , can be written as

$$\nabla^2 u - \frac{1}{v^2} \frac{\partial^2 u}{\partial t^2} = 0 \tag{11}$$

where v is the phase velocity of the wave. Physically speaking we are now considering a highly idealised situation where the wave under examination propagates far away from both the source and any materials that could influence the fields. However, our simplification should not be regarded as nonaccurate, because in any realistic situation the undulatory aspect will be present and as strongly pronounced as it is now. The only difference would be a complication of the differential equations involved due to (possibly complex) boundary conditions.

Since the electromagnetic radiation is known to propagate in vacuum with the speed of light c , we see that the value of the speed of light emerges from the classical electromagnetic theory and can be calculated using the electric permittivity and the magnetic permeability. From Eq. (10) it follows that

$$c = \frac{1}{\sqrt{\epsilon_0 \mu_0}}, \tag{12}$$

a relation discovered by Maxwell himself and already commented upon in Chapter 1.2 of the thesis.

The general solution of the electromagnetic wave equations in free space (far away from the source and materials) may be given in the complex form:

$$\mathbf{E}(\mathbf{r}, t) = \mathbf{E}_0 e^{-j(\mathbf{k} \cdot \mathbf{r} - \omega t)} \tag{13}$$

$$\mathbf{B}(\mathbf{r}, t) = \mathbf{B}_0 e^{-j(\mathbf{k} \cdot \mathbf{r} - \omega t)}. \tag{14}$$

\mathbf{k} represents the wave vector, i.e. the propagation direction of the wave, and ω is the angular frequency of the wave, related to the oscillation frequency f as $\omega = 2\pi f$. The physically measurable electromagnetic waves are obtained by taking the real parts of the expressions above.

If we now insert Eq. (13) and Eq. (14) into Eq. (5) and Eq. (6), we will eventually find that

$$\mathbf{k} \times \mathbf{B}_0 = -\omega \epsilon_0 \mu_0 \mathbf{E}_0$$

$$\mathbf{k} \times \mathbf{E}_0 = \omega \mathbf{B}_0.$$

It follows that the electric field is perpendicular to both the wave vector and the magnetic field, while the

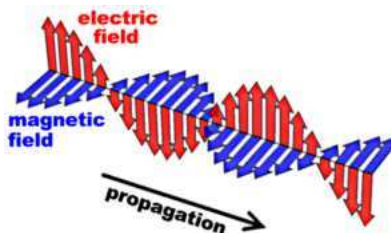


Figure 3: A schematic illustration of the spatial evolution of an electromagnetic wave. The electric and the magnetic fields are perpendicular to each other and to the direction of propagation. Figure reproduced from [50].

magnetic field is perpendicular to both the wave vector and the electric field. Thus, the propagation direction of the electromagnetic field, its electric part and its magnetic part are all perpendicular to each other.

We have chosen to present the simplest possible type of electromagnetic waves – i.e. plane monochromatic waves propagating in the free space – but any other case can be tackled as well with the help of Maxwell’s equations, for instance spherical waves or Gaussian beams (used as a good approximation to laser beams, see Ch. 5.3) [48]. Generally we also have to consider simultaneously different modes of the electromagnetic radiation, i.e. wave trains with different frequencies and polarizations which propagate through the system at the same time. The notion of modes will be formally introduced in the next section.

Besides, as mentioned above, in most practical situations we do not have the leisure of analyzing wave propagation in the vacuum, but instead we need solve an electrodynamical problem in some physical system consisting of several media. Then one has to use the general form of Maxwell’s equations, Eqs. (1)-(4), and apply appropriate boundary conditions. Usually solving the resulting differential equations is difficult from the mathematical point of view, but in principle it is always fully possible, at least numerically. Therefore the theory is able to describe the transmission of electromagnetic waves in waveguides and optical fibers or the behaviour of electromagnetic waves in a resonant cavity, just to mention a few examples [49].

Let us, however, keep the basic idea clear: According to the classical electromagnetic theory, light (and other forms of radiation) consists of linked electric and magnetic fields which travel through space in the same direction in a wavelike fashion.

2.2 The review of the quantum harmonic oscillator formalism

In the following intermediate subsection we will quickly review the algebraic solution of the quantum harmonic oscillator problem, because the photon number state and the coherent state formalisms are based directly upon it, and so in the remaining part of the chapter we will frequently refer to the results below. For the sake of brevity all proofs are omitted. They can be found in any textbook covering basic quantum mechanics, for instance in Shankar [51] (Chapter 7). The basic elements of the formalism of quantum mechanics is presented in Appendix A.

We want to solve the eigenvalue equation:

$$\hat{H} |n\rangle = E_n |n\rangle \tag{15}$$

where \hat{H} is the Hamilton (energy) operator for the harmonic oscillator:

$$\hat{H} = \frac{1}{2m}\hat{p}^2 + \frac{1}{2}m\omega^2\hat{x}^2. \quad (16)$$

All symbols are used in the usual way: m is the particle mass, ω is the angular frequency of oscillation, \hat{p} is the momentum operator and \hat{x} is the position operator. E_n is the energy of the eigenstate $|n\rangle$.

By introducing the so-called lowering and raising operators \hat{a} and \hat{a}^\dagger :

$$\hat{a} \equiv \sqrt{\frac{m\omega}{2\hbar}}\left(\hat{x} + \frac{i}{m\omega}\hat{p}\right) \quad (17)$$

$$\hat{a}^\dagger \equiv \sqrt{\frac{m\omega}{2\hbar}}\left(\hat{x} - \frac{i}{m\omega}\hat{p}\right) \quad (18)$$

which do not commute:

$$[\hat{a}, \hat{a}^\dagger] = 1, \quad (19)$$

one can show that the solution of (15) is given by eigenstates called $|0\rangle, |1\rangle, |2\rangle, \dots$ with the respective eigenvalues $\frac{1}{2}\hbar\omega, \frac{3}{2}\hbar\omega, \frac{5}{2}\hbar\omega, \dots$, so in general $E_n = (n + \frac{1}{2})\hbar\omega$. Now we can move on the “ladder” of the eigenstates using the lowering and raising operators (hence their names; they are also collectively called the ladder operators) in the following way:

$$\begin{aligned} \hat{a}|n\rangle &= \sqrt{n}|n-1\rangle \\ \hat{a}^\dagger|n\rangle &= \sqrt{n+1}|n+1\rangle. \end{aligned}$$

The square-root factors are normalization constants ensuring that $\langle m|n\rangle = \delta_{mn}$. It follows that:

$$|n\rangle = \frac{1}{\sqrt{n!}}(\hat{a}^\dagger)^n|0\rangle. \quad (20)$$

The eigenstates form a complete basis:

$$\sum_n |n\rangle\langle n| = 1 \quad (21)$$

$|0\rangle$ is the lowest possible state (in terms of energy), the so-called ground state. Acting on it with the lowering operator \hat{a} results in zero vector ($\hat{a}|0\rangle = 0$). We can also calculate the wave function of the ground state in the coordinate representation:

$$\varphi_0(x) = \langle x|0\rangle = \left(\frac{m\omega}{\pi\hbar}\right)^{1/4} e^{-\frac{1}{2}\frac{m\omega}{\hbar}x^2} \quad (22)$$

and then proceed with finding the wave functions of the higher eigenstates. As it happens, they are all related to the Hermite polynomials H_n :

$$\varphi_n(x) = \left(\frac{m\omega}{\pi\hbar}\right)^{1/4} \sqrt{\frac{1}{2^n n!}} H_n(x) e^{-x^2/2},$$

and the Hermite polynomials themselves are generated using the Rodriguez formula:

$$H_n(x) = e^{x^2} \left(-\frac{d}{dx} \right)^n e^{-x^2}.$$

Now the Hamilton operator (16) may be written in terms of the ladder operators:

$$\hat{H} = \left(\hat{a}^\dagger \hat{a} + \frac{1}{2} \right) \hbar \omega = \frac{1}{2} \hbar \omega (\hat{a}^\dagger \hat{a} + \hat{a} \hat{a}^\dagger), \quad (23)$$

as well as the position and momentum operators:

$$\hat{x} = \sqrt{\frac{\hbar}{2m\omega}} (\hat{a}^\dagger + \hat{a}) \quad (24)$$

$$\hat{p} = i \sqrt{\frac{m\hbar\omega}{2}} (\hat{a}^\dagger - \hat{a}). \quad (25)$$

Finally let us define the number operator, $\hat{N} \equiv \hat{a}^\dagger \hat{a}$, which may be used to “extract” the number n from an eigenstate $|n\rangle$ through another eigenvalue equation:

$$\hat{N} |n\rangle = n |n\rangle.$$

2.3 Quantization of the electromagnetic modes

In the following section we will study how one quantizes the electromagnetic radiation. We start by demonstrating how the (still classic) electric and magnetic fields \mathbf{E} and \mathbf{B} can be expressed in terms of two other electromagnetic quantities, the electromagnetic vector and scalar potentials \mathbf{A} and ϕ (Sect. 2.3.1). Then we expand \mathbf{A} as a sum over the electromagnetic modes, derive the wave equation, and show how it can be reduced to the harmonic oscillator equation for each mode (Sect. 2.3.2). Finally, by quantizing the harmonic oscillators, we obtain the photon number states for each mode (Sect. 2.3.3). The electric and magnetic fields \mathbf{E} and \mathbf{B} can be easily “recovered” from the model, but this time, obviously enough, as quantum mechanical operators $\hat{\mathbf{E}}$ and $\hat{\mathbf{B}}$.

We notice that Sects. 2.3.1-2.3.2 consist of derivations and the quantized model itself is presented and discussed in Sects. 2.3.3-2.3.4. In the course of the derivations some less important mathematical details will be omitted. The missing proofs can be found in, for instance, [52] or [53]. Besides, the path leading to the quantization which we will present is neither the only one possible nor the most rigorous one. An alternative way of quantizing the electromagnetic modes is briefly sketched in the footnote on page 25.

2.3.1 The electromagnetic potentials

We consider again one of the Maxwell’s equations, Eq. (3):

$$\nabla \cdot \mathbf{B} = 0$$

It demands the magnetic field to be non-divergent (i.e. the magnetic field never starts nor ends at a point, because there are no magnetic monopoles), but we know from vector algebra that the curl of an arbitrary vector field satisfies this condition. Thus, we can ensure the non-divergence of the magnetic field by assuming that it can be derived from some more fundamental field \mathbf{A} :

$$\mathbf{B} = \nabla \times \mathbf{A} \quad (26)$$

\mathbf{A} is called the magnetic vector potential. We can also use it to express the electric field \mathbf{E} , but then in addition we need a scalar potential ϕ . \mathbf{E} can then be defined as

$$\mathbf{E} = -\nabla\phi - \frac{\partial\mathbf{A}}{\partial t}. \quad (27)$$

The definition is consistent with Eq. (2), since $\nabla \times (\nabla\phi) = 0$ for any vector field ϕ . Before we insert the new definitions Eqs. (26) and (27) into Eqs. (1) and (4), let us impose an additional constraint on \mathbf{A} :

$$\nabla \cdot \mathbf{A} = 0. \quad (28)$$

This condition is called the Coulomb gauge or the radiation gauge. The reason for our use of it is the fact that without any such constraint we are free to transform the potentials:

$$\begin{aligned} \mathbf{A} &\rightarrow \mathbf{A}' = \mathbf{A} + \nabla\psi \\ \phi &\rightarrow \phi' = \phi - \frac{\partial\psi}{\partial t}, \end{aligned}$$

where ψ is an arbitrary scalar function. This freedom of transformation corresponds to non-physical quantities that we wish to eliminate by imposing some special condition, like the Coulomb gauge, Eq. (28).

Now we can apply Eqs. (27) and (28) to Eq. (4):

$$\nabla \cdot \mathbf{E} = \nabla \cdot \left(-\nabla\phi - \frac{\partial\mathbf{A}}{\partial t} \right) = -\nabla^2\phi - \frac{\partial(\nabla \cdot \mathbf{A})}{\partial t} = -\nabla^2\phi = \frac{\rho}{\epsilon},$$

and so we obtain Poisson's equation $\nabla^2\phi = -\frac{\rho}{\epsilon}$. This implies that the scalar potential defined by Eq. (27) is the ordinary electric potential from electrostatics given as:

$$\phi(\mathbf{r}, t) = \int \frac{\rho(\mathbf{r}', t)}{4\pi\epsilon|\mathbf{r} - \mathbf{r}'|} d^3\mathbf{r}'.$$

Thus ϕ has nothing to do with the electrodynamical part of the theory and the dynamics has to be contained within \mathbf{A} . We verify it by inserting Eqs. (26) and (27) into Eq. (1):

$$\nabla \times (\nabla \times \mathbf{A}) = \mu\mathbf{J} - \epsilon\mu\frac{\partial}{\partial t}\nabla\phi - \epsilon\mu\frac{\partial^2}{\partial t^2}\mathbf{A}.$$

Applying the vector identity $\nabla \times (\nabla \times \mathbf{A}) = \nabla(\nabla \cdot \mathbf{A}) - \nabla^2\mathbf{A}$, making use of the Coulomb gauge and setting $\epsilon\mu = c^{-2}$ where c is the speed of light in the given medium (see Eq. (12)), we end up with the complete field

equation for the electromagnetic potentials:

$$-\nabla^2 \mathbf{A} + \frac{1}{c^2} \frac{\partial(\nabla\phi)}{\partial t} + \frac{1}{c^2} \frac{\partial^2 \mathbf{A}}{\partial t^2} = \mu \mathbf{J}. \quad (29)$$

From the above expression we are going to extract the wave equation for the magnetic vector potential only. According to the fundamental theorem of vector calculus (Helmholtz's theorem), every vector field can be written as a sum of an irrotational (longitudinal) and a solenoidal (transverse) component vector field, i.e. for every vector field ψ one has $\psi = \psi_L + \psi_T$ where $\nabla \times \psi_L = 0$ and $\nabla \cdot \psi_T = 0$. Because of the Coulomb gauge Eq. (28) we see that the magnetic vector potential \mathbf{A} is wholly transverse, and we also know that $\nabla \times (\nabla\phi) = 0$, so $\nabla\phi$ is wholly longitudinal. Now, if we decompose the current \mathbf{J} , $\mathbf{J} = \mathbf{J}_L + \mathbf{J}_T$, we can readily split Eq. (29) into two parts:

$$\begin{aligned} -\nabla^2 \mathbf{A} + \frac{1}{c^2} \frac{\partial^2 \mathbf{A}}{\partial t^2} &= \mu \mathbf{J}_T \\ \frac{1}{c^2} \frac{\partial(\nabla\phi)}{\partial t} &= \mu \mathbf{J}_L. \end{aligned}$$

The first of these expressions is the one most interesting for our case, because it shows that the magnetic vector potential has to fulfill the wave equation with a source term given by the transverse component of the electric current. If the latter is present, it will be caused by atomic electrons, so solving the equation enables us then to consider the problem of radiation-matter interaction. But in a region of space with $\mathbf{J}_T = 0$ we simply get

$$-\nabla^2 \mathbf{A} + \frac{1}{c^2} \frac{\partial^2 \mathbf{A}}{\partial t^2} = 0 \quad (30)$$

and this is the case that we will study further.

2.3.2 Expansion in electromagnetic modes

Let us consider a cubic region of space of side L and volume $L^3 = V$. It is emphatically not a real physical cavity, merely a region of space limited by imaginary boundaries. Thus we may still work with running waves instead of reducing the problem to that of standing waves, but we have to apply to them appropriate periodic boundary conditions. Then a single component solution to Eq. (30) would be given as:

$$A_{\mathbf{k}\lambda}(\mathbf{r}, t) = A_{\mathbf{k}\lambda}(t)e^{i\mathbf{k}\cdot\mathbf{r}} + A_{\mathbf{k}\lambda}^*(t)e^{-i\mathbf{k}\cdot\mathbf{r}}, \quad (31)$$

where the lower index $\mathbf{k}\lambda$ labels a distinct mode (see below) characterised by the wave vector \mathbf{k} and one of the two possible polarization directions $\lambda = 1, 2$. $A_{\mathbf{k}\lambda}(t)$ is the time-dependent modal coefficient. Because of the periodic boundary conditions the components of \mathbf{k} take discrete values, so:

$$k_i = \frac{2\pi}{L}n_i, \quad n_i = 0, \pm 1, \pm 2, \dots, \quad i = x, y, z.$$

The general solution can then be written as the sum over all single-mode solutions,

$$\mathbf{A}(\mathbf{r}, t) = \sum_{\mathbf{k}, \lambda} \mathbf{e}_{\mathbf{k}\lambda} A_{\mathbf{k}\lambda}(\mathbf{r}, t) \quad (32)$$

where $\mathbf{e}_{\mathbf{k}\lambda}$ is the unit polarization vector of a given mode. Here the term “mode” denotes a particular, single-frequency oscillation pattern of the electromagnetic field [3]. The superposition of all modes gives the total electromagnetic field.

Inserting Eq. (31) into Eq. (30) results in the harmonic oscillator equation, a separate one for each mode:

$$k^2 A_{\mathbf{k}\lambda}(t) + \frac{1}{c^2} \frac{\partial^2 A_{\mathbf{k}\lambda}(t)}{\partial t^2} = 0,$$

or, by multiplying with c^2 and setting the modal angular frequency $\omega_{\mathbf{k}} = c|\mathbf{k}|$:

$$\frac{\partial^2 A_{\mathbf{k}\lambda}(t)}{\partial t^2} + \omega_{\mathbf{k}}^2 A_{\mathbf{k}\lambda}(t) = 0, \quad (33)$$

with the standard solution:

$$A_{\mathbf{k}\lambda}(t) = A_{\mathbf{k}\lambda} e^{-i\omega_{\mathbf{k}} t},$$

so Eq. (31) becomes:

$$A_{\mathbf{k}\lambda}(\mathbf{r}, t) = A_{\mathbf{k}\lambda} e^{i(\mathbf{k}\cdot\mathbf{r} - \omega_{\mathbf{k}} t)} + A_{\mathbf{k}\lambda}^* e^{-i(\mathbf{k}\cdot\mathbf{r} - \omega_{\mathbf{k}} t)}.$$

Now the formulas for the transverse electric field \mathbf{E}_T , the magnetic field \mathbf{B} can be easily derived from Eqs. (26) and (27).

$$\mathbf{E}_T(\mathbf{r}, t) = \sum_{\mathbf{k}, \lambda} \mathbf{e}_{\mathbf{k}\lambda} E_{\mathbf{k}\lambda}(\mathbf{r}, t) \quad (34)$$

$$E_{\mathbf{k}\lambda}(\mathbf{r}, t) = i\omega_{\mathbf{k}} (A_{\mathbf{k}\lambda} e^{i(\mathbf{k}\cdot\mathbf{r} - \omega_{\mathbf{k}} t)} - A_{\mathbf{k}\lambda}^* e^{-i(\mathbf{k}\cdot\mathbf{r} - \omega_{\mathbf{k}} t)}) \quad (35)$$

$$\mathbf{B}(\mathbf{r}, t) = \sum_{\mathbf{k}, \lambda} \frac{\mathbf{k} \times \mathbf{e}_{\mathbf{k}\lambda}}{|\mathbf{k}|} B_{\mathbf{k}\lambda}(\mathbf{r}, t) \quad (36)$$

$$B_{\mathbf{k}\lambda}(\mathbf{r}, t) = i|\mathbf{k}| (A_{\mathbf{k}\lambda} e^{i(\mathbf{k}\cdot\mathbf{r} - \omega_{\mathbf{k}} t)} - A_{\mathbf{k}\lambda}^* e^{-i(\mathbf{k}\cdot\mathbf{r} - \omega_{\mathbf{k}} t)}) \quad (37)$$

The formula for the total radiative energy U is somewhat more tedious to deduce, but starting from the standard expression, $U = \frac{1}{2} \int dV [\epsilon E_T^2(\mathbf{r}, t) + \mu^{-1} B^2(\mathbf{r}, t)]$, in the end we would obtain:

$$\begin{aligned} U &= \sum_{\mathbf{k}, \lambda} U_{\mathbf{k}\lambda} \\ U_{\mathbf{k}\lambda} &= \epsilon_0 V \omega_{\mathbf{k}}^2 (A_{\mathbf{k}\lambda} A_{\mathbf{k}\lambda}^* + A_{\mathbf{k}\lambda}^* A_{\mathbf{k}\lambda}) \end{aligned} \quad (38)$$

Of course, the contents of the last parenthesis could be put together in a single term, because classically these coefficients commute. However, in the next step we will quantize our model, and then the commutator will become non-zero.

2.3.3 The photon number states

The presence of the harmonic oscillator equation Eq. (33) in our model motivates us to quantize it by introducing the ideas from the quantum harmonic oscillator formalism presented in the last section. This procedure goes under the name canonical quantization. We simply assume⁵ that the quantum state for each

⁵This may seem like a big and unjustified leap in our reasoning. After all, in the quantum harmonic oscillator model we were working with the position and momentum operators contributing to the Hamilton operator Eq. (16), and our goal then

mode may be expressed in the basis consisting of the eigenstates $|n_{\mathbf{k}\lambda}\rangle$ where the integer $n_{\mathbf{k}\lambda}$ denotes the number of photons – discrete energy excitations – in the mode $\mathbf{k}\lambda$. We are using the ladder operators in the same manner as before, but this time they go under different names: the lowering operator becomes the annihilation operator and the raising operator becomes the creation operator, the obvious reason being that they can now be used to respectively destroy or create photons in the modes. Also, each mode has ascribed its own pair of the operators, and the operators from different modes commute. Thus we have the following relations:

$$\hat{a}_{\mathbf{k}\lambda} |n_{\mathbf{k}\lambda}\rangle = \sqrt{n_{\mathbf{k}\lambda}} |n_{\mathbf{k}\lambda} - 1\rangle \quad (39)$$

$$\hat{a}_{\mathbf{k}\lambda}^\dagger |n_{\mathbf{k}\lambda}\rangle = \sqrt{n_{\mathbf{k}\lambda} + 1} |n_{\mathbf{k}\lambda} + 1\rangle \quad (40)$$

$$[\hat{a}_{\mathbf{k}\lambda}, \hat{a}_{\mathbf{k}'\lambda'}^\dagger] = \delta_{\mathbf{k}\mathbf{k}'} \delta_{\lambda\lambda'}. \quad (41)$$

The state of the total field is written as a product of the single-mode states:

$$|\{n_{\mathbf{k}\lambda}\}\rangle \equiv |n_{\mathbf{k}_1 1}\rangle |n_{\mathbf{k}_1 2}\rangle |n_{\mathbf{k}_2 1}\rangle |n_{\mathbf{k}_2 2}\rangle \dots, \quad (42)$$

and using Eq. (20) we can write it as:

$$|\{n_{\mathbf{k}\lambda}\}\rangle = \prod_{\mathbf{k}\lambda} \left(\frac{1}{\sqrt{n_{\mathbf{k}\lambda}}!} (\hat{a}_{\mathbf{k}\lambda}^\dagger)^{n_{\mathbf{k}\lambda}} |0\rangle \right) \quad (43)$$

where $|0\rangle$ denotes the vacuum state, i.e. the state without any photons. The single-mode states $|n_{\mathbf{k}\lambda}\rangle$ are called the photon number states or the Fock states.

The Hamilton operator of the total radiation field is obtained by summing Eq. (23) over all modes:

$$\hat{H}_{tot} = \sum_{\mathbf{k}\lambda} \hat{H}_{\mathbf{k}\lambda} \quad (44)$$

$$\hat{H}_{\mathbf{k}\lambda} = \frac{1}{2} \hbar \omega_{\mathbf{k}} (\hat{a}_{\mathbf{k}\lambda} \hat{a}_{\mathbf{k}\lambda}^\dagger + \hat{a}_{\mathbf{k}\lambda}^\dagger \hat{a}_{\mathbf{k}\lambda}) = \hbar \omega_{\mathbf{k}} \left(\hat{a}_{\mathbf{k}\lambda}^\dagger \hat{a}_{\mathbf{k}\lambda} + \frac{1}{2} \right) \quad (45)$$

Now we are going to replace the magnetic vector field coefficients $A_{\mathbf{k}\lambda}$ with its corresponding quantum mechanical operators $\hat{A}_{\mathbf{k}\lambda}$, although we would like to express them in terms of the annihilation and creator operators. We do it by comparing Eq. (45) with Eq. (38), and so:

$$A_{\mathbf{k}\lambda} \rightarrow \hat{A}_{\mathbf{k}\lambda} = \sqrt{\frac{\hbar}{2\epsilon_0 V \omega_{\mathbf{k}}}} \hat{a}_{\mathbf{k}\lambda} \quad (46)$$

$$A_{\mathbf{k}\lambda}^* \rightarrow \hat{A}_{\mathbf{k}\lambda}^\dagger = \sqrt{\frac{\hbar}{2\epsilon_0 V \omega_{\mathbf{k}}}} \hat{a}_{\mathbf{k}\lambda}^\dagger \quad (47)$$

was to solve the eigenvalue equation Eq. (15). Here, however, we only have the magnetic vector potential \mathbf{A} which has to fulfill the harmonic oscillator equation Eq. (33) derived from the wave equation Eq. (30). It might be said that the analogy was stretched too far. But in fact, as explained for instance in [54], the energy of a general oscillating system is expressible as $U = \sum_i \frac{1}{2} (\dot{q}_i^2 + \omega_i^2 q_i^2)$ with q_i being the generalized coordinate of mode i and ω_i its associated angular frequency. Now the similarity to Eq. (16) is much clearer. The reason for us not choosing that way is that we wanted to work with the physical electric and magnetic fields from the start, instead of going through the Lagrange formalism with its somewhat more abstract concepts like generalized coordinates, canonical momenta and the Lagrangian of the electromagnetic field. Also keep in mind that the treatment is by no means meant to be exhaustive, and an interested reader may refer for more details to [53].

From Eqs. (34)-(37) we obtain now the electric field and the magnetic field operators:

$$\hat{\mathbf{E}}_T(\mathbf{r}, t) = \sum_{\mathbf{k}\lambda} i\sqrt{\frac{\hbar\omega_{\mathbf{k}}}{2\epsilon_0 V}} \left(\hat{a}_{\mathbf{k}\lambda} e^{i(\mathbf{k}\cdot\mathbf{r}-\omega_{\mathbf{k}}t)} - \hat{a}_{\mathbf{k}\lambda}^\dagger e^{-i(\mathbf{k}\cdot\mathbf{r}-\omega_{\mathbf{k}}t)} \right) \mathbf{e}_{\mathbf{k}\lambda} \quad (48)$$

$$\hat{\mathbf{B}}(\mathbf{r}, t) = \sum_{\mathbf{k}\lambda} i\sqrt{\frac{\hbar}{2\epsilon_0 V\omega_{\mathbf{k}}}} \left(\hat{a}_{\mathbf{k}\lambda} e^{i(\mathbf{k}\cdot\mathbf{r}-\omega_{\mathbf{k}}t)} - \hat{a}_{\mathbf{k}\lambda}^\dagger e^{-i(\mathbf{k}\cdot\mathbf{r}-\omega_{\mathbf{k}}t)} \right) (\mathbf{k} \times \mathbf{e}_{\mathbf{k}\lambda}) \quad (49)$$

2.3.4 Some problematic aspects of the quantized theory

While in the classical model the electromagnetic radiation is perceived as two (electric and magnetic) fields propagating through space in an undulatory manner, in the quantum model we are using the language of energy excitations, or photons. We assume that each radiation mode – characterized by the wave vector \mathbf{k} (together with the associated frequency $\omega_{\mathbf{k}} = c|\mathbf{k}|$) and the polarization λ – consists of a specific number n of these photons. The operators corresponding to physically measurable quantities, like the electric and the magnetic field, are expressed in terms of the annihilation and creation operators (which again can be applied to change the number of photons in each mode). There is no inherent wavelike propagation of the electromagnetic field, since the starting point of the quantum model is a Fock state given by Eq. (43), while in the classical mode we had the wave equation Eq. (10) following from the fundamental Maxwell equations Eqs. (1)-(4).

The main feature of the quantum view is discreteness of the radiation energy. The radiation *itself*, however, is not directly claimed by the theory to be of a corpuscular nature. An important point is that the optical field given by Eq. (42) has to be treated in its totality, because the quantization of the electromagnetic modes does not give us any natural way to localize a single photon in space. As Mandel and Wolf (see Chapter 12.11, [55]) pointed out, any attempts to extend the theory in this direction encounter fundamental difficulties, because no position operator exists for the photon. They showed that the intensity operator could be used as a measure of number of photons per unit volume, but limiting this volume to a spatial point lead to contradictions. Moreover, the volume considered must remain larger than the wavelengths of contributing modes. Also, a new problem arise if we try to apply the quantization scheme to polychromatic fields. If we strongly concentrate the photon position wave function near origin by appropriate superposition of different modes, we will find that the associated energy density is in fact spread out over space asymptotically like r^{-7} where r is the distance from the origin. Since photodetection probability is proportional to this energy density, it follows that a photodetection may occur at some distance from the origin even though per assumption photon is localized in the origin. More generally, the energy density can be non-zero at positions where the photon position wave function is zero.

We remarked in the Introduction that in principle the photonic idea is applied to whole electromagnetic spectrum, but in practice (i.e. when performing actual calculations and quantitative modelling) it is limited to the high-frequency part of the spectrum (the frequencies corresponding to the infrared region and higher). This limitation is partly due to theoretical reasons (as seen in the previous paragraph), and partly due to the fact that at low enough frequencies (for instance in the radio waves region) our measuring apparata are capable of tracing the evolution of electric and magnetic fields directly. One should thus consider to what degree the quantization of electromagnetic field is a conceptual artifact introduced in order to side-step the limitations caused by resolution capabilities of our present instruments. Alternatively, one could ask whether

there exists some rather sharp boundary in the frequency spectrum when the concept of photon loses its applicability. If no such boundary exists and if the wave-particle transition is “diffuse”, one should attempt to establish the physical character of this transition more clearly.

On the other hand, there is at least some “circumstantial” evidence suggesting that the photon is a real physical (though massless) particle, not merely a quantum of the radiation energy conveniently employed in the high-frequency region. Since $\hat{a}_{\mathbf{k}\lambda}^\dagger \hat{a}_{\mathbf{k}\lambda}$ acts as the number operator for mode $\mathbf{k}\lambda$ with $\hat{a}_{\mathbf{k}\lambda}^\dagger \hat{a}_{\mathbf{k}\lambda} |\omega\rangle = n_{\mathbf{k}\lambda} |n_{\mathbf{k}\lambda}\rangle$, we easily deduce from Eq. (45) that a single photon from that mode has energy equal to $E = \hbar\omega_{\mathbf{k}}$. In a similar way, starting from the classical field momentum formula

$$P = \int d^3\mathbf{r} \epsilon_0 (\mathbf{E} \times \mathbf{B})$$

one could show that a single photon from the given mode has momentum equal to $p = \hbar\mathbf{k}$. These relations are identical to de Broglie’s formulas describing physical particles (see Appendix C). Furthermore, using the relation $\omega_{\mathbf{k}} = c|\mathbf{k}|$ (which is generally valid for electromagnetic waves in vacuum) we see that a single photon energy can also be expressed as $E = cp$. The last equation emerges from the special theory of relativity as well, if one assumes that the photon is a massless relativistic particle. Finally, its two possible polarization states could be elegantly explained by ascribing the massless photon intrinsic spin of value 1.

We see that even though the corpuscularity of electromagnetic radiation may seem well grounded theoretically, the concept of photon – in the sense of “a particle of light” – must not be used uncritically. One has to be aware of the difference between quantizing the energy content of the electromagnetic field and postulating existence of massless corpuscular “carriers” of electromagnetic radiation; of the fundamental problems with localizing photons; and of the fact that the quantized theory is applicable only as long as the relevant volumes involved (as, for instance, volume of a photodetecting device) are much larger than the radiation wavelength.

The photon number states present us with another problem as well: their expectation values of the electric and the magnetic fields unrealistically vanish. Using Eq. (48) and Eq. (49) in Eq. (181) (see Appendix A, p. 167) we get for any general Fock state given by Eq. (43):

$$\langle \mathbf{E}_T(\mathbf{r}, t) \rangle = \langle \mathbf{B}(\mathbf{r}, t) \rangle = 0. \quad (50)$$

Thus, we do not observe any macroscopical coherent electric or magnetic field oscillations, no matter what Fock state we are considering. Even if the Fock state is highly excited, i.e. the numbers $n_{\mathbf{k}\lambda}$ are high for many modes, $\langle \mathbf{E}_T(\mathbf{r}, t) \rangle$ and $\langle \mathbf{B}(\mathbf{r}, t) \rangle$ will still vanish. It implies that the photon number states, though they possess a simple conceptual structure, have to be regarded as completely nonclassical states.

This problem, however, may be resolved by further development of the theory. In order to represent classical radiation with $\langle \mathbf{E}_T(\mathbf{r}, t) \rangle \neq 0$ and $\langle \mathbf{B}(\mathbf{r}, t) \rangle \neq 0$ new quantum states must be introduced. These are the coherent states $|z_{\mathbf{k}\lambda}\rangle$ where $z_{\mathbf{k}\lambda}$ is a complex number. We express them in terms of the photon number states in the following way:

$$|z_{\mathbf{k}\lambda}\rangle = e^{-|z_{\mathbf{k}\lambda}|^2/2} \sum_{n=0}^{\infty} \frac{z_{\mathbf{k}\lambda}^n}{\sqrt{n_{\mathbf{k}\lambda}!}} |n_{\mathbf{k}\lambda}\rangle, \quad (51)$$

The general coherent state, with all modes included, is given as (compare with Eq. (43)):

$$|\{z_{\mathbf{k}\lambda}\}\rangle = \prod_{\mathbf{k}\lambda} |z_{\mathbf{k}\lambda}\rangle.$$

The expectation values of the transverse electric and the magnetic fields for the coherent states are non-vanishing, and the calculations would be considerably shortened by the fact that the coherent state $|z_{\mathbf{k}\lambda}\rangle$ is defined as the eigenstate of the annihilation operator $\hat{a}_{\mathbf{k}\lambda}$ with the eigenvalue being simply $z_{\mathbf{k}\lambda}$. This definition, together with other important properties of the coherent states, will be elaborated on in the next section.

2.4 The coherent states

Although the number states may at first seem like the most natural basis for the quantum-mechanical representation of light, we have just seen that they present some difficulties because of their vanishing mean values of electric and magnetic fields. Moreover, they are not very convenient to use in practical situations due to our present experimental limitations – it is difficult to generate a state with a given number of photons except for the cases where this number is small, like in the high-energetic γ -rays [56]. Thus the need to use another set of states – the coherent states – arises⁶.

Coherent states, $\{|z\rangle\}$ with $z \in \mathbb{C}$, are defined as the eigenstates of the annihilation operator \hat{a} :

$$\hat{a}|z\rangle = z|z\rangle \tag{52}$$

\hat{a} is non-Hermitian, $\hat{a} = \hat{a}^\dagger$, so we have no immediate guarantee that the coherent states will be orthogonal or that they will form a complete basis. Alternatively some textbooks (for instance [57]) define the coherent states directly as in Eq. (51), but we choose to utilize the more elegant definition from Eq. (52) and show in Appendix B how Eq. (51) follows from it. The following properties of coherent states are also demonstrated in Appendix B:

- The coherent states are minimal uncertainty states. In Appendix A Heisenberg’s uncertainty principle is stated and proved: $(\Delta x)(\Delta p_x) \geq \frac{\hbar}{2}$. Δx denotes the standard deviation of the x -component of the position, and Δp_x is the standard deviation of the x -component of the momentum. For all coherent states Heisenberg’s uncertainty principle becomes an equality, $(\Delta x)(\Delta p_x) = \frac{\hbar}{2}$. Of course, x and p_x are used merely as examples – the uncertainty is minimal for any pair of a generalized coordinate and its conjugate momentum.
- A coherent state remains coherent during its time evolution. The evolution into another coherent states is periodic with period $\frac{2\pi}{\omega}$. Thus the uncertainty in any pair of a generalized coordinate and its conjugate momentum is always minimal.
- The coherent states form a basis for the representation of arbitrary quantum states. This basis, however, is non-orthogonal and over-complete. Over-completeness makes it possible to represent any coherent state in terms of other coherent states. Furthermore, if we wish to represent an arbitrary quantum state $|\Psi\rangle$ in terms of the coherent states, this representation is completely determined by its coefficients $\langle z|\Psi\rangle$ within some arbitrarily small but finite range of z .

⁶From now on we skip the lower index $\mathbf{k}\lambda$, since the distinction between different modes is of no importance in this section. Alternatively, let us just assume that we are talking about one specific mode only.

It is the coherent states, and not the number states, that are the quantum-mechanical equivalent of the classical electromagnetic field. For the coherent states the mean values of the electric and magnetic fields are non-vanishing. They are easily calculated because of the defining relation in Eq. (52). Eqs. (48) and (49) give:

$$\begin{aligned}\langle \mathbf{E}_T(\mathbf{r}, t) \rangle &= i\sqrt{\frac{\hbar\omega}{2\epsilon_0 V}} \left(z e^{i(\mathbf{k}\cdot\mathbf{r}-\omega t)} - z^* e^{-i(\mathbf{k}\cdot\mathbf{r}-\omega t)} \right) \mathbf{e} = \sqrt{\frac{2\hbar\omega}{\epsilon_0 V}} \Im \left(z e^{i(\mathbf{k}\cdot\mathbf{r}-\omega t+\pi)} \right) \mathbf{e} \\ \langle \mathbf{B}(\mathbf{r}, t) \rangle &= i\sqrt{\frac{\hbar}{2\epsilon_0 V\omega}} \left(z e^{i(\mathbf{k}\cdot\mathbf{r}-\omega t)} - z^* e^{-i(\mathbf{k}\cdot\mathbf{r}-\omega t)} \right) (\mathbf{k} \times \mathbf{e}) = \sqrt{\frac{2\hbar}{\epsilon_0 V\omega}} \Im \left(z e^{i(\mathbf{k}\cdot\mathbf{r}-\omega t+\pi)} \right) (\mathbf{k} \times \mathbf{e}),\end{aligned}$$

where again a single mode has been considered, but an extension to all modes can be made through a simple summation.

Even though a coherent state is not an eigenstate of any observable, one has to keep in mind that in practice the measurements related to the electromagnetic field are done through the process of photoelectric detection where the photons are being absorbed from the field (in the corpuscular picture; for more details concerning the photodetection process see Chapter 5.1). This process can be thus associated with the annihilation operator acting on the quantum state representing the field. Since we expect that the measurement should not disturb the classical electromagnetic field, and since the coherent state is per definition the eigenstate of the annihilation operator, we see how the relation between the coherent states and the classical electromagnetic field emerges. Furthermore it can be shown that the electromagnetic field produced by any deterministic current source is, in fact, in a coherent state (see Mandel and Wolf [55], p. 568).

The coherent states serve also as building blocks of the theory of quantum correlations [43]. Within this theory one represents electromagnetic field as a density matrix $\hat{\rho}$ which is a superposition of projection operators formed from coherent states:

$$\hat{\rho} = \int \phi(z) |z\rangle \langle z| d^2z.$$

$\phi(z)$ is a quasi-probability distribution which becomes ordinary probability distribution only when the electromagnetic field considered is classical (i.e. possesses no explicit quantum-mechanical properties). Above representation is called Glauber-Sudarshan P-representation (Mandel and Wolf [55], Chapter 11), but discussing it in detail lies outside the scope of the thesis. However, from the theory of quantum correlations emerge important results concerning statistical properties of optical fields which cannot be accounted for by the classical electromagnetism. We will come back to the issue of correlations in Chapter 4, and we will quote these special results in the final paragraphs of Chapter 4.4.

3 Experimental considerations of the wave-particle duality

Irrespective of how elegant, speculative or surprising a physical theory is, it is always the experimental evidence that is decisive for its verification or refutation. After having discussed physical models for electromagnetic radiation in Chapter 2, we are now going to familiarize ourselves with what several important experiments have to say about particlelike and wavelike behaviour of light. The somewhat controversial Afshar's experiment [45] is for the moment left out. We will present it in Chapter 8, because here we would rather focus on firmly established experiments.

The following chapter will be initiated by a short discussion of the black-body radiation (Ch. 3.1). Details will be avoided, because the measurements involved do not have any *direct* bearing on the wave-or-particle question. It can be easily reasoned that they demonstrate only the quantization of the energy transfer between light and matter, and, as remarked in the Introduction, we want to keep the quantization hypothesis (as applied generally to physical states) apart from the photon hypothesis.

Thereafter we analyze the phenomenon of light interference which occurs at both high and low intensities, and in our belief suffices to empirically ground the undulatory view of light (Ch. 3.2). We note, however, that this view is connected directly with the classical electromagnetic theory which have correctly predicted the results of countless experiments and has been validated through the workings of many different technological devices based on it (like power transmission lines or cellular phones, just to mention a few). Evidence of this kind has been excluded from the chapter, and we concentrate on interference alone.

When it comes to the corpuscular view of light, we critically analyze the photoelectric effect (Ch. 3.3) and the Compton effect (Ch. 3.4). In almost each modern textbook on quantum mechanics these two phenomena are mentioned as very strong proofs for the photon hypothesis, but we will also present their alternative explanations which make use of the undulatory view instead. We emphasize that these different models are by no means recent discoveries, but were conceived at about the same time when the original experiments were conducted. The question as to why these more conservative explanations of the photoelectric and the Compton effect never gained much appreciation, should be left for historians of physics to answer.

There is, however, another class of experiments suggesting that electromagnetic radiation indeed possesses a granular structure. In these experiments one measures anticorrelations between two parts of a light beam divided by a beam splitter, and finds that the anticorrelations are weaker than predicted by the classical electromagnetic model, but in accordance with the expression given by the photon hypothesis. In this context we will review the (anti)correlation experiment due to Grangier, Roger and Aspect, but we will also question some assumptions that their analysis is based on (Ch. 3.5). The discussion of photocount statistics associated with photomeasuring experiments will continue later in Chapter 5.1, where we will examine predictions of

the two main models of photodetection.

3.1 The black-body radiation

A black body is an object that completely absorbs the electromagnetic radiation that falls on it. With “complete absorption” we mean that the black body is perfectly opaque (no part of the radiation passes through it) and perfectly non-reflective. When the black body is at thermal equilibrium with its environment, it will on average emit as much radiative energy as it absorbs⁷. The radiation emitted by the black body can be measured and plotted as function of spectral energy density⁸ versus the radiative frequency (or, alternatively, wavelength). As it happens, the curve will have a distinct shape with a maximum for a particular frequency value, but the shape and the position of the maximum will vary with the temperature of the black body and its environment.

Planck’s law yields the functional dependence between the spectral energy density u and the frequency ν (or wavelength λ), with the temperature T as a parameter:

$$u(\nu) = \frac{8\pi h\nu^3}{c^3} \frac{1}{e^{h\nu/kT} - 1} \quad (53)$$

$$u(\lambda) = \frac{8\pi hc}{\lambda^5} \frac{1}{e^{hc/\lambda kT} - 1} \quad (54)$$

Here, c is the speed of light and k is the Boltzmann constant, while h is the nature constant discovered by Planck, subsequently called by his name and measured nowadays to be ca. 6.63×10^{-34} Js.

The rigorous derivation of Planck’s law lies outside the scope of this section. Suffice it to say that most modern textbooks starts the derivation by examining a single mode of electromagnetic radiation in a cavity [58]. The average energy in the mode is calculated with the help of the partition function from statistical mechanics. Then, one integrates the energy over all modes using the density of states as the weighting function. The density of states is determined from quantum-mechanical considerations, and this is how h is incorporated into the final expression for the spectral energy density.

As pointed out in Chapter 1.3, the original derivation due to Max Planck himself had to follow along different lines [59]. Planck described the black-body radiation in terms of monochromatic vibrations of resonators situated in a permanent stationary radiation field. He calculated the entropy of a single resonator and found a relationship between the entropy and the energy of the resonator. However, he had to make one crucial assumption: He postulated that the total energy of the system is distributed among the oscillators in finite amounts, i.e. that the energy share of each oscillator comes in discrete elements (quanta). Further considerations showed that the energy element ought to be proportional to the frequency of the radiation emitted by the oscillator. The numerical value of the proportionality constant was deduced from earlier experimental measurements of the black-body radiation; this was of course the Planck constant h .

It is easy to observe that in the limit of high frequencies the denominator of Eq. (53) simplifies, and the

⁷In many practical situations, however, this condition is not completely satisfied, but the formalism of the black-body radiation can still be used. A good example is the Sun. Our star is certainly not at thermal equilibrium with its environment, but the measurements of the radiation emitted by it show a very good agreement with the predictions of Planck’s law.

⁸Spectral energy density is energy per unit volume per unit frequency.

expression can be written as:

$$u(\nu) = \frac{8\pi h\nu^3}{c^3} e^{-h\nu/kT}.$$

This is Wien’s law (or Wien’s approximation), a formula proposed on the empirical basis by Wilhelm Wien in 1896 [29] which properly described the spectrum of the black-body radiation at high frequencies⁹ (see Ch. 1.3). On the other hand, in the limit of low frequencies (53) can be obviously written as:

$$u(\nu) = \frac{8\pi kT}{c^3} \nu^2.$$

This is the Rayleigh-Jeans law which yields the spectrum of the black-body radiation at low frequencies. Lord Rayleigh and Sir James Jeans managed in 1905 to rigorously demonstrate that this is the formula that follows from classical physical arguments (i.e. without the energy quantization hypothesis) [28]. It was immediately observed that the expression could not be completely correct, because the energy density went to infinity at very high frequencies (see the footnote about the “ultraviolet catastrophe” on p. 12).

The Planck’s law was proposed in order to give an explanation for the already measured black-body radiation. It succeeded in it exquisitely well, both by supplying an elegant theoretical model and by accurately reproducing the empirical data. In his article [59] Planck referred to measurements conducted by Lummer and Pringsheim [27], Rubens and Kurlbaum [60], and Beckmann [61]. Modern measurements of the black-body radiation (with the determination of cosmic background radiation being the most spectacular and precise of them all [62]) have further substantiated the validity of Planck’s law.

3.2 Interference (Michelson interferometry)

Interference of light is often defined by physical dictionaries as:

“The systematic attenuation and reinforcement of the amplitude over distance and time of two or more overlapping light waves that have the same or nearly the same frequency.” [63]

This definition is unfortunately not appropriate for our needs, because it *a priori* assumes existence of waves of some kind, while we would rather focus on the *phenomenological* aspect of the interference of light (without employing the term “waves” right from the start). Thus let us try to formulate our own, more careful definition:

Interference takes place if light (or, more generally, electromagnetic radiation of any kind) produces a detectable spatial (or temporal) pattern consisting of regions (or periods) where (during which) the response of our measuring apparatus seems to be alternately strengthened and weakened. Interference often occurs when two or more light beams combine in such a way that

⁹ Wien used other notation for the natural constants present in the expression. In particular, he did not consider the possibility for energy quantization at all, and thus was unable to explain h in its terms.

together they produce a pattern which is not a superposition of single patterns produced by each of the light beams on its own.

We notice that we have chosen to talk about “the response of our measuring apparatus” rather than about the amplitude of light or some other property belonging to the light itself.

The different variants of light interference¹⁰ can be divided into two types: 1) those where the directions of two parts of the light beam are changed and then recombined at a small angle, and 2) those where the light beam is divided completely into two parts and then reunited. We have already briefly mentioned in Chapter 1 colours of thin films, which belong to the latter class, but analyzing that phenomenon would not be very instructive. Other well-known examples of interferometers are Young’s apparatus with two pinholes (class 1), Michelson interferometer (class 2) and Mach-Zender interferometer (class 2). Performing Mach-Zender interferometry is actually a part of the experiment associated with the thesis (see Ch. 7.2), and a more detailed discussion (in the context of optical correlations) is to be found later (see Ch. 4.4). For that reason we will here use Michelson interferometry as our example. Our treatment below is loosely based on [64] and [67], but the original description due to Michelson can be found in [68].

Consider a simplified setup presented in Fig. 4. A coherent light source¹¹ L emits light toward a beam splitter¹² B . The beam is split into two new beams of approximately equal intensity. The first of these beams is reflected toward a movable mirror $M1$, while the second of the beams is transmitted toward a fixed mirror $M2$. $M1$ reflects the first beam back to B . Part of it is reflected by B back towards L , and part of it is transmitted to a screen S . The second beam is reflected by $M2$ back to B and then is again reflected by the back side of B toward S . With the careful directional alignment of mirrors (so that both beams are reflected back towards the same region of S , and they make a small angle relatively to each other), a spatial interference pattern will be observed on the screen. Moreover, the pattern will change if we move $M1$ along the MY -axis. The change will take place already after a very slight displacement of $M1$ (~ 10 nm or even less, if we are using visible light), and it will soon be observed to have a periodic character. (We assume that L is intense enough so the interference pattern can be seen with the naked eye, but we could also replace the screen with a more sensitive detector.)

The illustration of the interference pattern is presented in Fig. 5. The interference fringes can have many different forms depending on the exact alignment of the mirrors $M1$ and $M2$ (and other components), but the overall structure is each time similar and always consists of regions when the light is seen to be alternate strengthened and weakened. The simplest and most elegant explanation for the occurrence of this pattern

¹⁰We do not wish to elaborate on the rather subtle distinction between interference and diffraction. Diffraction can be generally defined as various phenomena which occur when a light beam encounters a particular kind of obstacle on its way, like a screen with a small slit. Different physical textbooks and dictionaries do not completely agree on the mutual nomenclatural relation of interference and diffraction. For instance, Monk [64] stresses that although diffraction also creates an interference pattern, it should not be confused with interference *per se*. On the other hand Daintith [65] simply states that diffraction is a class of physical phenomena where interference takes place, which *de facto* makes the diffraction phenomena an underclass of the interference phenomena. In our context the precise difference between diffraction and interference is not that important, because both produce an interference pattern, and it is that pattern that we would like to explain physically.

¹¹The coherence of light source is the necessary condition for producing an interference pattern. We deliberately defer the definition of coherence to Chapter 4, because the formal description is intimately connected with the undulatory aspect of radiation, and, as already remarked, for the sake of clarity we wish to avoid any *a priori* assumptions about the nature of light. For now we just assume, again in the phenomenological spirit, that coherence is a property that light sources in varying degree and which enables them to produce the interference pattern. In our discussion of the Michelson interferometry we are just assuming that the light source used has this property.

¹²Beam splitters are a crucial part of many interferometers, and we investigate their operational principles in Ch. 5.2. Right now we simply state that beam splitter is basically a half-reflecting mirror, i.e. a “imperfect” mirror that transmits half of the incoming light, and reflects the second half.

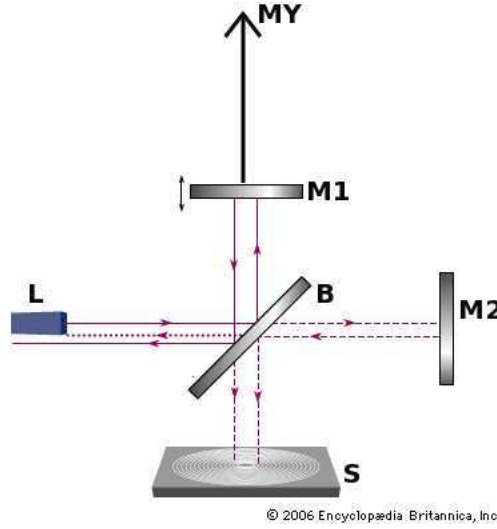


Figure 4: A schematic illustration of the Michelson interferometer. L is a coherent light source, B is a beam splitter, $M1$ is a mirror movable along MY -axis, $M2$ is a fixed mirror, S is a screen where the interference pattern is observed. Notice that the beams arriving at the screen ought to make a small angle relatively to each other. This is not seen in the figure. Source: *Encyclopedia Britannica [66]* (the picture has been modified)

and its dependence on the position of the movable mirror $M1$ is provided by the classical electromagnetic theory which describes light as electric and magnetic fields propagating together through space in a wavelike fashion (see Ch. 2.1). In Eqs. (13)-(14) we have expressed the electric and magnetic components as plane waves propagating through whole space:

$$\mathbf{E}(\mathbf{r}, t) = \mathbf{E}_0 e^{-j(\mathbf{k} \cdot \mathbf{r} - \omega t)} \quad (55)$$

$$\mathbf{B}(\mathbf{r}, t) = \mathbf{B}_0 e^{-j(\mathbf{k} \cdot \mathbf{r} - \omega t)} \quad (56)$$

Here, however, the light source does not need be monochromatic, so additional modes often have to be considered, but, more importantly, the light is spatially confined. It does not permeate the whole space as planar waves, but is represented as a narrow light beam propagating at all times in some single direction through the experimental setup. But, as we will more formally see in Ch. 5.3, such spatial confinements do not change the basic picture, because the amplitudes are simply modulated with a position-dependent envelope. Thus, the electric field, say, will become:

$$\mathbf{E}(\mathbf{r}, t) = \mathbf{U}(\mathbf{r}) e^{-j(\mathbf{k} \cdot \mathbf{r} - \omega t)}, \quad (57)$$

where the simple replacement $\mathbf{E}_0 \rightarrow \mathbf{U}(\mathbf{r})$ has been made. We have changed the letter to stress that now the amplitude may be represented as a complex number (with the physically measurable electric field being equal to the real part of the whole expression, just as before).

The term $e^{-j(\mathbf{k} \cdot \mathbf{r} - \omega t)}$ has been retained and thus in the real part of Eq. (57) there will still be present an oscillation which depends on $\mathbf{k} \cdot \mathbf{r}$, i.e. on position. Now, the beam splitter B divides the light beam into two parts, characterized by electrical fields $\mathbf{E}_1(\mathbf{r}, t)$ and $\mathbf{E}_2(\mathbf{r}, t)$. Both of them are proportional with $e^{-j(\mathbf{k} \cdot \mathbf{r} - \omega t)}$, because neither the wavelength nor the frequency have been changed through the interaction

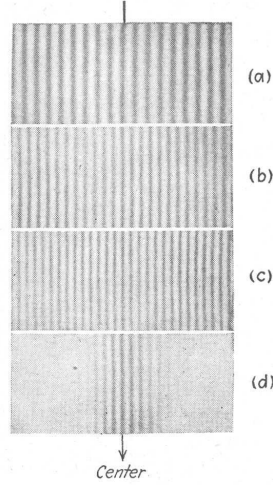


Figure 5: Interference fringes produced by a Michelson interferometer. (a), (b) and (c) are photographs obtained with respectively red, green and blue monochromatic radiations. (d) is the photograph of the white-light fringes. *Source: Monk [64]*

with B (per assumption). Furthermore, since the propagation of both beams occurs along straight lines, we can replace $\mathbf{k} \cdot \mathbf{r}$ with, say, kd where d is simply the distance travelled by the beam and k is the component of the wave vector \mathbf{k} corresponding to the direction along L - B (cf. Fig. 4) which was the original direction of propagation.

The path traversed by \mathbf{E}_1 can be symbolically expressed as B - $M1$ - B - S with the total distance d_1 , while the path traversed by \mathbf{E}_2 is given as B - $M2$ - B - S with the total distance d_2 . Right in front of the screen S at some time t_0 we thus get $\mathbf{E}_1 = \mathbf{U}_1 e^{-j(kd_1 - \omega t_0)}$ and $\mathbf{E}_2 = \mathbf{U}_2 e^{-j(kd_2 - \omega t_0)}$ with \mathbf{U}_1 and \mathbf{U}_2 being some complex numbers given by $\mathbf{U}(\mathbf{r})$ from Eq. (57). The two beams recombine at S and the superposition of their electric fields is:

$$\mathbf{E}_{res} = \mathbf{U}_1 e^{-j(kd_1 - \omega t_0)} + \mathbf{U}_2 e^{-j(kd_2 - \omega t_0)}$$

What we do observe on the screen, however, is not the resultant electric field, but the intensity I_{res} of the recombined beam. In the case of monochromatic light, the intensity can be taken to be proportional to the absolute square of the electric field. We obtain:

$$I_{res} \sim |\mathbf{E}_{res}|^2 = |\mathbf{U}_1|^2 + |\mathbf{U}_2|^2 + \mathbf{U}_1^* \mathbf{U}_2 e^{jk(d_1 - d_2)} + \mathbf{U}_1 \mathbf{U}_2^* e^{-jk(d_1 - d_2)}.$$

If we represent \mathbf{U}_1 and \mathbf{U}_2 exponentially as $\mathbf{U}_1 = \sqrt{I_1} e^{j\phi_1}$ and $\mathbf{U}_2 = \sqrt{I_2} e^{j\phi_2}$, the expression for I_{res} can be rewritten as:

$$I_{res} = I_1 + I_2 + \sqrt{I_1 I_2} \left(e^{j(k\Delta d + \Delta\phi)} + e^{-j(k\Delta d + \Delta\phi)} \right) = I_1 + I_2 + 2\sqrt{I_1 I_2} \cos(k\Delta d + \Delta\phi), \quad (58)$$

with $\Delta\phi \equiv \phi_2 - \phi_1$ and $\Delta d \equiv d_1 - d_2$.

Figure 6 shows a plot of Eq. (58). Its correspondence to Fig. 5 should be obvious. The intensity oscillation pattern observed on the screen results from the fact that the two beams have travelled different distances, and in the expression for the resultant intensity there is now an interference term, $2\sqrt{I_1 I_2} \cos(k\Delta d + \Delta\phi)$, due to the recombination of the two beams. The argument of the cosine term is influenced by the difference

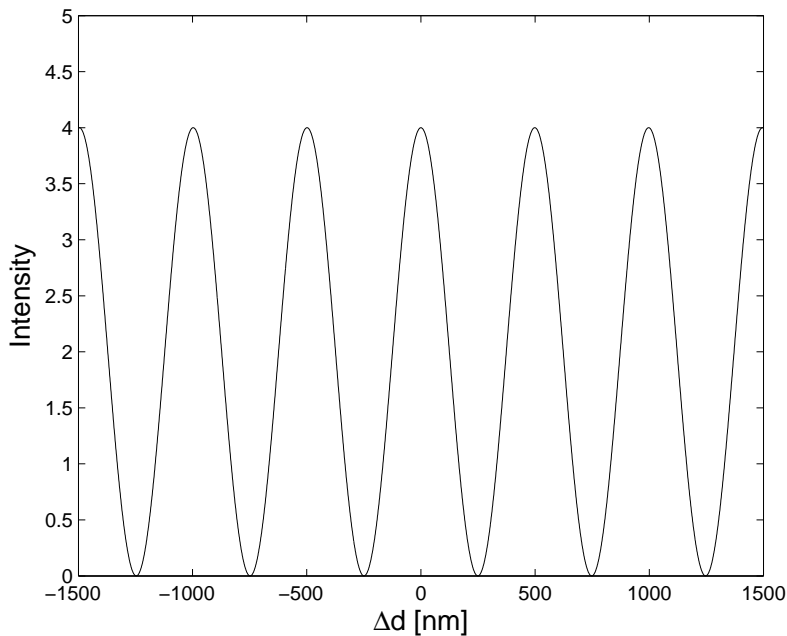


Figure 6: Plot of Eq. (58) as a function of Δd with $I_1 = I_2 = 1$, $\Delta\phi = 0$ and $k = 1.26 \times 10^7 \text{ m}^{-1}$ (calculated from $\lambda = 500 \text{ nm}$). The intensity observed on the screen varies when we change the difference in the distance travelled by the two beams, i.e. when we change the position of the movable mirror $M1$.

in the distances. Therefore moving the mirror $M1$ will result in a visible change of the pattern, because \mathbf{U}_1 (and thus ϕ_1) and d_1 will vary. The alteration of $\Delta\phi$ is dependent on the exact form of the envelopes of the beams, but the sensitivity of the cosine term for Δd is easily established by noticing that for an ordinary visible light with $\lambda \approx 500 \text{ nm}$ we have $k \approx 10^7 \text{ m}^{-1}$. Thus changing Δd by as little as $10^{-7} \text{ m} = 10 \text{ nm}$ will make a noticeable difference for the interference term.

In the above discussion we have implicitly assumed that the transversal size of the light beams is so small that on the screen we will observe only one single spot whose intensity will change according to Eq. (58) or Fig. 6. In practice it is not necessarily the case – what we see on the screen is an extended pattern of interference fringes for one chosen Δd (cf. Fig. 5), and it is the pattern that (periodically) changes when we vary Δd . We explain this easily by recalling that the light beams are not infinitesimally small in the transversal direction, so their different parts overlap in different ways on different regions of the screen. Besides, it is not the position of $M1$ along the MY -axis alone that decides how the interference pattern looks like, but also its directional alignment (relatively to the directional alignment of $M2$). Using different geometrical arguments [64] one is able to derive more complicated formulas for $\Delta d(\mathbf{r}_P)$ where \mathbf{r}_P denotes the position of some point P on the screen, and to describe the interference pattern in a quantitatively exact way¹³.

Thus, in order to explain the interference pattern that occurs in the Michelson interferometer, we may represent the light beam used as an electromagnetic field propagating through space in a wavelike fashion, with the electric and the magnetic components oscillating spatially and temporally. The Michelson interferometer divides this wave into two parts and later recombines them in such a way that an interference pattern is

¹³Many different forms of the interference fringes can also be obtained, not only straight lines, but also circles, parabolas, ellipses and hyperbolas.

produced. Mathematically, the most simple case of this procedure is given by Eq. (58). Descriptions of other variants of interference (and diffraction) may be much more complicated (due to the complex geometry of the given setting), but physically we can always assume the wavefronts of the two beams under consideration superpose so that in some regions they reinforce themselves, and in some other regions they attenuate themselves, these two occurrences being called respectively constructive and destructive interference.

The wave picture of light (or, more generally, of electromagnetic radiation) allows thus to describe interference in an elegant and consistent manner. The corpuscular view of light, however, does not. Let us see how far do we get with a heuristic approach. Imagine that our light source does not emit an electromagnetic, continuous field, but a stream of minute light particles called photons, which are sharply localized energy excitations travelling through space at the speed of light. The density of the stream is n photons per unit length. Let us also assume that the screen S is photoluminescent, so when a photon hits it, a flash of light is produced and our eyes register it. Now, the stream of photons meets first the beam splitter B on its way. For each of the photons the beam splitter randomly decides if it should be sent (undivided, per definition of the light quantum) towards $M1$ or $M2$ (the process of the beam splitting is examined in more detail in Ch. 5.2). Since the probability of sending a photon towards $M1$ is presumed to equal the probability of sending it towards $M2$, we end up with two new streams of photons travelling in two different directions, each having a density of approximately $\frac{n}{2}$ (some stochastic fluctuations are allowed, but they are of no consequence for us here). The mirrors reflect the two photon streams back to S , just like in the description of the interferometer above. They recombine and interact with the photoluminescent screen.

Intuitively, the corpuscular view of light does not make us expect any particular pattern to arise on the screen. If a single photon stream of density n would produce a light spot of intensity I on the photoluminescent screen, then a single photon stream of density $\frac{n}{2}$ should give¹⁴ a light spot of intensity $\frac{I}{2}$. Now, if we divide a single stream of density n into two equal parts, and then reunite them again and let the resultant beam interact with the screen, we expect a uniform light spot of intensity I given by a formula similar to Eq. (58), but without the interference term.

Empirically, however, we do obtain an interference pattern on the screen. Can it be explained using photons? What comes immediately to mind is that the photons from the two beams could interact with each other in some way, such that in some regions of the screen there arrives more of them than in some other regions. If the photons are perceived as corpuscles, they could for instance scatter from each other and, statistically, the scattering would result in a particular pattern observed on the screen. This line of thought could be followed on, were it not for the dependence of the pattern on Δd , the difference in distances travelled by the two beams. Because of it, we are forced to assume that there is some specific property possessed by the photon which changes as a function of the path length, and that this property is decisive for the manner in which the photons from the two beams interact during their recombination into one stream and their arrival upon the screen.

Were the photons ordinary physical particles, an obvious candidate for such a property would be velocity. Namely, we could assume that the photons are gradually slowing down on their way from L to S . The

¹⁴ We assume here that the photons are identical. Also, their density in each case is so large that a flash of light produced on the screen by a single photon does not have enough time to wane before the next photon hits the screen and a new flash of photoluminescence is generated. Therefore the screen does not produce discrete flashes of light corresponding to each photon hit separately, but instead we obtain an “accumulated” light spot with intensity proportional to the density of the incoming photon stream.

velocity would without a doubt be a very important factor in determining how the two beams interact during the recombination and what pattern is produced on the screen. However, a distinguished role of the velocity is of course ruled out in this context, because the light is known to have the constant speed c .

Moreover, the property needs change in a periodic fashion, if we wish to be able to reproduce the experimental results. It is thus hard to see what kind of property could it be, if one does not want to resort to the wave picture and to employ the phase. We could, however, try to equip the photon with some kind of internal “clock” that measures the distance the photon has travelled or the time that has passed since its emission¹⁵, and whose “hands” periodically return to the same values¹⁶, but this idea seems rather artificial.

The corpuscular picture of light not only has serious difficulties in explaining the interference pattern, but it also leads us to an additional problem that touches the heart of the wave-particle paradox. Assume that we represent the light as a stream of photons as before, and that each photon carries energy E given by Planck’s formula $E = \hbar\omega$, where ω is the angular frequency of the light, if the classical electromagnetic model were to be applied. Let us again use visible monochromatic light with wavelength $\lambda = 500$ nm. A simple calculation gives $\omega = 3.76 \times 10^{15} \text{ s}^{-1}$ and $E \approx 4 \times 10^{-19} \text{ J}$. If the effect of the light source combined with appropriate filters lies around 0.01 nW, the light source produces around 2.5×10^7 photons per second, i.e. approximately one photon each $4 \times 10^{-8} \text{ s}$. Let us make the size of the Michelson interferometer quite small, so that the longest of the two possible photon paths does not exceed 50 cm. A photon propagating with the speed of light needs only $1.6 \times 10^{-9} \text{ s}$ to traverse that distance, so we can safely assume that there is one photon in the apparatus at any given time – *if* the light source emits photons with equal (or almost equal) time intervals between two consecutive emissions (such regularity is formally described in the framework of photon and photocount statistics which we will discuss in Sects. 5.1.2-5.1.3).

We have therefore affirmed – working still in the framework of the corpuscular model – that a single photon is emitted from the light source, meets the beam splitter, is sent randomly towards either $M1$ or $M2$ (undivided), reflects back from one of the mirrors and after a fraction of nanosecond hits the photoluminescent screen. Thus we do not expect any interference pattern depending on the distance difference Δd , because in the absence of two separate streams of photons continuously bombarding the screen there is apparently no possibility for any inter-photon interactions that could lead to the creation of the pattern. Surprisingly enough, an interference pattern of exactly the same kind as before *will* be still observed, although this time its intensity will be understandably much smaller (because the intensity of the light source is now also very small), and we will be possibly forced to use detectors more sensitive than a combination of the photoluminescent screen and the naked eye.

The first observations of photonic self-interference in experimentally certain conditions are due to L. Jánossy who conducted appropriate measurements in Budapest in the 1950s [70]. Jánossy used monochromatic radiation with wavelength 546.1 nm and coherence length of approximately 1 m. The arm length of the Michelson interferometer employed was 14 m, and the total optical path for a photon traversing the apparatus was 30 m long. With intensity as low as ca. 10^4 photons emitted per second Jánossy was confident that only one photon was present in the interferometer at any given time¹⁷. The interference pattern was

¹⁵One could oppose such hypothesis by saying that, since the photon moves with the speed of light, its proper time is zero, and all lengths as measured from the “vantage point” of the photon are contracted to zero as well. The existence of such a “clock” would then be at odds with the special theory of relativity. Notice, however, that in the case of a *wave* of light, the position- and time-dependant phase of the wave plays a role equivalent to that of the postulated “clock”, and no objections are raised in that case.

¹⁶Actually, this is the approach embraced by Richard Feynman in his popular presentation of quantum electrodynamics [69].

¹⁷This crucial point was, however, criticized by Panarella [71]. According to Panarella Jánossy had not presented a conclusive proof that the photons were indeed isolated within the interferometer when they traversed it. Jánossy should have reduced

observed, and Jánossy had to conclude that “interference phenomena are perfectly normal even at such low intensities where at one time in average less than one photon is to be found in the arrangement; this is true even if the dimensions of the arrangement greatly exceed the coherence length of the photons giving rise to the patterns” [72].

The presence of the interference pattern in the case of single-photon interferometry leads us then easily to believe that the concept of the corpuscular nature of light is erroneous, and that light should be represented as an electromagnetic wave, even when the light source operates at very small intensities. This wave has then very small amplitude indeed, but it is nonetheless divided by the beam splitter and thereafter both parts get recombined, producing the interference fringes on the screen. This postulate could be verified by placing two detectors, $D1$ and $D2$, instead of the two mirrors $M1$ and $M2$, and letting them measure incoming light in coincidence. Unfortunately, results of such coincidence measurements – when conducted on classical states of light (generated by thermal sources and lasers) – are ambiguous, as we will see in our analysis in Chapter 7.1. However, in case of nonclassical states of light an appropriate experiment was conducted by Clauser [73], and the detectors worked indeed in anticoincidence, substantiating the corpuscular view of light.

An experiment similar to that of Clauser will be reviewed in Chapter 3.5, and in Section 5.1.4 we will summarize the differences between classical and nonclassical states of light. Then we will come back again to the issue of (anti)coincidence measurements in the context of our experiment in Chapter 7.1. In Chapter 7.2 the interference at the single photon level will be discussed again. For now we conclude that the classical electromagnetic theory elegantly deals with the development of the interference patterns, and that occurrence of these patterns at very low intensities of light indicates that the theory, or at least some central elements of it, remains valid in this regime.

3.3 The photoelectric effect

The photoelectric effect is the phenomenon where electrons are emitted from matter under an influence of electromagnetic radiation¹⁸. In Chapter 1 we presented its historical context, and now we will proceed to discuss the physical underpinnings of the phenomenon. In general terms it is easy to explain: A single electron is initially bound in the material with energy $E_0 < 0$, but it can absorb energy E_R from the radiation. If $E_0 + E_R$ is larger than zero, the electron frees itself from the potential well and is emitted from the material with the maximal kinetic energy equal to $E_R - |E_0|$.

In the classical electromagnetic theory the energy flux (energy per second per meter squared) of an electromagnetic field is given by the Poynting vector \mathbf{S} :

$$\mathbf{S} = \frac{1}{\mu} \mathbf{E} \times \mathbf{B},$$

where μ is the magnetic permeability and \mathbf{E} and \mathbf{B} vectorial quantities representing, respectively, the electric

further the intensity of light I and increased the counting time of the detector Δt in such a way that the product $I\Delta t$ was constant. If the interference pattern remained the same, it would demonstrate that the phenomenon is linear with light intensity, and the association of wave properties with a single particle would be substantiated. Otherwise one would discover that there is a regime of even lower intensity where the detector was unable to discern any interference pattern, and that the assumption about one photon being present in the apparatus at any time was wrong.

¹⁸This in fact the external photoelectric effect. The difference between the external and the internal photoelectric effects is explained in Chapter 5.1.

and the magnetic field (see Ch. 2.1). Thus the absolute value of the energy flux, $|\mathbf{S}|$, seems to depend only on the intensities of the component fields. We could then deduce that the emission of the electrons depends on these intensities alone. However, experimental results due to Philipp Lenard [74] showed that this is not the case, and that actually the frequency of the radiation plays an additional and essential role.

If, given a monochromatic radiation, the frequency is below some material-dependent value, no emission of electrons will take place, even if we increase the intensity further¹⁹. But if the frequency exceeds the threshold, then the emission will occur, even if the intensity remains low. Raising the frequency further will result in the increase of the speed of the photoelectrons (the emitted electrons), while raising the intensity will lead to more frequent emissions. In other words, the radiation frequency determines the kinetic energy of the photoelectrons, while the radiation intensity determines their number, i.e. the photocurrent.

Using Lenard's results Albert Einstein set out to explain the role of the frequency [31]. Einstein assumed that the incident light of frequency ν consists of energy quanta, each with energy E given by Planck's formula $E = h\nu$. A light quantum interacts with a single electron in the material and transfers all energy to the electron²⁰. Let us denote by W the minimum energy needed remove an electron from a solid to a point immediately outside the solid surface (the so-called work function). If E is larger than W , the electron leaves the material with maximal kinetic energy T_ν given simply by:

$$T_\nu = h\nu - W. \tag{59}$$

The formula reproduced Lenard's results to order of magnitude, and today the above explanation is taken to be the standard physical interpretation of the photoelectric effect. Fig. 7 presents exemplary experimental data describing the photoelectric effect, but since the original results of Lenard were unavailable for the author of the thesis, the data measured by Owen Richardson and K. T. Compton in 1912 [75] have been chosen instead.

We ask whether it is really necessary to assume the granular structure of light in order to give the physical reason for the photoelectric effect and the associated experimental data. From an intuitive point of view the conclusion of Einstein (that the light *consists* of energy quanta) may seem somewhat far-fetched, because all we need do is to quantize the interaction between electromagnetic radiation and matter (more precisely, the transfer of the energy from radiation to matter). Therefore we may ask whether it is possible to deduce Eq. (59) in some alternative way which does not make an explicit use of the concept of photon. Given that the approach of Einstein is taken for granted in almost every presentation of the photoelectric effect, it may seem surprising that the answer is positive [76].

As early as in 1912 Owen Richardson derived Eq. (59) without resorting directly to the corpuscular view of light (which at that time went under the name of "the unitary hypothesis") [32] [77]. Richardson based his model on statistical and thermodynamical principles combined with the laws of classical electrodynamics. In his approach the photoemission process might be compared with evaporation from a liquid surface and work function with latent heat of vaporization. Richardson considered a body being in thermal equilibrium with the surrounding radiation of temperature θ , and examined how the radiative energy will be divided among the electrons in the body. Now, if one electron acquires enough energy, it will be ejected. Richardson

¹⁹The emission may occur, however, if the intensity will become very large. This is the so-called anomalous photoelectric effect, and we will shortly discuss it in the closing paragraphs of Sect. 9.1.3.

²⁰Here we have to assume that multiple photons cannot interact with an electron at the same moment, and that the electron is not able to accumulate energy from different photons even if they interact with it rapidly one after another. Multiphoton scattering may occur, however, if the intensity is very large (see the previous footnote).

FIG. 9.

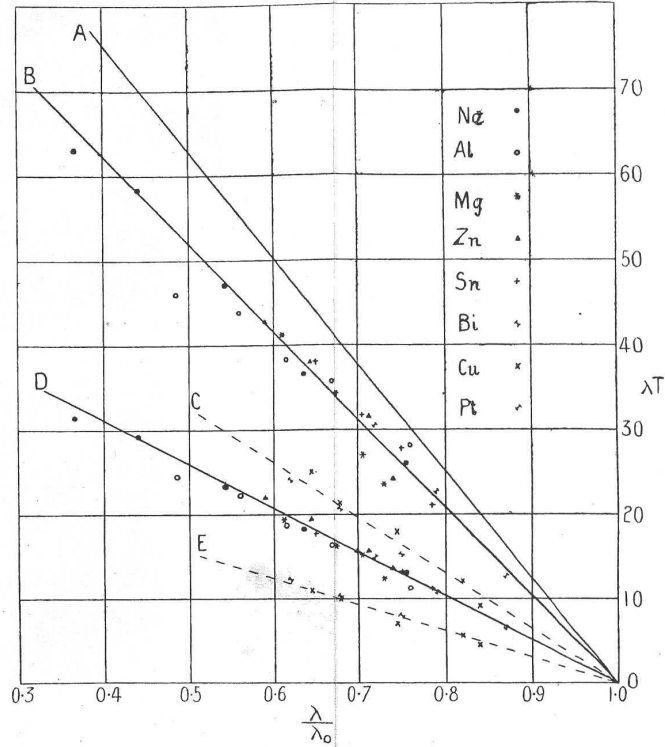


Figure 7: Experimental data describing the photoelectric effect and obtained by Owen Richardson and K. T. Compton in 1912. The scientists wanted to verify the formula postulated by Einstein in 1905, Eq. (59), giving the kinetic energy of the photoelectrons as the function of the frequency ν of the radiation. Denoting the minimal frequency necessary for the electronic emission by ν_0 we get $W = h\nu_0$, and Eq. (59) can be rewritten to $T_\nu = h(\nu - \nu_0)$. Alternatively, in terms of the wavelength $\lambda = \frac{c}{\nu}$, we have $\lambda T_\nu = ch \left(1 - \frac{\lambda}{\lambda_0}\right)$ where $\lambda_0 \equiv \frac{c}{\nu_0}$. For different wavelengths λ of the incoming radiation, the maximal kinetic energy of the photoelectrons was measured, and the results plotted with $\frac{\lambda}{\lambda_0}$ along the x-axis and λT_ν along the y-axis. These measurements were performed for different metals (corresponding to different types of points) and different types of experimental setups (lines OB, OC, OD and OE). We see that in all cases the kinetic energy decreases linearly to zero as the wavelength of the radiation approaches the limiting value λ_0 , and that the proportionality constant can be compared to h . The line OA gives the theoretical predictions. The agreement is apparently not very good, but Richardson and Compton managed to explain the deviations on the grounds of experimental limitations. Further measurements of the photoelectric effect confirmed the validity of Eq. (59) with greater precision. *Source: Richardson and Compton [75]*

demonstrated that the number N of electrons emitted from unit area of the body may be expressed either as the definite integral:

$$N = \frac{c}{4} \int_0^\infty \epsilon F(\nu, \theta) E(\nu, \theta) d\nu, \quad (60)$$

or explicitly as:

$$N = \alpha A \sqrt{\theta} \exp \left(\int \frac{w}{k\theta^2} d\theta \right). \quad (61)$$

The symbols used has the following meanings: c is the speed of light, ν is the radiation frequency, $\epsilon F(\nu, \theta)$ is the number of electrons emitted in the presence of unit electromagnetic radiation with temperature θ whose frequency lies between ν and $\nu + d\nu$, $E(\nu, \theta)$ is the spectral distribution of the electromagnetic energy density (in equilibrium), α is the fraction of the returning electrons which are absorbed (i.e. not reflected), A is a constant dependent on the material under consideration (but independent of θ), w is the internal latent heat of evaporation of one electron and k is Boltzmann's constant (in his treatment Richardson used R , the gas constant for one molecule, instead of k ; but k is per definition identical to the normalized gas constant).

Richardson, basing his reasoning on Eqs. (60) and (61), proceeded then to show how Eq. (59) will follow. First, let us notice that the right-hand sides of the above equations have to be equal, so these can be combined into a single integral equation true for all values of θ :

$$\frac{c}{4} \int_0^\infty \epsilon F(\nu, \theta) E(\nu, \theta) d\nu = \alpha A \sqrt{\theta} \exp \left(\int \frac{w}{k\theta^2} d\theta \right). \quad (62)$$

Since $E(\nu, \theta)$, A , α and w are either known (the spectral distribution is given by Planck's formula, and the material and proportion constants are determined from experiment) or can be approximated (the internal latent heat), we would like to solve the equation for $\epsilon F(\nu, \theta)$. Richardson assumed that

$$w = w_0 + \frac{3}{2} k\theta \quad (63)$$

for some constant w_0 , and instead of using the ordinary Planck formula:

$$E(\nu, \theta) = \frac{8\pi h\nu^3}{c^3} \frac{1}{e^{\frac{h\nu}{k\theta}} - 1},$$

he simplified it to:

$$E(\nu, \theta) = \frac{8\pi h\nu^3}{c^3} e^{-\frac{h\nu}{k\theta}}, \quad (64)$$

since the replacement only causes inaccuracies in the final result proportional to $e^{-w_0/k\theta}$ which is a very tiny fraction except at high temperatures (larger than ca. 5000 K). Putting Eqs. (63) and (64) into (62) the integral equation can be written as:

$$\begin{aligned} \frac{c}{4} \int_0^\infty \epsilon F(\nu, \theta) \times \frac{8\pi h\nu^3}{c^3} e^{-\frac{h\nu}{k\theta}} d\nu &= \alpha A \sqrt{\theta} \exp \left(\int \frac{w_0}{k\theta^2} d\theta \right) \exp \left(\int \frac{3}{2\theta} d\theta \right) \\ \frac{2\pi}{c^2} \int_0^\infty \epsilon F(\nu, \theta) h\nu^3 e^{-\frac{h\nu}{k\theta}} d\nu &= \alpha A \theta^2 \exp \left(\frac{-w_0}{k\theta} \right) \\ \int_0^\infty \epsilon F(\nu, \theta) h\nu^3 e^{-\frac{h\nu}{k\theta}} d\nu &= \alpha \frac{Ac^2}{2\pi} \theta^2 \exp \left(\frac{-w_0}{k\theta} \right) \end{aligned} \quad (65)$$

Assuming that $\alpha = 1$ (no reflection of the returning electrons), the above equation is satisfied by:

$$\epsilon F(\nu, \theta) = 0, \quad \text{if } 0 < h\nu < w_0 \quad (66)$$

$$\epsilon F(\nu, \theta) = \frac{Ac^2h}{2\pi k^2\nu^2} \left(1 - \frac{w_0}{h\nu}\right), \quad \text{if } w_0 < h\nu < \infty. \quad (67)$$

We observe that if the frequency ν of the electromagnetic radiation is so small that the product $h\nu$ is less than w_0 (which corresponds to the minimal energy required to free a single electron from its bounded state in the material), no photoelectrons will be emitted at all. Only past this value $\epsilon F(\nu, \theta)$ will be different from zero. Moreover, we see that $\epsilon F(\nu, \theta)$ is in fact independent of temperature, just like experiments indicate, so we should rather express it as $\epsilon F(\nu)$. One might possibly argue that the solution to Eq. (65) contained in Eqs. (66)-(67) is contrived in the sense that Eq. (65) has also other solutions without the discontinuity at $\nu_0 = \frac{w_0}{h}$. But this is not true – as Richardson showed, there is no single analytic function $\epsilon F(\nu, \theta)$ that solves the integral equation throughout the interval $\nu \in [0, \infty]$.

Choose now T_ν to be the average kinetic energy of a photoelectron which is emitted from the material due to radiation with frequency ν . The total energy E emitted is given by the integral:

$$E = \frac{c}{4} \int_0^\infty T_\nu \epsilon F(\nu, \theta) E(\nu, \theta) d\nu$$

One can show that the energy streaming towards the material in unit time by virtue of the thermal motion of the external electrons is $2Nk\theta$. If $0 \leq \beta \leq 1$ is the fraction of these electrons that are absorbed, we have in equilibrium:

$$E = 2\beta Nk\theta.$$

By setting $\beta = 1$ (total absorption) and using Eq. (61) for N and Eq. (64), we end up with another integral equation:

$$\frac{2\pi}{c^2} \int_0^\infty T_\nu \epsilon F(\nu, \theta) h\nu^3 e^{-\frac{h\nu}{k\theta}} d\nu = 2\alpha Ak\theta^{3/2} \exp\left(\int \frac{w}{k\theta^2} d\theta\right).$$

With $\alpha = 1$, w approximated as before and $\epsilon F(\nu, \theta)$ given by the solution above, we can find the following expression for T_ν :

$$T_\nu = h\nu - w_0, \quad \text{if } w_0 \leq h\nu < \infty, \quad (68)$$

T_ν having no meaning if $h\nu < w_0$, because then no photoelectrons are emitted. Thus, also here we have derived the correct (from the experimental point of view) formula for the kinetic energy of a photoelectron “without making use of the hypothesis that free radiant-energy exists in the form of “Licht-quanten,” unless this hypothesis implicitly underlies the assumptions: (A) that Planck’s formula radiation is true; (B) that, *ceteris paribus*, the number of electrons emitted is proportional to the intensity of monochromatic radiation” [75]. Of course, we can conveniently *explain* Eq. (68) in terms of electromagnetic radiation consisting of photons, but from a formal point of view the notion of quantized light is not necessary in order to *deduce* this formula. However, we do have to make use of Planck’s results and the constant h which suggest that the energy exchange between light and matter is somehow quantized. Still, this does not prevent us from perceiving light as such as a continuous electromagnetic wave.

Although the form of Eq. (68) with the discontinuity at $\nu = \frac{w_0}{h}$ is not a reason strong enough to fully accept Einstein’s hypothesis, we can in addition consider the principle of the energy conservation in the case of the photoelectric effect. Assume that we use electromagnetic radiation – perceived, to begin with, as a

wave and described classically by Poynting vector \mathbf{S} – to irradiate a material with an area described by vector \mathbf{A} . Assume also that in order to make the material emit a single photoelectron we need supply it energy E_0 (i.e. this is the work function). This energy will be delivered from the radiation to the material after time T given by the equation:

$$\int_0^T dt \int_A \mathbf{S} \cdot d\mathbf{A} = E_0,$$

if we assume that the irradiation started at time $t = 0$. Now, we could experimentally measure T_{min} , the minimum time between the beginning of the irradiation and the emission of the first photoelectron. If we would find $T_{min} > T$, it would show that the radiative energy flows into the metal in a continuous manner and thus the undulatory view of light would be supported²¹. On the other hand, if we would find $T_{min} < T$, we would have to theoretically allow for the situation where the necessary energy E_0 is delivered “immediately” (or at least much quicker than the classical theory allows), and this is most easily explained in the virtue of the corpuscular view, i.e. in the virtue of radiation travelling through space as discrete energy packets.

The experiment in question was conducted by C. E. Tyler [78] who found that $T_{min} < T$. However, his results were partially inconclusive, because in the setup for switching the light beam on and off he had employed an electro-optical shutter which attenuated the beam ca. 200 times instead of shutting it off completely. Davis and Mandel performed another version of Tyler’s experiment where they replaced the electro-optical shutter with a mechanical one that allowed for a full stoppage of the light beam [79]. T was assigned the value of $20 \mu s$. The reasoning based on the undulatory view predicted thus that no photoelectron should be emitted for irradiation times shorter than $20 \mu s$, no more than one photoelectron should be emitted for irradiation times shorter than $40 \mu s$, etc. However, Davis and Mandel found both that $T_{min} < T$ and that the probability distribution $P(n, \tau)$ for emission of n photoelectrons during the irradiation time τ was actually independent of τ (Fig. 8).

These results were taken as a proof for the corpuscular view of light. However, we observe that several loopholes remained. In the first place, the minimal resolution in the experiment was $5 \mu s$, so the experiment did not substantiate the claim that energy transfer was instantaneous. All that could be said with certainty was that this transfer took $5 \mu s$ or less. Secondly, it was conceivable that fluctuations were present in the electromagnetic field on the time scale of $5 \mu s$, and that their intensity was occasionally high enough to excite photoelectrons before the “required” $20 \mu s$ have passed. In other words, one could argue that the short-time ($< 5 \mu s$) average of the energy transmitted by the wave was not necessarily equal to the long-time ($> 5 \mu s$) average. Thirdly, Davis and Mandel postulated that each electron was characterized by the same work function E_0 . This assumption was an idealization, since the material consisted of a very large amount of electrons, so their work functions might somewhat vary. Alternatively one could point out that the authors did not irradiate single and separated electrons having fixed binding energy, but rather a complicated solid-state structure consisting of many electrons and atoms. E_0 was thus an average value.

We see that the basic features of the photoelectric effect do not – as is often dogmatically claimed in textbooks – force upon us the corpuscular view of light, because the well-known formula given by Eq. (68) can be deduced without resorting to that view explicitly. The consideration of the energy conservation law presents us with additional questions, so it would be interesting to repeat Davis and Mandel’s experiment

²¹We should stop here and ask how the continuous flow of energy could be reconciled with the aforementioned quantized energy exchange between light and matter. After all, even if T_{min} is indeed found to be larger than T , Eq. (68) is still valid and the constant h stems from the Planck theory which implicitly postulates *some* kind of energy discretization. However, this discretization could be attributed to the irradiated material alone (i.e. to the discrete excitation of photoelectrons) as the semiclassical model of photodetection demonstrates (see Sect. 5.1.2).

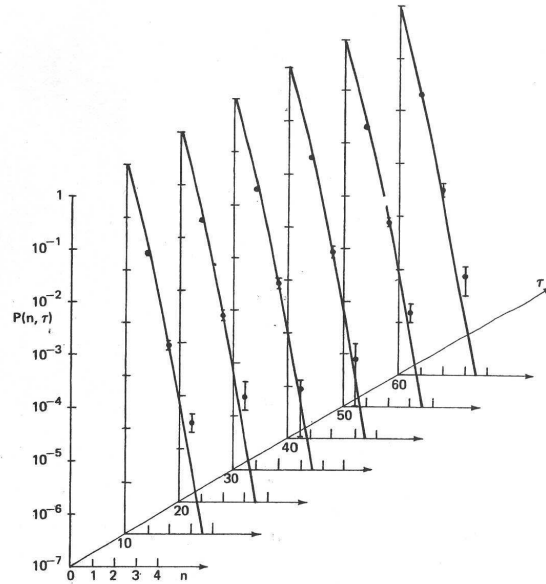


Figure 8: The photoemission probability distribution $P(n, \tau)$ given as a function of the number of photoelectrons n and the irradiation time τ . The plot presents the experimental data of Davis and Mandel [79]. The probability distribution is independent of τ (given in μs). Source: Leonard Mandel [80], reproduced from Davis and Mandel [79].

with other light sources, other materials, larger time resolution and faster shutter.

3.4 The Compton effect

In addition to the photoelectric effect there is another physical phenomenon commonly presented as a proof of the corpuscular nature of light. This phenomenon, called the Compton effect (or the Compton scattering), was discovered in 1923, much later than the photoelectric effect, by Arthur Compton (cf. Ch. 1.3) [33]. The Compton scattering is a type of scattering of electromagnetic waves by matter, where the scattered wave changes its wavelength (or, equivalently, frequency). Usually, the matter under consideration is electrons belonging to an atom. Also, in the first experiments due to Compton the change of wavelength was positive, i.e. the wavelength increased, the frequency decreased and the emerging radiation was less energetic than the incoming radiation. However, inverse Compton scattering with a negative change of wavelength is also possible [81].

Before the Compton effect was discovered, the Thomson model had successfully explained previously known cases of scattering of electromagnetic radiation. It assumed that the incoming electromagnetic field accelerated a charged particle which subsequently re-emitted the radiation in different direction. However, the explanation of Compton's experimental data in the framework of Thomson scattering did not appear to be possible, because of the distinct wavelength change involved. Instead, Compton successfully employed²² the quantum theory of light (combined with relativistic formulas for energy and momentum) in order to explain his results [33].

²²A similar model was developed independently by Peter Debye in the same year [82].

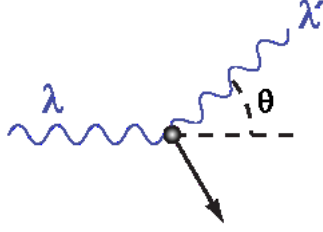


Figure 9: Illustration of the Compton effect: An incoming electromagnetic quasi-monochromatic radiation with wavelength λ interacts with an electron at rest and is scattered to angle θ . Also, the wavelength changes to λ' . The Compton effect can be understood and explained in terms of photons where a single photon collides with the electron in such a way that the total energy and the total momentum of the system is conserved. *Source: http://en.wikipedia.org/wiki/Compton_effect, retrieved on 26.01.2009*

Let us represent the electromagnetic radiation as photons moving through space, and let us consider a single photon. It enters some material, collides with an electron at rest and travels off in the direction given by θ , where θ is the angle between the original direction of the photon propagation and the direction of the photon propagation after the collision²³. Both the photon and the electrons are imagined to be minute particles (or point particles). Let us denote the photon before the collision by γ , the photon after the collision by γ' , the electron before the collision by e and the electron after the collision by e' . The energy and the momentum of the photon before the collision is E_γ and \mathbf{p}_γ , of the electron before the collision E_e and \mathbf{p}_e , and so on (see Fig. 9). Our starting point are the conservation principles for energy and momentum:

$$E_\gamma + E_e = E_{\gamma'} + E_{e'} \quad (69)$$

$$\mathbf{p}_\gamma + \mathbf{p}_e = \mathbf{p}_{\gamma'} + \mathbf{p}_{e'}. \quad (70)$$

In our reference frame the electron is at rest before the collision, so $\mathbf{p}_e = 0$. Eq. (70) can be rewritten as:

$$\mathbf{p}_{e'} = \mathbf{p}_\gamma - \mathbf{p}_{\gamma'}.$$

Squaring both sides gives:

$$p_{e'}^2 = p_\gamma^2 + p_{\gamma'}^2 - 2p_\gamma p_{\gamma'} \cos(\theta),$$

where $p_i \equiv |\mathbf{p}_i|$ for an arbitrary index i . Relativistically, energy and momentum of a photon are related as $E = cp$, but the energy could be also given using Planck's formula, $E = h\nu$, where ν is the frequency of the (quasi-monochromatic) radiation that the photon is a part of. In other words, the photonic momentum could be expressed as $p = \frac{h\nu}{c}$, and from the above formula we get:

$$p_{e'}^2 c^2 = h^2 \nu_\gamma^2 + h^2 \nu_{\gamma'}^2 - 2h^2 \nu_\gamma \nu_{\gamma'} \cos \theta. \quad (71)$$

Let us go back to Eq. (69). As remarked above, the photonic energy can be expressed as $E = h\nu$. On the other hand, the total energy of an electron with momentum p and mass m is given by the relativistical

²³Alternatively one can think of the original photon as being destroyed in the process, and assume that a new photon emerges after the collision at the angle θ . This subtlety makes no difference for our further treatment. Although it is the latter view that is usually employed in the much more general framework of quantum electrodynamics, let us notice that, strictly speaking, the Compton effect by itself does not substantiate it, since there is no time delay involved in the scattering. More precisely, such time delay, if exists, must be less than 0.5 ns [83].

formula $E = \sqrt{p^2c^2 + m^2c^4}$. Remembering that the momentum of the electron before the collision is zero, Eq. (69) gives:

$$h\nu_\gamma + m_e c^2 = h\nu_{\gamma'} + \sqrt{p_e'^2 c^2 + m_e'^2 c^4}.$$

The electron rest mass is invariant, so $m_e = m_e' \equiv m$. We solve the above equation for $p_e'^2 c^2$:

$$\begin{aligned} p_e'^2 c^2 &= \left(h\nu_\gamma + mc^2 - h\nu_{\gamma'} \right)^2 - m^2 c^4 \\ p_e'^2 c^2 &= h^2 \left(\nu_\gamma - \nu_{\gamma'} \right)^2 + 2hmc^2 \left(\nu_\gamma - \nu_{\gamma'} \right) \end{aligned} \quad (72)$$

We have now two independent equations for $p_e'^2 c^2$, Eq. (71) and Eq. (72). Equating and simplifying gives:

$$\begin{aligned} h^2 \nu_\gamma^2 + h^2 \nu_{\gamma'}^2 - 2h^2 \nu_\gamma \nu_{\gamma'} \cos \theta &= h^2 \left(\nu_\gamma - \nu_{\gamma'} \right)^2 + 2hmc^2 \left(\nu_\gamma - \nu_{\gamma'} \right) \\ -2h^2 \nu_\gamma \nu_{\gamma'} \cos \theta &= -2h^2 \nu_\gamma \nu_{\gamma'} + 2hmc^2 \left(\nu_\gamma - \nu_{\gamma'} \right) \\ -\cos \theta &= -1 + \frac{mc^2}{h} \left(\frac{1}{\nu_{\gamma'}} - \frac{1}{\nu_\gamma} \right) \\ \frac{1}{\nu_{\gamma'}} - \frac{1}{\nu_\gamma} &= \frac{h}{mc^2} (1 - \cos \theta), \end{aligned}$$

or, in terms of the wavelength $\lambda = \frac{c}{\nu}$:

$$\Delta\lambda \equiv \lambda_{\gamma'} - \lambda_\gamma = \frac{h}{mc} (1 - \cos \theta) = \frac{2h}{mc} \sin^2 \frac{\theta}{2}. \quad (73)$$

The difference in wavelength $\Delta\lambda$ is sometimes called the Compton shift, and the fraction of physical constants $\frac{h}{mc}$ is defined as the Compton wavelength λ_c with value 2.43×10^{-13} m. Eq. (73) is referred to as the Compton scattering formula. This was the equation that Arthur Compton used to explain his experimental results, as illustrated in Fig. 10.

The description of the Compton scattering in terms of a photon interacting with an electron in a particlelike fashion is indeed elegant, but just like in the case of the photoelectric effect we need inquire if an explanation based on the wave view is admissible. First, let us notice that the Compton model relies on a crucial simplification: the incident radiation is assumed to interact with a single electron only. In reality, however, the situation is not necessarily that idealistic. The material that Compton irradiated in his experiments hardly consisted of well separated electrons. The radiation interacted rather with atomic electrons, i.e. with groups of electrons collected in atoms. Therefore we could ask if it is possible for the radiation (this time perceived solely as a classical electromagnetic wave) to interact collectively with all electrons in a single atom, and produce the effect described by Eq. (73). It was C. V. Raman who followed this line of thought in 1928 [84].

In his model Raman proposed to represent an atom as a spherically symmetric enclosure with Z electrons imprisoned inside. The electrons are moving inside, subjected to the influence of a central field of force, and the probability of finding any specific electron within a volume element is given as some distribution. The atom model is then allowed to interact with a plane monochromatic electromagnetic wave. The electric force associated with the electric component of the wave would accelerate the encountered electrons along the direction of the component, and due to the oscillating nature of the electric force the electrons would

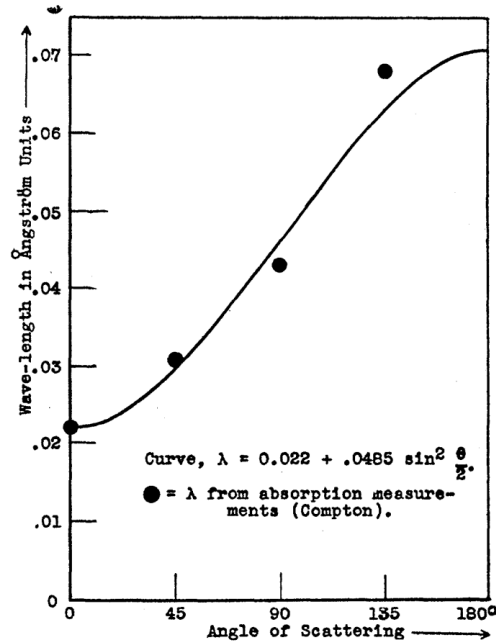


Figure 10: A comparison of Compton's experimental results (points) with the theoretical predictions given by the Compton scattering formula, Eq. (73). The wavelength shift $\Delta\lambda$ is measured as a function of the scattering angle θ . In the experiment X-rays from molybdenum were scattered by graphite. *Source: Arthur Compton [33]*

be made to vibrate. The vibrating electrons would then emit their own radiation (known as secondary radiation) which the observer would perceive as the original electromagnetic wave being scattered. But since the electrons are in different positions and move independently of each other inside the atom, their vibrations would have the same amplitude, but different phases. The total secondary radiation (the superposition of secondary radiations from all electrons) would then have to be calculated using the theory of random interferences, and it is conceivable that it would be characterized by the wavelength shift identical with the Compton shift (possibly some additional constraints and assumptions would have to be employed).

C. V. Raman did not demonstrate directly that this was the case. He argued for it using qualitative arguments, but in the end tried to explain the alteration of the frequency with the Doppler effect applied to a single electron only. However, using the theory of random interferences, Raman showed that the intensity I of the radiation scattered by the atom, and measured at distance r from the atom and at angle θ with the incident radiation, can be divided in two parts, $I = I_1 + I_2$, where:

$$I_1 = \frac{e^4 \sin^2 \theta}{m^2 c^4 r^2} Z^2 F^2$$

$$I_2 = \frac{e^4 \sin^2 \theta}{m^2 c^4 r^2} Z(1 - F^2).$$

with e being the elementary electric charge, m the electron mass and F^2 some particular integral. Despite the formal similarity between I_1 and I_2 , their physical nature is different. I_1 corresponds to the diffracted radiation from the atom, while I_2 represents the statistical average of intensity fluctuations caused by the "random" (in the sense explained above) radiative contributions from the moving electrons. Such fluctuations

are indeed observed during the Compton scattering, and the Raman's model allows to understand their nature. The Compton shift, however, is *not* rigorously deduced from the random interference assumption.

Still, let us see how the Doppler effect can be used to explain the Compton scattering when we limit our attention to an interaction with a single electron. The generalized Doppler shift of light in the relativistic framework is described by the formula:

$$\lambda' = \lambda \frac{1 - \frac{v}{c} \cos \alpha}{\sqrt{1 - \frac{v^2}{c^2}}},$$

where λ is the emitted wavelength (as measured in the rest frame of the emitter), λ' is the observed wavelength, v is the speed of the emitter (as measured by the observer) and α is the angle between the direction of light toward the observer and the velocity of the emitter. We consider now the situation illustrated in Fig. 9. First, we consider the incoming radiation from the vantage point of the electron. We assume that the electron recoils in the direction of propagation of the incident light²⁴, so $\alpha = \pi$ and the above formula simplifies to:

$$\lambda' = \lambda \frac{1 + \frac{v}{c}}{\sqrt{1 - \frac{v^2}{c^2}}}, \quad (74)$$

where λ' is the wavelength received by the electron recoiling with speed v . Now the electron becomes the emitter and scatters the radiation in the direction given by θ (cf. Fig. 9). The scattered wavelength λ'' is measured to be:

$$\lambda'' = \lambda' \frac{1 - \frac{v}{c} \cos \alpha}{\sqrt{1 - \frac{v^2}{c^2}}} = \lambda \frac{\left(1 + \frac{v}{c}\right) \left(1 - \frac{v}{c} \cos \theta\right)}{1 - \frac{v^2}{c^2}}.$$

We calculate the wavelength shift:

$$\Delta\lambda = \lambda'' - \lambda = \lambda \frac{\frac{v}{c}(1 - \cos \theta)}{1 - \frac{v^2}{c^2}} \quad (75)$$

Kidd, Ardini and Anton [85] noticed that Eq. (75) is identical to Eq. (73) if $\lambda \frac{v}{c} (1 - \frac{v}{c})^{-1} = \frac{h}{mc}$ and argued that this similarity has to be something more than a mere coincidence. Their paper was stimulated by an article due to Mellen [86] which had demonstrated how the equivalence between both formulas might be achieved, if one applied the de Broglie hypothesis (see Appendix C). Let us express Eq. (75) in terms of λ' (given by Eq. (74)) which is the wavelength of the incident light as measured from the point of view of the electron:

$$\Delta\lambda = \lambda' \frac{\frac{v}{c}}{\sqrt{1 - \frac{v^2}{c^2}}} (1 - \cos \theta).$$

In the classical model λ' would be the wavelength of the oscillations of the electron as measured in its own reference frame. But if we now assume that this is *also* de Broglie wavelength of the electron when influenced by the external radiation, we get through Eq. (205) (see Appendix C):

$$\Delta\lambda = \frac{h}{p} \times \frac{\frac{v}{c}}{\sqrt{1 - \frac{v^2}{c^2}}} (1 - \cos \theta) = \frac{h}{mc} (1 - \cos \theta),$$

since the momentum p is (relativistically) given as $p = mv \left(1 - \frac{v^2}{c^2}\right)^{-\frac{1}{2}}$ with m being the electron rest mass.

²⁴It can be argued that this will happen on average; furthermore, this is the limiting value for the recoil direction when the Compton wavelength is much greater than the wavelength of the incident radiation, cf. [85].

Thus we obtain again the Compton formula, Eq. (73).

Incorporating de Broglie relationship into the alternative model for Compton scattering demands a proper justification. It would be of course wrong to imagine an electron as a point particle oscillating due to the incident radiation, and then blindly apply Eq. (205) in order to obtain the Compton scattering formula in the end. We are rather forced to think in terms of de Broglie wave from the beginning. In this scheme the electron is not a corpuscle, but a physical object of some kind represented as a wave in accordance with Eqs. (205)-(206). This electron-object interacts with the incident radiation and scatters it, while recoiling itself with speed v . However, in order for the scattering to occur with maximal efficiency, de Broglie wavelength of the electron has to equal the wavelength of the incident radiation. This suggests that some kind of resonance has to take place in the system. Otherwise the intensity of the scattered radiation ought to be reduced, i.e. given a (quasi-)monochromatic incident radiation with wavelength λ_1 , the scattered radiation measured at angle θ should have a maximum at λ_2 (as given by Eq. (73)), but also should be broadened about it. Such effect is indeed observed, but usually it is interpreted solely as Doppler broadening caused by the motion of the target electrons [87].

The Compton effect, together with the photoelectric effect examined in the previous subsection, are today frequently presented as main experimental pillars of the photon theory of light. In the historical context it was the Compton effect – the combination of the experimental data obtained by Compton in 1923 and his derivation of Eq. (73) – that forced many skeptics to accept the photon hypothesis. However, just as in the case of the photoelectric effect, we have seen that it is not necessary to assume the corpuscular nature of light in order to understand the origin of the Compton scattering formula. Specifically, instead of assuming the corpuscular nature of both the incident radiation and the electron, we could as well interpret both the radiation and the electron as waves (the latter as de Broglie wave). The presence of Planck’s constant h in the resulting formula stems then directly from the de Broglie relations, Eqs. (205)-(206). However, it may also suggest in addition that the energy transfer between the radiation and the electron has to be quantized but, again as in the case of the photoelectric effect, the granular structure of light should not be considered to be an inevitable consequence of the energy quantization scheme²⁵.

3.5 The photon anticoincidence effect

The question of the nature of light is intimately connected with the photon anticoincidence effect. Consider a radiative source which sends short, (quasi-)monochromatic outbursts of radiation. Let us assume that we know with certainty that the radiation is not a continuous wave²⁶, but we would like to experimentally determine whether these outburst are inherently discrete (photons) or have a wave packet nature. Now, the fundamental difference between the photons and the wave packets is that the photons, being energy *quanta*,

²⁵Another derivation of Eq. (73) in which the radiation is described as classical electromagnetic waves can be found in Dodd [88]. Dodd does not resort to the idea of de Broglie waves and simply combines the Doppler effect with the assumption that electron energy changes discretely.

²⁶Because if we would measure its intensity directly, we would find long periods of zero intensity separating short periods of non-zero intensity. This is, per definition, the nature of the source employed. In practice performing such a measurement with high accuracy could be difficult due to the various effects associated with the source, the detector and the background radiation. Principally, however, the source could send high-intensity outbursts with large time intervals in between (relatively to the temporal resolution of the detector), and this would minimize the uncertainty of the measurement.

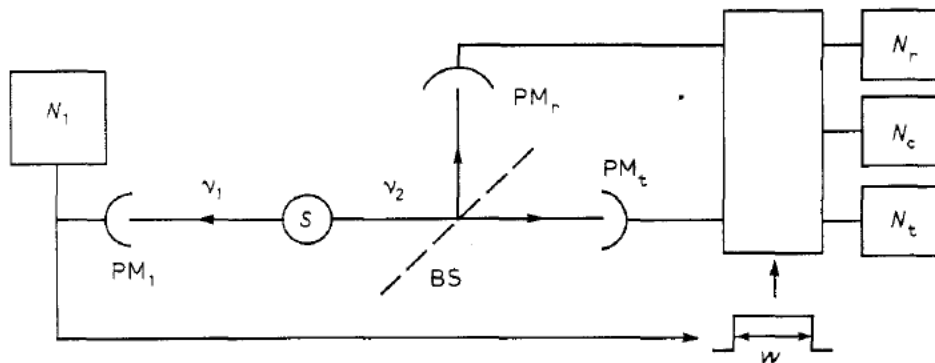


Figure 11: The setup of the triggered photon counting experiment. The source S emits two radiation outbursts in two different directions. The frequencies of the outbursts are ν_1 and ν_2 . The ν_1 -outburst triggers a gate which allows the measurement of the ν_2 -outburst during a short time interval. That second outburst impinges on a beam splitter and is sent further to detectors denoted in the figure by PM_t and PM_r (in the text we just use letters t and r). Source: Grangier et al. [89]

cannot be divided in two (or more) parts in such a way that we might measure all the parts independently²⁷. Wave packets, however, being continuous distributions of energy in space (but of limited spatial extent), can be divided in that way. Thus, we can easily conceive an experiment, where the radiation outbursts are sent through a beam splitter behind which there are placed two detectors. The corpuscular hypothesis implies that their responses should be completely anticoincidental, while the undulatory hypothesis suggests that a very strong correlation will occur.

This simple scheme will be complicated by several difficulties encountered in practice. Arguably the most important of these is the presence of a background noise in detectors which is partially due to photons coming from sources other than the main source, and partially due to the noise of the electronic circuits inside the detectors. The influence of the external noise can be strongly reduced by performing a triggered photon counting experiment. If our radiative source is known to emit two outbursts (almost) simultaneously, then one of them can serve as a trigger for a gate generator enabling the two detectors in view of the second outburst. An experiment of this kind was conducted by Clauser [73], but in the following we will review a similar one due to Grangier, Roger and Aspect [89].

The radiation emitter used here is an atomic beam of calcium which sends pairs of radiation outbursts²⁸ characterized by different frequencies ν_1 and ν_2 [90]. The time interval between the emissions of two outbursts is exponentially distributed. The mean lifetime of the intermediate state of the cascade (after the emission of the first outburst, but before the emission of the second one) is $\tau = 4.7$ ns. The detection of ν_1 -outburst triggers a gate generator for two photomultipliers observing the ν_2 -outburst. The gate duration is $\Delta t = 2\tau = 9.4$ ns. The photomultipliers are placed behind a beam splitter and labelled by letters t and r (for “transmitted” and “reflected”). Fig. 11 shows the experimental setup.

If we assume that the ν_2 -outburst is indivisible (as in the corpuscular model), the beam splitter will send

²⁷The refinement “in such a way that we may measure all the parts independently” is very important. Notice that in the framework of quantum mechanics interference is explained in terms of superposition of two (or more) different photon states. Thus, the standard interpretation of the theory asks us to imagine a photon which has not been really divided, but which still is localized in more than one place at once. However, any measurement performed on it will result in localizing the *whole* photon at *one*, and only one, place. These issues are discussed further in Chapter 9.2.

²⁸As opposed to Grangier et al., we avoid using the term “photon” already at the introductory stage

it either to t or to r ; otherwise, it is possible that the two photomultipliers will register a coincidence. We denote by N_1 the rate of gates (the rate of the photon measurements by the gating detector), and by N_t and N_r the separate (singles') rates of t and r . N_c denotes the rate of coincident measurements by t and r . The experimental results yield the probabilities p_t and p_r for singles' counts during Δt , and the probability p_c for coincidental counts during Δt :

$$p_t = \frac{N_t}{N_1}, \quad p_r = \frac{N_r}{N_1}, \quad p_c = \frac{N_c}{N_1}.$$

Grangier et al. examined the theoretical relation between p_c and the product of p_t and p_r , as given by the classical electromagnetic description and by the quantum-mechanical formalism. The classical theory starts with ascribing to the emitted ν_2 -outbursts a time-dependent intensity $2I(t)$ (the factor 2 is for convenience only). If the beam splitter divides the outburst in two equal parts (with regard to the intensity), the time-averaged intensity of one such part for the n -th gate is:

$$i_n = \frac{1}{\Delta t} \int_{t_n}^{t_n+\Delta t} I(t) dt,$$

where t_n is the time at which the gate is opened. Choosing N_{tot} to be the total number of gates during the experiment, the ensemble average of the time-averaged intensities is:

$$\langle i_n \rangle = \frac{1}{N_{tot}} \sum_{n=1}^{N_{tot}} i_n,$$

and the ensemble average of the time-averaged intensities squared is:

$$\langle i_n^2 \rangle = \frac{1}{N_{tot}} \sum_{n=1}^{N_{tot}} i_n^2$$

The semiclassical model of photodetection (cf. Mandel and Wolf [55], p. 447) yields:

$$p_t = \epsilon_t \Delta t \langle i_n \rangle, \quad p_r = \epsilon_r \Delta t \langle i_n \rangle, \quad p_c = \epsilon_t \epsilon_r (\Delta t)^2 \langle i_n^2 \rangle, \quad (76)$$

with ϵ_t and ϵ_r being the total detection efficiencies of t and r . Now, we have:

$$\langle i_n^2 \rangle \geq \langle i_n \rangle^2$$

due to the Cauchy-Schwarz inequality. Thus we see that:

$$p_c \geq p_t p_r,$$

which means that the probability for a ‘‘real’’ coincidence (i.e. a situation where a divided radiation outburst was registered simultaneously at both detectors) is at least as large as the probability for a ‘‘accidental’’ coincidence (i.e. a situation where two different radiation outbursts were registered). The relation above can be written as:

$$\alpha \equiv \frac{p_c}{p_t p_r} = \frac{N_c N_1}{N_t N_r} \geq 1. \quad (77)$$

This is the prediction of the classical theory, or, more specifically, the prediction based on the four assump-

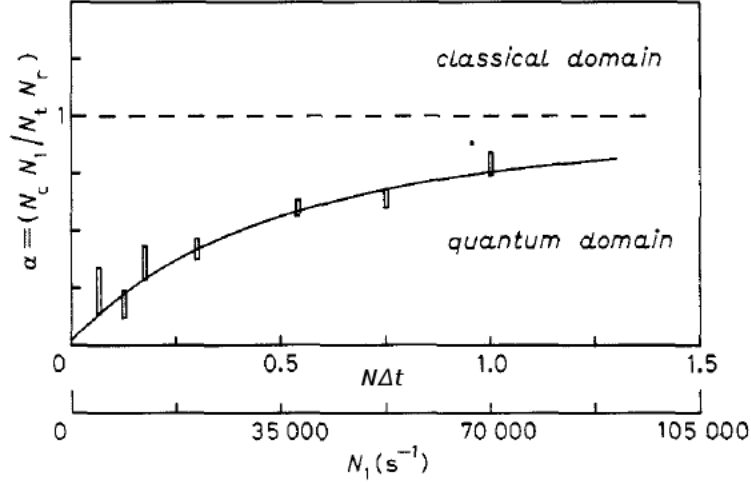


Figure 12: The results of the triggered photon counting experiment. The classical model predicts that the anticoincidence parameter α should be greater than 1. However, it is measured to be less than 1 in accordance with the corpuscular model. Source: Grangier et al. [89]

tions: 1) that the outbursts coming from the radiative source are of a finite spatial extent described by the continuous intensity distribution $2I(t)$; 2) that the beam splitter divides the intensity in two equal parts; 3) that Eqs. (76) hold; 4) and that the detection efficiency can be simply described using the constant parameters ϵ_t and ϵ_r .

A simple quantum-mechanical calculation combined with the postulate that the emitted outbursts are discrete and indivisible, results in an altogether different prediction. We denote with N the emission rate of the cascade (the outbursts in one pair taken together) and with ϵ_1 the total efficiency of the gating detector. We have:

$$\begin{aligned}
 N_1 &= \epsilon_1 N \\
 N_t &= N_1 \epsilon_t [f(\Delta t) + N \Delta t] \\
 N_r &= N_1 \epsilon_r [f(\Delta t) + N \Delta t] \\
 N_c &= N_1 \epsilon_t \epsilon_r [2f(\Delta t) N \Delta t + (N \Delta t)^2].
 \end{aligned}$$

The quantity $f(\Delta t)$ is the product of the factor $1 - e^{-\Delta t/\tau}$ (overlap between the gate and the exponential decay in the cascade) with a factor slightly greater than 1 and related to the angular correlation between ν_1 and ν_2 . The ratio α from Eq. (77) is now:

$$\alpha = \frac{2f(\Delta t)N\Delta t + (N\Delta t)^2}{[f(\Delta t) + N\Delta t]^2} \quad (78)$$

which is obviously smaller than one. This expression tends to 0 when $f(\Delta t) \gg N\Delta t$. We observe that a term $f(\Delta t)^2$ is “missing” from the numerator, and this is due to the fact that in the corpuscular model a single outburst of radiation (now: a photon) can be detected only once, even if it passes through a beam splitter. This is the essential point and the main cause that makes $\alpha < 1$.

Experimental data obtained by Grangier et al. are presented in Fig. 12. The authors could conclude that

their anticoincidence measurements confirmed the corpuscular model; $N\Delta t$ was varied and α was measured to be indeed smaller than one and in accordance with Eq. (78). Their analysis and empirical results are rather solid, but nonetheless there are several loopholes that should be pointed out.

Firstly, we can question the second assumption from the list above: Grangier et al. assumed that the beam splitter either divides the intensity of a single radiation outburst in two equal parts (in the undulatory model) or does not divide it at all (in the corpuscular model). If we now limit our attention to the undulatory model, it is certainly true that the beam splitter works on the 50:50 principle, *if* the time scale involved is long enough, i.e. if we integrate the intensity coming from the two outputs of the beam splitter over sufficiently long time. The question remains whether the 50:50-manner of splitting up the incoming radiation occurs also in the very low intensity regime. If not, then the derivation of Eq. (77) would be incorrect. Shortcomings of the standard beam splitter models will be discussed in Section 5.2.3; we notice that a classical model improved in this respect could account for the observation of $\alpha < 1$.

Secondly, Panarella [71] pointed out that the quantum efficiency of the detectors used (which was not explicitly stated) had to be limited, so out of N of the (postulated) photons impinging on the detector only a minor fraction could lead to an emission of photoelectrons. The remaining photons went altogether unnoticed by the apparatus, so any information about their arrangement in space (whether they were indeed isolated in space, as the authors assumed, or rather grouped together). A model with “photon clumps”, also due to Panarella, will be discussed in Chapter 9.1.

Thirdly, it should be noticed that the analysis due to Grangier et al. was done more carefully in the case of the corpuscular model than in the case of the undulatory one, since only in the first one they consider the overlap between the gate and the exponential decay and the angular correlation between ν_1 and ν_2 .

Finally (but this argument is by no means least important) the experiment involved a nonclassical light source. A similar anticoincidence effect would not be observed in the case of a classical light source like laser, as we will see in Chapter 7.1, and differences between classical and nonclassical light sources in the context of photocounting measurement will be discussed in Sect. 5.1.4. Thus we have to keep in mind that the corpuscular behaviour exhibited in the anticoincidence experiment was demonstrated neither for thermal light source nor for coherent light source.

4 Classical description of optical coherence and correlations

In the following two chapters we will present the theoretical background for our preliminary measurements in Chapter 6 and experimental illustration of the wave-particle duality in Chapter 7. We begin by elaborating on the concept of optical coherence and optical correlations, the inclusion of which is necessary in any discussion of the interference phenomena. For this reason the term “coherence” had to be used already in Chapter 3.2 in our treatment of the Michelson interferometer, but there we have avoided definitions and detailed considerations. This will be made up for in the present chapter which is based on Saleh and Teich [48] (Chapter 11), Loudon [52] (Chapter 3) and Mandel and Wolf [55] (Chapters 2, 4 and 12).

The examination of optical coherence can be conducted both on the classical and the quantum-mechanical grounds. We will use the first approach, but we will also mention the important result implied by the quantum theory that is absent in the classical one (final paragraphs of Ch. 4.3). More emphasis is put on the classical description, because it seems to be the most natural way of describing conditions under which interference occurs. However, the quantum model seems to be indispensable in specific experimental situations where so-called antibunching phenomena arise, and we will come back to this issue in Sect. 5.1.4, after we have reviewed different photodetection models.

This chapter starts with the presentation of the complex analytic signal, a commonly used representation of the optical field (Ch. 4.1). The concept of optical coherence is introduced in the next two sections, first in a rather qualitative way (Ch. 4.2), and then rigorously, using the so-called coherence degrees (Ch. 4.3). As illustrations we use results from a numerical simulation of the thermal emission of light. The theory of optical coherence is then applied to interferometry experiments, and a simple formula describing the interference fringes emerges (Ch. 4.4).

4.1 The complex analytic signal

When working with optical fields it is desirable to find a convenient mathematical representation of the physically measurable signals. Since the electric field \mathbf{E} and the magnetic field \mathbf{B} are related through Maxwell’s equations, in far-field approximations limiting our attention to only one of them, say \mathbf{E} , is enough. Furthermore, to simplify the analysis, one frequently works with a single component of the electric field. Thus the optical field is considered to be a scalar wavefield characterized by that component, and it can be represented as the so-called complex analytic signal. A full vectorial treatment is also possible, but will be unnecessary

for us. We present the concept of the complex analytic signal in the scalar framework, and our description is based on Chapter 3.1 of Mandel and Wolf [55], but some calculational details have been changed. The formalism of the complex analytic signal as applied to vector wavefields is to be found in *ibid.*, Chapter 6.

Assume that our real signal, $x(t)$, is one of the components of the electric field. The real signal $x(t)$ can be expressed in terms of its Fourier transform $\tilde{x}(\omega)$:

$$x(t) = \frac{1}{\sqrt{2\pi}} \int_{-\infty}^{\infty} \tilde{x}(\omega) e^{-i\omega t} d\omega \quad (79)$$

where the Fourier transform (alternatively called the spectral amplitude) is given as:

$$\tilde{x}(\omega) = \frac{1}{\sqrt{2\pi}} \int_{-\infty}^{\infty} x(t) e^{i\omega t} dt. \quad (80)$$

The frequency variable ω , however, does not need to run from $-\infty$ to $+\infty$, because information about $\tilde{x}(\omega < 0)$ is already contained in $\tilde{x}(\omega > 0)$ (or vice versa). This is due to the fact that $x(t)$ is real, because with $x^*(t) = x(t)$ we have:

$$\tilde{x}(-\omega) = \frac{1}{\sqrt{2\pi}} \int_{-\infty}^{\infty} x(t) e^{-i\omega t} dt = \frac{1}{\sqrt{2\pi}} \int_{-\infty}^{\infty} x^*(t) e^{-i\omega t} dt = \tilde{x}^*(\omega).$$

This motivates the introduction of a new function $z(t)$ defined again as the Fourier integral. This function is the complex analytic signal associated with $x(t)$:

$$z(t) \equiv \frac{1}{\sqrt{2\pi}} \int_{-\infty}^{\infty} \tilde{z}(\omega) e^{-i\omega t} d\omega \quad (81)$$

where:

$$\tilde{z}(\omega) \equiv \begin{cases} \tilde{x}(\omega), & \omega \geq 0 \\ 0, & \omega < 0, \end{cases}$$

so $z(t)$ can be written as:

$$z(t) = \frac{1}{\sqrt{2\pi}} \int_0^{\infty} \tilde{x}(\omega) e^{-i\omega t} d\omega. \quad (82)$$

In other words we have to set to zero the negative frequencies in the Fourier expression for $x(t)$, Eq. (79). However, despite the formal similarity between $x(t)$ and $z(t)$, the latter is generally not real, because:

$$z^*(t) = \frac{1}{\sqrt{2\pi}} \int_0^{\infty} \tilde{x}^*(\omega) e^{i\omega t} d\omega = \frac{1}{\sqrt{2\pi}} \int_0^{\infty} \tilde{x}(-\omega) e^{i\omega t} d\omega = \frac{1}{\sqrt{2\pi}} \int_{-\infty}^0 \tilde{x}(\omega) e^{-i\omega t} d\omega \neq z(t).$$

On the other hand this gives us a simple relation between $x(t)$ and its complex analytic signal:

$$x(t) = \frac{1}{\sqrt{2\pi}} \int_{-\infty}^{\infty} \tilde{x}(\omega) e^{-i\omega t} d\omega = \frac{1}{\sqrt{2\pi}} \left(\int_{-\infty}^0 + \int_0^{\infty} \right) \tilde{x}(\omega) e^{-i\omega t} d\omega = z(t) + z^*(t) = 2\Re[z(t)]. \quad (83)$$

If we define a function $y(t)$ to be twice the imaginary part of the complex analytic signal, we may write:

$$z(t) = \frac{1}{2}[x(t) + iy(t)]. \quad (84)$$

Several relations between $x(t)$ and $y(t)$ could be demonstrated, but they are of no interest to us. Let us consider a simple example instead. Assume that the real signal is a monochromatic cosinusoidal wave of amplitude A , frequency ω_0 and phase θ , $x(t) \equiv A \cos(\omega_0 t + \theta) = \frac{A}{2} (e^{i(\omega_0 t + \theta)} + e^{-i(\omega_0 t + \theta)})$. Using Eq. (80) we find:

$$\tilde{x}(\omega) = \frac{A\sqrt{2\pi}}{2} [e^{i\theta} \delta(\omega + \omega_0) + e^{-i\theta} \delta(\omega - \omega_0)],$$

where $\delta(x)$ is the Dirac-delta function. Putting this into Eq. (82) produces $z(t)$:

$$z(t) = \frac{A}{2} e^{-i\theta} e^{-i\omega_0 t} = \frac{A}{2} e^{-i(\omega_0 t + \theta)} = \frac{A}{2} \cos(\omega_0 t + \theta) - \frac{iA}{2} \sin(\omega_0 t + \theta), \quad (85)$$

so Eq. (83) can be readily verified, and we see that in this case $y(t) = -A \sin(\omega_0 t + \theta)$.

The main reason for dealing with the complex analytic signal is that it allows us to elegantly accommodate the fluctuations of the real signal. Consider a signal $x(t)$ whose spectrum contains several frequencies ω centered around ω_0 . The width of the frequency range is defined as Δ , so $|\omega| \in [\omega_0 - \frac{1}{2}\Delta, \omega_0 + \frac{1}{2}\Delta]$. If Δ is much smaller than ω_0 , then the signal is quasi-monochromatic. Thus $x(t)$ resembles a simple wave, but with amplitude and phase that are slowly changing in time. These changes may be perceived as fluctuations of a cosinusoidal wave, and we can write:

$$x(t) = A(t) \cos[\omega_0 t + \theta(t)], \quad (86)$$

with $A(t)$ positive. Now, given a quasi-monochromatic signal $x(t)$, there are many different pairs of the functions $A(t)$ and $\theta(t)$ that would satisfy the above equation. However, we want the associated complex analytic signal to look similar to that from Eq. (85):

$$z(t) = \frac{A(t)}{2} e^{-i[\omega_0 t + \theta(t)]}, \quad (87)$$

and that puts a restriction on the choice of $A(t)$ and $\theta(t)$:

$$\begin{aligned} A(t) &= 2|z(t)| \\ \theta(t) &= \phi(t) - \omega_0 t, \end{aligned}$$

where $\phi(t) = \arccos \frac{x(t)}{2|z(t)|}$. We see that once the complex analytic signal has been determined, the time-dependent amplitude and the phase of the real signal follow in a straight-forward manner.

We insert the complex representation of the quasi-monochromatic signal, Eq. (87), into the original

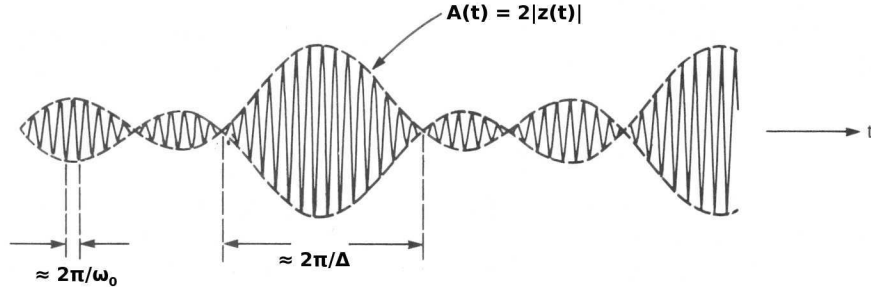


Figure 13: Illustration of the (real) envelope $A(t)$ of a quasi-monochromatic signal $x(t)$. $x(t)$ is the rapidly oscillating function inside the envelope. We notice that the characteristic time scale of $A(t)$ is approximately equal to the inverse bandwidth $\frac{2\pi}{\Delta}$ which is much less than the oscillation period $\frac{2\pi}{\omega_0}$. Source: Mandel and Wolf [55]

expression for $z(t)$, Eq. (81):

$$\begin{aligned}
\frac{A(t)}{2} e^{-i[\omega_0 t + \theta(t)]} &= \frac{1}{\sqrt{2\pi}} \int_{-\infty}^{\infty} \tilde{z}(\omega) e^{-i\omega t} d\omega \\
\frac{A(t)}{2} e^{-i\theta(t)} &= \frac{1}{\sqrt{2\pi}} \int_{-\infty}^{\infty} \tilde{z}(\omega) e^{-i(\omega - \omega_0)t} d\omega \\
\frac{A(t)}{2} e^{-i\theta(t)} &= \frac{1}{\sqrt{2\pi}} \int_{-\infty}^{\infty} \tilde{z}(\nu + \omega_0) e^{-i\nu t} d\nu \\
\frac{A(t)}{2} e^{-i\theta(t)} &= \frac{1}{\sqrt{2\pi}} \int_{-\infty}^{\infty} \zeta(\nu) e^{-i\nu t} d\nu
\end{aligned} \tag{88}$$

with the substitution $\nu \equiv \omega - \omega_0$, and with the definition of new spectral amplitude $\zeta(\nu) \equiv \tilde{z}(\nu + \omega_0)$. This represents a simple frequency shift, and since $\tilde{x}(\omega)$ is supposed to be negligible outside the range $[\omega_0 - \frac{1}{2}\Delta, \omega_0 + \frac{1}{2}\Delta]$, we see that after the substitution the new spectrum is effectively confined to $[-\frac{1}{2}\Delta, \frac{1}{2}\Delta]$. In other words, $A(t)$ and $\theta(t)$ need vary slowly over any time interval τ much smaller than the inverse bandwidth $\frac{2\pi}{\Delta}$. This interval, however, may still be much larger than the inverse of the central frequency, $\frac{2\pi}{\omega_0}$. This is illustrated in Fig. 4.

Going back to Eq. (87), we see that $2z(t)e^{i\omega_0 t} = A(t)e^{-i\theta(t)}$ is the complex envelope of the quasi-monochromatic signal $x(t)$. The envelope modulates the signal whose basic frequency is ω_0 . It is natural to expect that the bandwidth of the time-dependent amplitude of the envelope $A(t)$ is somehow related to the bandwidth of the signal. The theorem due to Dugundji [91] quantifies this relation. We quote it without reproducing the proof: If the spectral amplitude of $x(t)$ is *strictly* confined to the interval $[\omega_0 - \frac{1}{2}\Delta, \omega_0 + \frac{1}{2}\Delta]$, then the squared amplitude $A^2(t)$ is bandlimited to the interval $[-\Delta, \Delta]$.

4.2 Describing optical coherence

A sinusoidal plane wave (or its one-dimensional equivalent) extending uniformly over all space from $x, y, z = -\infty$ to $x, y, z = \infty$ is a mathematical idealization which does not have any counterpart in the physical world. The essential concept of optical coherence arises when we start to consider more realistic forms of

the undulatory propagation of the electromagnetic field. We initiate the discussion by asking how light is generated in an ordinary, everyday thermal light source like an incandescent light bulb or the Sun.

A thermal source consists of a very huge amount of atoms and electrons in vibrational and translatory motion. They constantly collide with each other and get excited to higher energy levels. This thermal energy is supplied by some mechanism specific for the given light source – in case of a light bulb it is electric current delivered by an external circuit, and in case of the Sun it is the fusion process ongoing in the core of the Sun. Each excitation is followed by a rapid de-excitation where the excess energy is emitted in the form of electromagnetic radiation. Now, depending on the view on the nature of light that we adopt, we can either think in terms of photons being sent out from an atom after each de-excitation (the corpuscular model), or in terms of undulatory outbursts of radiation (the wave model). In order to discuss the classical optical coherence, we have to make use of the latter picture.

Obviously the excitations, de-excitations and corresponding emissions are random processes. We choose to model each radiation outburst starting at t_0 as a one-dimensional wave packet characterized by amplitude A , damping time τ , angular frequency ω , wave vector \mathbf{k} and phase θ . Then a single component of the electric field of the wave packet can be described by the function:

$$E_{WP}(\mathbf{r}, t) = \begin{cases} 0 & t < t_0 \\ Ae^{-(t-t_0)/\tau} \cos[\omega(t-t_0) - \mathbf{k} \cdot \mathbf{r} + \theta] & t \geq t_0 \end{cases} \quad (89)$$

For simplicity, let us suppose that the radiation is spherically symmetrical and that we measure it at some fixed point in space. Thus the scalar product $\mathbf{k} \cdot \mathbf{r}$ becomes a constant and may be incorporated into θ . E_{WP} will then be a function of time only.

We are unable to predict when each emission will take place, so the total number of the wave packets in a given time interval is a random variable. It is reasonable to assume that each wave packet will somewhat differ in form, so A , τ , ω and θ are random as well, although their deviations from some mean values are not necessarily large (except for the phase which is uniformly distributed over the interval $[0, 2\pi]$)²⁹. If we now superpose contributions from all atoms, the resulting total electric field, and thus the field intensity (given as the electric field squared), will fluctuate randomly. The fluctuations can be made subject to a quantitative analysis, and this will be done in the next section. First, we would like to illustrate them qualitatively through a numerical computation.

We use a time array consisting of 100.000 elements, where each element corresponds to an arbitrarily chosen time unit. The time scale will be kept dimensionless, because we are not aiming for a precise simulation of some specific thermal source. There is 0.05 probability that an emission will occur during any single time unit, and zero probability that two or more emissions will occur. Each emission gives rise to a wave packet described by Eq. (89). A is uniformly distributed over the interval $[0.9, 1.1]$, where we again operate with completely arbitrary units for the amplitude. The damping time τ is uniformly distributed over the interval $[900, 1100]$. The oscillation period T of a single wave packet is fixed, $T = 100$, so ω is constant and approximately equal to 0.0628.

Fig. 14-17 presents the results of the simulation. In Fig. 14 we see how a single wave packet from our

²⁹We stress that the model chosen by us is one of several possible. Loudon (Chapter 3.1 in [52]) made use of another one. He considered a single atom, and called t_1 the mean time between a de-excitation and the subsequent excitation, and t_2 the mean time during which the atom stays in the excited level. If both t_1 and t_2 were much shorter than $T \equiv \frac{2\pi}{\omega}$, which is the oscillation period of an outburst, then one could imagine that each atom emits a continuous wave of radiation. This wave, however, changed its phase abruptly and randomly at random times.

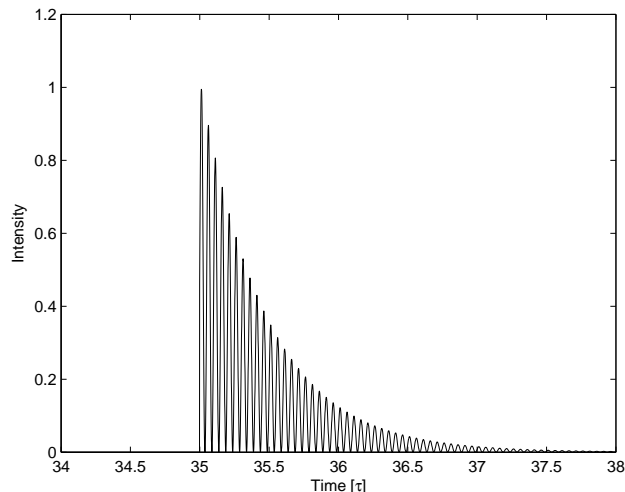


Figure 14: An intensity distribution of a single wave packet from our simulation. Such wave packet is assumed to represent the radiation outburst emitted by an atom due to its excitation and the subsequent de-excitation. The start amplitude, the phase and the damping time are chosen randomly for each packet, but all of them are of the same form as the one depicted in the figure. Notice that the time is given in the units of τ where τ is the damping time. The same time scale is employed in the next three figures.

model looks like. Fig. 15 shows the development of the intensity over the whole time interval (the so-called time series). It is highly irregular, but it is also characterized by a presence of easily discernible “spikes”. In Fig. 16 we zoom in a part of the previous figure. Now the rapid oscillations corresponding to the wave packet frequency ω are visible. More importantly, we observe that during short time intervals (but still larger than T), the intensity develops in at least partially predictable way, rising and then declining again. One such interval has been marked with a double arrow labelled as τ_c which stands for coherence time, and the name has been chosen with the foresight of the further results.

Qualitatively speaking, the coherence time represents the time interval over which the evolution of an electromagnetic wave is regular. Obviously a plane electromagnetic wave has infinite coherence time. On the other hand, even a highly erratic radiation pattern, as the one modelled in Fig. 15-16, has a coherence time that is small, but finite. The coherence time can be quantified in at least two different ways, and we will examine the rigorous mathematical definitions in the next section.

Finally, Fig. 17 presents the same part of the plot as Fig. 16, but with the intensity cycle-averaged. In this way we have removed the basic oscillatory pattern, but the plot is now less smooth. This is because the time resolution in our simulation was not very large to begin with. Fig. 17 is included for the sake of graphical completeness, since sometimes graphs like Fig. 15 or 16 are presented with the intensity cycle-averaged.

The discussion of the intensity fluctuations of a thermal source has allowed us to introduce the concept of coherence time in a natural way. In fact, the same concept can be defined very simply on the phenomenological grounds as well. Consider an interferometry experiment of the Michelson type as presented in Chapter 3.2. Assume that the light source emits quasi-monochromatic radiation of bandwidth Δf , and that the time delay introduced between the two partial beams is equal to Δt . Now, it is a well-known experimental fact (Mandel

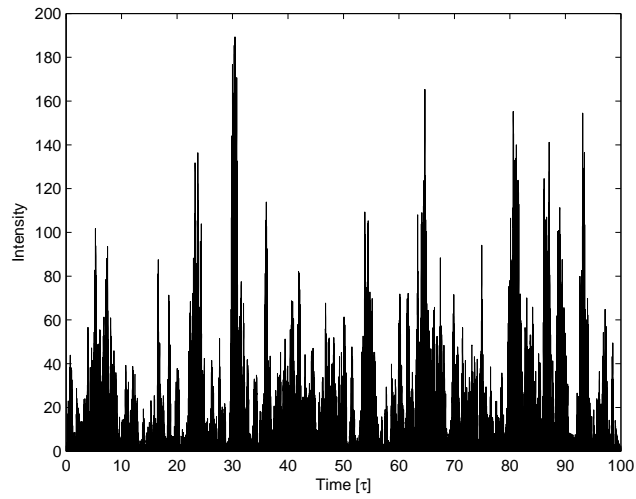


Figure 15: The total time duration of our simulation is 100τ . The resultant field is the superposition of all wave packets such as the one from the previous figure. These wave packets are distributed randomly in time, so the resulting intensity distribution is highly erratic. However, some regular features can be recognized on short time scales, as the next figure shows.

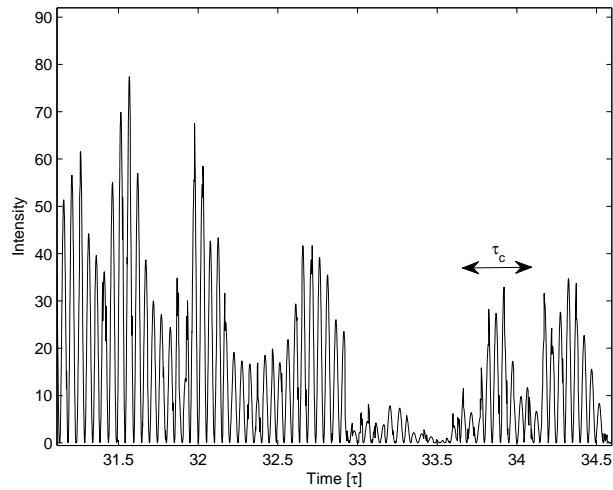


Figure 16: A magnification of a part of the previous figure. Irregularities are still present, but now the basic oscillatory pattern is visible, and we observe that the distribution consists of regular regions where the intensity first rises, and then declines in a more or less predictable way. One of these regions are marked with a double arrow. Its width is approximately equal to the coherence time τ_c of the distribution.

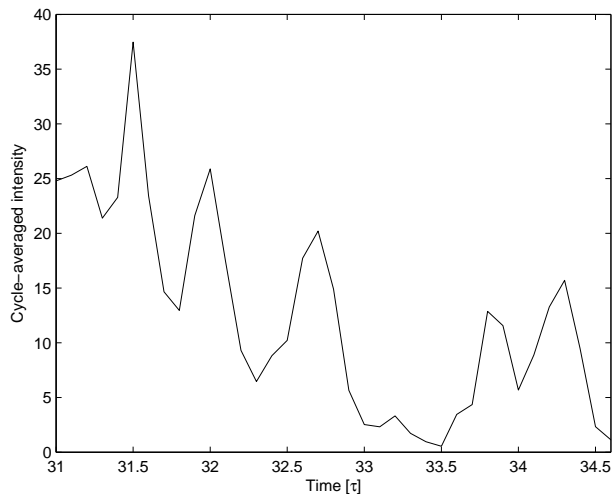


Figure 17: A magnification of the same part of Fig. 15 as showed in Fig. 16, but with the intensity cycle-averaged. Cycle-averaging makes the plot less smooth (because the time resolution used in our simulation was relatively small), but now the “regular regions” of the distribution mentioned in the caption of the previous figure are more visible.

and Wolf [55], p. 148) that the interference fringes will occur on the screen if

$$\Delta t \lesssim \frac{1}{\Delta f}. \quad (90)$$

Thus, at least in this context, we can try to define coherence time as

$$\tau_c \equiv \frac{1}{\Delta f}. \quad (91)$$

Now we have to verify whether the coherence time of Eq. (91) is approximately equal to the coherence time defined in Fig. 16. The bandwidth in our simulation was not explicitly given in the input parameters, because, even though the wave packets were modelled using the constant angular frequency ω , the spectrum of such a spatially localized wave packet consists of many different frequencies. Furthermore, in the simulation a large amount of wave packets was superposed, and it was the resultant intensity distribution that was being analyzed.

Given these considerations, let us simply perform a numerical Fourier transform of the intensity distribution from Fig. 15. The spectrum is presented in Fig. 18. The right peak is centered at twice the basic frequency $\frac{\omega}{2\pi}$ of the underlying wave packets (the factor two is due to the squaring of the electric field in order to obtain the intensity distribution), and its width corresponds to the bandwidth of our field. After magnifying the original figure we estimate it as 0.002. The inverse of that is 500 time units, or 0.5τ . This is approximately the coherence time as seen in Fig. 16. Thus, there is a clear agreement between definition in Eq. (91) and our evaluation of the intensity distribution plot.

It is easy to see how the condition given by Eq. (90) arises in an interferometric context. The original beam is not monochromatic, so the two partial beams (perceived as electromagnetic waves) consist of many frequency components. Each frequency component corresponds to a particular periodic distribution of the electromagnetic field in space. In order for the interference fringes to occur, the different distributions must

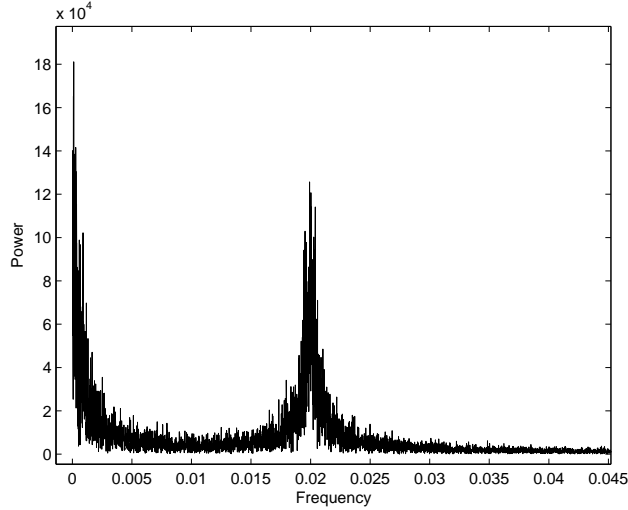


Figure 18: The Fourier spectrum of the intensity distribution from Fig. 16. The frequency along the x-axis is given in units being the inverse of the arbitrary units used in the simulation and in Fig. 14-17. The right peak is centered at twice the basic oscillatory frequency, i.e. at $\frac{\omega}{\pi}$ (the basic oscillatory frequency corresponded to the oscillations of the electric field while now we consider the intensity oscillations). Its width corresponds to the bandwidth Δf from Eq. (91) that gives the coherence time.

be superposed. The time delay between them, however, cannot be too large, because then the maxima and minima belonging to different frequency components will get out of step with each other, and no distinct interference pattern will result. Now, the inverse of the bandwidth gives us a natural measure of the time interval over which the field evolves approximately like a regular plane wave³⁰. If the time delay is larger, we end up with adding together seemingly uncorrelated field disturbances, and no interference fringes will emerge. The term “uncorrelated” has been used here in a rather loose way, but we will see in the next section how its precise quantification may serve to define the coherence time in a rigorous manner.

The time delay Δt from Eq. (90) corresponds to the path difference $\Delta l = c\Delta t$ where c is the speed of light in the medium considered. Thus it seems natural to define the longitudinal coherence length³¹ $\ell_c^{(l)}$ as:

$$\ell_c^{(l)} = c\tau_c = \frac{c}{\Delta f} = \frac{\lambda^2}{\Delta\lambda} \quad (92)$$

where λ is the central wavelength of the radiation, and $\Delta\lambda$ is the wavelength bandwidth, calculated from $f = \frac{c}{\lambda} \Rightarrow df = \frac{-c}{\lambda^2} d\lambda$ with the minus suppressed.

In similar vein we can consider the transverse coherence length, but now it is necessary to extend our discussion of interference to a three-dimensional setup. Consider Young’s interference experiment as presented in Fig. 19. A square-shaped thermal source of transverse length Δs is placed in plane M . In plane N there is a screen with two pinholes called P_1 and P_2 . Their positions are symmetrical with respect to the axial

³⁰To substantiate this postulate, consider two extreme cases: a simple sinusoidal wave and a single Dirac-delta spike. The sinusoidal wave is per definition characterized by a single frequency, so $\Delta f = 0$ and $\Delta t = \infty$. On the other hand, the spike is obtained by superposing sinusoidal waves of all possible frequencies, so $\Delta f = \infty$ and $\Delta t = 0$. These results are of course in full agreement with what can be deduced by inspection from the plots of the wave and the spike. The first one evolves as a sinusoidal wave from $t = -\infty$ to $t = \infty$ (per definition), and the spike does not resemble a sinusoidal wave even at very short Δt .

³¹It may be also called temporal coherence length, but we will consistently use the adjective “longitudinal”, as opposed to “transverse coherence length”, see below.

point Q . The distance between the two planes is $R \gg \Delta s$. The second screen is placed behind the first one, in plane O , and on that screen interference fringes might be possibly formed. Their appearance is a manifestation of the so-called spatial coherence between light beams reaching some point on the screen O from the pinholes.

Consider a vertical boundary point of the source, say, on its upper edge. Call d_1 the distance from the source point to P_1 and call d_2 the distance from the source point to P_2 . Then d_2 is obviously longer than d_1 , the difference being $d_2 - d_1 \equiv \Delta d$. In order for the interference fringes to form on the screen O , Δd should be shorter than a central wavelength of the radiation, λ (which is assumed much shorter than Δs). The reason is that if the radiation is to exhibit any central wavelength, then its character must remain the same during spatial intervals that are of magnitude λ (see Ch. 4.1). Since the pinholes, as seen from the screen O , act as point sources, the fields emitted by (or transmitted through) them must have similar spatial pattern in order for the interference pattern to emerge.

A simple geometric argument shows that the condition $\Delta d \lesssim \lambda$ translates to:

$$\Delta\theta \lesssim \frac{\lambda}{2\Delta s}, \quad (93)$$

where $\Delta\theta$ is the angle between the optical axis and the line joining the (center of the) source and one of the pinholes. If $\Delta\theta$ is small, then we can approximate the distance $\overline{QP_1} = R \tan(\Delta\theta)$ as $R\Delta\theta$. Thus, in order to observe fringes in O , the pinholes must be situated within an area A_c of N centered at Q and given approximately as

$$A_c \approx (2R\Delta\theta)^2 \approx \frac{R^2\lambda^2}{(\Delta s)^2}. \quad (94)$$

A_c is called the coherence area (hence the subscript c), and its square root may be called transverse coherence length $\ell_c^{(t)}$:

$$\ell_c^{(t)} \approx \frac{\sqrt{R}\lambda}{\Delta s}. \quad (95)$$

We see that a new quantity of dimension volume can be easily obtained by multiplying the longitudinal coherence length $\ell_c^{(l)}$ with the coherence area A_c :

$$V_c \equiv \ell_c^{(l)} A_c. \quad (96)$$

The subscript c announces that we are going to call V_c the coherence volume. If the optical field considered is quasi-monochromatic and emitted from a thermal source, then we can substitute for $\ell_c^{(l)}$ from Eq. (92) and for A_c from (94). Eq. (96) yields then:

$$V_c \approx \frac{R^2\lambda^4}{\Delta\lambda(\Delta s)^2}, \quad (97)$$

where the symbols λ , $\Delta\lambda$ and Δs have the same meaning as before, and R is simply the distance from the source to some arbitrary point in space around which we wish to calculate the coherence volume (but again assuming that $R \gg \Delta s \gg \lambda$).

The concept of coherence volume has an interesting meaning in the context of quantum mechanics and the corpuscular theory of light. Using the Heisenberg uncertainty relation (cf. Appendix B) and de Broglie's wavelength formula (cf. Eq. (205), Appendix C) one can show that in a spatial region of volume V_c the photons belonging to the optical field are intrinsically indistinguishable from each other (Mandel and Wolf

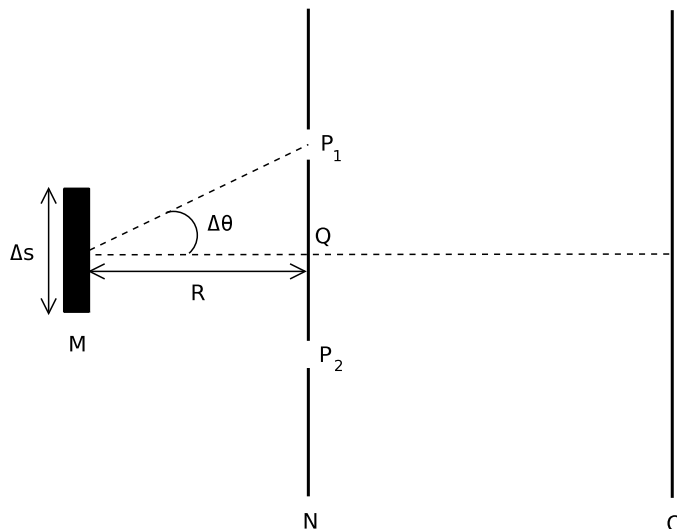


Figure 19: A schematic illustration of Young's interferometry experiment used to introduce the concepts of coherence area and transverse coherence length, cf. Eq. (94) and Eq. (95). The setup is three-dimensional, but the figure presents its two-dimensional cross-section for the sake of simplicity.

[55], pp. 156-159).

4.3 Quantifying optical coherence

In the previous section we have described the concept of optical coherence qualitatively using a numerical model of the thermal emission of light. The coherence time, the transverse coherence length and the coherence area have also been defined on the phenomenological grounds, i.e. they have been related to the conditions under which the interference pattern forms. In that context we have seen that coherence is somehow related to correlations of the random light fluctuations. A closer examination of these correlations will now allow us to present a theoretical definition of the coherence time.

We consider again the situation where we measure, from some fixed point in space, the intensity of light emitted from a thermal source. The time duration of each measurement is T , and we perform N such measurements where N is a very large number (ideally it should tend to infinity). Together they form an ensemble, and the result of each measurement is similar to the distribution depicted in Fig. 15. Although we observe an random process, we assume that it is ergodic, i.e. that the character of fluctuations of the optical field in each realization is the same. Also, we assume the process to be statistically stationary which means that the statistical averages of the measurable quantities related to the optical field are invariant in time (even if they instantaneous values fluctuate wildly).

The intensity is perhaps the most obvious example of such a quantity. We represent the i -th realization of optical field by its associated complex analytic signal $z^{(i)}(\mathbf{r}, t)$ (see Ch. 4.1), and we call the instantaneous

intensity of the i -th realization $I^{(i)}(\mathbf{r}, t)$. The intensity averaged over the ensemble, $I(\mathbf{r})$, is then given as:

$$I(\mathbf{r}) = \frac{1}{N} \sum_{i=1}^N I^{(i)}(\mathbf{r}, t) = \frac{1}{N} \sum_{i=1}^N \left| z^{(i)}(\mathbf{r}, t) \right|^2 \equiv \langle |z(\mathbf{r}, t)|^2 \rangle.$$

It is customary to use brackets $\langle \dots \rangle$ to denote the ensemble average. The time variable disappears, because due to the statistical stationarity the average will be time-independent per definition. However, when both the ergodicity and stationarity assumptions hold, the averaging can be performed using a single realization only. T must then be long enough, i.e. much longer than any characteristic time scale of the fluctuations involved. Ideally it should tend to infinity, just as N above. Thus we have:

$$I(\mathbf{r}) = \langle |z(\mathbf{r}, t)|^2 \rangle = \lim_{T \rightarrow \infty} \frac{1}{T} \int_{-T/2}^{T/2} |z(\mathbf{r}, t)|^2 dt.$$

The formal proof that under the described circumstances the ensemble average equals the time average can be found, for instance, in Mandel and Wolf [55] (Sect. 2.2.2).

The characteristic time scale of the fluctuations involved in a random process is a central parameter describing the process. We can quantify it by introducing a function which describes correlations between two arbitrary temporal points of the optical field. This function, $\Gamma(t_1, t_2)$, is called the autocorrelation function, the two-time correlation function or the temporal coherence function. We will use the first name. The autocorrelation is defined as:

$$\Gamma(t_1, t_2) \equiv \langle z^*(t_1)z(t_2) \rangle$$

Both Γ and z depend implicitly on the position in space, but since we assume that all measurements are performed in the same spatial point, the variable \mathbf{r} has now been omitted. Furthermore, since the processes considered are statistically stationary, the autocorrelation function depends on its time arguments only through the difference between them. Thus we can express it as:

$$\Gamma(\Delta t) = \langle z^*(t)z(t + \Delta t) \rangle, \quad (98)$$

where Δt is the time delay and t can be chosen arbitrarily. We notice that the autocorrelation function is a kind of “generalized intensity”, because for $\Delta t = 0$ it yields:

$$\Gamma(0) = \langle z^*(t)z(t) \rangle = I$$

It is customary to use the intensity in order to normalize the autocorrelation function so its absolute value will be bounded by 0 and 1. Therefore we define the complex first-order degree of temporal coherence, $\gamma(\Delta t)$, as:

$$\gamma(\Delta t) \equiv \frac{\Gamma(\Delta t)}{\Gamma(0)} = \frac{\langle z^*(t)z(t + \Delta t) \rangle}{I} = \frac{\langle z^*(t)z(t + \Delta t) \rangle}{\langle z^*(t)z(t) \rangle}, \quad (99)$$

and it can be shown (Mandel and Wolf [55], Section 4.3.1) that with this definition $0 \leq |\gamma(\Delta t)| \leq 1$. By inspection, we see also that $\gamma(0) = 1$, so any temporal point is maximally correlated with itself which makes good sense. Finally, the first order degree of temporal coherence is symmetric in Δt , because $\gamma(\Delta t) =$

$\gamma(-\Delta t)^*$. This follows at once from:

$$\Gamma(-\Delta t) = \langle z^*(t)z(t - \Delta t) \rangle = \langle z^*(t + \Delta t)z(t) \rangle = \langle z^*(t)z(t + \Delta t) \rangle^* = \Gamma^*(\Delta t),$$

where the second equality is due to the fact that the process is statistically stationary, so only the absolute value of the time delay matters.

We are now in position to examine rigorous definitions of the coherence time τ_c . The plural form is used, because several of them can be found in the literature [94]. The first one stems from the theory of analytic signals (see Ch. 4.1) and was introduced by Wolf [95]:

$$\tau_c^{(1)} = \frac{\int_{-\infty}^{\infty} (\Delta t)^2 |\Gamma(\Delta t)|^2 d(\Delta t)}{\int_{-\infty}^{\infty} |\Gamma(\Delta t)|^2 d(\Delta t)} = \frac{\int_{-\infty}^{\infty} (\Delta t)^2 |\gamma(\Delta t)|^2 d(\Delta t)}{\int_{-\infty}^{\infty} |\gamma(\Delta t)|^2 d(\Delta t)}. \quad (100)$$

The second one is due to Mandel [96] who was motivated by considerations of the fluctuation properties of light beams:

$$\tau_c^{(2)} = \int_{-\infty}^{\infty} |\gamma(\Delta t)|^2 d(\Delta t). \quad (101)$$

Let us take a glance back at our numerical simulation from the previous section. We generate $N = 100$ realizations of the emission process. The intensity plot of each resembles Fig. 15, but the fluctuations vary randomly in each realization. From Eq. (99) we calculate the complex first order degree of temporal coherence, and plot its absolute value versus the time difference Δt which ranges from -50000 to 50000 in our arbitrary time units. The plot is shown in Fig. 20. We observe the distinct peak in the middle that corresponds to strong correlations when the time difference is small. The peak decays abruptly as $|\Delta t|$ increases, but $|\gamma(\Delta t)|$ does not go to zero as $|\Delta t|$ approaches its maximal value. Instead the function is seen to fluctuate weakly. This weak fluctuations are due to the fact that we have used only 100 realizations (to spare the computational time). If N had been much larger, the central peak would remain unchanged, but $|\gamma(\Delta t)|$ would converge to zero outside it.

Using Eq. (101) we calculate the coherence time. We truncate the integral to the range $\Delta t \in [-2000, 2000]$, because the contributions from the aforementioned fluctuations of $|\gamma(\Delta t)|$ are undesirable. Such a numerical evaluation of Eq. (101) yields $\tau_c^{(2)} \approx 433 \approx 0.5\tau$ where τ is the mean damping time of a single wave packet from the simulation. The same result was determined from Fig. 16. Furthermore, this is also the FWHM of the peak of $|\gamma(\Delta t)|$ as can be seen from Fig. 21.

It can be demonstrated that for “typical” quasi-monochromatic chaotic radiation with Lorentzian or Gaussian spectra³² the two definitions of coherence time given in Eqs. (100)-(101) are equivalent, $\tau_c^{(1)} = \tau_c^{(2)}$ [94]. However, if the spectral profile of the optical field is more complicated (for instance, if it contains several peaks, as is the case of multimode laser light), then the coherence times calculated from different definitions may differ from each other with many orders of magnitude. In our further work, when considering thermal sources, we will focus on such “typical” fields only, so we will set $\tau_c^{(1)}$ equal to $\tau_c^{(2)}$, and in calculations we will

³²The form of the Lorentzian spectrum is $\tilde{x}_L(\omega) = \frac{A}{(\omega - \omega_0)^2 + A^2}$ where A is the inverse height and ω_0 is the central frequency. The Lorentzian broadening of spectral lines is due to homogeneous mechanisms such as lifetime broadening (where the radiative energy emitted by an excited atom is to some degree uncertain due to Heisenberg’s principle) or collisional broadening (where the constant collisions between the atoms interrupt the light emission process). The form of the Gaussian spectrum is $\tilde{x}_G = Ae^{-(\omega - \omega_0)^2/B}$ where A is the amplitude (height) and $\frac{B}{2}$ is the variance. The Gaussian broadening of spectral lines is caused by inhomogeneous mechanisms. The most important example of an inhomogeneous mechanism is Doppler broadening where the radiation emitted is Doppler-shifted due to the random thermal motions of the emitting atoms. Further details regarding the line broadening phenomena are to be found, for instance, in Loudon [52] and Fox [57].

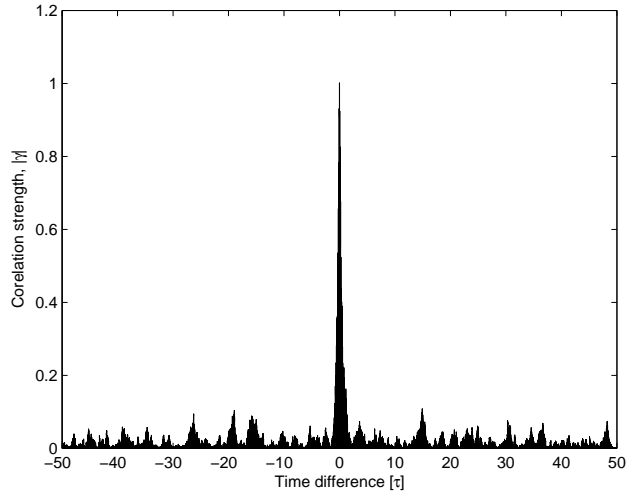


Figure 20: Quantification of the correlation strength in an optical field. The absolute value of the complex first-order degree of coherence, $|\gamma|$, is plotted as a function of the time difference Δt . The optical field under consideration is again a superposition of many randomly distributed wave packets with the mean damping time τ . The time difference Δt is given in the units of τ . We observe a distinct, narrow peak surrounded by weak fluctuations. The fluctuations are due to the limited number of simulation realizations. Ideally, when this number tends to infinity, $|\gamma|$ should converge to zero outside the peak.

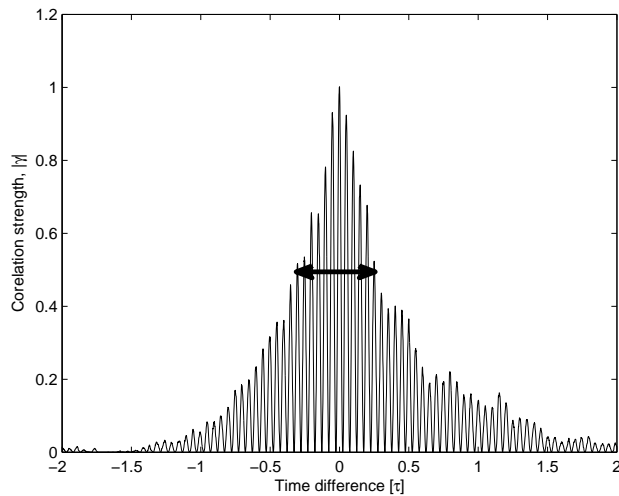


Figure 21: The central peak of $|\gamma|$ from Fig. 20. We observe that $|\gamma|$ decreases non-monotonically, and that the FWHM (marked by the double arrow) of the peak is approximately equal to the coherence time, 0.5τ . The peak is clearly asymmetric, but again this is due to the limited number of realizations (too small ensemble).

use Eq. (101).

We can now quantify the relation between the coherence time and the spectral width. We have seen that the spectral profile $\tilde{z}(\omega)$ is given as the Fourier transform of the signal:

$$\tilde{z}(\omega) = \frac{1}{\sqrt{2\pi}} \int_{-\infty}^{\infty} z(t) e^{-i\omega t} dt$$

Since each realization is of finite length T , the Fourier transform must in fact be first truncated:

$$\tilde{z}_T(\omega) = \frac{1}{\sqrt{2\pi}} \int_{-T/2}^{T/2} z(t) e^{-i\omega t} dt,$$

and then we can consider the limit as $T \rightarrow \infty$. Taking the absolute value squared, ensemble averaging and dividing by T yields a new quantity $S(\omega)$:

$$S(\omega) = \lim_{T \rightarrow \infty} \frac{1}{T} \langle |\tilde{z}_T(\omega)|^2 \rangle.$$

This is the power spectral density, and $S(\omega) d\omega$ represents the average power per unit area per unit (angular) frequency [48]. One can show that $S(\omega)$ is the Fourier transform of the autocorrelation function $\Gamma(\Delta t)$:

$$S(\omega) = \frac{1}{\sqrt{2\pi}} \int_{-\infty}^{\infty} \Gamma(\Delta t) e^{-i\omega(\Delta t)} d(\Delta t).$$

Furthermore, the total average intensity is given as the integral of $S(\omega)$:

$$I = \int_0^{\infty} S(\omega) d\omega.$$

The spectral width $\Delta\omega$ can be determined from the power spectral density. Again there are two different definitions, each of which corresponds to one of the definitions of the coherence time τ_c from Eqs. (100) and (101). The first one is:

$$\Delta\omega^{(1)} = \frac{\int_0^{\infty} (\omega - \bar{\omega})^2 S^2(\omega) d\omega}{\int_0^{\infty} S^2(\omega) d\omega},$$

with

$$\bar{\omega} = \frac{\int_0^{\infty} \omega S^2(\omega) d\omega}{\int_0^{\infty} S^2(\omega) d\omega}.$$

The second one is:

$$\Delta\omega^{(2)} = \frac{(\int_0^{\infty} S(\omega) d\omega)^2}{\int_0^{\infty} S^2(\omega) d\omega}.$$

These two spectral widths are related to the two coherence times in the following ways [94]:

$$\begin{aligned} \tau_c^{(1)} &\geq \frac{1}{2\Delta\omega^{(1)}} \\ \tau_c^{(2)} &= \frac{2\pi}{\Delta\omega^{(2)}}. \end{aligned}$$

In particular we observe that the second pair of definitions reproduces the experimentally grounded coherence time formula given by Eq. (91) (remember that $\Delta\omega = 2\pi\Delta f$). However, in both cases the coherence time is

not allowed to be shorter than approximately the inverse of the spectral width.

Up till now the position variable \mathbf{r} has been suppressed in our treatment, i.e. we have assumed that all measurements of the optical field are performed in the same point of space. This has allowed us to quantitatively examine the *temporal* coherence. Let us now generalize the formalism to two spatial points \mathbf{r}_1 and \mathbf{r}_2 . We introduce the cross-correlation function (also called the mutual coherence function):

$$\Gamma(\mathbf{r}_1, \mathbf{r}_2, \Delta t) = \langle z^*(\mathbf{r}_1, t) z(\mathbf{r}_2, t + \Delta t) \rangle, \quad (102)$$

and the complex first-order degree of mutual coherence:

$$\gamma(\mathbf{r}_1, \mathbf{r}_2, \Delta t) = \frac{\Gamma(\mathbf{r}_1, \mathbf{r}_2, \Delta t)}{\sqrt{\Gamma(\mathbf{r}_1, \mathbf{r}_1, 0)}\sqrt{\Gamma(\mathbf{r}_2, \mathbf{r}_2, 0)}} = \frac{\Gamma(\mathbf{r}_1, \mathbf{r}_2, \Delta t)}{\sqrt{I(\mathbf{r}_1)I(\mathbf{r}_2)}}, \quad (103)$$

where we normalize the cross-correlation function with the help of the average intensities at the two spatial points. Notice that we have called these two functions by the same Greek letters as the ones used before, Γ and γ , in order to emphasize that the quantities from Eqs. (98)-(99) follow directly from the above expressions (when $\mathbf{r}_1 = \mathbf{r}_2$). The absolute value of γ is still bounded between zero and unity, and, loosely speaking, the larger it is, the stronger are the correlations of the optical field in two spacetime points.

Consider now again an extended thermal source of dimension Δs lying in the origin O , and a point P (in position \mathbf{r}_1) in space lying at distance $R \gg \Delta s$ from the source. If we wish to determine the coherence area around the point P , we can calculate the complex first-order degree of mutual coherence at different points around P . Let us call one of these points Q (in position \mathbf{r}_2). If the distance difference $|\overline{OQ} - \overline{OP}|$ is much smaller than the longitudinal coherence length $\ell_c^{(l)} = c\tau_c$, so that the optical field in P and Q is almost completely temporally coherent, then we are effectively calculating $\gamma(\mathbf{r}_1, \mathbf{r}_2, \Delta t \approx 0)$. For $\mathbf{r}_1 = \mathbf{r}_2$ the degree of mutual coherence is 1. When $|\mathbf{r}_2 - \mathbf{r}_1|$ increases, $\gamma(\mathbf{r}_1, \mathbf{r}_2, \Delta t \approx 0)$ will decrease. As long as its value stays relatively high (i.e. larger than some prescribed value), we say that the two points P and Q are partially coherent in the spatial sense., and that Q is within coherence area relatively to P .

We will now introduce the concept of the complex second-order degree of coherence. It is obvious that $\gamma(\mathbf{r}_1, \mathbf{r}_2, \Delta t)$ from Eq. (103) quantifies the correlations between field *components* in two different points of the optical field. However, in many scenarios (the most notable being Hanbury Brown-Twiss interferometry experiment [97] [98]) it is desirable to examine the correlations between the *intensities*. A proper generalization of γ is readily obtained:

$$\gamma^{(2)}(\mathbf{r}_1, \mathbf{r}_2, \Delta t) \equiv \frac{\langle \xi(\mathbf{r}_1, t)\xi(\mathbf{r}_2, t + \Delta t) \rangle}{I(\mathbf{r}_1)I(\mathbf{r}_2)},$$

with $\xi(\mathbf{r}, t) = |z(\mathbf{r}, t)|^2$ which is the instantaneous intensity. This is the definition of the second-order degree of coherence. Using Cauchy's inequality one can show (Loudon [52], Chapter 3.7) that

$$\begin{aligned} \infty &\geq \gamma^{(2)}(\mathbf{r}, \mathbf{r}, \Delta t) \geq 1, & \Delta t = 0 \\ \infty &\geq \gamma^{(2)}(\mathbf{r}, \mathbf{r}, \Delta t) \geq 0, & \Delta t \neq 0. \end{aligned} \quad (104)$$

These general inequalities are to be compared with $\gamma(\mathbf{r}, \mathbf{r}, 0) = 1$ and $1 \geq |\gamma(\mathbf{r}, \mathbf{r}, \Delta t)| \geq 0$ in the case of the complex first-order degree of coherence which we will henceforth call $\gamma^{(1)}$. Even though the second-order

degree of coherence has no upper bound, it can be shown that

$$\gamma^{(2)}(\mathbf{r}, \mathbf{r}, 0) \geq \gamma^{(2)}(\mathbf{r}, \mathbf{r}, \Delta t). \quad (105)$$

For the particular case of a quasi-monochromatic chaotic radiation these two coherence degrees are related:

$$\gamma^{(2)}(\mathbf{r}, \mathbf{r}, \Delta t) = 1 + \left| \gamma^{(1)}(\mathbf{r}, \mathbf{r}, \Delta t) \right|^2,$$

and the limiting values of the second-order degree of coherence are thus:

$$\begin{aligned} \gamma^{(2)}(\mathbf{r}, \mathbf{r}, 0) &= 2 \\ \gamma^{(2)}(\mathbf{r}, \mathbf{r}, |\Delta t| \rightarrow \infty) &\rightarrow 1. \end{aligned}$$

In the foregoing discussion of the second-order degree of coherence we have set $\mathbf{r}_1 = \mathbf{r}_2 \equiv \mathbf{r}$. If we now consider again two distinct spatial points $\mathbf{r}_1 \neq \mathbf{r}_2$, we say that the optical field at these two points is second-order coherent with time delay Δt if $|\gamma^{(1)}(\mathbf{r}_1, \mathbf{r}_2, \Delta t)| = 1$ and $\gamma^{(2)}(\mathbf{r}_1, \mathbf{r}_2, \Delta t) = 1$ are both satisfied. Therefore the chaotic light will not be second-order coherent no matter what spatial points of the field are being examined.

Finally we would like to mention an important result stemming from the theory of quantum correlations which aims at describing and quantizing correlations of the quantized electromagnetic fields. This theory represents electromagnetic fields as statistical mixtures of coherent states (see Ch. 2.4) using general distribution functions (which often cannot be reduced to ordinary probability distributions). It was developed mainly by Glauber [43]. The presentation of his model in a satisfactory manner would be rather lengthy and technical. Therefore for a full treatment we simply refer to Mandel and Wolf [55] (Chapter 12) or Loudon [99], and here we quote only the result concerning the second-order degree of coherence which is of central importance in our context. Namely, the theory of quantum correlations allows for a situation with:

$$\gamma^{(2)}(\mathbf{r}, \mathbf{r}, 0) < 1 \quad (106)$$

$$\gamma^{(2)}(\mathbf{r}, \mathbf{r}, 0) < \gamma^{(2)}(\mathbf{r}, \mathbf{r}, \Delta t \neq 0) \quad (107)$$

In other words, if the electromagnetic fields are quantized, then correlations of their fluctuations may be weaker than the classical description predicts. These weak correlations correspond then to a high degree of regularity in the stream of photons. For this reason light with $\gamma^{(2)}(\mathbf{r}, \mathbf{r}, 0) < \gamma^{(2)}(\mathbf{r}, \mathbf{r}, \Delta t \neq 0)$ (for some $\Delta t \neq 0$, not necessarily for all Δt) is called antibunched, while light with $\gamma^{(2)}(\mathbf{r}, \mathbf{r}, 0) > \gamma^{(2)}(\mathbf{r}, \mathbf{r}, \Delta t \neq 0)$ is called bunched. Thus a situation with $\gamma^{(2)}(\mathbf{r}, \mathbf{r}, 0) > \gamma^{(2)}(\mathbf{r}, \mathbf{r}, \Delta t \neq 0)$ is admissible both in the classical and in the quantum description of correlations. In the first case we explain it as a presence of high-intensity fluctuations, in the second case as a presence of bunches of photons. The classical description, however, cannot account for $\gamma^{(2)}(\mathbf{r}, \mathbf{r}, 0) < \gamma^{(2)}(\mathbf{r}, \mathbf{r}, \Delta t \neq 0)$.

We will discuss experimental demonstrations of photon antibunching in Sect. 5.1.4 in the context of different photodetection models. There we will also comment on the link between photon bunching/antibunching and photocount statistics.

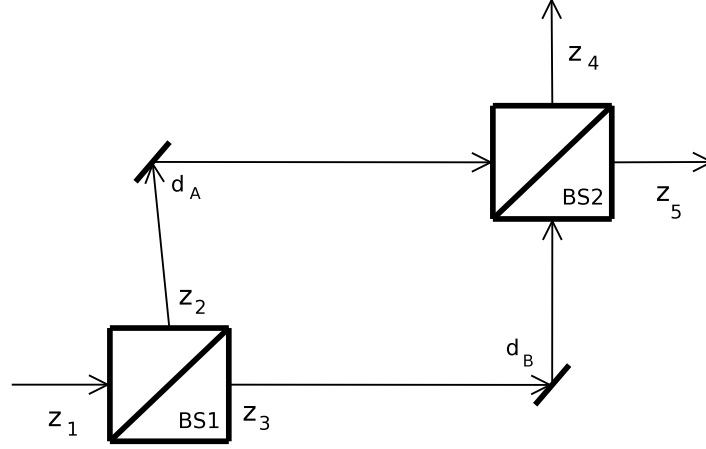


Figure 22: A Mach-Zender interferometer consists of two beam splitters. The distances between them may be different for each optical path. Usually one path length is fixed, and only the second one is varied.

4.4 Application to interferometry

We will now show how the theory of correlations can be applied to interferometers and the formation of interference pattern. We will use Mach-Zender interferometer as our example, but the same principles apply to Michelson interferometer (Ch. 3.2) as well.

Refer to Fig. 22 for a schematic description of a Mach-Zender interferometer. It consists of two beam splitters labeled BS1 and BS2. The optical field, represented again as a complex analytic signal z_1 , enters through one of the input ports of BS1 (the second port remains closed). The beam is partially reflected (z_2) and partially transmitted (z_3). If R is the reflection coefficient of the beam splitter, and T the transmission coefficient³³, we have:

$$\begin{aligned} z_2(t) &= Rz_1(t) \\ z_3(t) &= Tz_1(t), \end{aligned}$$

with the assumption that the transit time through the beam splitter is negligible. Now, the distances between BS1 and BS2 may be different for each optical path, so generally $d_A \neq d_B$. Thus if a beam segment has arrived at BS1 at time t_0 and was (per assumption immediately) divided into two subsegments, the subsegment following the upper path will arrive at BS2 at time $t_0 + t_A \equiv t_0 + \frac{d_A}{c}$ and the subsegment following the lower path will arrive at BS2 at time $t_0 + t_B \equiv t_0 + \frac{d_B}{c}$. Thus we have, assuming that both beam splitters are identical and the same coefficients can be used in the case of BS2:

$$\begin{aligned} z_4(t) &= Rz_2(t - t_A) + Tz_3(t - t_B) = R^2z_1(t - t_A) + T^2z_1(t - t_B) \\ z_5(t) &= Tz_2(t - t_A) + Rz_3(t - t_B) = RT[z_1(t - t_A) + z_1(t - t_B)] \end{aligned}$$

We measure the intensity at some spatial point behind BS2, say, along the z_4 -direction. Its time-averaged

³³The full description of beam splitters belongs to Chapter 5.2.

value³⁴ is:

$$I_{\text{out}} = \left\langle |z_4(t)|^2 \right\rangle = |R|^2 |T|^2 \left\langle |z_1(t-t_A)|^2 + |z_1(t-t_B)|^2 + z_1^*(t-t_A) z_1(t-t_B) + z_1(t-t_A) z_1^*(t-t_B) \right\rangle. \quad (108)$$

Due to the statistical stationarity of the process, each of the two first terms in the brackets give the average intensity I_{in} of the input beam:

$$\left\langle |z_1(t-t_A)|^2 \right\rangle = \left\langle |z_1(t-t_B)|^2 \right\rangle = I_{\text{in}}. \quad (109)$$

The two last terms, however, can be rewritten and expressed with the help of the complex first-order degree of coherence:

$$\langle z_1^*(t-t_A) z_1(t-t_B) + z_1(t-t_A) z_1^*(t-t_B) \rangle = 2\Re[\langle z_1^*(t-t_A) z_1(t-t_B) \rangle] = 2\Re[\langle z_1^*(t) z_1(t+\Delta t) \rangle],$$

with $\Delta t \equiv t_A - t_B = \frac{d_A - d_B}{c}$ and where the last equality is justified again by the statistical stationarity. We continue:

$$2\Re[\langle z_1^*(t) z_1(t+\Delta t) \rangle] = 2\Re[\Gamma(\Delta t)] = 2I_{\text{in}} \Re[\gamma^{(1)}(\Delta t)], \quad (110)$$

with the help of Eqs. (98), (99) and (109). Putting back Eqs. (109)-(110) into Eq. (108) we obtain a simple expression for the time-averaged output intensity:

$$I_{\text{out}} = 2I_{\text{in}} |R|^2 |T|^2 \left(1 + \Re[\gamma^{(1)}(\Delta t)] \right) \quad (111)$$

We see that the output intensity of the Mach-Zender interferometer is related in a rather simple way to the (real part of the) complex first-order degree of coherence. In the total absence of first-order correlations, i.e. when $\gamma^{(1)}(\Delta t) = 0$, the output intensity is constant and equal to $2I_{\text{in}} |R|^2 |T|^2$. However, the interference fringes³⁵ will occur when $\gamma^{(1)}(\Delta t) \neq 0$, because then $\Re[\gamma^{(1)}(\Delta t)]$ can be positive or negative. We conclude that the formation of the fringes is dependent on the correlations in the input beam; or, equivalently, by varying Δt and measuring the output intensity, we can deduce the form of $\Re[\gamma^{(1)}(\Delta t)]$.

The above analysis of the Mach-Zender interferometry is applicable for both chaotic radiation from a thermal source, for partially coherent light beam with coherence time long compared to the time needed for the light to pass through the apparatus, and for perfectly coherent, idealized light beam with infinitely long coherence time. In the first case, when $|\Delta t|$ increases, $|\gamma^{(1)}|$ will tend to zero, and the interference fringes will be less and less visible, until at last I_{out} achieves the constant value of $2I_{\text{in}} |R|^2 |T|^2$. In the second case $|\gamma^{(1)}|$ will also diminish with increasing $|\Delta t|$, but less rapidly. In the third case, one can show (Loudon [52], Chapter 3.4) that $\gamma(\Delta t) = e^{-i\omega\Delta t}$ where ω is the angular frequency of the monochromatic light. Eq. (111)

³⁴ We are using brackets, because we assume again that the emission process is ergodic, so the ensemble average equals the time average.

³⁵ The term ‘‘interference fringes’’ is used here in a different way than in Chapter 3.2 where we discussed the Michelson interferometer. Now we are not talking about any *spatial* interference pattern, because the spatial variable \mathbf{r} has been suppressed in our treatment of the Mach-Zender interferometer (as it is usually done). What we now mean with ‘‘fringes’’ is that when $\Delta d \equiv d_A - d_B$ (and thus Δt) is varied, the output intensity I_{out} measured at a single spatial point will get larger or smaller according to whether $\Re[\gamma^{(1)}(\Delta t)]$ increases or decreases.

implies that then I_{out} will oscillate in a sinusoidal fashion between 0 and $4I_{\text{in}}|R|^2|T|^2$.

In practice the above theory can be used to estimate coherence time τ_c (or, equivalently, longitudinal coherence length $\ell_c^{(l)}$) of a light beam. One sends the beam through an interferometer and varies³⁶ the path length difference $\Delta d = c\Delta t$ between the two partial beams. The partial beams are recombined and the visibility of interference fringes measured as a function of Δd . As long as visibility remains high, Δd must be much less than $\ell_c^{(l)}$. When Δd tends to $\ell_c^{(l)}$ the visibility will decrease, and when the path length difference exceeds the longitudinal coherence length, the interference pattern will no longer form, because then the fluctuations in the two partial beams will be uncorrelated. This principle will be used in Chapter 6.2 where we will measure the coherence length of our laser beam.

³⁶For geometrical reasons it is more easily done with Michelson interferometer than Mach-Zender interferometer.

5 The main elements of the experimental setup: theoretical review

The following two chapters are dedicated to the three main elements of the experimental setup from Chapter 7 – the photodetector, the beam splitter and the laser beam. In this chapter we review the theoretical background, and in the next chapter we state specifications of the elements and conduct some preliminary measurements. Since the setup is being prepared from scratch, and since most of the components have not been used before, such measurements are necessary. It seems only natural that their presentation is coupled together with a review of the theoretical background. However, investigation of this background will give us further insight into the wave-particle duality problem, because we will make use of different physical models which assume that light is either an undulatory or a corpuscular phenomenon, and because we will discuss how they differ and what their shortcomings are.

In Chapter 5.1 we are going to speak qualitatively about several different photodetection schemes (Sect. 5.1.1), and then discuss the photocount statistics in the framework of the semiclassical (Sect. 5.1.2) and the corpuscular (Sect. 5.1.3) model. Concluding remarks regarding the two models are given in Sect. 5.1.4.

In Chapter 5.2 we present two theoretical models describing the beam splitter. The presentation will be first done in a textbook manner (Sect 5.2.1-5.2.2), but then we will discuss the shortcomings of both models (Sect. 5.2.3).

In Chapter 5.3 we will investigate the shape of the laser beam, since discussion of the beam shape is necessary to properly set up optical elements in any laser experiment. That chapter is rather technical and consists mainly of derivations – the central results, important for our further work in Chapter 6.1, are Eqs. (158)-(165). The question of how the laser beam is actually generated has been left out. Although this subject without a doubt is of relevance, its complexity makes the author unable to cover it in the thesis as well. We can only refer to, for instance, Saleh and Teich [48], Milonni and Eberly [100] or Siegman [101].

In the following chapter both views on the nature of light will be used: the undulatory model (e.g. when classically describing the beam splitter), and the corpuscular models (e.g. when reviewing the fully quantum-mechanical theory of photocount statistics). Our treatment will therefore again exhibit the problem of wave-particle duality, but the conceptual conflict between these different approaches will not be emphasized in this chapter. Let us keep in mind, however, that it may serve as a fine illustration of the duality (in addition to the different considerations discussed in Chapter 3).

5.1 Photodetector

Consider a photon-counting experiment where we measure the incoming light beam with a single-photon detector. The working of such a device is based on the (external or internal) photoelectric effect (for a description of internal photoelectric effect see Ch. 3.3). As long as the intensity is not too high and we avoid saturation, the response of the detector will consist of a series of discrete signals called photocounts. In the following section we will develop basic statistical models that describe the distribution of the signals in time and relate it to the type and intensity of the input radiation. We shall present two main approaches: the semiclassical theory (Sect. 5.1.2) and the fully quantized model (Sect. 5.1.2). In our presentation we will focus on the fundamental difference between the two models: That the latter is able to predict arbitrarily small variance of the photocount number, while the semiclassical model sets a lower bound for it. We begin, however, by reviewing different types of photodetectors (Sect. 5.1.1). The description is kept rather short and qualitative, because the detailed examination would require us to review elements of solid-state and semiconductor physics which are outside the scope of this thesis.

5.1.1 Types of photodetectors

A photodetector measures the intensity of electromagnetic radiation by converting its energy into a measurable form. Photodetecting devices fall into two broad classes: photoelectric detectors that convert the intensity into an electric current, and thermal detectors that convert the intensity into heat. The working of the photoelectric detectors is based on the photoelectric effect which was explored in detail in Chapter 3.3. In that section we focused on the external photoelectric effect where electrons leave the photoelectric material under an influence of electromagnetic radiation. In the case of the internal photoelectric effect the excited electrons remain inside the photoelectric material, but increase its conductivity in a measurable way.

A typical example of a photodetector based on the external photoelectric effect is a photomultiplier tube (also called a photomultiplier). When light impinges on the photocathode, the photoelectrons are emitted and travel to the anode maintained at a higher electric potential. However, between the photocathode and the anode there are several dynodes which amplify the electron current by the means of the secondary emission – a phenomenon where a material emits additional electrons when impacted by an electron (or other material particle) with sufficient energy. The amplified photoelectric current (the total amplification can be as high as 10^8 [48]) is then measured, and related to the intensity of the incoming light.

In recent times, due to the progress in the fabrication of semiconductors, photodetectors based on the internal photoelectric effect have gained popularity. For such devices the electromagnetic radiation transfers its energy to an electron bound in the photosensitive part of the detector. The energy is not sufficient to eject the electron from the material, but large enough to excite and move it from the lower energy level, called the valence band, to the upper energy level, called the conduction band (thus the energy has to be greater than the energy difference between the bands, called the band gap). Furthermore, the electron leaves behind it, in the valence band, an excess of positive charge, called hole. The application of external electric field to the material transports the excited electrons (and the holes) through it, thus producing a measurable electric current. The electrons and the holes are collectively called carriers.

Similarly as in the case of photomultipliers, the internal photoelectric effect can be amplified by introducing

a gain mechanism into the structure of the semiconductor. This is what happens in the avalanche photodiodes (APD) where the electric field is strong enough for a carrier to excite a new pair of carriers through the impact ionization. In the process of impact ionization the original carrier has enough kinetic energy to promote a bound electron to a state in the conduction band, thus creating a new electron-hole pair. The process is repeated many times, so even low light intensity at the input would produce a relatively strong electrical signal at the output. One could believe that increasing the strength of the external electric field would just lead to a larger gain. However, several side-effects must be considered. The amplification is time consuming, so large gain reduces the bandwidth of the detector. Furthermore, the process of amplification is inherently random, so large gain will correspond to large noise. Finally, if the external electric field is too strong, there will be spontaneous breakdowns, i.e. situations where the generation of the first carrier pair occurs because of the field and not as the result of the impinging radiation.

If the (avalanche-amplified) electric signal caused by a single photocount is quickly quenched, but nonetheless registered on the output, then we are able to separate the signals corresponding to different photocounts. Thus the response of the detector will be binarized – a single photocount will correspond to a short and isolated output signal. With proper auxiliary electronic circuits in the detector module a high temporal resolution (less than 1 ns) can be achieved, and the problem of noise reduced. However, there are several drawbacks of such detection scheme. The detector will saturate much more easily, so the measured count rate cannot be very high. The photocount statistics will be somewhat biased by the presence of dark counts, i.e. “false” photocounts caused by random thermal excitations of the electrons in the detector. Undesired afterpulses, as explained in Chapter 6.4, will also occur. Finally, we have to remember that two subsequent photocounts cannot be registered with an arbitrary short time interval between them, because the detector response is characterized by a “dead time” during which the electric signal from the previous photocount is being quenched.

The devices described in the above paragraph are, naturally enough, called single-photon counting modules, single-photon avalanche photodetectors or Geiger-mode avalanche photodiodes. This is the photodetector type that we will be using in our experimental setup (see Ch. 6.4).

5.1.2 The semiclassical model

The statistical results of light measuring experiments are of great importance for the question regarding the nature of light. Up until the 1970s physicists were able to explain all experimental results using the semiclassical model. In that model the quantum-mechanical rules were applied to the detector only, and the light itself was treated as a classical electromagnetic wave. Thus the complete quantization of the electromagnetic field, although resting on solid theoretical foundations, was not necessary from the empirical point of view. The situation changed in 1970s when the technological progress made it possible to conduct new types of experiments, the results of which could not be reconciled with the predictions of the semiclassical model. As the consequence, the complete quantum model of both radiation and the interactions between radiations and matter (detectors) started to gain much more appreciation [92] [93].

In the semiclassical theory of optical detection we represent the quasi-monochromatic light impinging on a detector as a electromagnetic plane wave, but we assume that the interaction between the light and the detector is quantized. More precisely, we treat the electrons bounded in the photosensitive part of the

detector quantum-mechanically, but the radiation is represented classically as an external potential that perturbs the electrons. It follows that the responses of the detector to the incoming light are discrete, even though the light itself is modelled as a continuous phenomenon (compare with the alternative model for the photoelectric effect presented in Chapter 3.3).

Let us denote by $p(t)dt$ the probability that the detector registers a single photocount between time t and $t + dt$, where dt is so short that the probability for registering two or more photocounts is negligible. Then it is reasonable to assume that:

$$p(t)dt \sim \bar{I}(t)dt,$$

i.e. the probability ought to be proportional to the cycle-averaged intensity of the radiation at the same time, $\bar{I}(t)$ [96]. The proportionality constant is the total efficiency ϵ of the photodetector. With “total” we mean that both internal (e.g. sensitivity to the incoming radiation) and external (e.g. alignment) factors are considered in the determination of ϵ . Notice, however, that generally ϵ would be a function of both the radiation frequency (because of the threshold given by the work function, cf. Eq. (59) in Chapter 3.3) and the radiation intensity (because the dependance needs not to be linear). For simplicity we just set:

$$p(t)dt = \epsilon \bar{I}(t)dt. \quad (112)$$

The validity of Eq. (112) in the framework of the semiclassical theory can be, in fact, rigourously demonstrated (Mandel and Wolf [55], Ch. 9.3). One would then find that ϵ is given as:

$$\epsilon = \left(\frac{e}{m\hbar} \right)^2 N \sigma(E_0 + \hbar\omega) g(E_0 + \hbar\omega) |\langle E_0 + \hbar\omega | \hat{\mathbf{p}}(t) | E_0 \rangle \cdot \mathbf{u}|^2 2\pi\hbar,$$

if $|E_0| > \hbar\omega$, and $\epsilon = 0$ otherwise. e is the electron charge, m the electron mass and \hbar the Planck constant divided by 2π ; N denotes the number of electrons in the photoelectric surface, σ the density of electron states and g the response function (a sort of weighting function which is needed because detection process may favor electrons with certain energies); E_0 is the negative energy of a bound electron, ω is the angular frequency of the impinging radiation, $\hat{\mathbf{p}}$ is the momentum operator, \mathbf{u} is the unit polarization vector of the radiation; and, finally, the bra and the ket denote energy eigenstates of the electron. Eq. (112) holds as long as the intensity of the light is not extremely high, and the photoemissions do not influence each other.

In the spirit of Loudon [52], we define now $P_n(t_1, t_2)$ as the probability for the event that n photocounts took place between times t_1 and t_2 , with $t_2 \geq t_1$. We consider $P_n(t_1, t_2 + dt_2)$ with dt_2 being again a time interval so short that the probability of more than one photocount occuring between t_2 and $t_2 + dt_2$ is negligible. The event can be realized in two ways: Either there will be n photocounts between t_1 and t_2 , but none between t_2 and $t_2 + dt_2$, or there will be $n - 1$ photocounts between t_1 and t_2 , and a single one between t_2 and $t_2 + dt_2$. Thus we have:

$$\begin{aligned} P_n(t_1, t_2 + dt_2) &= P_n(t_1, t_2)[1 - p(t_2)dt_2] + P_{n-1}(t_1, t_2)p(t_2)dt_2 \\ P_n(t_1, t_2 + dt_2) - P_n(t_1, t_2) &= [P_{n-1}(t_1, t_2) - P_n(t_1, t_2)]p(t_2)dt_2 \\ \frac{P_n(t_1, t_2 + dt_2) - P_n(t_1, t_2)}{dt_2} &= [P_{n-1}(t_1, t_2) - P_n(t_1, t_2)]\epsilon \bar{I}(t_2), \end{aligned}$$

where we have substituted for $p(t_2)dt_2$ from Eq. (112). In the limit $dt_2 \rightarrow 0$ the left hand side can be

expressed as a differential, so we get:

$$\frac{dP_n(t_1, t_2)}{dt_2} = [P_{n-1}(t_1, t_2) - P_n(t_1, t_2)]\epsilon\bar{I}(t_2). \quad (113)$$

If we naturally define the meaningless expression $P_{-1}(t_1, t_2) \equiv 0$ for all t_1 and t_2 , then we obtain from the above formula:

$$\begin{aligned} \frac{dP_0(t_1, t_2)}{dt_2} &= -\epsilon\bar{I}(t_2)P_0(t_1, t_2) \\ \frac{dP_0(t_1, t_2)}{P_0(t_1, t_2)} &= -\epsilon\bar{I}(t_2)dt_2 \\ \ln\left(\frac{P_0(t_1, t_1+T)}{P_0(t_1, t_1)}\right) &= -\epsilon\int_{t_1}^{t_1+T}\bar{I}(t_2)dt_2 \end{aligned}$$

where we integrate with t_2 as the variable from t_1 to some time t_1+T . It is obvious from the definition that $P_0(t_1, t_1) = 1$. If we denote the time-averaged intensity impinging on the detector between t_1 and t_1+T as $\bar{I}(t_1, t_1+T) \equiv \frac{1}{T}\int_{t_1}^{t_1+T}\bar{I}(t_2)dt_2$, we obtain:

$$P_0(t_1, t_1+T) = e^{-\epsilon\bar{I}(t_1, t_1+T)T}. \quad (114)$$

With the help of Eqs. (113)-(114) and the obvious fact that $P_{n>0}(t_1, t_1) = 0$, we can calculate the formulas for $P_n(t_1, t_1+T)$ with $n > 0$. The general result is:

$$P_n(t_1, t_1+T) = \frac{[\epsilon\bar{I}(t_1, t_1+T)T]^n}{n!}e^{-\epsilon\bar{I}(t_1, t_1+T)T}$$

which can be proved by induction (Loudon [52], Ch. 3.9).

In practical situations the cycle-averaged intensity $\bar{I}(t)$ will fluctuate and therefore has to be represented as a random process. However, in many cases it is reasonable to use two simplifying assumptions: that the process is stationary (the character of the fluctuations does not change with time) and ergodic (every realization of the process is similar). Then the probability for registering n photocounts during a time interval of length T is:

$$P_n(T) = \left\langle \frac{[\epsilon\bar{I}(t_1, t_1+T)T]^n}{n!}e^{-\epsilon\bar{I}(t_1, t_1+T)T} \right\rangle \quad (115)$$

where the angular brackets denote a statistical average over the intensity fluctuations. The mean number of photocounts in a detection time T is given as:

$$\mu = \sum_n nP_n(T) = \langle \epsilon\bar{I}(t_1, t_1+T)T \rangle.$$

In the idealized case of a stable plane wave, $\bar{I}(t)$ is constant and the statistical averaging in Eq. (115) is unnecessary. Thus, given a perfect detector, we obtain the Poisson distribution of photocounts:

$$P_n(T) = \frac{\mu^n}{n!}e^{-\mu} \quad (116)$$

with the mean $\mu = \epsilon\bar{I}T$ and the variance $\sigma_n^2 = \mu$. However, this Poisson distribution occurs also when the light intensity fluctuates (in a stationary and ergodic manner), as long as the detection time T is much

longer than the characteristic scale of the fluctuations (the coherence time, see Ch. 4.2-4.3), because then the integration in the expression for $\bar{I}(t_1, t_1 + T)$ “smoothens out” the fluctuations and \bar{I} is now the long-time average intensity. On the other hand, if the period given by T is much shorter than the coherence time, the instantaneous intensity $\bar{I}(t)$ is approximately constant over the period and we have $\bar{I}(t_1, t_1 + T) = \bar{I}(t_1)$. The calculation then yields:

$$P_n(T) = \frac{\mu^n}{(1 + \mu)^{1+n}},$$

again with $\mu = \epsilon \bar{I} T$. It suggests that the distribution of photocounts for chaotic light (i.e. with fluctuating intensity) with relatively long coherence time resembles the photocount distribution for a single mode of thermal light given by the Bose-Einstein distribution [52].

If the integration time is neither very short or very long relatively to the coherence time, there is no general formula that describes the distribution, and the evaluation of Eq. (115) has to be performed numerically. However, it is possible to find an analytic expression for the variance of the photocount distribution (Loudon [52], Ch. 3.9):

$$\sigma_n^2 = \epsilon \langle \bar{I}(t_1, t_1 + T) \rangle T + \epsilon^2 T^2 [\langle \bar{I}(t_1, t_1 + T)^2 \rangle - \langle \bar{I}(t_1, t_1 + T) \rangle^2]. \quad (117)$$

The first term is again does not depend on the intensity fluctuations. It is called the shot noise of the photodetection process, and it is due to the discrete nature of the photoelectric ionizations. The second term, however, is determined by the intensity fluctuations. For the perfectly coherent light consisting of a continuous wave with constant amplitude and unique frequency $\bar{I}(t_1, t_1 + T)$ is a constant, so the two terms in the square brackets cancel each other, and we are left with:

$$\sigma_n^2 = \mu.$$

This is the variance of the Poisson distribution, the lowest variance possible in the semiclassical model.

An important feature of the Poissonian light is that times between two subsequent events are exponentially distributed with parameter μ [102] where μ is, as before, mean value of photocounts. Thus, if instead of measuring number of photocounts in each time interval, we choose to measure times Δt between two subsequent photodetections, the theoretical prediction for the distribution $P_{\Delta t}$ of these times will be given as:

$$P_{\Delta t} = \mu e^{-\mu \Delta t}. \quad (118)$$

This can be demonstrated very easy. Consider a process described by the Poisson distribution, and assume that a photodetection takes place between time t_0 and time $t_0 + dt$, and the next photodetection between $t_0 + \Delta t$ and $t_0 + \Delta t + dt$. Here t_0 is an arbitrarily chosen reference point, Δt is a finite time interval, and dt is infinitesimally small. On average there will occur $\mu \Delta t$ photodetections in this interval, so the probability that no photodetections will occur ($n = 0$) is given by the Poisson distribution as $e^{-\mu \Delta t}$. However, the probability for one photodetection occurring between $t_0 + \Delta t$ and $t_0 + \Delta t + dt$ is μdt . Multiplying the two probabilities yields $e^{-\mu \Delta t} \mu dt$ which is the probability density that two consecutive photodetections will be separated by a time interval Δt . This leaves us with the exponential distribution given by Eq. (118).

In photon-counting experiments we irradiate the detector with a light beam coming from some source we want to examine. If we just want to measure the photon statistics of a single beam (i.e. no beam splitting and no coincidence measurements are involved), the basic scheme is to irradiate the detector in short, subsequent time intervals. We register the number of photocounts in each interval, calculate their mean number μ , plot

the results as a histogram, and compare it with the theoretical Poisson distribution. The variance is used as a quantitative measure in such comparison. If it is smaller than μ , then we have observed the distinct signature of the so-called nonclassical light that the semiclassical model cannot account for. We examine an appropriate model in the next section.

5.1.3 The corpuscular model

If the measured variance of the photocount number, σ_n^2 , is larger than the measured mean photocount number, μ , the light beam is characterized by super-Poissonian statistics³⁷. This would reflect a lack of perfect coherence, since the large photon number fluctuations must be due to intensity fluctuations of the source. This situation was predicted by the semiclassical model, cf. Eq. (117). On the other hand the inequality $\sigma_n^2 < \mu$ defines sub-Poissonian light, i.e. light characterized by sub-Poissonian statistics. The inequality implies that the intensity of sub-Poissonian light fluctuates even less than the intensity of perfectly coherent light beam which is clearly a contradiction, because a perfectly coherent light beam does not fluctuate at all. Thus we are forced to use the fully quantized model in order to theoretically allow for the case $\sigma_n^2 < \mu$. In contrast to the situation in the semiclassical model, this model is able to predict arbitrarily small variances of the photocount distribution.

We employ the formalism of the photon number states (see Sect. 2.3.3), and we limit our attention to one particular mode characterized by a wave vector \mathbf{k} and polarization λ . Thus we drop the lower index $\mathbf{k}\lambda$, and instead of using the general Fock state $\{|n_{\mathbf{k}\lambda}\rangle\}$ we simply write $|n\rangle$ where n denotes the well-defined number of photons in that mode.

The electromagnetic field can be represented as a wave function $|\psi\rangle$. Since $\{|n\rangle\}$, $n \in \mathbb{N}$ is a complete basis, it can be used to expand $|\psi\rangle$. Thus we easily find that the probability of finding n photons in the electromagnetic field is:

$$P(n) = |\langle n|\psi\rangle|^2.$$

However, if the electromagnetic field is a photon number state, i.e. $|\psi\rangle = |m\rangle$, then we know with certainty that m photons will be observed there:

$$P(n) = |\langle n|m\rangle|^2 = \delta_{nm}.$$

With $\hat{n} \equiv \hat{a}^\dagger \hat{a}$ acting as the number operator, it is trivial to calculate the mean $\langle n \rangle$ and the variance $\langle (\Delta n)^2 \rangle$ of the photon number for such a state:

$$\mu \equiv \langle n \rangle = \langle m|\hat{n}|m\rangle = \langle m-1|\sqrt{m}\sqrt{m}|m-1\rangle = m \quad (119)$$

$$\sigma_n^2 \equiv \langle (\Delta n)^2 \rangle = \langle m|\hat{n}^2|m\rangle - \langle m|\hat{n}|m\rangle^2 = m^2 - m^2 = 0. \quad (120)$$

³⁷Provided the detector is perfect and there are no optical losses in the system, so to each emitted photon corresponds a single photocount. In practice such a perfect correspondence would be difficult to obtain, but at least there are no theoretical hindrances to it. This 1:1-correspondence will be implicitly assumed till the end of the section. However, notice that the presence of optical losses and the less-than-unity efficiency of the detector will effectively lead to a random selection of photons from the original photon stream, and such selection will degrade the photon statistics to the Poisson distribution. In other words, the super-Poissonian and sub-Poissonian (see below) distributions can be lost due to the lack of 1:1-correspondence in the detection system, but any deviations from the Poissonian distribution will be related to the character of the source, not to the random selection. We elaborate on this degradation in the final paragraphs of the section.

These results are of course obvious, because $|m\rangle$ contains m photons per definition, so every measurement of the photon number must result in m . We see that in the framework of this model it is fully possible to have a photocount distribution with variance zero which is less than the mean number of photocounts. On the other hand the photon number states are highly unclassical, because the mean value of their transverse electric field \mathbf{E}_T and the magnetic field \mathbf{B} are zero, $\langle \mathbf{E}_T \rangle = \langle \mathbf{B} \rangle = 0$ (cf. Eq. (50) in Sect. 2.3.3). Therefore we would like to repeat the above analysis for the coherent state $|z\rangle$ defined by Eq. (52) and expressed in terms of the photon number states as in Eq. (51):

$$|z\rangle = e^{-|z|^2/2} \sum_{n=0}^{\infty} \frac{z^n}{\sqrt{n!}} |n\rangle, \quad z \in \mathbb{C},$$

where we again consider a single mode only. In Appendix B we demonstrate that the probability distribution for having n photons in the coherent state $|z\rangle$ is given by the Poissonian distribution (Eq. (202)):

$$P_{|z\rangle}(n) = e^{-\langle n \rangle} \frac{\langle n \rangle^n}{n!},$$

where the mean number of photons is $\mu = |z|^2$ and the variance of the number of photons is μ as well. In other words, the photon statistics of the coherent state $|z\rangle$ corresponds to the photocount statistics of a perfectly coherent classical beam. Of course, this was to be expected, since the coherent states are the quantum-mechanical equivalent of classical electromagnetic waves.

We now ask whether there exists states for which the measured variance is non-zero, but less than the mean photon number. The obvious candidate is a superposition of the photon number states. Consider, for instance, $|\psi\rangle = a|1\rangle + b|2\rangle$, where $|a|^2 + |b|^2 = 1$ due to the usual normalization condition. We calculate the mean number of photocounts for $|\psi\rangle$:

$$\mu = \langle \psi | \hat{n} | \psi \rangle = |a|^2 + 2|b|^2,$$

and the variance:

$$\sigma_n^2 = \langle \psi | \hat{n}^2 | \psi \rangle - \langle \psi | \hat{n} | \psi \rangle^2 = |a|^2 + 4|b|^2 - (|a|^2 + 2|b|^2)^2 = |a|^2 + 4|b|^2 - |a|^4 - 4|b|^4 - 4|a|^2|b|^2.$$

Both expressions can be simplified by the fact that $|b|^2 = 1 - |a|^2$:

$$\begin{aligned} \mu &= |a|^2 + 2 - 2|a|^2 = 2 - |a|^2 \\ \sigma_n^2 &= |a|^2 - |a|^4, \end{aligned}$$

so it is always true that $\sigma_n^2 < \mu$.

Another possibility is to consider a pure photon number state, but this time we assume that the efficiency of the detector is less than one or that there are optical losses in the system (or both). Thus we examine a situation where it is not true that every emitted photon is registered by the detector (see the footnote on p. 83). A non-perfect detector can be modelled by an optical system consisting of a lossless beam splitter placed in front of a perfect detector, because it is irrelevant whether the photons are lost inside or outside of the detector. Such a model is based on the rigorous statistical theory of quantum photodetection developed by Kelley and Kleiner [103], but we will follow the less formal treatment given by Funk and Beck [104].

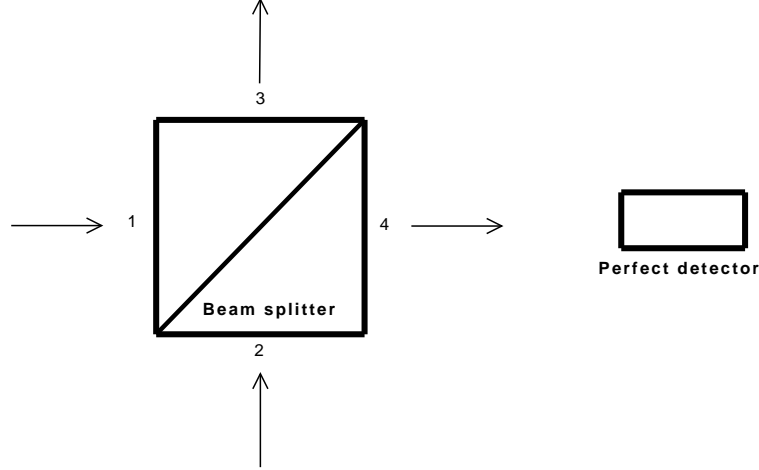


Figure 23: Modelling a non-perfect photodetector with the help of a lossless beam splitter placed in front of a perfect detector. The numbers 1-4 label the input ports (1 and 2) and the output ports (3 and 4) of the beam splitter.

The optical system under consideration is presented in Fig. 23. The light beam enters through the input port no. 1 of the beam splitter and is represented as a photon number state $|n\rangle_1$. The input port no. 2 is unused, so we relate to it the zero energy state $|0\rangle_2$ (refer to Sect. 5.2.2 for the presentation of the quantum model of the beam splitter). Therefore the total input state can be written as the tensor product $|n\rangle_1 \otimes |0\rangle_2$ abbreviated in the following to $|n; 0\rangle$. The perfect photodetector is placed in front of the output port no. 3, and all four ports are represented as the annihilation operators \hat{a}_i where i is the port number. We relate the output ports to the input ports using the reflection coefficients R_1 and R_2 and the transmission coefficients T_1 and T_2 of the beam splitter (see Eq. (142) on p. 93):

$$\begin{aligned}\hat{a}_3 &= R_1\hat{a}_1 + T_2\hat{a}_2 \\ \hat{a}_4 &= T_1\hat{a}_1 + R_2\hat{a}_2\end{aligned}$$

Because the beam splitter is lossless, the number of photons passing through it (and hence the energy) has to be conserved, and the coefficients have to satisfy conditions given later in Eqs. (131)-(132) (p. 90). We choose a solution where $R_1 = -R_2 \equiv R$ and $T_1 = T_2 \equiv T$, so the above expressions can be rewritten as:

$$\begin{aligned}\hat{a}_3 &= R\hat{a}_1 + T\hat{a}_2 \\ \hat{a}_4 &= T\hat{a}_1 - R\hat{a}_2.\end{aligned}$$

Since the photodetector is placed behind the output port no. 4, we calculate the photon statistics related to \hat{a}_4 . We determine the photon number operator \hat{n}_4 :

$$\begin{aligned}\hat{n}_4 &= \hat{a}_4^\dagger\hat{a}_4 = (T^*\hat{a}_1^\dagger - R^*\hat{a}_2^\dagger)(T\hat{a}_1 - R\hat{a}_2) = |T|^2\hat{a}_1^\dagger\hat{a}_1 + |R|^2\hat{a}_2^\dagger\hat{a}_2 - T^*R\hat{a}_1^\dagger\hat{a}_2 - R^*T\hat{a}_2^\dagger\hat{a}_1 = \\ &|T|^2\hat{n}_1 + |R|^2\hat{n}_2 - T^*R\hat{a}_1^\dagger\hat{a}_2 - R^*T\hat{a}_2^\dagger\hat{a}_1,\end{aligned}$$

Now can find the mean number of photons emerging from the output port no. 4:

$$\langle n_4 \rangle = \langle n; 0 | \hat{n}_4 | n; 0 \rangle = \langle n; 0 | \left(|T|^2 \hat{n}_1 + |R|^2 \hat{n}_2 - T^* R \hat{a}_1^\dagger \hat{a}_2 - R^* T \hat{a}_2^\dagger \hat{a}_1 \right) | n; 0 \rangle = |T|^2 n, \quad (121)$$

and the corresponding variance:

$$\begin{aligned} (\Delta n_4)^2 &= \langle n; 0 | \hat{n}_4^2 | n; 0 \rangle - \langle n; 0 | \hat{n}_4 | n; 0 \rangle^2 = |T|^4 n^2 + |T|^2 |R|^2 n - |T|^4 n^2 = \\ &|T|^2 |R|^2 n = (1 - |T|^2) \langle n_4 \rangle, \end{aligned} \quad (122)$$

where in the end we have used the fact that $|R|^2 + |T|^2 = 1$ for a lossless beam splitter, and in order to calculate $\langle n; 0 | \hat{n}_4^2 | n; 0 \rangle$ we have employed the commutation relation $[\hat{a}_i, \hat{a}_j] = \delta_{ij}$. Since the detector placed behind the output port no. 4 is assumed to be perfect, Eqs. (121)-(122) give us also the mean photocount number and the variance of photocounts. Now, $|T|^2$ represents the intensity transmission of the beam splitter, so we see that high $|T|^2$ results in low losses of the photons and vice versa. In our model $|T|^2$ is equivalent to the efficiency ϵ of a non-perfect detector. We observe that as $|T|^2 \equiv \epsilon$ tends to 1, the measured variance tends to zero, Eq. (122) becomes Eq. (120) and we have the sub-Poissonian photocount distribution. On the other hand, as ϵ tends to zero and the detector becomes less and less efficient, $(\Delta n_4)^2 \rightarrow \langle n_4 \rangle$, so the photocount distribution degrades to the Poissonian case.

Using the same formalism it could be shown that for a coherent state input $\langle n_4 \rangle = (\Delta n_4)^2 = \epsilon n$ [104]. Thus the attenuation of the coherent light beam decreases the mean number of photocounts, but the relation between the mean and the variance remains typical for the Poissonian distribution. This relation can be in general quantified by introduction of the Fano factor F defined as the ratio of the variance to the mean:

$$F \equiv \frac{(\Delta n)^2}{\langle n \rangle}.$$

We see that $F = 1$ for the Poissonian distribution, $F < 1$ for the sub-Poissonian distribution and $F > 1$ for the super-Poissonian distribution. Alternatively, the signal-to-noise ratio SNR might be used (Saleh and Teich [48], Chapter 18). It is defined as:

$$SNR = \frac{\langle n \rangle^2}{(\Delta n)^2},$$

so $SNR = \langle n \rangle$ in the case of the Poissonian distribution.

We have seen how it is possible to obtain the sub-Poissonian distribution of photocounts in the corpuscular theory. Taking into account the photon losses in the optical system, we have made a simple model where the variance of photocounts varies smoothly between 0 and 1, something that was not possible in the semiclassical model. Since the random selection of photons from the original stream played an important role in the above discussion, we end it by presenting (without proof) the general formula for the final (measured) photocount distribution $P(n)$ given the initial distribution of emitted photons $P_0(r)$ and the total intensity transmittance $|T|^2 \equiv \mathcal{T}$ of the optical system (Saleh and Teich [48], Chapter 12):

$$P(n) = \sum_{r=n}^{\infty} \binom{r}{n} \mathcal{T}^r (1 - \mathcal{T})^{r-n} P_0(r).$$

5.1.4 Concluding remarks

In the foregoing two sections we have reviewed the theory of photocount statistics in the framework of the semiclassical and the corpuscular model. In Chapter 4 we also examined the classical theory of optical coherence and correlations, and in the closing paragraphs of Chapter 4.4 we presented results that follow only from the theory of quantum correlations (i.e. when the electromagnetic field is quantized). Now we can summarize the crucial differences between the (semi)classical and quantum models of radiation with respect to fluctuation correlations and photocount statistics:

- Quantization of the electromagnetic field allows for weaker correlations of intensity fluctuations than are possible within the classical model. “Weaker” must be understood in the sense of breaking inequalities given by Eq. (104)-(105) (p. 72):

$$\begin{aligned}\gamma^{(2)}(\mathbf{r}, \mathbf{r}, 0) &\geq 1 \\ \gamma^{(2)}(\mathbf{r}, \mathbf{r}, 0) &\geq \gamma^{(2)}(\mathbf{r}, \mathbf{r}, \Delta t \neq 0)\end{aligned}$$

A situation where $\gamma^{(2)}(\mathbf{r}, \mathbf{r}, 0) < \gamma^{(2)}(\mathbf{r}, \mathbf{r}, \Delta t \neq 0)$ (not necessarily for all $\Delta t \neq 0$) is commonly interpreted as antibunching of photons.

- The semiclassical model of the photodetection process sets a lower theoretical bound for the variance, and this bound is equal to the mean value of photocounts (Eq. (117)). The variance in the corpuscular model, however, can be arbitrarily low (sub-Poissonian). This is due to the fact that in the corpuscular model light may be represented in terms of the highly nonclassical photon number states, and in the case of pure number states the variance is zero per definition (see Sect. 2.3.3). In fact, the occurrence of sub-Poissonian photocount statistics is equivalent (at least for a stationary field) to a situation where $\gamma^{(2)}(\mathbf{r}, \mathbf{r}, 0) < 1$ (Zou and Mandel, [105]).

It remains to ask whether antibunching and/or sub-Poissonian photocount statistics were observed experimentally, and the answer is positive. Sub-Poissonian statistics was obtained for instance by Short and Mandel [106] employing resonance fluorescence of a single atom, by Teich and Saleh [107] who excited mercury atoms using a regularized electron flow, and by Tapster, Rarity and Satchell [108] who used parametric down-conversion. Antibunched light was generated (among others) by Kimble et al. [109] using resonance fluorescence, by Kurtsiefer et al. [110] who examined single photons generated from vacancy centers in diamond and by Santori et al. [111] who measured light emitted from a quantum dot. These were all instances of nonclassical light that the (semi)classical theories could not account for³⁸.

We immediately note, however, that the applicability of the semiclassical model is somewhat limited. Let us focus on the photocount statistics, and let us consider a simple, but illustrative example with a classical source. With “classical” we mean that the source is thermal (but made quasi-monochromatic using appropriate filtering) or partially coherent (as a laser), so results of any photocount measurement performed on emitted light should be in accordance with the semiclassical model. Let us now, however, equip the source

³⁸Antibunching and sub-Poissonian statistics are often directly associated with each other, but in fact these two phenomena are not equivalent [105]. In other words, $\gamma^{(2)}(\mathbf{r}, \mathbf{r}, 0) < 1$ does not imply $\gamma^{(2)}(\mathbf{r}, \mathbf{r}, 0) < \gamma^{(2)}(\mathbf{r}, \mathbf{r}, \Delta t \neq 0)$ (for some Δt), or vice versa.

with a shutter which opens and closes periodically in such a way that it remains open for time T_O and then is closed for time T_C . These time durations are chosen in order to satisfy $T_C \gg T_O \approx \tau_{\text{dead}}$ where τ_{dead} is dead time of the detector employed, and this detector may well be a single-photon counting module. If the value of τ_{dead} is realistically chosen to lie around the order of magnitude 10^{-9} - 10^{-8} ns (see Ch. 6.4), the shutter has to work very fast and the scheme may be very difficult to realize in practice, but is certainly possible in principle.

The radiative field produced by our combination of the source and the shutter is obviously (using the undulatory picture) a sequence of wave packets. The width of each wave packet is approximately T_C and the distance between their midpoints is T_O . Such a field may be easily described classically. Now, when a single wave packet reaches the detector, it will give rise to maximally one photocount (because $T_O \approx \tau_{\text{dead}}$), and if the radiation is intense enough, most wave packets will be registered by the detector in this way. Thus the detector output would consist of a very regular sequence of photocounts where the variance is clearly lower than the mean.

The paradox may be resolved easily: The semiclassical model is not able to account for such a situation, because we have regularized the light beam and took into explicit consideration the detector dead time. It could then be argued that in our setup we do not examine the classical light source *per se*, but only a radiation field emerging from this source and prepared in a very special manner. Thus our photocount statistics would not have any real significance.

Let us notice, however, that in the aforementioned experiments involving nonclassical light the situation might be somewhat similar. The nonclassical light sources consist of small groups of atoms (or, preferably, single atoms) which are resonantly and regularly excited using laser, so comparison with the shutter setup seems appropriate. Besides, the stationarity condition – on which predictions of the different models usually rest – is not paid explicit attention by most of the authors [106] [108] [109] [110] [111]. Teich and Saleh [107] claim that their sub-Poisson source is stationary, but they neither elaborate on it or substantiate it. It seems that both the stationarity condition and the detector dead time limitation should be examined with greater care in the case of nonclassical light sources, because only if the first is fully satisfied and the latter deemed unimportant, the semiclassical model could be unambiguously dismissed. On the other hand, one could try to extend the semiclassical model in order to accommodate regularizing effects, and then try to apply this modified model to nonclassical light sources. Our above example with the shutter experiment shows that such extensions are certainly possible.

There are also other possible ways of improving the semiclassical model. One could examine the photodetection process itself in greater detail: seek involvement of new effects at very low intensities of impinging light and put more emphasis on fluctuations inherent to the detector. Furthermore, the semiclassical model is built around the very simple Eq. (112) (p. 80). Admittedly this equation can be demonstrated in a rigorous way, but the proof assumes that the interaction time between the electromagnetic field is much longer than the period of the field oscillation and much shorter than the coherence time. This assumption is not necessarily unreasonable, but nonetheless the length of the interaction time is chosen *a priori*. It would be interesting to see what alternatives to Eq. (112) another choice of interaction time would yield, and whether the semiclassical model could be modified considerably on such basis.

5.2 Beam splitter

The beam splitter is apparently a very simple optical component, but its workings may be investigated from several angles. We review the basic features of the classical (Sect. 5.2.1) and the quantum (Sect. 5.2.2) model of the beam splitter behaviour where we will loosely follow Bachor and Ralph [112] and Loudon [52] with some calculations carried out explicitly. In the end we discuss shortcomings of both models (Sect. 5.1.3) and sketch some alternatives.

In the experiments we are in fact using two types of beam splitters: polarizing and non-polarizing. The polarizing beam splitters combined with half wave plates play the role of filters and their sole task is to attenuate the light beam (in addition to the neutral density filters). The non-polarizing beam splitters, however, are used to split or to split and then recombine again the light beam prior to the measurements, so their workings have direct impact on the experimental results. Thus in the following presentation we will focus on the properties of non-polarizing beam splitters.

5.2.1 The classical description

In order to develop a classical model of the behaviour of a (non-polarizing) beam splitter, we need choose a proper representation of the incoming light beams. It is sufficient to limit our attention to the electric field strength of the fields, and we represent them again as complex analytic signals (see Ch. 4.1). Thus the light beam entering through the input port no. 1 is labeled as z_1 and the beam entering through the port no. 2 as z_2 (see Fig. 24). Assume the light beams to be monochromatic and perfectly coherent electromagnetic waves. Then we can write:

$$z_1(\mathbf{r}, t) = \alpha_1 e^{i\phi_1(\mathbf{r}, t)} \quad (123)$$

$$z_2(\mathbf{r}, t) = \alpha_2 e^{i\phi_2(\mathbf{r}, t)}, \quad (124)$$

where α_i is a constant amplitude and $\phi_i(\mathbf{r}, t)$ is a phase given as $\phi_i(\mathbf{r}, t) = \mathbf{k} \cdot \mathbf{r} - \omega t$ (\mathbf{k} , \mathbf{r} , ω and t have the usual meanings). In the same spirit we can represent the outgoing light beams (see Fig. 24) as

$$z_3(\mathbf{r}, t) = \alpha_3 e^{i\phi_3(\mathbf{r}, t)} \quad (125)$$

$$z_4(\mathbf{r}, t) = \alpha_4 e^{i\phi_4(\mathbf{r}, t)}, \quad (126)$$

where again the lower indices 3 and 4 stand for the output ports no. 3 and 4 of the beam splitter.

The incoming beams are partially transmitted and reflected by the beam splitter (possibly with different transmission and reflection coefficients for each beam), so the z_3 and z_4 are linear combinations of z_1 and z_2 :

$$z_3 = R_1 z_1 + T_2 z_2 \quad (127)$$

$$z_4 = T_1 z_1 + R_2 z_2. \quad (128)$$

Here R_i and T_i denote, respectively, the reflection and transmission coefficients for the electric field strength of beam i . These relations can be also written as a single matrix equation:

$$\mathbf{z}_{\text{out}} = \mathbf{M} \mathbf{z}_{\text{in}}, \quad (129)$$

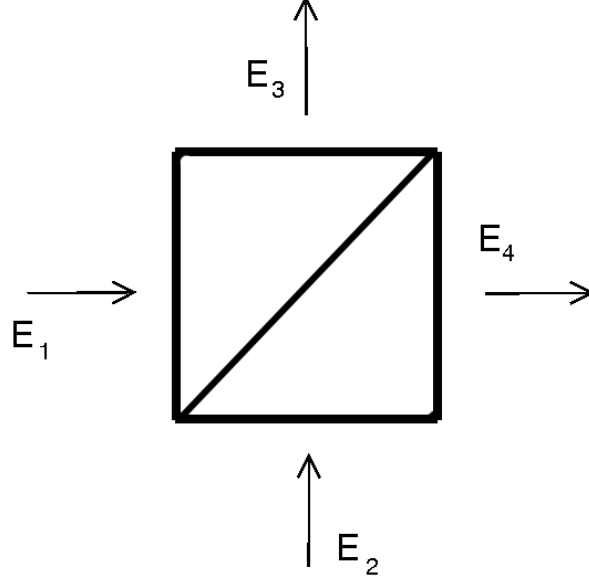


Figure 24: A schematic illustration of a beam splitter. The input ports are represented by the left and the lower side of the square; the output ports by the right and the upper side. The diagonal line is an all-dielectric coating on the boundary between two prisms constituting the beam splitter. The coating partially reflects and partially transmits the incoming light beams. The light beams are represented as complex analytic signals.

with $\mathbf{z}_{\text{out}} \equiv [z_3, z_4]^T$, $\mathbf{z}_{\text{in}} \equiv [z_1, z_2]^T$ and M being the beam splitter matrix defined as:

$$M \equiv \begin{bmatrix} R_1 & T_2 \\ T_1 & R_2 \end{bmatrix}.$$

We assume that the beam splitter is lossless, and from the energy conservation law we derive two constraints on the elements of M . The energy ϵ_i of a light beam i is proportional to the absolute square of the related complex analytic signal z_i . Thus we must have:

$$|z_1|^2 + |z_2|^2 = |z_3|^2 + |z_4|^2. \quad (130)$$

We substitute for z_3 and z_4 from Eqs. (127)-(128):

$$\begin{aligned} |z_1|^2 + |z_2|^2 &= (|R_1|^2 + |T_1|^2) |z_1|^2 + (|T_2|^2 + |R_2|^2) |z_2|^2 + \\ &\quad (R_1^* T_2 + T_1^* R_2) z_1^* z_2 + (T_2^* R_1 + R_2^* T_1) z_2^* z_1. \end{aligned}$$

This equation has to be valid for all z_1, z_2 , so it yields the two constraints on the elements of the beam splitter matrix:

$$|R_1|^2 + |T_1|^2 = |T_2|^2 + |R_2|^2 = 1 \quad (131)$$

$$R_1 T_2^* + T_1 R_2^* = 0, \quad (132)$$

so we observe at once that M is a unitary matrix:

$$M^\dagger M = \begin{bmatrix} R_1^* & T_1^* \\ T_2^* & R_2^* \end{bmatrix} \begin{bmatrix} R_1 & T_2 \\ T_1 & R_2 \end{bmatrix} = \begin{bmatrix} 1 & 0 \\ 0 & 1 \end{bmatrix} = I.$$

Let us now write the coefficients in a complex form. We define $R_j \equiv |R_j|e^{i\beta_{Rj}}$ and $T_j \equiv |T_j|e^{i\beta_{Tj}}$ with $j = 1, 2$. Then Eq. (132) gives:

$$\begin{aligned} |R_1||T_2|e^{i(\beta_{R1}-\beta_{T2})} + |T_1||R_2|e^{i(\beta_{T1}-\beta_{R2})} &= 0, \\ \frac{|R_1|}{|T_1|}e^{i(\beta_{R1}-\beta_{T2})} + \frac{|R_2|}{|T_2|}e^{i(\beta_{T1}-\beta_{R2})} &= 0 \end{aligned}$$

and, with the help of a phasor diagram, we observe that:

$$\frac{|R_1|}{|T_1|} = \frac{|R_2|}{|T_2|} \quad (133)$$

$$\beta_{R1} + \beta_{R2} - \beta_{T1} - \beta_{T2} = \pm\pi \quad (134)$$

Eq. (133) together with Eq. (131) gives:

$$|R_1| = |R_2| \equiv |R| \quad (135)$$

$$|T_1| = |T_2| \equiv |T|. \quad (136)$$

Thus if the beam splitter is observed to split at least one of the incoming beams into two equal parts (in the sense of energy balance), then the second beam will also be divided into two equal parts, and we will have $|R| = |T| = \frac{1}{\sqrt{2}}$.

Because of Eq. (134) we have a certain freedom in relating the phase factors of the reflection and transmission coefficients to each other. For instance, we could choose:

$$\beta_{R1} = \beta_{R2} = \beta_{T1} = 0, \quad \beta_{T2} = \pi, \quad (137)$$

which leads to:

$$R_1 = R_2, \quad T_1 = -T_2. \quad (138)$$

In other words, the incoming light beam no. 2 during the transmission is phase-displaced with π . A more symmetric choice would be:

$$\beta_{R1} = \beta_{R2} \equiv \beta_R, \quad \beta_{T1} = \beta_{T2} \equiv \beta_T, \quad (139)$$

which gives:

$$R_1 = R_2 \equiv R = |R|e^{i\beta_R}, \quad T_1 = T_2 \equiv T = |T|e^{i\beta_T}. \quad (140)$$

Eq. (134) yields then the necessary relation between β_R and β_T :

$$\beta_R - \beta_T = \pm\frac{\pi}{2}. \quad (141)$$

After this simple model has been established, we need go back and review some of our simplifying assumptions. These were: 1) perfect coherence and 2) monochromaticity of the incoming light beams, and

3) no energy loss in the beam splitter. We see at once that 1) is easiest to remove, because in our original expressions for the electric field strengths, Eqs. (123)-(126), the amplitudes α_i , instead of being constants, can vary in time. Such time-dependance is of no importance for the further treatment, so arbitrary input fields may be considered. When it comes to 2), if the light beam is not monochromatic, we could in principle express it as a sum (or an integral) over all single-frequency modes, then apply the above model for each mode separately, and in the end superpose again the outgoing modes. In such a situation the reflection and transmission coefficients would probably vary with modes, so we would have to use different beam splitter matrix M for each mode. An important requirement in such a situation is that the beam splitter would process modes linearly, i.e. that amplitudes belonging to different modes would not be mixed.

Finally, the possible energy loss ϵ_{loss} in the beam splitter is easily accounted for by rewriting Eq. (130) as:

$$|z_1|^2 + |z_2|^2 = |z_3|^2 + |z_4|^2 + \epsilon_{\text{loss}}.$$

Mathematically, the energy loss will be reflected by the fact that the beam splitter matrix will no longer be unitary (the sum of moduli squared of the reflection and transmission coefficients will no longer equal 1). The presence of ϵ_{loss} in the energy conservation formula will change the form of the resulting equations, but similar expressions for R_i and T_i will be still obtained in the end, and an description of the beam splitter analogous to the one above will emerge.

In our analysis we have not regarded the polarization of the electric fields involved, because, as remarked before, we wanted to consider the beam splitter of the non-polarizing type. The difference between non-polarizing and polarizing beam splitters reduces to the simple fact that, in the case of the latter, the reflection and transmission coefficients are polarization dependent. Thus the polarizing beam splitter can be used to split a incident beam into two beams of different polarizations. In this context one sometimes talks about S and P linear polarization states where P is defined as the direction of the electric vector field parallel to the surface of the mirror, and S is defined as the direction perpendicular to P [112].

5.2.2 The quantum model

We will now describe the properties of a beam splitter using the language of quantum mechanics. It is customary (see for instance Bacher and Ralph [112] or Loudon [52]) to represent the input and output ports as photon annihilation operators $a_{\mathbf{k}\lambda}$ ³⁹ (see Sect. 2.3.3). The lower indices $\mathbf{k}\lambda$ denote a particular mode of the electromagnetic field characterized by the wave vector \mathbf{k} and the polarization λ on which any given operator acts. $\hat{a}_{\mathbf{k}\lambda}$ is of course accompanied by its Hermitian adjoint $\hat{a}_{\mathbf{k}\lambda}^\dagger$ interpreted as the photon creation operator. In the following discussion we will again consider only monochromatic radiation, so the lower index $\mathbf{k}\lambda$ will be suppressed.

We would like to relate the input and output ports, and we draw analogy from the classical model. Thus we rewrite Eq. (129) as:

³⁹Some authors are slightly vague at this point, and say that the photon annihilation operators represent the input and output electromagnetic *fields*. However, as we will soon see, the fields are in fact expressed in terms of the photon number states. The photon annihilation operators should be thus unambiguously assigned to the input and output *ports* of the beam splitter. This makes of course sense, since the quantum-mechanical operators act on the quantum states, just as the beam splitter acts on the light beam. On the other hand, because the photon annihilation operators are not self-adjoint, it is not obvious what observable – if any – should they represent in this model.

$$\begin{bmatrix} \hat{a}_3 \\ \hat{a}_4 \end{bmatrix} = \begin{bmatrix} R_1 & T_2 \\ T_1 & R_2 \end{bmatrix} \begin{bmatrix} \hat{a}_1 \\ \hat{a}_2 \end{bmatrix}, \quad (142)$$

so once more we utilize the complex reflection and transmission coefficients. The matrix in the above expression may be for convenience again called the beam splitter matrix, but now we have to remember that the operators \hat{a}_i are also a part of the mathematical description of the beam splitter.

A peculiarity of the quantum model emerges at once. In the classical theory we could assume that there is only one incoming light beam, and set, for instance, $E_2(\mathbf{r}, t) = 0$. Then we would simply get from Eqs. (127)-(128) $E_3 = R_1 E_1$ and $E_4 = T_1 E_1$. However, neglecting one of the ports in the quantum model leads to a contradiction, because then we find:

$$\begin{aligned} \hat{a}_3 &= R_1 \hat{a}_1 \\ \hat{a}_4 &= T_1 \hat{a}_1 \\ [\hat{a}_3, \hat{a}_3^\dagger] &= R_1^2 [\hat{a}_1, \hat{a}_1^\dagger] = R_1^2 \\ [\hat{a}_4, \hat{a}_4^\dagger] &= T_1^2 [\hat{a}_1, \hat{a}_1^\dagger] = T_1^2 \\ [\hat{a}_3, \hat{a}_4^\dagger] &= R_1 T_1^* [\hat{a}_1, \hat{a}_1^\dagger] = R_1 T_1^*. \end{aligned}$$

We have used here the canonical commutation relation $[\hat{a}_i, \hat{a}_j^\dagger] = \delta_{ij}$ (cf. Eq. (41)). But because of the same relation, we expect to obtain:

$$\begin{aligned} [\hat{a}_3, \hat{a}_3^\dagger] &= 1 \\ [\hat{a}_4, \hat{a}_4^\dagger] &= 1 \\ [\hat{a}_3, \hat{a}_4^\dagger] &= 0 \end{aligned}$$

(Notice that \hat{a}_3 and \hat{a}_4 correspond to two different modes, because even if their frequencies and polarizations are identical, they propagate in different directions, so \mathbf{k}_3 and \mathbf{k}_4 differ.) Thus, the comparison of the two sets of equations yields $R_1^2 = 1$, $T_1^2 = 1$ and $R_1 T_1^* = 0$ which is nonsensical. However, if we include \hat{a}_2 in our equations, then we get:

$$\begin{aligned} [\hat{a}_3, \hat{a}_3^\dagger] &= [R_1 \hat{a}_1 + T_2 \hat{a}_2, R_1^* \hat{a}_1^\dagger + T_2^* \hat{a}_2^\dagger] = \\ &= [R_1 \hat{a}_1, R_1^* \hat{a}_1^\dagger] + [R_1 \hat{a}_1, T_2^* \hat{a}_2^\dagger] + [T_2 \hat{a}_2, R_1^* \hat{a}_1^\dagger] + [T_2 \hat{a}_2, T_2^* \hat{a}_2^\dagger] = \\ &= (|R_1|^2 + |T_2|^2) [\hat{a}_1, \hat{a}_1^\dagger] + (|T_1|^2 + |R_2|^2) [\hat{a}_2, \hat{a}_2^\dagger] \\ [\hat{a}_3, \hat{a}_4^\dagger] &= (R_1 T_1^* + T_2 R_2^*), \end{aligned}$$

so now the requirements are:

$$\begin{aligned} |R_1|^2 + |T_2|^2 &= |T_1|^2 + |R_2|^2 = 1 \\ R_1 T_1^* + T_2 R_2^* &= 0. \end{aligned}$$

These conditions differ slightly from Eqs. (131)-(132), but in the end they would yield the same results, i.e.

Eqs. (131)-(133). As far as the determination of the reflection and transmission coefficients is concerned, there is a consistency between the classical and the quantum model. In the quantum model, however, the electromagnetic fields from both input ports of the beam splitter must always be taken into consideration, even if the light beam is being sent only through one of them. The paradox is resolved by the existence of the omnipresent vacuum energy modes. In the absence of a “real” beam in one of the input ports (or, equivalently, when one of the ports is closed), it is the vacuum mode that contributes to the output modes, so we can never set \hat{a}_1 or \hat{a}_2 equal to zero.

We will now develop a simple mathematical description where one photon is being sent through the beam splitter. The evolution through the beam splitter is represented by a unitary operator \hat{U} . Let us denote by $|n\rangle_{i=1,2}$ the photon number state of the light beam with n photons entering the input port no. $i = 1, 2$, and by $|n\rangle_{j=3,4}$ the state with n photons leaving through the output port no. $j = 3, 4$. Thus $|1\rangle_1 |0\rangle_2$ represents a state with one photon entering through the input port no. 1 and none entering through the input port no. 2. We examine how the beam splitter acts on $|1\rangle_1 |0\rangle_2$:

$$\hat{U} |1\rangle_1 |0\rangle_2 = \hat{U} \hat{a}_1^\dagger |0\rangle_1 |0\rangle_2 = \hat{U} \hat{a}_1^\dagger (\hat{U}^\dagger \hat{U}) |0\rangle_1 |0\rangle_2 = \hat{U} \hat{a}_1^\dagger \hat{U}^\dagger |0\rangle_3 |0\rangle_4,$$

where the last equality is a logical consequence of the fact that if no photons are sent into the beam splitter, then surely none will emerge from it (the number of photons is preserved). $\hat{U} \hat{a}_1^\dagger \hat{U}^\dagger$ represents the time-reversed evolution through the beam splitter, so with the help of Eq. (142) we represent \hat{a}_1^\dagger in terms of \hat{a}_3^\dagger and \hat{a}_4^\dagger , and obtain:

$$\hat{U} \hat{a}_1^\dagger \hat{U}^\dagger |0\rangle_3 |0\rangle_4 = \left(R_1^* \hat{a}_3^\dagger + T_1^* \hat{a}_4^\dagger \right) |0\rangle_3 |0\rangle_4 = R_1^* |1\rangle_3 |0\rangle_4 + T_1^* |0\rangle_3 |1\rangle_4.$$

The result is a superposition of two photon number states: In the first one the input photon leaves through the output port no. 3, and in the second one the input photon leaves through the output port no. 4. The probability amplitudes of the superposition are the complex conjugates of the appropriate reflection and transmission coefficients. Given the postulated indivisibility of the photons, such a result could be intuitively expected.

Let us now consider a situation where two photons are sent into the beam splitter, one through each input port⁴⁰, so the input photon number state is $|1\rangle_1 |1\rangle_2$. We have:

$$\begin{aligned} \hat{U} |1\rangle_1 |1\rangle_2 &= \hat{U} \hat{a}_1^\dagger \hat{a}_2^\dagger |0\rangle_1 |0\rangle_2 = \hat{U} \hat{a}_1^\dagger \hat{U}^\dagger \hat{U} \hat{a}_2^\dagger \hat{U}^\dagger \hat{U} |0\rangle_1 |0\rangle_2 = \left(\hat{U} \hat{a}_1^\dagger \hat{U}^\dagger \right) \left(\hat{U} \hat{a}_2^\dagger \hat{U}^\dagger \right) |0\rangle_3 |0\rangle_4 = \\ &= \left(R_1^* \hat{a}_3^\dagger + T_1^* \hat{a}_4^\dagger \right) \left(T_2^* \hat{a}_3^\dagger + R_2^* \hat{a}_4^\dagger \right) |0\rangle_3 |0\rangle_4 = \\ &= \sqrt{2} R_1^* T_2^* |2\rangle_3 |0\rangle_4 + \sqrt{2} T_1^* R_2^* |0\rangle_3 |2\rangle_4 + (R_1^* R_2^* + T_1^* T_2^*) |1\rangle_3 |1\rangle_4 \end{aligned}$$

We remember that the coefficients must satisfy some specific conditions. Using, for instance, Eq. (137)-(138),

⁴⁰It seems natural to require that the photons are present at both inputs at the same time. Notice, however, that the time aspect is altogether absent in this rather crude model. When we work with the photon number states, we have to consider the optical field in its totality, and we are unable to track the propagation of single photons through space (see the remarks in Sect. 2.3.4). We will come back to this issue in the next section.

and assuming that we are using a 50:50 beam splitter (where $|R_i| = |T_i| = \frac{1}{\sqrt{2}}$), we obtain:

$$\hat{U} |1\rangle_1 |1\rangle_2 = \frac{1}{\sqrt{2}} |2\rangle_3 |0\rangle_4 + \frac{1}{\sqrt{2}} |0\rangle_3 |2\rangle_4. \quad (143)$$

Thus, with right conditions, there will occur a situation where we send one photon through each of the input ports, and the resulting state will be a superposition of $|2\rangle_3 |0\rangle_4$ and $|0\rangle_3 |2\rangle_4$. The subsequent measurement of the output arms will either show that both photons have left the beam splitter through the output port no. 3, or that the photons have left through the port no. 4. We will not, however, observe the case where there are single photons in each output, because the term $|1\rangle_3 |1\rangle_4$ has cancelled. This is an example of quantum interference effect. We notice that this quantum interference could be discussed in the context of quantum entanglement of which the RHS of Eq. (143) is an instance. As remarked in the Introduction, the complex subject of the quantum entanglement lies outside the scope of the thesis, so we will not follow this line of reasoning further.

We examine also the case of the beam splitter acting on an coherent state $|z\rangle$ in one of the input ports. We will make use of the shift operator $\hat{D}(z)$ defined in Appendix B.3 (Eq. (197)):

$$\begin{aligned} \hat{U} |z\rangle_1 |0\rangle_2 &= \hat{U} \hat{D}_1(z) |0\rangle_1 |0\rangle_2 = \hat{U} \hat{D}_1(z) \hat{U}^\dagger \hat{U} |0\rangle_1 |0\rangle_2 = \hat{U} \hat{D}_1(z) \hat{U}^\dagger |0\rangle_3 |0\rangle_4 = \hat{U} \left(e^{z\hat{a}_1^\dagger - z^* \hat{a}_1} \right) \hat{U}^\dagger |0\rangle_3 |0\rangle_4 = \\ &= \left(e^{zR_1^* \hat{a}_3^\dagger + zT_1^* \hat{a}_4^\dagger - z^* R_1 \hat{a}_3 - z^* T_1 \hat{a}_4} \right) |0\rangle_3 |0\rangle_4 = \left(e^{zR_1^* \hat{a}_3^\dagger - z^* R_1 \hat{a}_3} \right) \left(e^{zT_1^* \hat{a}_4^\dagger - z^* T_1 \hat{a}_4} \right) |0\rangle_3 |0\rangle_4 = \\ &= \hat{D}(zR_1^*) \hat{D}(zT_1^*) |0\rangle_3 |0\rangle_4 = |zR_1^*\rangle_3 |zT_1^*\rangle_4 \end{aligned}$$

The factorization of exponentials was possible because $[\hat{a}_3, \hat{a}_4^\dagger] = [\hat{a}_3, \hat{a}_4] = 0$. We see that output state is a product of coherent states. In a similar way we can calculate the output state when there are two different coherent states entering the input ports of the beam splitter, $|z_A\rangle$ and $|z_B\rangle$. The final result is:

$$\hat{U} |z_A\rangle_1 |z_B\rangle_2 = e^{(z_A^* z_B R_1 T_2^* - z_A z_B^* R_1^* T_2)/2} |z_A R_1^* + z_B T_2^*\rangle_3 |z_A T_1^* + z_B R_2^*\rangle_4.$$

The output state is again a product of coherent states, but this time the input coherent states are mixed in the output, and there is an additional phase factor.

5.2.3 Shortcomings of the beam splitter model

After having presented the basic features of the classical and the quantum beam splitter, we would like now to point out and discuss shortcomings of both models. We are not claiming that they are erroneous in any direct way. The models have been successfully applied in the descriptions of many different experiments, and they are also essential elements of the frameworks of larger optical and quantum-optical theories. We will rather try to make a case that there are certain subtle, unclear aspects of the models that may bear relevance when one examines the nature of light by experimental means.

To begin with we notice that the beam splitter is treated as a black box. It is described in terms of its transfer characteristics which, given an input state, produce an output state. The models say almost nothing about the internal workings of the beam splitter. One could of course argue that a beam splitter is essentially a half-silvered mirror, so no detailed description of such simple a device should be ever needed.

However, exactly the same line of reasoning shows that the workings of the beam splitter is intimately connected with the principles governing the interaction between light and matter. After all, the half-silvered mirror is supposed to absorb the radiation incoming from two directions and then re-emit it again in two other directions. Since the issue of the light-matter interactions is given a lot of detailed thought in other situations (like the photoelectric effect, see Ch. 3.3; not to mention the whole theory of quantum electrodynamics), there is no reason for not raising it in the case of the beam splitter.

This lack of interest in the inner workings of the device is made apparent by the constancy of the reflection and transmission coefficients, $R_{i=1,2}$ and $T_{i=1,2}$. These coefficients are completely independent of the incoming radiation fields, and they neither possess any explicit time-dependence. This may seem unjustified when we recall that the electrons constituting the mirror of the beam splitter absorb and re-emit the radiation involved, so the dynamical properties of the electrons surely need to influence the whole process of beam splitting. On the other hand, these very properties are influenced by the radiation, so it is reasonable to believe that the characteristics of the radiation fields affect the way the fields themselves are divided inside the beam splitter. In other words, the description in terms of constant coefficients could be well appropriate in the equilibrium, but as soon as the first “segment” (however we define it) of the electromagnetic field irradiates the beam splitter, its behaviour changes and the next “segments” are processed differently. The aforementioned explicit time-dependence would be caused by the fact that even in the absence of any radiation the beam splitter system is not in a perfect equilibrium, but, for instance, oscillates around it in the phase space due to thermal influences.

In order to illustrate this problem, let us take a look at the classical model, and imagine that an electromagnetic field enters the beam splitter through the input port no. 1. We represent again the electromagnetic field with the help of the complex analytic signal $z_1(\mathbf{r}, t)$ where $z_1(\mathbf{r}, t)$ may be a general function of position and time. As noticed before, the field is split into $z_3 = R_1 z_1$ leaving through the port no. 3 and $z_4 = T_1 z_1$ leaving through the port no. 4. Thus the splitting of the original field is ideal, because the form of z_1 is not changed *at all*; and besides *no* fluctuations are introduced due to the interaction with the beam splitter⁴¹. From the strictly practical point of view, such ideal splitting is impossible. One could argue that any additional effects caused by the beam splitter, even if present, are minute, so there is no need for taking them into account. This is certainly true in experiments where the process of beam splitting is only a minor part of the general setup, and where during any single measurement of the split beam we integrate over relatively long time scales. However, in the experiments examining the wave-particle duality, the beam splitter is often the central element of the setup (as in coincidence measurements, or in a Mach-Zender interferometer), and the time scales corresponding to the passage of a “single photon” or a “single wave packet” may be very short. This leads us to the question whether a more elaborate model of the beam splitter would allow us to interpret the results of these experiments differently.

We will now consider one simple way the existing classical beam splitter model could be improved. It is not our goal to develop here a complete description, but only to show how the mathematics might be modified. We introduce the dependence on the electromagnetic field explicitly into the coefficients. For instance, the reflection coefficient R_1 could be written:

$$R_1 = \text{const.} \quad \rightarrow \quad R_1(t) = R_{1,0} + f_{R_1} [z_1(t - \tau), z_2(t - \tau)]$$

⁴¹Of course the *original* fluctuations will be transmitted through the beam splitter (and if there were two input fields, their fluctuations will be also mixed in the output). However, *no new* fluctuations will be produced.

where $R_{1,0}$ is the original constant value and f_{R_1} represents the change due to the influence of the input fields z_1 and z_2 at time $t - \tau$ where t is the time the value of R_1 is calculated for. More realistically, f_{R_1} should not depend on any single past values of z_1 and z_2 , because the influence is continuous. Thus we would write:

$$R_1(t) = R_{1,0} + f_{R_1}(S)$$

where S is the integral:

$$S = \int_{t-\tau}^t g(t') h[z_1(t'), z_2(t')] dt'.$$

Here $g(t')$ is an appropriate weighting function, and $h[z_1(t'), z_2(t')]$ decides how the past values of electric field strengths contribute to the present behaviour of the beam splitter. f_{R_1} would be then used in order to calculate the contribution of the integral to R_1 . Notice that τ would correspond to the relaxation time, and that the maximal value of $f_{R_1}(S_1, S_2)$ should be much smaller than $R_{1,0}$ – because, as remarked before, such additional beam splitter effects must be minute. Similar relations to that for $R_1(t)$ could be derived for $R_2(t)$, $T_1(t)$ and $T_2(t)$. In the case of the lossless beam splitter the constraints given by Eqs. (131)-(132) are assumed to be still valid, so these could be used in order to examine the relations between $R_{1,0}$, $R_{2,0}$, f_{R_1} , f_{R_2} and so on. Deducing the actual form of all these new function would not be an easy task. Apart from “intelligent guessing”, one could try to apply principles of quantum electrodynamics describing the light-matter interactions. Then we would have to look for any new predictions regarding the behaviour of the beam splitter and try to confirm them (or refute) empirically⁴².

In the case of the quantum model, the same remarks still apply, because the reflection and transmission coefficients are used here as well (as a matter of fact they are taken directly from the classical model). In addition, however, there is the problem of the Fock states being unable to say anything about how positions of single photons change with time. As noted in Section 2.3.4, the photon number states formalism treats the electromagnetic field holistically. Consider, for instance, the situation described by Eq. (143). The model tells us that if one photon enters the beam splitter through the input port no. 1, and another one through the input port no. 2, and if we place two perfect detectors in front of the output ports, then we will either register two photons leaving the beam splitter through the output port no. 3, or two photons leaving through the output port no. 4. It is striking that the model do not make any claims on the original photons entering the beam splitter simultaneously⁴³. Thus we do not know what is the maximal time interval allowed between these two events, and how the time difference involved would affect the output state (if at all). We do not know neither how the photons in the output state will be distributed in time.

In many experimental situations these kinds of information may be unnecessary for the correct prediction of the results. However, the same cannot be said about the experiments regarding the wave-particle duality. There are three reasons for this state of affairs. First and foremost, in order to resolve (or at least understand better) the duality problem, we crave to gain an intimate knowledge about what happens with a segment of

⁴²Another possibility worth considering would be to model the beam splitter in terms of driven harmonic oscillations: $\ddot{z}_3 + b\dot{z}_3 + kz_3 = f(z_1, z_2)$, where z_3 is an output field, b and k are constants, and the function $f(z_1, z_2)$ describes the influence of the input fields. The emergence of resonance for some specific z_1 and z_2 would reflect the fact that the reflection and transmission coefficients vary with modes, particularly with the wavelength, as seen in Fig. 33 on p. 112. Furthermore, some choices of the function f would naturally lead to interesting additional effects, also at low intensities of the incoming fields.

⁴³Unless this simultaneity requirement is implicitly present in a definition of a state like $|1\rangle_1 |1\rangle_2$, i.e. unless we read $|1\rangle_1 |1\rangle_2$ as “a situation where a photon number state $|1\rangle$ enters the input port no. 1 and at the same time another photon number state $|1\rangle$ enters the input port no. 2”. However, this solution cannot be applied to cases with photon number states $|n > 1\rangle$, because we cannot require that all n photons from a photon number state $|n > 1\rangle$ are present at the same point in spacetime.

a light beam⁴⁴ between its emission from the source and its detection at the source. Any shortcomings of the quantum model as problematic as the ones mentioned in the previous paragraph could hardly help us in achieving such knowledge. Secondly, the experiments involving the wave-particle duality rely heavily on coincidence and interferometry measurements where the time aspect plays a prominent role. Any improvements on the model which would stop treating “photons” holistically could thus help us in predicting, describing and quantifying possible new effects. And, finally, such holistic approach to the electromagnetic field is of no help when we try to understand better the nature of a “photon”, because it does not allow us to speculate about what “photon” is.

We note that the critical remarks from the last two paragraphs do not apply only to the quantum model of the beam splitter, but to the photon number states formalism on which this model is based. This is an important point, because the successes the corpuscular theory of light have achieved on the quantitative field make us easily forget that the same theory has serious problems when it comes to answering qualitative questions about the physical reality of different phenomena. It is curious that the situation of the classical model of light may be seen as the reverse of the situation of the quantum model – the (semi)classical model is (so far) not able to properly predict all experimental results (see Sect. 5.1.4), but it presents us with a much clearer physical picture of the beam splitting process. If we refer to the three items from the previous paragraph, we see that 1) the classical model assumes that the light beam propagates from the source to the detector as an electromagnetic wave, or, more precisely, as a wavelike variation of the electromagnetic field; 2) the propagation of this electromagnetic wave can be easily analyzed as a function of time; and 3) the light may be depicted as an electromagnetic wave with varying degree of coherence (see Chapter 4).

We conclude the above section by saying that there is room for improvement in both the classical and the quantum model of the beam splitter. However, while an improvement of the classical model could be achieved by introducing new factors to the model without revising the underlying theory of light, an improvement of the quantum model will likely require us to modify some elements of its theoretical foundations.

5.3 The shape of the laser beam

The aim of the following section is to give a quantitative description of the laser beam shape. First we show how one can spatially confine an ordinary plane wave using an appropriate envelope. We derive the paraxial Helmholtz equation that the envelope has to satisfy (Sect. 5.3.1). Then we present a simple solution of the equation which embodies the complex envelope of the Gaussian beam; the subsequent analysis of the expression for the complex amplitude allows us to recognize several quantities of physical significance (Sect. 5.3.2). Also, we quickly review the ABCD law which is an important tool in examining how different optical elements influence the Gaussian beam (Sect. 5.3.3).

In our presentation we follow mainly Saleh and Teich [48] and Milonni and Eberly [100], but the formula for the complex amplitude of the Gaussian beam, Eq. (157), will be derived more explicitly than it is usually done.

Note that this chapter is rather technical and we aim at establishing the mathematical theory that will be used in Chapter 5.3.3. Specifically, the shape of the laser beam will not be discussed in the context of the wave-particle duality as different models of photodetection (Section 5.1.4) and beam splitters (Sect. 5.2.3) were.

⁴⁴The phrase “segment of a light beam” may sound artificial in this context, but we want to avoid the terms “wave packet” or “photon” which suggest undulatory or corpuscular view of light, respectively.

5.3.1 The paraxial Helmholtz equation

In terms of the classical theory the laser beam consists of an electromagnetic field propagating undulatorily through space, the laser being its source. The electromagnetic field has to satisfy the Maxwell equations, Eq. (2.1)-(2.4), and thus the wave equation, Eq. (2.10), or, alternatively, Eq. (2.11). In the following we will use the latter form:

$$\nabla^2 u - \frac{1}{v^2} \frac{\partial^2 u}{\partial t^2} = 0. \quad (144)$$

We recall that u denotes any component of the electric or magnetic field constituting the beam, and v is the phase velocity of the component. This velocity is generally given as $v = \frac{c}{n}$, where c is the speed of light in vacuum and n is the refractive index of the medium. Eq. (144) has to be satisfied for all six components (three electric and three magnetic), but we will focus on only one of them, the treatment of the other five being completely similar. Thus the scalar function of position \mathbf{r} and time t , $u(\mathbf{r}, t)$, can for instance represent a single component of the electric field. $u(\mathbf{r}, t)$ is sometimes called the wavefunction (not to be confused with the wave function of quantum mechanics). It could be represented with the help of the complex analytic signal (see Ch. 4.1), but it is unnecessary to apply the formalism of the complex analytic signal in the discussion of the laser beam shape.

We saw in Chapter 2.1 that the simplest solution of the wave equation is a plane wave described by a vector parameter \mathbf{k} (the wave vector) related to the spatial argument, and a scalar parameter ω (the angular frequency) related to the temporal argument. But obviously these solutions, given by Eqs. (2.13)-(2.14), cannot be applied in the case of the laser beam, because the laser beam is strongly limited in space, i.e. the wavefunction has to tend rapidly to zero outside some relatively narrow region (see the remark in Ch. 3.2). Specifically, we need a solution that gives us a paraxial wave characterized by a wavefront normal which makes a small angle with the optical axis of the system (the propagation axis). Also, the paraxial wave needs lie close to the axis. Such a solution can be obtained by modulating a plane wave solution with a proper position-dependent envelope $A(\mathbf{r})$. If we choose the z -axis of the coordinate system to be the optical axis of our model, we get:

$$u(\mathbf{r}, t) = A(\mathbf{r})e^{-j(kz - \omega t)}. \quad (145)$$

It remains to see what conditions constrain $A(\mathbf{r})$ so Eq. (144) is satisfied. First and foremost, the envelope has to vary slowly in the z -direction within a distance that is small relatively to the wavelength $\lambda = \frac{2\pi}{k}$, because we want the wavefunction to resemble a plane wave (propagating in the z -direction) at small spatial scale. The partial derivatives $\frac{\partial A}{\partial z}$ must change slowly for the same reason. If ΔA denotes the change of A within a small (i.e. equal to the wavelength) distance Δz in the positive z -direction, we have:

$$|\Delta A| = \left| \frac{\partial A}{\partial z} \right| \Delta z = \left| \frac{\partial A}{\partial z} \right| \lambda \ll |A| \Rightarrow \left| \frac{\partial A}{\partial z} \right| \ll \frac{|A|}{\lambda} \sim k|A|. \quad (146)$$

Similarly, if $\Delta \frac{\partial A}{\partial z}$ denotes the change of the partial derivative of A , we obtain:

$$\left| \Delta \frac{\partial A}{\partial z} \right| = \left| \frac{\partial^2 A}{\partial z^2} \right| \Delta z = \left| \frac{\partial^2 A}{\partial z^2} \right| \lambda \ll \left| \frac{\partial A}{\partial z} \right| \ll k|A| \Rightarrow \left| \frac{\partial^2 A}{\partial z^2} \right| \ll \frac{k|A|}{\lambda} \sim k^2|A|, \quad (147)$$

(If $A(\mathbf{r}, t)$ is a complex function, as is usually the case, the inequalities have to apply separately to the

absolute values of real and imaginary parts.) We substitute now from Eq. (145) in Eq. (144):

$$\begin{aligned} & \nabla^2 \left[A(\mathbf{r})e^{-j(kz-\omega t)} \right] - \frac{1}{v^2} \frac{\partial^2}{\partial t^2} \left[A(\mathbf{r})e^{-j(kz-\omega t)} \right] = \\ & (\nabla_T^2 A)e^{-j(kz-\omega t)} + \frac{\partial}{\partial z} \left[\frac{\partial A}{\partial z} e^{-j(kz-\omega t)} - jkAe^{-j(kz-\omega t)} \right] + A \frac{\omega^2}{v^2} e^{-j(kz-\omega t)} = \\ & \left[\nabla_T^2 A + \frac{\partial^2 A}{\partial z^2} - 2jk \frac{\partial A}{\partial z} - k^2 A + A \frac{\omega^2}{v^2} \right] e^{-j(kz-\omega t)} = \nabla_T^2 A - 2jk \frac{\partial A}{\partial z} = 0 \end{aligned}$$

∇_T^2 is the transverse Laplacian, $\nabla_T^2 \equiv \frac{\partial^2}{\partial x^2} + \frac{\partial^2}{\partial y^2}$, and in the second to last transition we have set $\frac{\omega}{v} = k$ and we have neglected $\frac{\partial^2 A}{\partial z^2}$ in accordance with Eq. (147). Thus we have obtained a differential equation that the envelope $A(\mathbf{r})$ needs to satisfy:

$$\nabla_T^2 A(\mathbf{r}) - 2jk \frac{\partial A(\mathbf{r})}{\partial z} = 0. \quad (148)$$

The equation is called the slowly varying envelope approximation of the Helmholtz equation or the paraxial Helmholtz equation.

5.3.2 The Gaussian beam

A possible solution of Eq. (148) is the paraboloidal wave:

$$A(\mathbf{r}) = \frac{A_1}{z} e^{-jk \frac{x^2+y^2}{2z}}, \quad (149)$$

with A_1 being a constant. The validity of the paraboloidal solution as a possible envelope can be checked by direct substitution from Eq. (149) into (148). By defining $\rho^2 \equiv x^2 + y^2$ it is possible to derive an auxillary expression:

$$\nabla_T^2 f(\rho^2) = 4[\rho^2 f''(\rho) + f'(\rho)]$$

where prime denotes differentiation with respect to ρ^2 . Then we obtain:

$$\begin{aligned} \nabla_T^2 A(\mathbf{r}) &= 4 \left[-\rho^2 \frac{k^2}{4z^2} A(\mathbf{r}) - \frac{jk}{2z} A(\mathbf{r}) \right] = \left[-\frac{\rho^2 k^2}{z^2} - \frac{2jk}{z} \right] A(\mathbf{r}) \\ 2jk \frac{\partial A(\mathbf{r})}{\partial z} &= 2jk \left[-\frac{1}{z} A(\mathbf{r}) + jk \frac{\rho^2}{2z^2} A(\mathbf{r}) \right] = \left[-\frac{2jk}{z} - \frac{\rho^2 k^2}{z^2} \right] A(\mathbf{r}) \end{aligned}$$

and the paraxial Helmholtz equation is obviously satisfied, the difference of both terms being identically zero.

It is, however, not the paraboloidal envelope that is most often used to model the laser beam, but the Gaussian envelope. The Gaussian solution can be simply obtained from the paraboloidal one by substituting z with $q(z) \equiv z - \xi$. If ξ is real, this corresponds to a trivial shift of the point \bar{z} on the z -axis about which the paraboloidal wave is centered in the xy - or the xz -plane (from $\bar{z} = 0$ to $\bar{z} = \xi$). However, ξ can be also taken to be complex, and then the new solution acquires altogether new properties. Choosing ξ to be purely imaginary, say $\xi = -jz_0$, results in the complex envelope of the Gaussian beam:

$$A(\mathbf{r}) = \frac{A_1}{q(z)} e^{-jk \frac{\rho^2}{2q(z)}}, \quad q(z) = z + jz_0 \quad (150)$$

$q(z)$ is known as the q-parameter of the Gaussian beam, and z_0 as the Rayleigh range.

The exponent in Eq. (150) is now not purely imaginary, but complex. Let us separate explicitly the real and the imaginary part of $q^{-1}(z)$:

$$\frac{1}{q(z)} = \frac{1}{z + jz_0} = \frac{z}{z^2 + z_0^2} - j \frac{z_0}{z^2 + z_0^2} \equiv \alpha - j\beta \quad (151)$$

We insert the expression for $q^{-1}(z)$, Eq. (151), into Eq. (150):

$$A(\mathbf{r}) = A_1(\alpha - j\beta) \exp\left[-jk\frac{\rho^2}{2}\alpha\right] \exp\left[-k\frac{\rho^2}{2}\beta\right]. \quad (152)$$

The complex number in the prefactor can be written in exponential form: $\alpha - j\beta = \tilde{W}e^{j\tilde{\zeta}}$ where both \tilde{W} and $\tilde{\zeta}$ are functions of the position z :

$$\begin{aligned} \tilde{W}(z) &\equiv \sqrt{\alpha^2 + \beta^2} = \frac{1}{\sqrt{z^2 + z_0^2}} = \frac{1}{z_0\sqrt{1 + \frac{z^2}{z_0^2}}} \\ \tilde{\zeta}(z) &\equiv \arctan\left(-\frac{\beta}{\alpha}\right) = \arctan\left(-\frac{z_0}{z}\right) = \arctan\left(\frac{z}{z_0}\right) - \frac{\pi}{2} \end{aligned}$$

We may now write α and β as:

$$\alpha = \frac{z}{z^2 + z_0^2} = z\tilde{W}^2(z) \equiv \frac{1}{R(z)} \quad (153)$$

$$\beta = \frac{z_0}{z^2 + z_0^2} = z_0\tilde{W}^2(z) \equiv \frac{\lambda}{\pi W^2(z)} \quad (154)$$

These curious definitions will be justified shortly, as we will see that the quantities $R(z)$ and $W(z)$ are of physical significance. Eq. (152) can be now expressed as:

$$A(\mathbf{r}) = A_1\tilde{W}e^{j\tilde{\zeta}} \exp\left[-jk\frac{\rho^2}{2R(z)}\right] \exp\left[-\frac{\rho^2}{W^2(z)}\right] \quad (155)$$

From Eq. (154) we extract the relationship between $\tilde{W}(z)$ and $W(z)$:

$$W(z) = \sqrt{\frac{\lambda}{\pi z_0}} \frac{1}{\tilde{W}(z)} = \sqrt{\frac{\lambda z_0}{\pi}} \sqrt{1 + \frac{z^2}{z_0^2}} \equiv W_0 \sqrt{1 + \frac{z^2}{z_0^2}}$$

where $W_0 \equiv \sqrt{\frac{\lambda z_0}{\pi}}$. Eq. (155) becomes:

$$\begin{aligned} A(\mathbf{r}) &= \frac{A_1}{z_0} \frac{W_0}{W(z)} \exp\left[-\frac{\rho^2}{W^2(z)}\right] \exp\left[-jk\frac{\rho^2}{2R(z)} + j\tilde{\zeta}(z)\right] = \\ &= \frac{A_1}{jz_0} \frac{W_0}{W(z)} \exp\left[-\frac{\rho^2}{W^2(z)}\right] \exp\left[-jk\frac{\rho^2}{2R(z)} + j\zeta(z)\right] \equiv \\ &= A_0 \frac{W_0}{W(z)} \exp\left[-\frac{\rho^2}{W^2(z)}\right] \exp\left[-jk\frac{\rho^2}{2R(z)} + j\zeta(z)\right] \end{aligned} \quad (156)$$

where we have defined

$$A_0 \equiv \frac{A_1}{jz_0}, \quad \zeta(z) \equiv \arctan\left(\frac{z}{z_0}\right)$$

Substituting for the envelope from Eq. (156) in the wavefunction, Eq. (145), yields our final result:

$$u(\mathbf{r}, t) = A_0 \frac{W_0}{W(z)} \exp\left[-\frac{\rho^2}{W^2(z)}\right] \exp\left[-jkz - jk\frac{\rho^2}{2R(z)} + j\zeta(z)\right] \exp(j\omega t), \quad (157)$$

which is the complex amplitude of the Gaussian beam. Eq. (157) must be considered together with the formulas for beam parameters $W(z)$, W_0 , $R(z)$ and $\zeta(z)$:

$$W(z) = W_0 \sqrt{1 + \frac{z^2}{z_0^2}} \quad (158)$$

$$W_0 = \sqrt{\frac{\lambda z_0}{\pi}} \quad (159)$$

$$R(z) = z \left(1 + \frac{z_0^2}{z^2}\right) \quad (160)$$

$$\zeta(z) = \arctan\left(\frac{z}{z_0}\right) \quad (161)$$

The physical meaning of these parameters can be inferred from Eq. (157). $W(z)$ is a radial measure of the beam width, because we see that the term $e^{-\rho^2/W^2(z)}$ will attenuate the amplitude when we move away from the optical z -axis (i.e. when $\rho^2 = x^2 + y^2$ grows). The beam width, however, depends on the position along the z -axis, and since it increases with increasing $|z|$, the beam will diverge as we move away from the plane $z = 0$. At that plane the beam width is yielded by W_0 . $z = 0$ is the so-called beam waist, and W_0 is called the waist radius.

At $z = z_0$ the beam width $W(z)$ assumes the value $\sqrt{2}W_0$. Thus we see that the Rayleigh range z_0 is the scaling factor for the divergent behaviour of the beam. The depth of focus (also known as confocal parameter) is defined as twice the Rayleigh range:

$$r_{\text{d.o.f.}} \equiv 2z_0 = \frac{2\pi W_0^2}{\lambda}. \quad (162)$$

$R(z)$ represents the wavefront radius of curvature. This is not seen directly from Eq. (157), and a more careful analysis is needed [100]. We notice that $R(z)$ is infinite at the beam waist, so the wavefronts are planar there. $R(z)$ obtains a minimum, $2z_0$, at $z = \pm z_0$, and when $z \gg z_0$ the radius of curvature increases linearly with z .

Finally, $\zeta(z)$ is the phase retardation brought in by the envelope, known as the Gouy phase [101]. It ranges from $-\frac{\pi}{2}$ at $z \rightarrow -\infty$ to $\frac{\pi}{2}$ at $z \rightarrow \infty$.

Two other important quantities can be determined with the help of Eqs. (157)-(161). The first of these is the optical intensity I of the beam:

$$I(\rho, z) = |u(\mathbf{r}, t)|^2 = \frac{I_0 W_0^2}{W^2(z)} \exp\left[-\frac{2\rho^2}{W^2(z)}\right], \quad I_0 \equiv |A_0|^2. \quad (163)$$

We see now clearly that the intensity decrease is caused at all z by a Gaussian function, with the radial distance ρ as the argument. Hence the name of the beam. We can easily calculate the total optical power

carried by the beam at any transverse plane:

$$\begin{aligned} P(z) &= \int_0^\infty \int_0^{2\pi} I(\rho, z) \rho d\phi d\rho = 2\pi \int_0^\infty I(\rho, z) \rho d\rho = \frac{2\pi I_0 W_0^2}{W^2(z)} \int_0^\infty \rho \exp\left[-\frac{2\rho^2}{W^2(z)}\right] d\rho = \\ &= \frac{\pi I_0 W_0^2}{W^2(z)} \int_0^\infty \exp\left[-\frac{2u}{W^2(z)}\right] du = \frac{1}{2}\pi I_0 W_0^2 = \frac{1}{2}I_0(\pi W_0^2), \end{aligned}$$

so the total optical power is half the maximal intensity multiplied by the beam waist area (defined as the circle with radius equal to the waist radius W_0).

Let us also find the divergence angle of the Gaussian beam. From Eq. (158) we see that when $z \gg z_0$, the beam diverges linearly as:

$$W(z) \approx W_0 \frac{z}{z_0} \equiv z \sin \theta,$$

with the definition $\sin \theta \equiv \frac{W_0}{z_0}$ for the divergence angle θ . However, usually we have $W_0 \ll z_0$ (the waist radius is much smaller than the Rayleigh range), so we obtain:

$$\theta = \frac{W_0}{z_0} = \frac{1}{z_0} \sqrt{\frac{\lambda z_0}{\pi}} = \frac{\lambda}{\pi W_0}. \quad (164)$$

Thus a highly directional laser beam can be obtained by using a short wavelength and a large waist radius.

5.3.3 The ABCD law

The shape of the Gaussian beam is completely described by the beam width $W(z)$ and by the wavefront curvature radius $R(z)$. These quantities, given that the wavelength λ is known, can be determined from the q-parameter, Eq. (151). Using it together with Eqs. (153)-(154) we get:

$$\frac{1}{q(z)} = \frac{1}{R(z)} - j \frac{\lambda}{\pi W^2(z)}.$$

The shape of the beam changes both during propagation in a homogenous medium (as seen from Eqs. (158) and (160)) and due to a transfer through some optical component, a thin lens and a curved interface being probably the most important examples. In the latter case it can be demonstrated (cf. Milonni and Eberly [100] or Gerrard and Burch [113]) that the beam remains Gaussian, but its q-parameter is transformed, $q \rightarrow q'$, in accordance with the ABCD law:

$$q' = \frac{Aq + B}{Cq + D}, \quad (165)$$

where A , B , C and D are parameters describing the given optical component. These parameters can be collected in a matrix M :

$$M = \begin{bmatrix} A & B \\ C & D \end{bmatrix}.$$

For a thin lens of focal length f the matrix is:

$$M_{\text{TL}} = \begin{bmatrix} 1 & 0 \\ -\frac{1}{f} & 1 \end{bmatrix},$$

and for a refraction at curved interface:

$$M_{\text{CI}} = \begin{bmatrix} 1 & 0 \\ \frac{n_1 - n_2}{Sn_2} & \frac{n_1}{n_2} \end{bmatrix},$$

where S is the curvature radius (with centre of curvature after the interface), n_1 is the initial index of refraction and n_2 is the final index of refraction. If the interface is flat, $S \rightarrow \infty$ and M_{CI} becomes diagonal.

Eq. (165) applies also when the beam propagates in a homogenous medium. Then the appropriate matrix is:

$$M_{\text{P}} = \begin{bmatrix} 1 & d \\ 0 & 1 \end{bmatrix}$$

with d being the optical length, i.e. the physical length multiplied with the refractive index of the medium. In the case of propagation in free space the application of Eq. (165) is obviously equivalent with the straightforward formulas given by Eq. (158) and Eq. (160).

The relevance of the matrix representation of the optical elements is contained in the mathematical fact that this representation is invariant to cascading of the elements. If we have a system consisting of many optical elements labeled by numbers 1, 2, 3, ..., n , where the labeling reflects the succession of the elements, the influence of the whole system on the Gaussian beam can be described simply by a matrix M_{TOT} being the product of the matrices representing the elements separately:

$$M_{\text{TOT}} = M_n \dots M_3 M_2 M_1.$$

The free space between elements have to be included as optical elements on their own, making use of M_{P} above.

The method described above, i.e. the ABCD law combined with the matrix representation of the optical elements, is a popular technique used for designing and analyzing optical systems. The calculations involved, however, are tedious from the algebraic point of view, so usually they are carried out numerically with the help of an appropriate computer program.

For the sake of completeness we notice that the method is closely related to another important technique in ray optics where one wants to trace a paraxial ray using two variables, r and ϕ . r is the transverse offset of the ray and ϕ the offset angle (both measured relatively to the optical axis). These variables are collected as a vector $[r \ \phi]^T$ which the optical elements transform through an ordinary matrix multiplication. The matrix representation of these elements are the same as for the Gaussian beam, and the cascading invariance still applies.

6 The main elements of the experimental setup: specifications and preliminary measurements

After the purely theoretical treatment of the previous chapter, we will here give specifications of the laser (Tab. 1 on p. 106), the non-polarizing beam splitters (Tab. 2 on p. 111) and the detectors (Tab. 3 on p. 114) used in our experimental setup. Furthermore we will present results of some preliminary measurements regarding the laser and the detectors. First we measure and model the laser beam; we demonstrate that it is indeed approximately Gaussian, we describe it graphically and we determine its parameters (Ch. 6.1). Then we will measure the coherence length of the beam (Ch. 6.2) using the principle presented in Ch. 4.4. Afterwards we give specifications of our non-polarizing beam splitter (Ch. 6.3) and experimentally verify that for our photodetectors the response to the impinging radiation is linear (in the low photocount rate regime) (Ch. 6.4). Finally we measure the photocount statistics, demonstrate that it is Poissonian and determine the afterpulse probability of the detector (Ch. 6.5).

6.1 Modelling the laser beam shape

We are using a helium-neon laser produced by Thorlabs. The specifications are given in Tab. 1. The output power was measured to be ca. 12.1 mW approximately 10 cm from the output coupler. We were using pyroelectric energy sensor ES120 [121] connected to digital power metre console PM100 [122] (both manufactured by Thorlabs).

We proceed to measure the transverse profile of the laser beam. Here, we use a CCD device, and the beam has to be attenuated with neutral density filters (NDF) in order to avoid saturation of the CCD. NDF's, as any other optical element, will distort the beam profile. In the case of NDF's this is due to several factors. The filters used in the experiment do not have anti-reflective coatings, so stray light has not been reduced. Besides, we assemble and align the optical components manually, and it is impossible to achieve an alignment that is completely perpendicular to the optical axis. The third reason is that the filter surfaces are not perfectly homogenous, since the absorbing substance that covers the glass is granular at the microscopic scale.

We check qualitatively how large the distortion actually is already at this introductory stage, since during the experiment it will be crucial to obtain an even stronger attenuation with several NDF's, Therefore the CCD is used to measure⁴⁵ the profile of the beam attenuated with one and with four NDF's, the total

⁴⁵Notice, however, that we have assumed a linear response of the CCD to the incoming light intensity, at least in the intensity

Type, model, manufacturer	He-Ne, HRR120, Thorlabs
Wavelength	633 nm
Output power	12.0-50.0 mW
Mode structure	TEM ₀₀ > 99%
Waist radius	0.44 mm
Divergence angle	0.46 mrad
Polarization	random
Longitudinal mode spacing	316 MHz
Coherence length	20 cm

Table 1: Specifications of the laser. Coherence length was in fact missing from the technical documentation, but the author obtained it from ThorLabs via e-mail. It will be verified in Ch. 6.2. *Source: Thorlabs [120]*

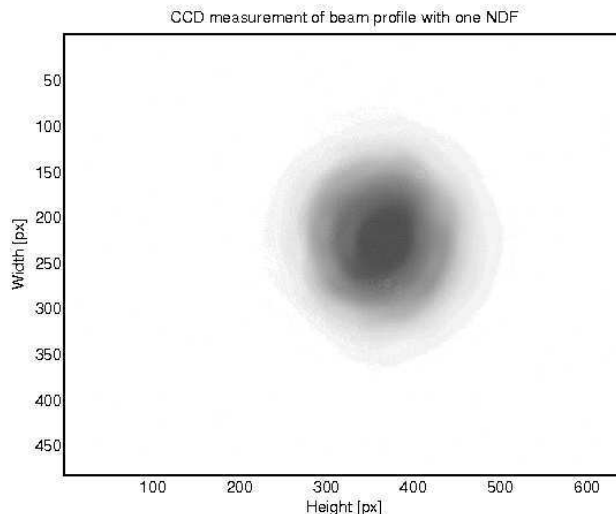


Figure 25: CCD measurement of the beam profile in a transverse plane. The beam has been attenuated with one neutral density filter. The dimensions (height/width) are reversed, because the CCD was rotated 90 degrees. The circular specks are due to dust particles on the laser aperture, the neutral density filters and/or the CCD device.

attenuation factor being in both cases identical. Fig. 25 and 26 present the results. The distortion due to four NDF's is noticeable, and the intensity of the beam profile is only approximately Gaussian in both cases, cf. Fig. 27. Despite the discrepancy between the measurements and the theoretical model, we will keep using the formalism presented in Chapter 5.3. This is justified since, as we will shortly see, the predictions of the ABCD law (see Sect. 5.3.3) will nonetheless match very closely our measurements of the beam width.

We perform now a series of measurements in order to determine the position of the waist and its radius W_0 . The beam waist is in fact localized inside the laser casing, so we are not able to measure it directly. However, both the position and W_0 can be computed numerically by fitting Eq. (158). We use a simple apparatus consisting of a photodetector and a narrow metal ruler of width l which swings like a pendulum. Initially the laser beam impinges on the photodetector. Then the ruler is swung and, during a single pass, it blocks the laser beam: partially for a time interval Δt_1 , completely for a time interval Δt_2 , and again partially for a time interval Δt_3 . The velocity of the ruler is calculated as $v = \frac{l}{\Delta t_2}$, and the beam diameter as $2W = v \frac{\Delta t_1 + \Delta t_3}{2} = l \frac{\Delta t_1 + \Delta t_3}{2\Delta t_2}$. After several measurements W can be plotted as a function of the distance

range that we work with. This assumption has not been verified experimentally.

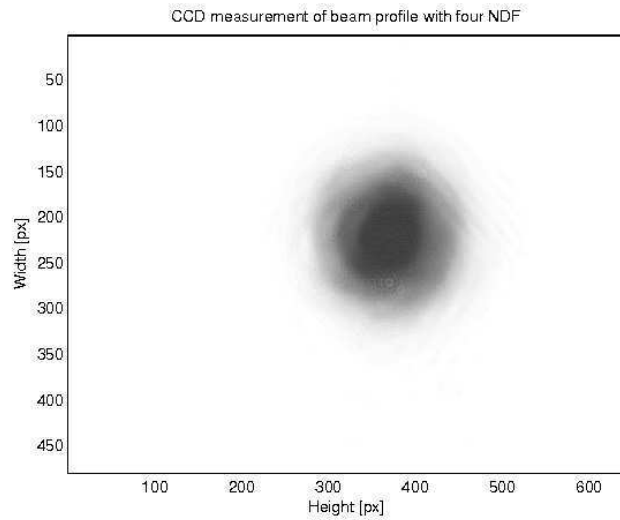


Figure 26: CCD measurement of the beam profile in a transverse plane. The beam has been attenuated with four neutral density filters. The distortion is conspicuous; notice especially the skew fringes in the upper left and the upper right corner of the beam. For other details refer to the caption of the previous figure.

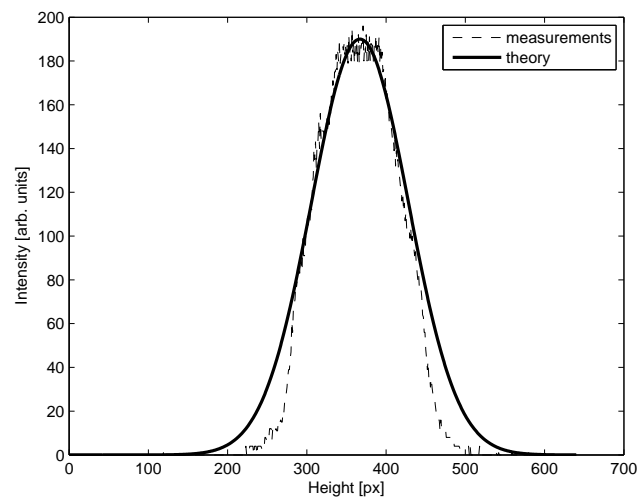


Figure 27: The dashed line is the intensity of the beam as measured along row 225 in Fig. 25. The solid thick line is a Gaussian fit. We observe that the measured intensity profile is approximately Gaussian, although it differs from a Gaussian distribution in three respects: 1) the top is flat with relatively strong fluctuations, 2) the profile is slightly asymmetrical, and 3) the intensity tends to zero too quickly. Notice that here we consider a horizontal section (horizontal in the sense of Fig. 25), and an analogous plot was obtained (but not presented here) along the vertical axis. However, along some diagonal axes the deviation from a pure Gaussian function was even larger, as is obvious from Fig. 25.

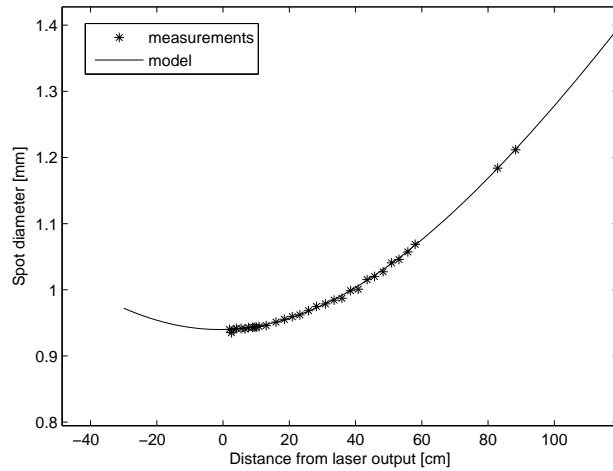


Figure 28: Measurements of the beam diameter fitted by the theoretical model in accordance with Eq. (158). Development of the beam diameter is seen to be typical for a Gaussian beam. The beam waist is placed at $z = -1$ cm (measured relatively to the laser aperture). The waist diameter is $2W_0 = 0.94$ mm which confirms the value from Tab. 1 with ca. 7% error. The Rayleigh range is then $z_0 = 110$ cm.

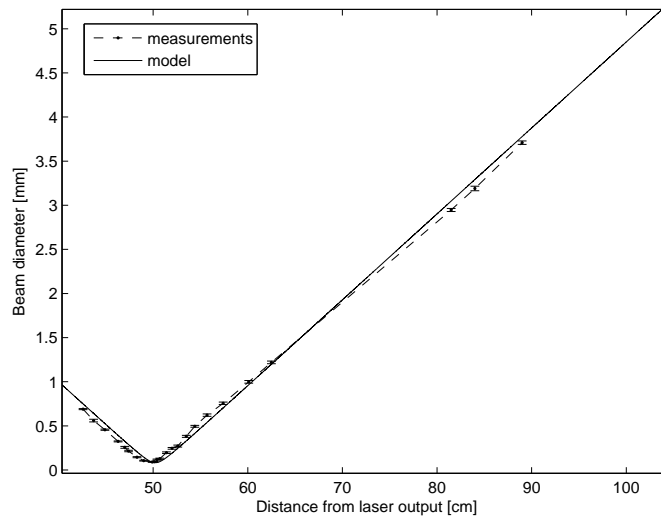


Figure 29: Measuring the beam diameter after a planoconvex thin lens with focal length 100 mm has been inserted 40 cm in front of the laser aperture. Eq. (158) combined with the ABCD law give a good description of the behaviour of the beam, ensuring us that it can be represented with the help of the Gaussian envelope.

z from the laser aperture (not the distance from the beam waist), and the fitting can be performed, see Fig. 28.

The experimentally obtained parameters can be verified in a different optical setup where a planoconvex thin lens with focal length 100 mm is inserted 40 cm in front of the laser aperture. The development of the waist radius is again measured, and we compare the results with the predictions given by Eq. (158), see Fig. 29. The agreement is good enough for our needs, so in setting up the experiments described in Chapter 7 we will again apply the ABCD law while choosing appropriate lenses for coupling the laser beam to the detectors.

6.2 Measuring the coherence length

After the laser beam shape has been modelled, we will now measure longitudinal coherence length of the beam and verify that it is approximately 20 cm. We will use a Michelson interferometer which has been set up as a part of another experiment in the laboratory. The Michelson interferometer was described in Ch. 3.2 and schematically presented in Fig. 4 on p. 35 which we reproduce below for convenience.

The emergence of interference fringes is conditioned by correlations in phase between the two partial beams. As explained in Ch. 4.4, this condition can be related to the general theory of optical correlations through the complex first-order degree of coherence $\gamma^{(1)}$ (cf. Eq. (111) on p. 75). In that chapter we used Mach-Zender interferometer as an example, but the same theory can be applied to other types of interferometers where the original beam is split by a beam splitter, and the two partial beams traverse paths with different lengths before they are recombined in order to produce an interference pattern (see Fig. 30). When the path length difference Δd increases, the visibility of interference fringes decreases, and when Δd is approximately equal to the longitudinal coherence length of the beam $\ell_c^{(l)}$ (or larger), the fringes are no longer visible, because the interference cannot take place any longer (see Ch. 4.2-4.4). Thus, by measuring the visibility as a function of Δd we are able estimate the coherence length.

In our measurements Δd is varied by adjusting the longitudinal position of one of the mirrors ($M1$ in Fig. 30). For each choice of Δd the second mirror $M2$ is moved $50 \mu\text{m}$ longitudinally using a motorized translational stage (and the position of $M2$ is reset after each measurement). $50 \mu\text{m}$ corresponds to ca. 80 wavelengths ($\lambda = 633 \text{ nm}$), so the intensity in the plane S varies with ca. 80 oscillations due to repeated occurrence of constructive and destructive interference fringes. A photodetector placed in S registers this variation, and its output is demonstrated in Fig. 31.

We could use the standard formula for the fringe visibility V (see Ch. 7.2.3), but here we choose to introduce a more pragmatic measure Q instead. We define it as $Q \equiv \frac{W_1}{W_2}$ where W_1 is the interference “strength” (the spread in intensity when $M2$ moves) and W_2 is the fluctuations amplitude (the spread in intensity when $M2$ stands still). W_1 and W_2 are presented graphically in Fig. 31.

Our final results are presented in Fig. 32. We observe that Q stays high while $\Delta d \lesssim 10 \text{ cm}$, starts to decrease rapidly around $\Delta d = 15 \text{ cm}$ and reaches the minimal level around $\Delta d = 22 \text{ cm}$. If we define the longitudinal coherence length $\ell_c^{(l)}$ as that Δd for which Q is equal to 10% of its maximal value, we find that $\ell_c^{(l)} \approx 18 \text{ cm}$. However, since uncertainties were rather large when Q was small, we conclude that the nominal value of the longitudinal coherence length of the He-Ne beam, $\ell_c^{(l)} = 20 \text{ cm}$, is approximately correct. We notice that it corresponds to coherence time τ_c of ca. 700 ps or to ca. 300,000 wavelengths.

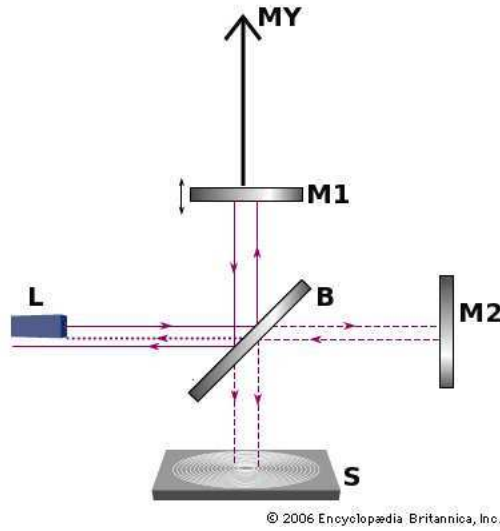


Figure 30: A schematic illustration of the Michelson interferometer used to measure coherence length of the helium-neon laser. The beam enters the apparatus from the left (L), reaches a beam splitter (B) and is sent to two mirrors ($M1$ and $M2$). The mirrors reflect the partial beams back to the beam splitter and they continue to the plane S where they recombine at a small angle relatively to each other (not shown in the figure) and interfere. A photodetector is placed in S . $M1$ is movable so that we can vary the path length difference between the distance $d_1 = \overline{B - M1}$ (i.e. from B to $M1$) and the fixed distance $d_2 = \overline{B - M2}$. The path length difference is then given as $\Delta d = 2d_2 - 2d_1$, and we measure the visibility of the interference fringes as a function of it. $M2$ is connected to a motorized translational stage. In each measurement the stage moves it $50 \mu\text{m}$ longitudinally (in steps of 40 nm) in order to vary the interference pattern. The photodetector registers intensity variation corresponding to constructive maxima and destructive minima of the pattern (see the main text for details). Source: *Encyclopædia Britannica* [66] (the picture has been modified)

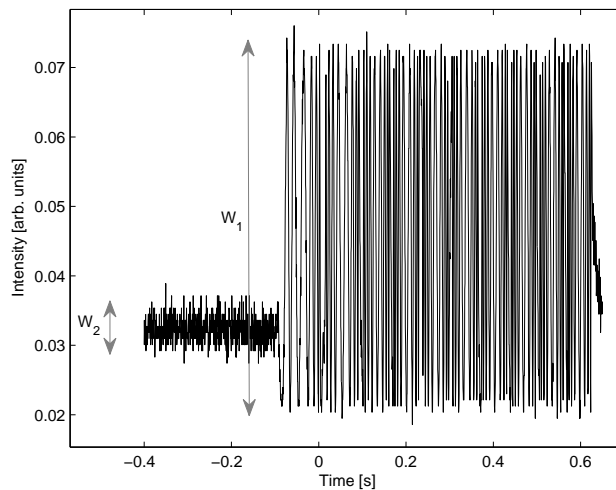


Figure 31: An example of interference measurement for $\Delta d = 3.4 \text{ cm}$. In the central part of the figure (approximately between 0 s and 0.7 s) we observe strong intensity variation due to the rapid development of interference fringes. It is caused by movement of $M2$ across $50 \mu\text{m}$. The right double arrow marks the interval W_1 over which intensity during this development varies. W_1 corresponds to interference “strength”, i.e. to the difference in intensity between bright and dark fringes of the pattern. The left double arrow marks the interval W_2 over which intensity varies when $M2$ stands still. This variation is irregular and caused by random fluctuations in the beam and instability of the setup. When we increase Δd , W_1 decreases and W_2 increases, reducing the visibility of the interference fringes. We quantify the visibility simply as a ratio Q between W_1 and W_2 , $Q = \frac{W_1}{W_2}$ (which is different from the standard formula for visibility).

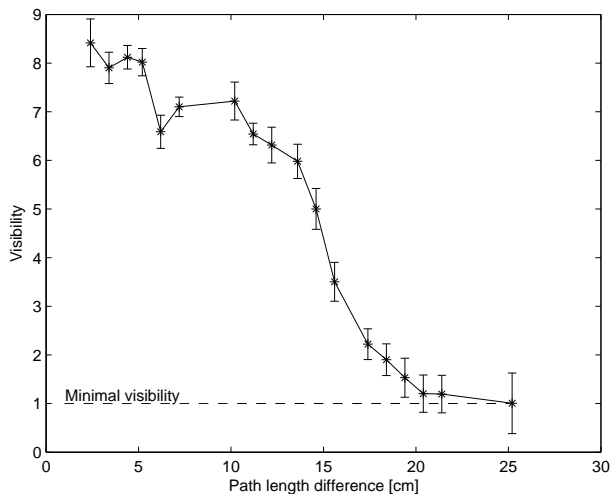


Figure 32: Visibility V (defined in the caption of the previous figure) as a function of path length difference Δd . The uncertainties are rather large, but we see clearly that V decreases rapidly around $\Delta d = 15$ cm and reaches minimal level at around $\Delta d = 20$ cm. This is the approximate coherence length of the beam. Notice that the smallest path length difference used was $\Delta d = 2.4$ cm. It could not be reduced to 0 cm due to practical space limitations on the optical table.

Model and manufacturer	05BC16NP.4, Newport
Wavefront distortion	$\leq \frac{\lambda}{4}$ at 632.8 nm over the clear aperture
Transmission	50%±3%, independent of polarization
Reflection	50%±3%, independent of polarization
Transmitted beam deviation	≤ 5 arcmin
Reflected beam deviation	$90^\circ \pm 5$ arcmin
Angle of incidence	$0^\circ \pm 2^\circ$
Antireflection coating	multilayer coating with R<0.5%
Damage threshold	2 kW/cm ² with CW, 1 J/cm ² with 10 ns pulses

Table 2: The specifications of the non-polarizing beam splitter used in our setup. *Source: Newport [119]*

6.3 Specifications of the beam splitter model

The non-polarizing beam splitters used in our experimental setup is 05BC16NP.4 model produced by Newport [119]. They are shaped as cubes with dimension 12.7 mm, and each consists of a pair of right-angle prisms cemented carefully together. The prisms are made of BK7 grade A fine annealed optical glass. The hypotenuse of one of the prisms has an all-dielectric coating optimized for 632.8 nm laser light (which is the wavelength of the laser light we are using, see Ch. 6.1). The coating behaves in principle as a half-silvered mirror, so the incoming radiation from the two sides of the cube (the input ports) is partially reflected, and partially transmitted, and then sent out through the other two sides (the output ports). The transmission and reflection coefficients for the two input ports are both 50%±3% (for 632.8 nm radiation), and independent of polarization. The specifications are presented in Tab. 2 and Fig. 33.

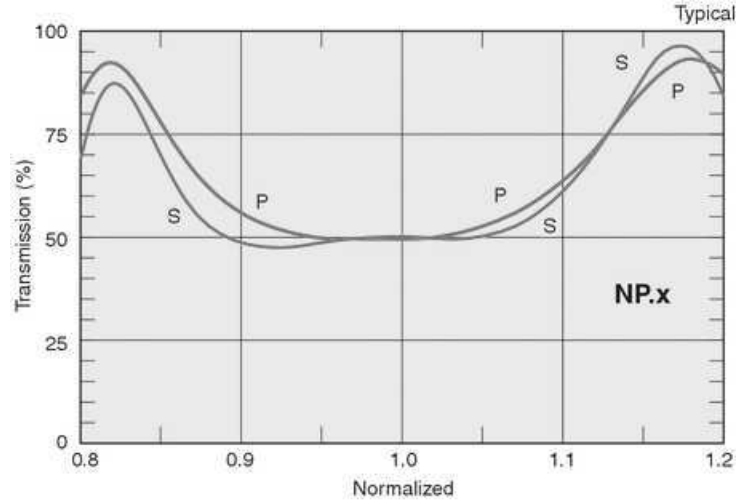


Figure 33: The transmission coefficient of the beam splitter as a function of the wavelength. The wavelengths are normalized to the optimal wavelength of 632.8 nm. The two curves correspond to two polarizations states, and the meaning of the S and P labels is explained at the end of Sect. 5.2.1. *Source: Newport [119]*

6.4 The single-photon counting module

We perform our photocounting measurements using a single-photon counting module (SPCM) manufactured by PerkinElmer. The model we are using is called SPCM-AQRH-16 [114]. The module is based on a silicon avalanche photodiode, and according to the description from the producer “detects single photons of light”. In our context such phrasing should of course be avoided, so we rather say that the module is able to register separate photocounts with high temporal precision.

SPCM is sensible to light from the wavelength interval 400-1060 nm, and achieves peak detection efficiency of more than 70% at 700 nm (Fig. 34). Its photosensitive area is circular and 180 μm in diameter. The maximum⁴⁶ count rate is at least 10 million photocounts per second (10 MC/s), but in practice we will operate far below this value, and the photocount rate in our experiments will seldom exceed 20-30 kC/s. Thus we do not expect that it will be necessary to use a correction factor for adjusting the measured count rate, because according to the table provided by the manufacturer this factor is 1.00 at 14.1 kC/s and only 1.02 at 34.7 kC/s. However, the linear relation between the measured count rate and the intensity of the light beam will be verified experimentally at the end of this section.

The module is supplied by 0.3 A current and 5.0 V voltage. Each photocount is signaled by a 2.5 V output pulse (with a 50 Ω load) or by a 5.0 V output pulse (with a 1 M Ω load) with FWHM approximately equal to 17 ns in both cases (Fig. 35). The typical dead time of a photocount is approximately 30 ns (width of the photocount pulse included). The nominal dark count rate is 25 C/s, but we observe it to be considerably higher. Two SPCM modules are employed in the coincidence measurements (see Ch. 7.1), and a single module in all other measurements (which are the interferometry measurements, see Ch. 7.2, and the preliminary measurements described in this section, and in the rest of this chapter). We label our modules as Det. 1 and Det. 2 (their serial numbers are, respectively, 15720 and 15719). The dark count rate of Det. 1 is measured to be 800 ± 100 C/s, and the dark count of Det. 2 is measured to be 150 ± 50 C/s. Therefore,

⁴⁶That is, corresponding to the saturation point. Further increase of the count rate could lead to an overload and a permanent damage of the module.

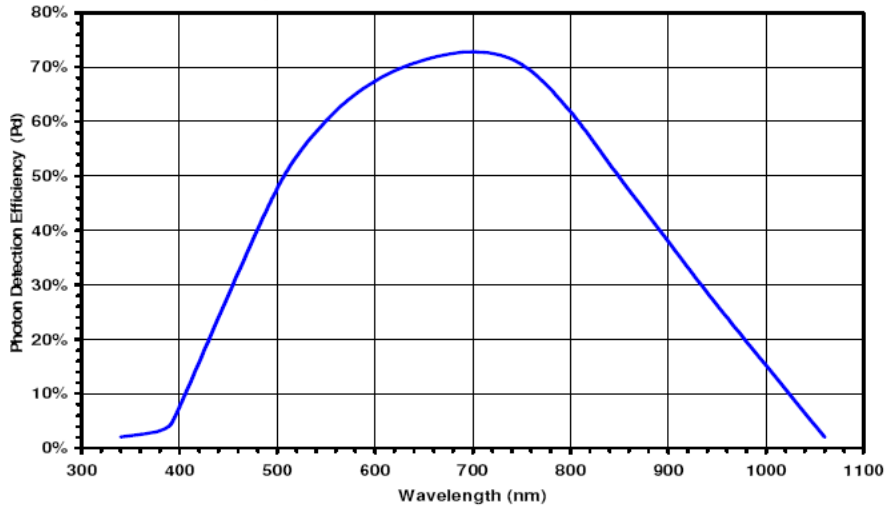


Figure 34: The efficiency of the SPCM as a function of the wavelength of the incoming light. In the corpuscular picture of light the efficiency is to be understood as the ratio of the number of detected photons (i.e. the number of photocounts) to the number of incident photons. In the undulatory picture of light (the semiclassical model) the efficiency is the probability coefficient ϵ for the detection process, cf. Eq. (112) and the discussion around it. *Source: PerkinElmer [115]*

when only one module is needed, we will be using Det. 2. Obviously, the very high dark count rate of Det. 1 suggests a malfunction of some kind.

An inconvenient feature of the module is the phenomenon known as afterpulsing: Sometimes, immediately after a photocount, another photocount is apparently registered, but in fact this second photocount does not correspond to the external stimulation of the module by the measured light source. Afterpulsing is due to some inherent effect in the semiconductor material, and it is outside our scope to describe it in detail⁴⁷. Afterpulsing is very important in our measurements, because it can easily bias any coincidence measurements. Unfortunately, the phenomenon is only vaguely quantified in the module specifications – the total afterpulse probability from 100 ns to 500 ns is simply given as 0.5 %. Eventually we will try to give a better estimate of the afterpulse probability, but the measurements are relegated to Chapter 6.5.

The most important specifications of the SPCM are summarized in Tab. 3.

Now we will examine whether the linear relation between the intensity of light and the photocount rate holds in the regime of low photocount rate. The light is the laser beam emitted from a He-Ne laser that was examined in Chapter 6.1 (cf. Tab. 1 on page 106 for specifications). The intensity of the beam can be controlled in two different ways: in discrete steps, with the help of neutral density filters, and continuously, with the help of a combination of polarizing beam splitters and a zero order half wave plate, which together act as a polarization filter. The polarizing beam splitters are 05BC16PC.4 manufactured by Newport [116], and the half wave plate is WPH05M-633 manufactured by Thorlabs [117]. The neutral density filters are absorptive with optical densities ranging from 0.1 to 5.0, and manufactured by Thorlabs as well [118].

⁴⁷ Partially it is also caused by the fact that when the avalanche region of the module detects incoming light, a small amount of light is emitted from the region. This emitted light can possibly back-scatter on the avalanche region, and result in an afterpulsed photocount.

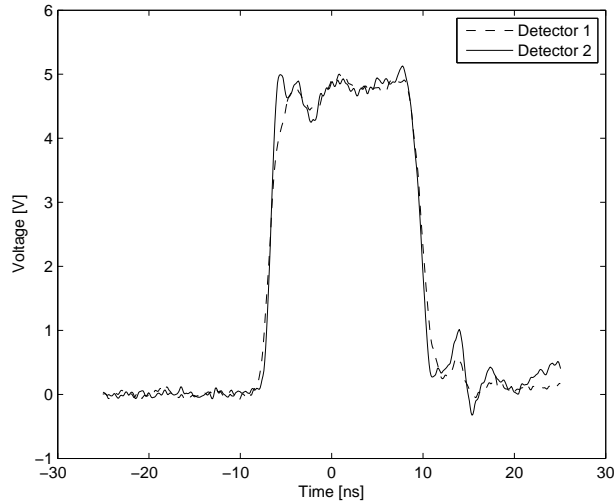


Figure 35: Single pulse outputs from the detectors employed in the experimental setup. Since the output is binarized, a single pulse corresponds to a single photocount as registered by the detector. The single pulse voltage is 5 V, because the oscilloscope coupling was set at 1 M Ω .

Model and manufacturer	SPCM-AQRH-16, PerkinElmer
Dark count	nominal: 25 C/s, measured: 800 \pm 100 (Det. 1), 150 \pm 50 C/s (Det. 2)
Maximum photocount rate	20-29 Mc/s
Pulse width (FWHM)	nominal: 15 ns, measured: 17 ns
Dead time	nominal: 32-40 ns, measured: 25 ns (pulse width incl.)
Active area diameter	170 μ m
Afterpulsing probability	nominal: 0.5%, measured: see Ch. 6.5

Table 3: Specifications of the single-photon counting module. Notice that in several cases the nominal and the measured values differ. The nominal afterpulsing probability is given very roughly by the manufacturer. For a more elaborate estimate refer to Chapter 6.5. Source: *PerkinElmer [115]*

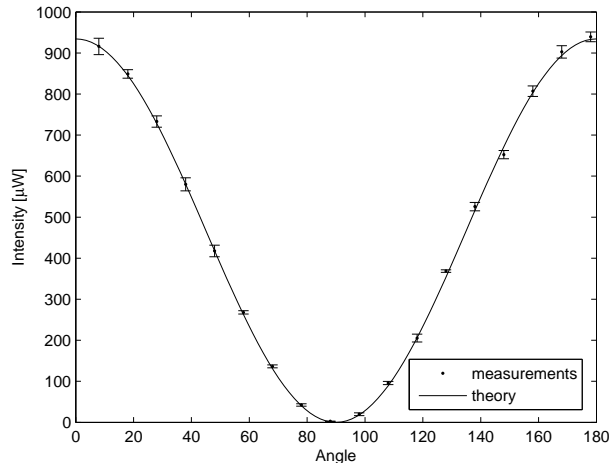


Figure 36: Instead of using a simple polarization filter, in our setup we are employing a combination of polarizing beam splitters and a half wave plate. Therefore we wish to verify that Malus' law for intensity attenuation holds. We vary the intensity by rotating the half wave plate. The theoretical prediction is given by $I = I_0 \cos^2 \theta$ with $\theta \equiv [2(\phi - 1.0^\circ)]$ where ϕ is the half wave plate angle. We plot I versus θ and see that the experimental results agree with the formula very well. The maximal intensity I_0 is approximately $940 \mu\text{W}$.

First, we quickly establish the relation between the half wave plate angle and the measured intensity. The intensity is measured again by a pyroelectric energy sensor ES120 [121] connected to a digital power metre console PM100 [122] (both manufactured by Thorlabs). As expected, this relation is given by Malus' law:

$$I = I_0 \cos^2 \theta, \quad (166)$$

where I is the intensity and I_0 is the maximal intensity. θ is related to the half wave plate alignment angle ϕ as:

$$\theta = 2(\phi - 1.0^\circ), \quad (167)$$

where the constant 1.0° is due to a non-perfect alignment of the half wave plate in its holder, and the factor 2 is related to the way the half wave plate works [47]. Fig. 36 shows the results of the measurements.

Now we can check whether the response of the module changes linearly when intensity is varied. In order to avoid saturation, we have to work in the low photocount rate regime, but this is exactly the regime that is of interest for us. Using four neutral density filters having the total attenuation factor equal to $10^{10.5}$ we manage to weaken the laser beam, so that the variation of the angle θ given by Eq. (167) between 0° and 180° results in the minimal and maximal photocount rates of 200 C/s and ca. 36500 C/s, respectively. The beam is not attenuated completely, because the combination of the polarizing beam splitters with the half wave plate does not constitute a perfect polarizing filter.

We measure the photocount rate as a function of the expected photocount rate (i.e. the actual intensity) which is again determined as a function of θ with help of Malus' law, Eq. (166). I_0 equals 36500 C/s. Fig. 37 shows the linearity of the detector response. The minor deviations have to be mainly attributed to the alignment uncertainty of the half wave plate, $\Delta\phi \approx 0.5^\circ \Rightarrow \Delta\theta \approx 1^\circ$.

We conclude that the photocount rate of the photodetector is indeed linearly dependent on the intensity of the incoming light, at least in the low photocount rate regime (< 40000 C/s). There are no unexpected and

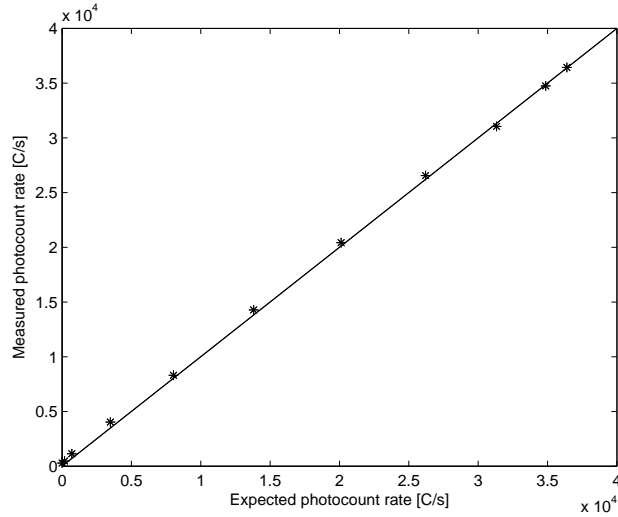


Figure 37: The verification of the linear response of the detector in the low photocount regime. The measured photocount rates are plotted as points versus the expected photocount rates calculated from Eq. (166). The dark count rate has been subtracted. The response is seen to be linear. When the expected photocount rate is 0, we measure ca. 200 C/s, but this corresponds both to uncertainty in the alignment of the half wave plate and to the fact that the combination of the polarizing beam splitter with the half wave plate does not constitute a perfect polarizing filter.

undesirable effects here that must be accounted for when we will be interpreting the main results in Chapter 7. It should be noted that the above linearity test was run on both detectors, but there were no notable differences between these two (except that in the case of Det. 1 we had to account for much larger dark count rate).

6.5 Measuring the photocount statistics

We perform a photon-counting measurement with the single-photon counting module SPCM-AQRH-16 (Tab. 3) where we measure the light beam emitted by the He-Ne laser (Tab. 1). The output power is approximately 12.0 mW which corresponds to ca. 4×10^{16} photons per second (the laser wavelength is 633 nm). This number is far beyond the capacity of the detector, and we want to reduce it to less than 20.000 photons per second. The attenuation of the beam is obtained with a combination of polarizing beam splitters (PBS) and half wave plates, and with neutral density filters (NDF). The final photocounting rate is approximately 13.400 per second (corresponding to 4.2×10^{-15} W). The total transmittance of the optical system is thus $\mathcal{T} \approx 10^{-31}$.

The response signals of the detector are gathered by a digital oscilloscope WavePro 7100A (manufactured by LeCroy [123]) and processed in real time on a computer with the help of a simple Matlab routine. Each single measurement (sweep) consists of 250.000 sampling points with temporal resolution of 4 ns per point, so the total duration of a sweep is 1 ms. The sweeps are triggered by photocounts with maximum delay, and the triggering photocounts are not present in the sweeps. We want to measure the distribution of photocounts and the distribution of time differences between two consecutive photocounts. As noticed in the previous section, because of the very strong filtering of the light beam we expect a degradation of the photon statistics to the Poissonian case (given the corpuscular model).

Measurements lasted ca. 3 h. In total, time distribution of photocounts from almost 15.000 sweeps were

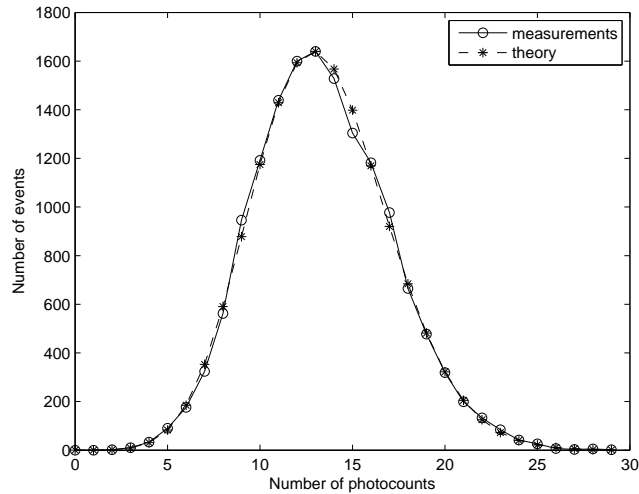


Figure 38: The measured photocount distribution (solid line) compared with the theoretical Poisson distribution with the same mean (dashed line). Although the resemblance is large, the two distributions slightly differ. A simple simulation of a Poisson process shows that after 160.000 sweeps there should be a stronger overlap. The deviation from the theoretical Poisson distribution is due to afterpulsing.

gathered. The maximal number of photocounts in a sweep was 29. Fig. 38 presents the photocount distribution compared with the theoretical Poisson distribution of the same mean. The mean number photocounts is measured to be $\mu = 13.38$, and the variance is $\sigma_n^2 = 13.47$. The Fano factor is thus $F = 1.007$ which suggests that the distribution is very nearly Poissonian. Fig. 38 confirms it.

An inspection of the distribution of the time differences between two consecutive photocounts reveals helps us to quantify the afterpulsing effect that was mentioned in Sections 5.1.1 and in Chapter 6.4. We expect the distribution to be exponential in accordance with Eq. (118), but as Figs. 39-40 show, the shortest time intervals occur much more frequently than we expect them to. With “shortest” we mean the time intervals from 24 ns to ca. 60 ns; notice that there are none time intervals shorter than 24 ns, because, as remarked in Chapter 6.4, the detector dead time is approximately 25 ns (recall that the resolution is 4 ns per sampling point). This accumulation of photocounts cannot be caused by some characteristic feature of the laser beam, because any such feature would be removed by the strong filtering. The reason must be an imperfection of the detector used, namely, the afterpulsing effect. As explained in Chapter 6.4, after each photocount there is a small, but finite probability that the detector will emit another output pulse (independently of the input signal). The probability distribution of the afterpulsing is unknown, but we can try to model it on the computer and compare the numerical results with the experimental ones. We get a good fit by assuming that immediately after a photocount the afterpulse probability is 5×10^{-4} per sampling point, and that it decreases linearly to zero during 60 ns. Any photocount registered during this time will cause a new afterpulsing. The total afterpulse probability is then ca. $0.0038 = 0.38\%$ which is rather close to the value of 0.5% given by the manufacturer (see Tab. 2 on page 111).

The start value of the afterpulse probability has to be compared with the probability that an “ordinary” photocount will be observed during 4 ns. The latter is around one order of magnitude lower, approximately 5.4×10^{-5} .

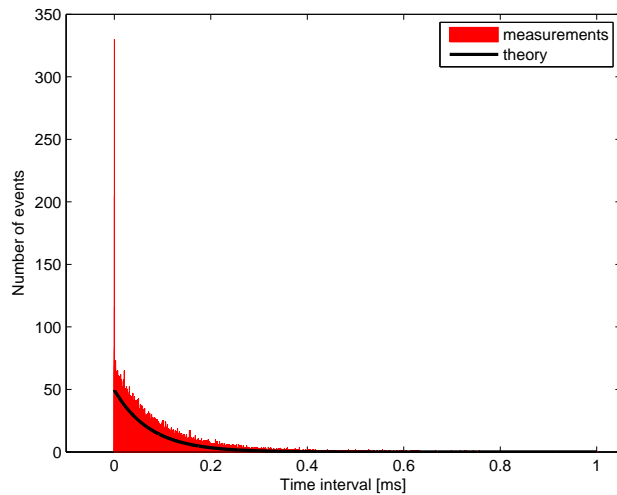


Figure 39: The distribution of time intervals between two consecutive photocounts. We compare the experimental results with the theoretical prediction given by the exponential distribution. The experimental results are presented as a histogram. Each bin is 20 ns wide. Notice the pronounced peak to the left which tells us that relatively often there was a situation where a photocount was quickly followed by another one. It seems that the theoretical curve is always lower than the histogram bars which would suggest some normalization error. However, the histogram bars are in fact often lower than the curve, but this is not possible to see in the figure due to the very fine bin partitioning.

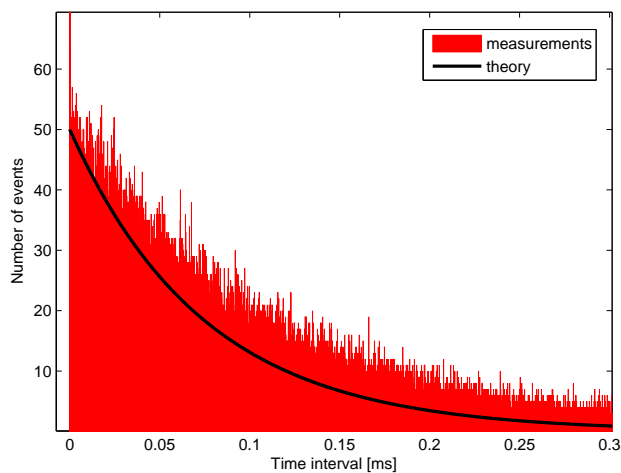


Figure 40: A magnification of a part of the histogram from Fig. 39. The pronounced peak is seen to the left, but not in its entirety. It still seems that the theoretical curve is always lower than the histogram bars, but an even stronger magnification would reveal that the bars are often lower than the curve.

7 An experimental illustration of wave-particle duality

In the following section we present and analyze the results from two “typical” experiments concerning the nature of light which were conducted in our laboratory. They are: coincidence measurements where two single-photon detectors measure photon statistics of two partial beams obtained after sending a laser beam through a beam splitter (Ch. 7.1); and Mach-Zender interferometry performed in the low-intensity regime (Ch. 7.2).

The main elements of the optical setup in both experiments have been already presented and carefully examined in the previous chapter. Instead of giving their description once more in an abbreviated form, we simply refer to the proper sections of that chapter. Thus:

- The detectors used are single-photon counting modules manufactured by Perkin-Elmer, model SPCM-AQRH-16 [114]. Its parameters have been given in Chapter 6.4 (see Tab. 3 on page 114). In the same section we have verified that the detector response is linear in the low-intensity regime.
- The non-polarizing beam splitter used to divide and recombine the laser beam is model called 05BC16NP.4 and manufactured by Newport [119]. For its description refer to Tab. 2 on page 111 and Chapter 6.3.
- The laser beam used is emitted from the He-Ne laser [120] with 633 nm central wavelength. Other parameters have been specified in Tab. 1 on page 106. In Chapter 6.1 we have modelled the shape of the beam, in Chapter 6.2 we have verified its coherence length, and in Chapter 6.5 we have measured its photon statistics.
- The laser beam is attenuated **1**) using combinations of polarizing cube beam splitters (model 05BC16PC.4 manufactured by Newport [116]) and a zero order half wave plate (WPH05M-633 manufactured by Thorlabs [117]), and **2**) using absorptive neutral density filters with optical densities ranging from 0.1 to 5.0 (manufactured by Thorlabs [118]).
- When the need arises to measure the intensity of the beam in the high-intensity regime with a photometer, we use pyroelectric energy sensor ES120 [121] connected to digital power metre console PM100 [122] (both manufactured by Thorlabs).
- The response signals from the detectors is collected using a digital oscilloscope Le Croy WavePro 7100A [123]. The data is then processed in real time and saved to memory by a simple Matlab routine.

7.1 The coincidence measurements

7.1.1 Description

The coincidence measurements are performed in order to examine the corpuscular hypothesis which states that the laser light consists of indivisible particles (called photons) of very small size (i.e. much smaller than the central wavelength λ_0 of the quasi-monochromatic laser beam). Due to the indivisibility, if we place two single-photon detectors behind the output ports of a beam splitter, we expect that any such light particle entering the beam splitter will be registered either by the first or by the second detector (given they are 100% efficient), but not by both of them simultaneously.

The experiment can be considered as an alternative version of the experiment due to Grangier, Roger and Aspect [89] where a cascade light source was employed (see Ch. 3.5). There are following differences between these two:

1. The light source employed by us is a laser beam with coherence length of 20 cm while Grangier et al. used a radiative cascade originating from excited calcium atoms. The coherence length of the cascade was not explicitly given, but it is assumed that it was much shorter than 20 cm.
2. Our experiment is not triggered by means of correlated emission, so background photocounts might present a problem. However, since the dark count rates of detectors are very low, the results should not be biased (this assumption will be confirmed during our analysis).
3. We analyze the results by comparing them with the results of numerical models (see Sect. 7.1.4), while Grangier et al. made an analytical (but simplified) comparison with the semiclassical and the fully quantum-mechanical models.

We stress that we do not set out to disprove the results of Grangier et al. We simply want to conduct a similar experiment in order to illustrate how the the wave-particle duality of light may be discussed in the context of coincidence measurements performed on a coherent laser beam which is a “classical” light source as opposed to the light source employed by Grangier et al.

7.1.2 Setup and discussion of photocount rates

The experimental setup is presented in Fig. 41. The attenuated beam reaches the non-polarizing beam splitter and the two partial beams continue to the detectors. The optical path length between the laser aperture and the beam splitter is 1.49 m; the optical path length between the beam splitter and Det. 1 (Det. 2) is 55 cm (98 cm). Division by the speed of light c yields the time needed for the emitted laser light to reach the detectors: it is 6.8 ns for Det. 1 and 8.2 ns for Det. 2. The difference between these two is negligible, because it is smaller than the time resolution employed in our setup (see Sect. 7.1.3). The partial beams are focused into the detector apertures using two convex thin lenses with focal lengths 100 mm. The beam radius W (see Eq. (158) on p. 102) at the positions of the apertures can be calculated as $45.0 \pm 5.0 \mu\text{m}$ (for

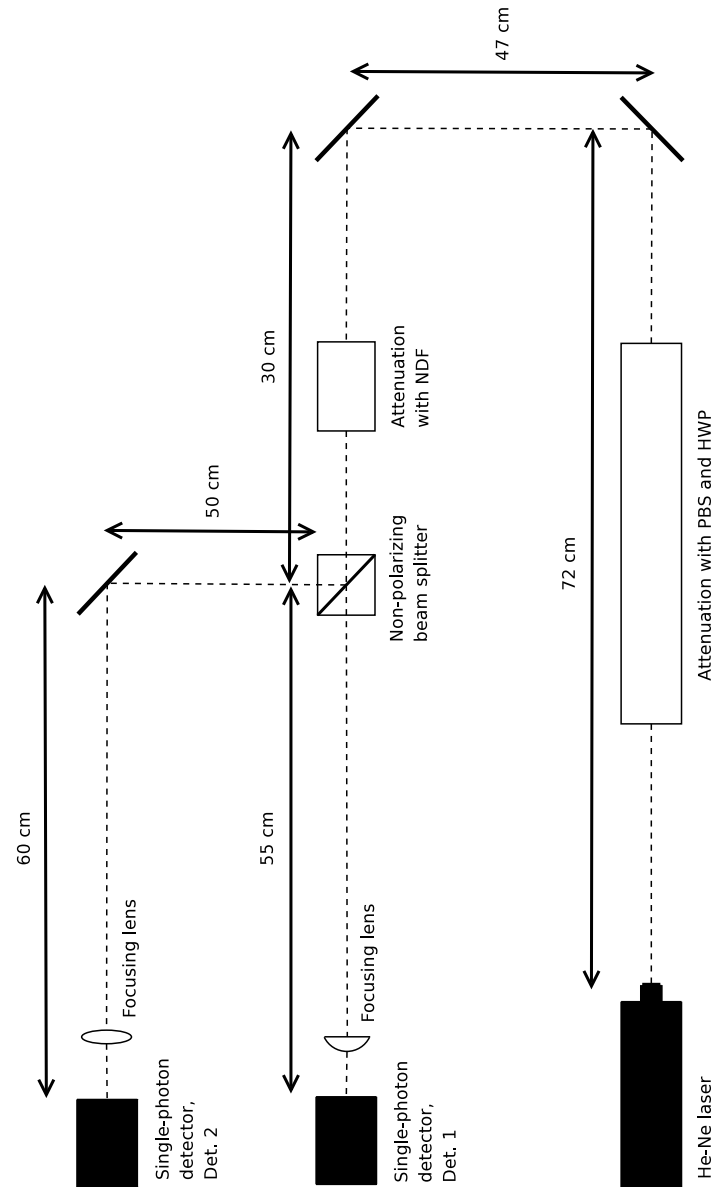


Figure 41: The complete experimental setup employed for coincidence measurements. The light beam emitted from He-Ne laser is attenuated with help of polarizing beam splitters (PBS) combined with half wave plates (HWP), and then with neutral density filters (NDF). The attenuated beam reaches non-polarizing beam splitter, and the two partial beams are sent to two single-photon counting modules labeled Det. 1 and Det. 2. There is a plano-convex lens placed 10 cm in front of Det. 1, and a biconvex lens placed 10 cm in front of Det. 2, both with 100 mm focal lengths.

both beams) which is well below the active area radius of apertures ($85 \mu\text{m}$, see Tab. 3 on p. 114).

During the measurements the mean total photocount rate of Det. 1 was $N_{1,\text{tot}} = 14700 \text{ C/s}$ (counts per second⁴⁸), and the mean total photocount rate of Det. 2 was $N_{2,\text{tot}} = 7800 \text{ C/s}$. The total background photocount rate⁴⁹ of Det. 1 is $N_{1,\text{BG}} = 850 \text{ C/s}$, and the total background photocount rate of Det. 2 is $N_{2,\text{BG}} = 200 \text{ C/s}$. Thus the photocount rate due to the split laser beam alone is, for Det. 1:

$$N_{1,\text{las}} = N_{1,\text{tot}} - N_{1,\text{BG}} = 13850 \text{ C/s},$$

and, for Det. 2:

$$N_{2,\text{las}} = N_{2,\text{tot}} - N_{2,\text{BG}} = 7600 \text{ C/s}.$$

We would expect N_1 and N_2 to be approximately equal, since the original beam is split using a 50:50 beam splitter. The splitting, however, might be non-perfect due to misalignment of the beam splitter. In order to check this, we measure the intensity with a photometer directly in front of Det. 1 and Det. 2. We find then that the intensity of the split beam going to Det. 2 equals 88% of the intensity of the split beam going to Det. 1. Nonetheless it does not explain that N_1 is almost twice as large as N_2 , so we have to conclude that the effectivity of Det. 2 is considerably smaller than the effectivity of Det. 1.

The intensity of the laser beam right after emission is 12.0 mW . After attenuating the beam with polarizing beam splitters and half wave plates, its intensity is reduced to $925 \mu\text{W}$. The total attenuation due to neutral density filters is $10^{-10.79}$, so the intensity is reduced further to 0.015 pW . It is impossible to measure such extremely low intensity directly with a photometer, so it has been inferred from the optical densities of the filters.

Since the (central) wavelength of the light employed is 633 nm , formula $E = hf = \frac{hc}{\lambda}$ yielding single photon energy tells us that 0.015 pW corresponds to approximately 50.000 photons per second (if we work within the corpuscular model). We then find that Det. 1 should receive ca. 26500 photons per second, and that Det. 2 should receive ca. 23500 photon per second. Given the Poissonian distribution of the photons, the mean time interval between two consecutive photons reaching Det. 1 or Det. 2 is approximately $40 \mu\text{s}$. This is much larger than the time needed for the laser light to reach detectors after being emitted from the laser aperture (which is less than 10 ns , see figures quoted above), so we can assume that at any time there is maximally one photon present in the apparatus.

At 633 nm central wavelength the nominal quantum efficiency of the detectors is $\epsilon_{N,1} = \epsilon_{N,2} = 70\%$ (cf. Fig. 34 on page 113). Thus we expect that Det. 1 should measure 18600 C/s and that Det. 2 should measure 16500 C/s (from the partial beams alone). These numbers have to be confronted with $N_{1,\text{las}}$ and $N_{2,\text{las}}$. We estimate that the efficiency of Det. 1 is in fact $\epsilon_1 = 51\%$, and that the efficiency of Det. 2 is $\epsilon_2 = 32\%$. These ratios are low compared to the nominal quantum efficiency. However, we have to remember that the coupling of the partial beams into the detector apertures is not necessarily perfect. Furthermore, it is possible that the beam intensity after attenuation is lower than 0.015 pW , since the optical densities of the neutral density filters have been measured and calculated in the high-intensity regime, and in the low-intensity regime some additional effects could occur.

The suspected low efficiencies will not, however, pose a real problem for obtaining good statistics, since

⁴⁸Uncertainty for all photocount rates is estimated as $\pm 100 \text{ C/s}$

⁴⁹With the total background photocount rate we mean the dark count rate plus the photocount rate due to the stray light in the laboratory. The measurements of the laser beam are not performed in total darkness, because of several LED's belonging to different laboratory devices. We keep in mind that the dark count rate of Det. 1 is considerably higher than that of Det. 2 (cf. Tab. 3 on page 114).

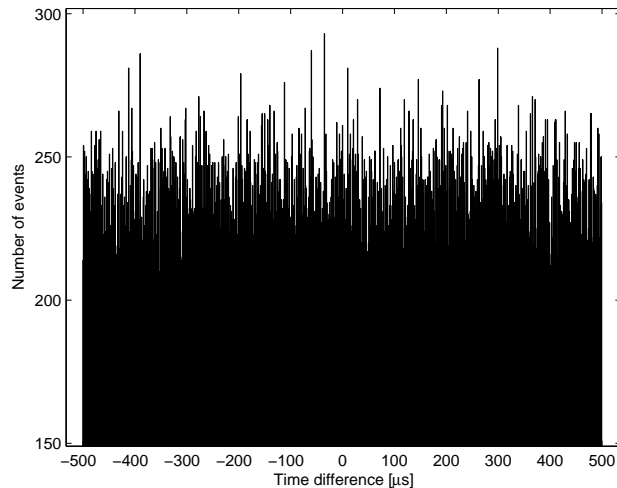


Figure 42: A histogram presenting the results of the coincidence measurements. The width of each bar is $1 \mu s$. We plot the number of events versus the time difference Δt between the triggering photocount registered by Det. 2 and the photocounts registered by Det. 1 during the actual time window. No regular pattern is observed, and no top or dip occurs at $\Delta t \approx 0$ (which would suggest, respectively, correlations or anticorrelations of the photocounts).

one of the detectors will be used only as a triggering device for the second one. As long as the ratio between noise and signal remains low, we can use the detector with the worse effectivity as the triggering device, and gather the actual data using the detector with the better effectivity. Thus the ratios between the noise and the signal calculated for the two detectors are more important than their total efficiencies. These ratios can be calculated as $\eta_1 = \frac{N_{1,BG}}{N_{1,las}} = 6.1 \pm 0.7\%$ and $\eta_2 = \frac{N_{2,BG}}{N_{2,las}} = 3 \pm 1.3\%$. The fact that $\eta_2 < \eta_1$ makes us choose Det. 2 to be the triggering device. We know that ca. 3 out of 100 triggers will be “false”, i.e. caused by “accidental” photocounts, not by laser beam photocounts.

7.1.3 Results

The experiment proceeds as follows: A photocount pulse from Det. 2 triggers measurement of Det. 1 which registers all photocounts during 1 ms time window centered about the triggering pulse (i.e. the triggering has zero delay). The sampling rate of Det. 1 (as well as that of Det. 2) is 250,000 points per time window, so the resolution is 4 ns/pt. Each time window yields ca. 14 photocounts, and there are 16281 time windows (i.e. single measurements) in total⁵⁰. For each photocount we calculate the time difference between the photocount and the zero point defined by the triggering pulse. The time differences are plotted as a histogram shown in Fig. 42.

7.1.4 Analysis and comparison with numerical simulations

The pattern observed in the coincidence histogram in Fig. 42 is apparently random in the whole time

⁵⁰One could easily believe that the total duration of the experiment was only 16 seconds, but in fact it took approximately 5 hours. The reason is that for each time window a considerable amount of data had to be processed, and the processing time was much longer than 1 ms. Therefore we could not choose the time resolution much smaller than 4 ns/pt, because then obtaining good statistics would be too time-consuming.

interval, and its Fourier analysis does not reveal any regularities. More importantly, there is no dip around the region where $\Delta t \approx 0$. The occurrence of such a dip would serve as a proof that at the moment of triggering Det. 2 with a photocount Det. 1 registers photocounts only seldom. This would again suggest that the photons going through the beam splitter are indeed indivisible, and, furthermore, that they do not travel in clusters (or, if they do, that the clusters are not being divided by the beam splitter, but rather sent along one of the optical paths in their entirety, see also Ch. 9.1).

Two issues must be considered. Firstly, we ask to what degree the presence of dark counts, background photocounts and afterpulses affect the coincidence statistics. We know that the rate of all these effects combined is small compared to the photocount rate associated with the partial beams of the laser. Nonetheless we have to admit the possibility that in the case of *coincidence* measurements some bias will be introduced due to these “accidental” photocounts.

Secondly, we know from the photocount statistics measurements described in Chapter 6.5 that the distribution of the laser photocounts in time is Poissonian. As explained in Section 5.1.3, even if the original emission of light had been characterized by sub-Poissonian or super-Poissonian distribution of photons (within the corpuscular model), this distribution would be reduced to the Poissonian one anyway because of the very strong attenuation of the beam. Thus we have to find out what coincidence histogram is expected in the case of Poissonian distribution.

In order to answer the above questions simultaneously and in an illustrative way we have written a Matlab program which simulates the coincidence measurements (the code is included in Appendix D). The program takes into account all features of the detection process hitherto discussed (dark and background counts, afterpulsing, detector dead time). Furthermore it allows us to manipulate freely the parameters describing the original distribution of the photons, the beam splitting process and the detection process (i.e. the conversion of photons to photocounts).

The program can be easily modified in order to accommodate different models of light. Thus we will not only see what coincidence histogram should be experimentally expected when we picture light as Poisson-distributed, indivisible photons, but also what histograms should result from other models. The scenarios considered are:

1. A stream of indivisible photons that are well-separated in space
 - (a) a completely regular stream
 - (b) a Poisson-distributed stream
 - (c) a Poisson-distributed stream with weak bunching effect
 - (d) a Poisson-distributed stream with weak antibunching effect
2. A stream of divisible, narrow wave packets that are well-separated in space
 - (a) a Poisson-distributed stream
 - (b) a Poisson-distributed stream with weak bunching effect
 - (c) a Poisson-distributed stream with weak antibunching effect
3. Continuous radiation

In the following the parameters corresponding to dark and background counts, afterpulsing, detector dead time are chosen to be the same as in our setup. The temporal resolution and length of each realization are also identical to the ones in the actual experiment.

We begin by examining the implications of model **1a**. This is an ideal situation, but it helps us to establish that our numerical routines work properly. The coincidence histogram is presented in Fig. 43. The regular stream of photons results in no correlations around zero time difference, $\Delta t \approx 0$, but very strong correlations start to show at $|\Delta t| = 20 \mu\text{s}$ and they repeat themselves with $20 \mu\text{s}$ interval which of course corresponds to the time interval between two consecutive photons in the original beam. The uniformly distributed dark and background counts are clearly visible in the bottom of the histogram.

The simulation results for models **1b** and **1c** are presented, respectively, in Figs. 44 and 45. Histogram in Fig. 44 resembles our original histogram created from the experimental data. The variation of the number of events as a function of time difference is apparently random in the whole interval. No top or dip occurs at $\Delta t \approx 0$, and Fourier analysis does not reveal any regularities. Histogram in Fig. 45 shows that in the case of bunched⁵¹ photons one should expect a top at $\Delta t \approx 0$. This top reflects the frequently occurring situation where two photons, originally located close to each other, pass through the beam splitter and where one of them is sent to Det. 2 and acts as a trigger, while the second of them is (almost) coincidentally registered by Det. 1. The simulation results for model **1c** is not shown explicitly, but commented upon in the caption of Fig. 45 – in the case of weakly antibunched photons we would simply obtain a dip at $\Delta t \approx 0$, for converse reasons. We remember that in our setup the beam has been strongly attenuated, so in the standard corpuscular model only the Poisson distribution is possible, but it is instructive to examine all three scenarios.

We now change the basic hypothesis by assuming that the beam splitter is able to split any single photon in two parts. In other words, instead of photons we work now with wave packets that are well-separated in space and of very short duration⁵². The modelled beam splitter divides now each wave packet in two parts of approximately equal intensity (some stochastic variation is allowed), the parts are sent on to the detectors, and the detection probability (i.e. the photocount probability) is proportional to the intensity of the incoming signal. The results for model **2b** (with a weak bunching of wave packets) are shown explicitly in Fig. 46. We observe a very sharp peak at $\Delta t = 0$ corresponding to the coincidences caused by the splitting of the single wave packets in the beam splitter. This central coincidental bar is surrounded by a much smaller top which is reminiscent of the top from Fig. 45. Of course, this top is due to bunching of wave packets. In models **2a** and **2c** we would see (the histograms are not shown), respectively, no such top and a dip instead of a top. However, the central coincidental peak is present in all cases, and no such peak has been observed in our experimental results.

Finally we consider model **3** where light is modelled as strongly attenuated, but nonetheless continuous radiative field. The fundamental frequency of this field, corresponding to 633 nm, is 4.74×10^{14} Hz which yields an oscillation period of 2.11×10^{-15} s. This is several orders of magnitude less than resolution capability of the detector (which is around 1 ps [114]), so as far as this capability is concerned, the intensity of the field is constant. In addition we have to consider coherence time. However, longitudinal coherence length of the beam is only 20 cm, so coherence time is only 700 ps. Since our time resolution (4 ns) is almost six times longer than the coherence time, we will be unable to measure any correlations on the coherence time scale (see Chapter 4) and the resulting coincidence histogram will be random and bereft of any features, as

⁵¹The photon occurrence probability in a time step is originally 0.0002. To simulate bunching, this probability increases to 0.00035 immediately after a photon has occurred, and then decreases linearly back to 0.0002 during time interval of 1000 time steps ($4 \mu\text{s}$ in our models). The antibunching is simulated in a similar way. Notice that the modelled beam splitter still processes photons independently, even if they are bunched or antibunched.

⁵²With “very short duration” we mean that their temporal length is much shorter than dead time of the detectors, so one wave packet may give rise to maximally one photocount.

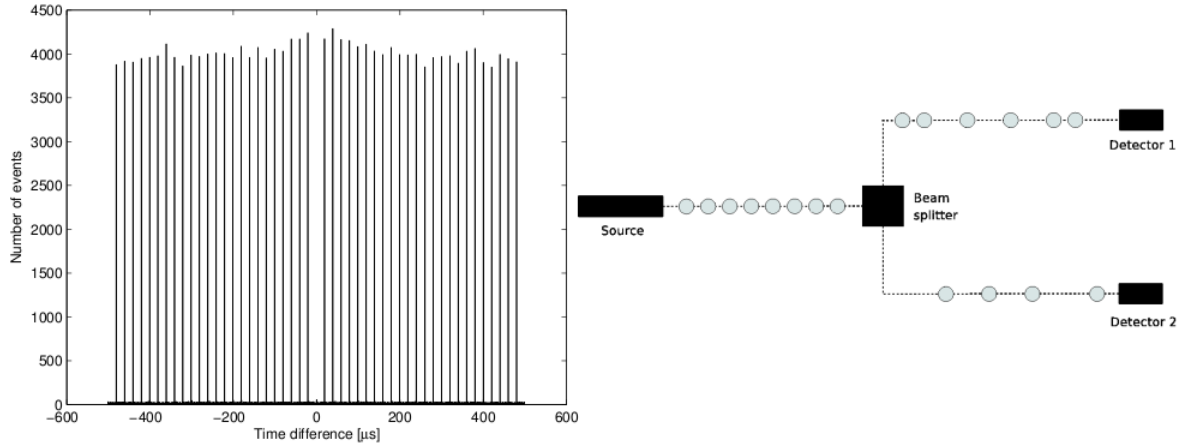


Figure 43: To the left we see a histogram presenting the results of the coincidence simulation for the case of a regular stream of photons (model **1a**). The width of each bar (histogram bin) is $1 \mu\text{s}$ – this applies to all remaining histograms in this section. The regularity of the bars reflects the constant time interval between two consecutive photons in the stream. To the right we schematically illustrate the model used. The photon size is exaggerated.

histograms from Figs. 42 and 44.

We could ask, however, what would happen if we had worked with a source of coherent time considerably longer than the dead time⁵³, say $3 \mu\text{s}$ (this corresponds to coherence length of 1 km). In our numerical model of the field we need then allow for some intensity variation with $3 \mu\text{s}$ as characteristic time scale. We choose to model this variation as a sinusoidal envelope:

$$I(t) = A \cos(\omega t + \phi) + 4A, \quad (168)$$

where $\omega = \frac{2\pi}{3 \mu\text{s}}$, $\phi \in [0, 2\pi]$ is phase randomly determined for each run of the simulation, and A is intensity amplitude. A is proportional to the detection probability and is chosen such that in each run of the simulation we obtain approximately as many detector photocounts as in the previous models (and as in the actual experiment). The term $4A$ is the “basic” cycle-averaged intensity (as registered by the detector with its limited resolution), and the sinusoidal term modulates it, so that this cycle-averaged intensity oscillates between $3A$ and $5A$. This is a very simplified model of coherent continuous radiation, and the intensity variation should be in fact both weaker and less regular. However, application of this model in our numerical simulation results in the coincidence histogram shown in Fig. 47 which is very similar to the one from model **1b** and to the experimentally obtained one.

7.1.5 Conclusion

The lack of any distinctive characteristics in the experimentally obtained histogram shows that two models of light are tenable: stream of indivisible, Poisson-distributed corpuscles (the standard particle model) and continuous coherent radiation (the wave model). However, our numerical simulation has been simplified in

⁵³Alternatively we could work with much better time resolution, say, 100 ps/pt. However, as explained in footnote 50, it would be then too time-consuming to obtain good statistics. We demonstrate numerically in the following that even if the coherence time were (much) larger than the time resolution, no new coincidence effects would occur.

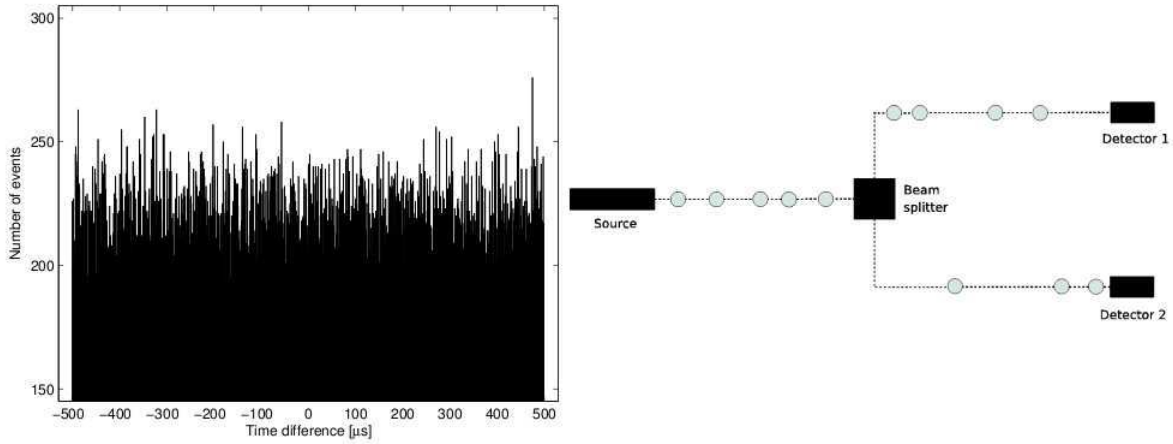


Figure 44: Results of the coincidence simulation for a stream of Poisson-distributed photons (model 1b). No feature is observed around the zero time difference, $\Delta t \approx 0$.

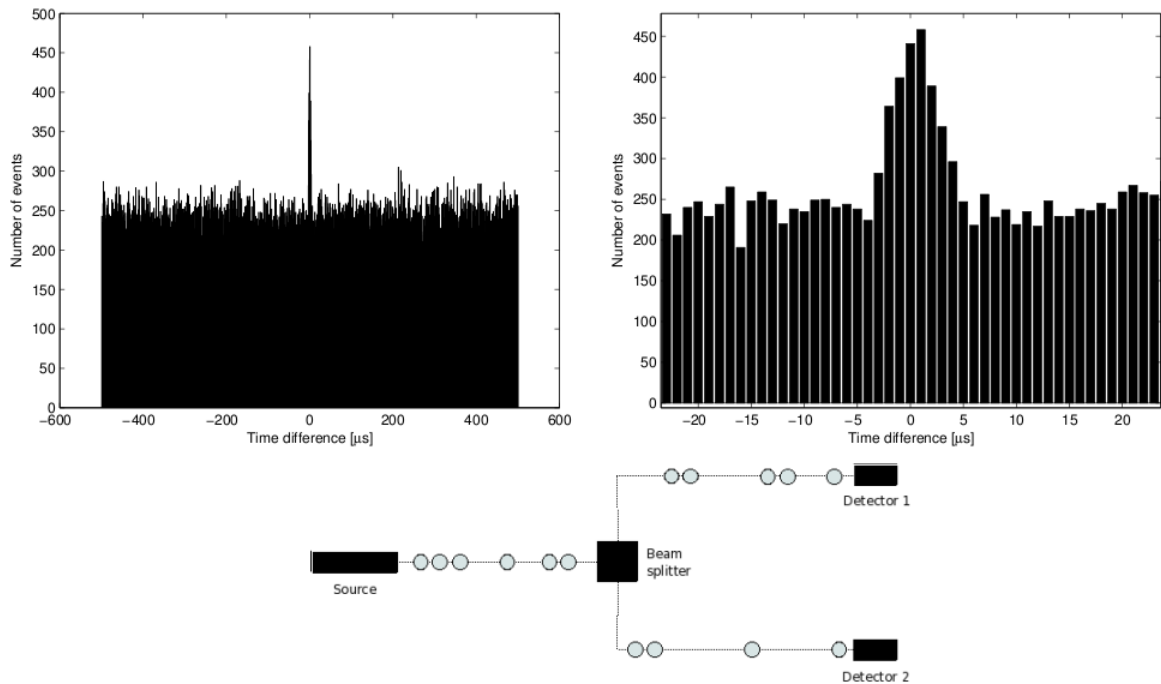


Figure 45: Results of the coincidence simulation for a stream of bunched photons (model 1c). The distinctive top at $\Delta t \approx 0$ from the “main” histogram (to the left) is seen magnified to the right. In case of a stream of antibunched photons (model 1d) we would simply observe a dip instead of a top at $\Delta t \approx 0$.

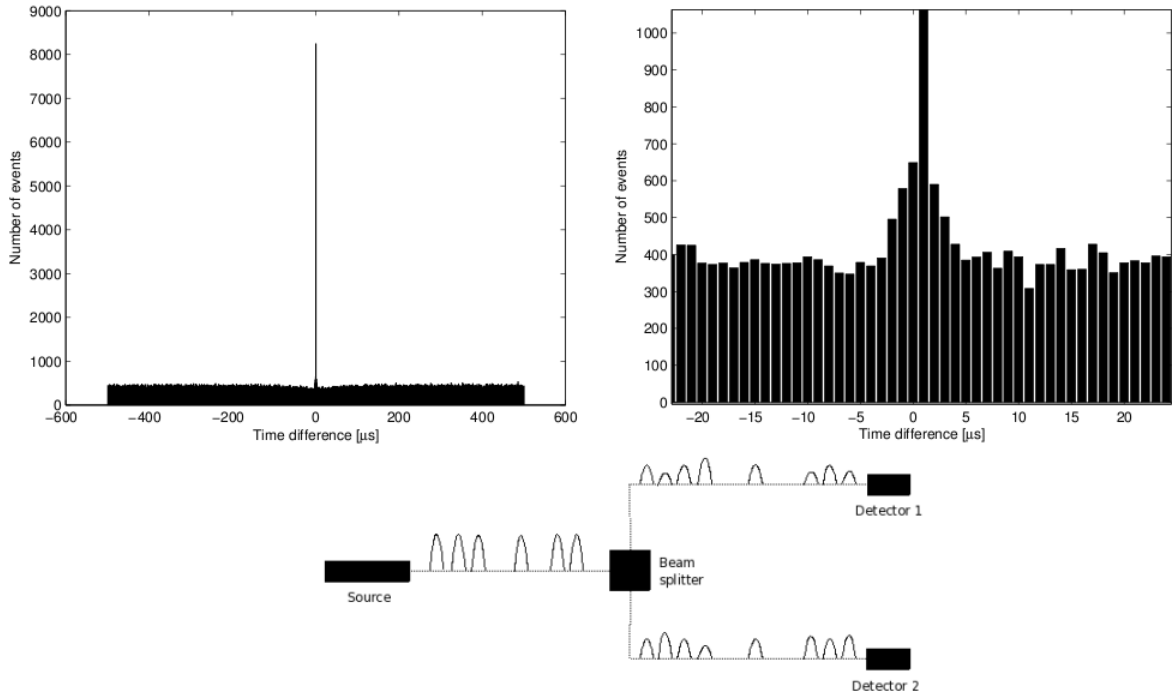


Figure 46: Results of the coincidence simulation for a stream of bunched wave packets (model 2b). We observe a very sharp coincidence peak which reflects the splitting of wave packets in the beam splitter. This peak is surrounded by a top similar to that from the previous figure which is due to the bunching of the wave packets. Without the bunching effect the top would disappear (model 2a), or it would be replaced by a dip in case of an antibunching effect (model 2c), but these histograms are not shown. However, the central sharp peak would be present in all three cases. The wave packet width in the illustration below is exaggerated.

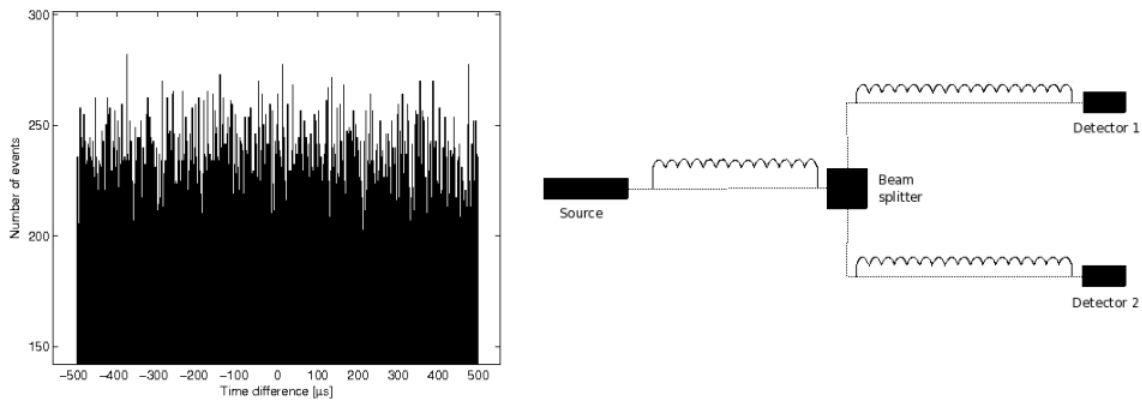


Figure 47: Results of the coincidence simulation for a continuous coherent field (model 3). No features are observed, and Fourier analysis does not reveal any regularities in the histogram.

some respects and has built on specific assumptions in others, so at least two reservations must be immediately made:

1. Since we work in the low-intensity regime, we are not guaranteed that the beam splitter exhibits standard behaviour. It is conceivable that model **2a** could be corroborated if we had included in the simulation some additional effects that might be associated with the functioning of the beam splitter at very low intensities. This claim should be compared with what have been said about shortcomings of the standard beam splitter models in Chapter 5.2.3. As the program code from Appendix D shows, in our simulation the beam splitter model used is very simple indeed.
2. Our model of coherent radiation is admittedly simplistic. However, its simplicity may be perceived as an asset, because it demonstrates that even if the intensity envelope would be as regular as in Eq. (168) (and the intensity variation as strong), the resulting coincidence histogram would nonetheless be similar to the one we had obtained in the experiment. A more careful modelling of continuous coherence radiation would introduce more random elements into the radiative pattern and lessen its variation, so it is difficult to see how these elements could lead to a different histogram (in the sense of possessing coincidental or anticoincidental features).

We conclude that the coincidence measurements performed on a strongly attenuated coherent laser beam does not demonstrate its corpuscular properties unambiguously, because the same results can be obtained on the basis of classical model. This is in accordance with what have been said in Chapter 4.3 and Section 5.1.4 about, respectively, the classical description of coherence and the semiclassical model of photodetection. Thus our results are by no means novel, but simply serve as an experimental and numerical illustration of the theory. As remarked in Sect. 7.1.1, presenting such an illustration was our goal in this chapter.

7.2 The Mach-Zender interferometry

7.2.1 Description

We perform a Mach-Zender interferometry experiment with a single-photon counting module in order to confirm the occurrence of interference fringes in the low-intensity regime. The crucial connection between the interference fringes and the wave aspect of electromagnetic radiation has been elaborated on in Chapter 3.2, while in Chapter 4.4 we have presented the Mach-Zender interferometry in the framework of optical correlations theory. The latter, however, will not be employed here.

7.2.2 Setup

The experimental setup is shown in Fig. 48. Up until the first non-polarizing beam splitter it is identical to the one employed in the coincidence measurements and depicted in Fig. 41. The split beam is then sent along two different optical paths to the second non-polarizing beam splitter where the partial beams are recombined. The length of the Path 1 (refer to Fig. 48) is 81 cm, the length of the Path 2 is 90 cm. The

path length difference is 9 cm, well within the coherence length of the beam (20 cm; see also Fig. 32 on page 111). The length of the Path 1 may be delicately adjusted using a mirror whose position is controlled by a piezoelectric element. The maximal adjustment possible is approximately $\pm 1 \mu\text{m}$.

The recombined beam is focused into the detector aperture using a biconvex thin lens with focal length 100 mm. Using a photodetector we can first verify that the partial beams are properly mixed at the second beam splitter and that the interference pattern occurs in the high-intensity regime (Fig. 49). Then the intensity is strongly decreased using neutral density filters, and the measurements are repeated with the single-photon counting module. By varying the length of the Path 1, we confirm that the interference pattern occurs in the low-intensity regime as well.

In order to obtain better visibility of the pattern (see below) we employ an iris placed between the second beam splitter and the focusing lens, and we measure only the central part of the beam. There are two drawbacks of this scheme: the original intensity must be somewhat increased to recompense for the loss of intensity at the iris, and the beam shape loses its Gaussian form (see Ch. 5.3). However, the intensity remains nonetheless very low (see below for actual values), and the beam couples to the detector well enough for obtaining an unambiguous intensity pattern.

7.2.3 Results and analysis

The intensity of the original beam is attenuated to 0.093 pW which, using again the corpuscular model and the formula $E = \frac{hc}{\lambda}$, corresponds to ca. 300.000 photons per second. The iris attenuates the beam further, so the photocount rate measured along Path 1 (with Path 2 covered) is 6530 C/s, while the photocount rate measured along Path 2 (with Path 1 covered) is 6290 C/s (background counts have been subtracted). When both paths are uncovered, the measured photocount rate varies when we adjust the length of Path 1, and the variation is taken as an indication of the presence of an interference pattern.

We encounter a problem with the stability of the setup. The interference pattern does not stay the same (when the length of Path 1 is kept fixed), but drifts randomly. The time scale of the random drift is shown in Fig. 50. We see that the measurements of the interference pattern have to be conducted quickly, so there is no time for long averaging in each single measurement. This introduces an uncertainty to the results, but the stability problem nonetheless does not prevent us from obtaining a distinct interference curve.

This curve is shown in Fig. 51 and it shows variation of the intensity as a function of the length of Path 1. The experimental results are compared with the prediction of Eq. (58) on p. 36. That equation was derived for the case of Michelson interferometer, but it is also valid in the case of Mach-Zender interferometer, since in the latter the interference fringes are also understood to be a result of the superposition of the electromagnetic waves. The equation states:

$$I = I_1 + I_2 + 2\sqrt{I_1 I_2} \cos(k\Delta d + \Delta\phi), \quad (169)$$

where I is the measured intensity, I_1 is the intensity from Path 1 alone, I_2 is the intensity from Path 2 alone, k is the wave number of the (quasi-)monochromatic radiation involved, Δd is the difference in the path lengths, and $\Delta\phi$ is the difference in phases of the partial beams. In our case the intensities are given as photocount rates with $I_1 = 6530 \text{ C/s}$ and $I_2 = 6290 \text{ C/s}$. Δd has to be measured relatively to some arbitrary zero point, since we are not able to measure the total path lengths with nanometer precision. Then we can set $\Delta\phi = 0$. The wavelength $\lambda = 633 \text{ nm}$ yields $k = 9.93 \times 10^6 \text{ m}^{-1}$.

Fig. 51 shows a very good agreement between the experimental results and the theoretical prediction.

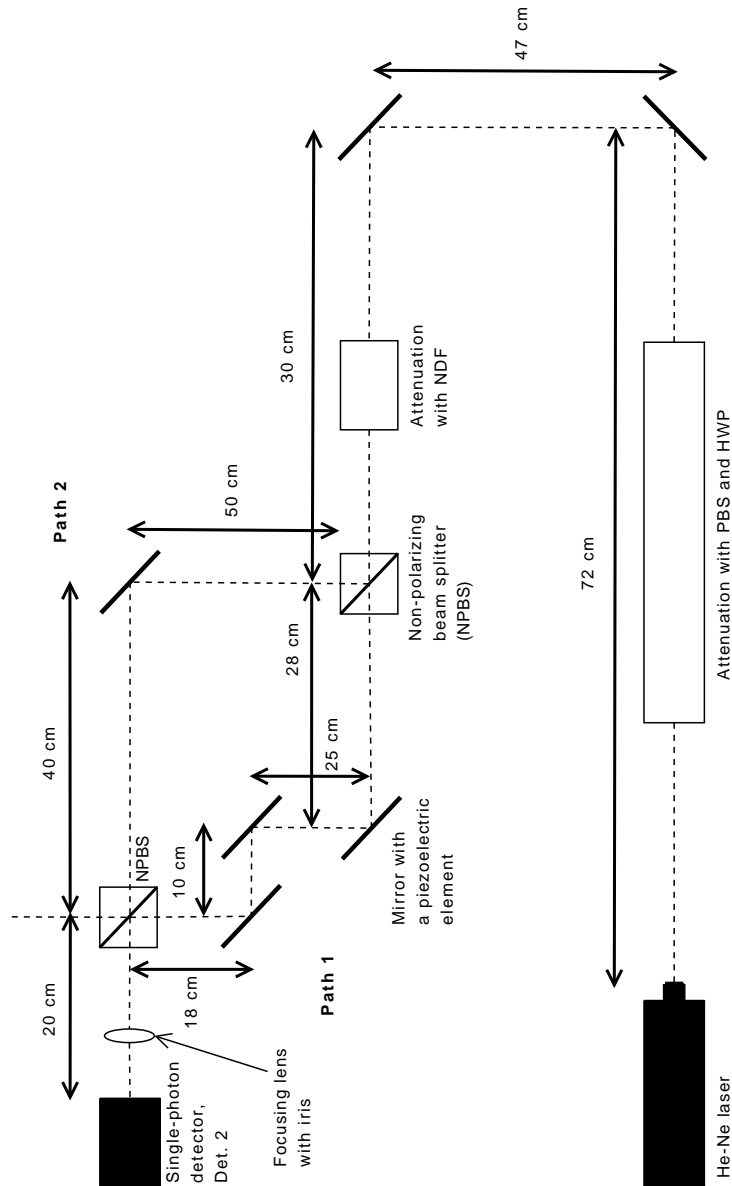


Figure 48: The complete experimental setup employed for the Mach-Zender interferometry experiment. The light beam emitted from He-Ne laser is attenuated with help of polarizing beam splitters (PBS) combined with half wave plates (HWP), and then with neutral density filters (NDF). The attenuated beam reaches non-polarizing beam splitter, and the two partial beams are sent to the second non-polarizing beam splitter along two optical paths labeled as Path 1 and Path 2. The length of Path 1 may be adjusted using a mirror whose position is controlled by a piezoelectric element. Two additional mirrors allow us to align the beam properly, so the two partial beams may be recombined at the second beam splitter. The recombined beam is sent to the single-photon detector which is the same as Det. 2 employed in the coincidence measurements (see Ch. 7.1). There is a biconvex lens with 100 mm focal length placed 10 cm in front of the detector which focuses the beam into the aperture. An iris placed between the lens and the aperture makes us measure only the (transversally) central part of the beam.

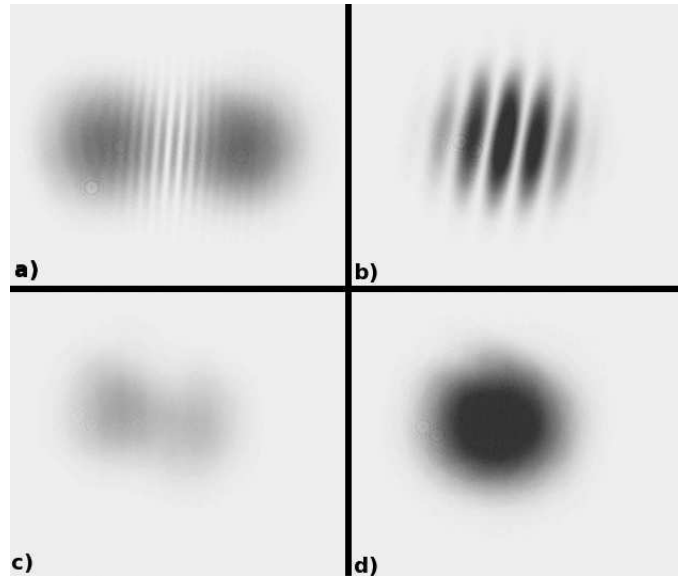


Figure 49: Interference fringes measured in the high-intensity regime using a CCD device. In **a)** the two partial beams overlap partially, and the interference pattern starts to emerge. We align the beams better and in **b)** they overlap almost completely, so the distinct fringes are visible. When the overlap is complete (or, rather, as good as the setup allows), a single fringe extends to whole transverse area of the recombined beam, so we either get **c)** a dark spot or **d)** a bright spot. Colours are inverted in order to obtain a better contrast.

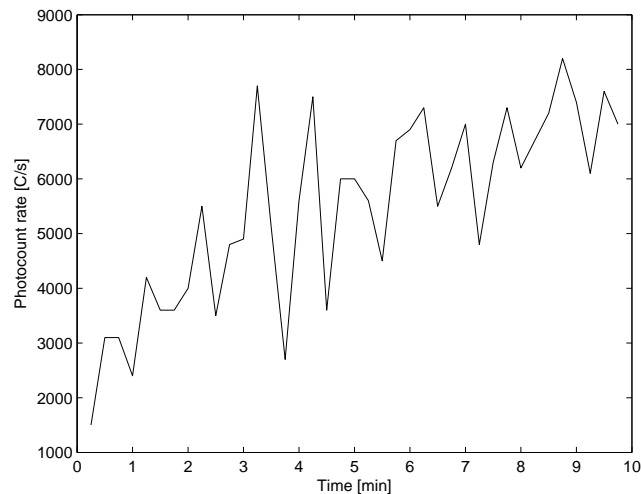


Figure 50: Demonstration of the setup instability. By adjusting the length of Path 1 we localize the interference minimum, and continue to measure the intensity for 10 minutes during which the interference pattern is supposed to be fixed. However, we see that the intensity slowly increases which indicates that the difference in path length “drifts off” from the value which allows us to obtain an interference minimum. The velocity of this drift is estimated to be 7 nm per minutes, both on short scale (within 15 seconds) and on long scale (within 10 minutes).

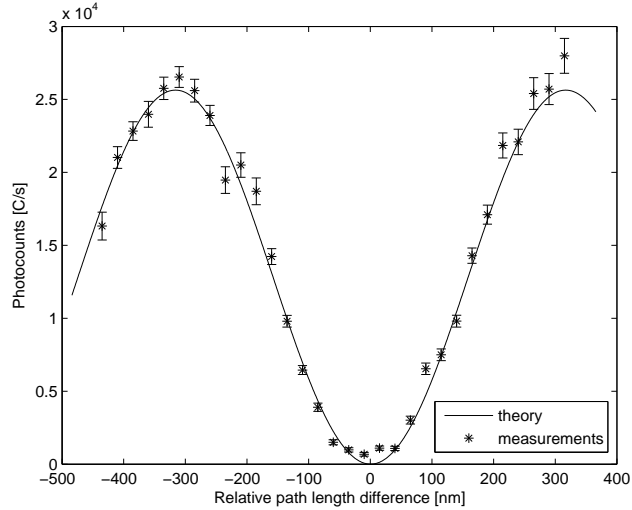


Figure 51: The intensity curve obtained in the Mach-Zender interferometry experiment. The variation of the intensity (or the photocount rate) reflects the presence of an interference pattern there minima and maxima are moving across the detector aperture when we vary the difference in path lengths of the two partial beams. Note that the path length difference Δd is relative, i.e. we give it relatively to the value where there occurs an intensity minimum. Δd is varied by regulating voltage V of the piezoelectric element which controls the position of one of the mirrors. We assume that the relation between V and Δd is linear, and that after we have increased V in order to “move” from one intensity maximum to the next one, then Δd has changed with one wavelength, or 633 nm. We observe that the agreement between the theory and the experimental results is very good, and the rather large uncertainties are due to short averaging of every measurement.

The uncertainties (i.e. the standard deviations) are rather large, but this is due to the setup instability and the aforementioned necessity of short averaging (only 10 single photocount measurements⁵⁴ for a given value of Δd). The visibility V of the interference pattern is, according to the standard formula:

$$V \equiv \frac{I_{\max} - I_{\min}}{I_{\max} + I_{\min}} = 95.3\% \pm 5.9\%,$$

where I_{\max} (I_{\min}) is the maximal (minimal) observed intensity. The value of V is high, although the large uncertainty is again due to the short averaging of single measurements.

7.2.4 Conclusion

The emergence of the interference pattern must be considered in the context of the very low intensity regime that the experiment has been performed in. We have seen above that the intensity of the original beam corresponds, in the corpuscular model, to ca. 300.000 photons per second. Given their necessary Poissonian distribution (see simulations in Ch. 7.1) the mean distance between two consecutive photons in the beam is 1 km. This distance is almost three orders of magnitude larger than the dimension of the interferometer (ca. 2.5 m). Thus we naturally expect that at almost any given time there is only one photon present in the apparatus, and the wave aspect of the radiation – which causes the interference phenomenon – has to be associated with single photons.

⁵⁴A single photocount measurement extends over a time window of 1 μ s, but in practice each measurement takes 1.5 s due to the necessity of data processing.

On the other hand we saw in Chapter 4.4 that correlations in electromagnetic field (perceived classically) play a crucial role in the formation of interference fringes, because the time delay (path length difference) introduced between two partial beams must be shorter than the coherence time (the coherence length). This condition persists in the very low intensity regime, so the notion of coherence length cannot be dismissed at the single-photon level, since the interference pattern is rather easily exhibited at this level as well. However, there is no clear-cut relation between the concept of a light corpuscle and the associated coherence time (or length). For instance, one could try to describe position of a photon in terms of a quantum-mechanical wave function. If this wave function is spatially limited and thus possesses wave packet character, its approximate length could be set equal to longitudinal coherence length. Unfortunately, we saw in Chapter 2.3.4 that attempts at localizing single photons in space, either by means of position operators or by means of wave functions, encounter fundamental difficulties. Therefore it seems that we have to seek another way of the dilemma.

In Chapter 9.1 we will present an alternative model of light which reconciles the concept of coherence length with the concept of light corpuscles by postulating that these corpuscles travel through space in specific geometric arrangements. In Chapter 9.2 we will discuss the standard view of wave-particle duality embedded within the Copenhagen interpretation of quantum mechanics. According to this view, one can employ the principle of complementarity, and simply state that the corpuscularity of light and the coherence length are mutually exclusive concepts, because the latter applies to the wave view only. In Chapter 9.3 we will see that Bohm's interpretation of quantum mechanics makes the concept of light particle altogether redundant.

Finally we notice that an experiment very similar to ours was conducted by Grangier, Roger and Aspect [89] in connection with their anticoincidence experiment described in Chapter 3.5. By the means of low-intensity Mach-Zender interferometry they also aimed at demonstrating that undulatory behaviour occurs at "the single-photon level". Due to stable setup they managed to obtain better visibility than we, $V > 98\%$; they also varied Δd over ca. 5λ . Their results, although more precise in the numerical sense, give rise to the same conclusions as ours: the characteristic intensity curve with interference maxima and minima emerges also when intensity is so low that it seems justified to claim that not more than one photon is present in the interferometer at any given time.

8 The Afshar experiment

The Afshar experiment which has recently revived the discussion surrounding the wave-particle duality has not been considered in Chapter 3. Due to its recent character and controversial nature we have chosen to postpone the presentation of the experiment to the present chapter. It will serve us to illustrate the duality problem from a general point of view, and motivate our examination of alternative physical models of light and alternative interpretations of quantum mechanics in Chapter 9.

We begin the following chapter by describing the setup and the results of the experiment (Ch. 8.1). Then we discuss Afshar’s analysis in the light of the criticism that has been raised against it, and the response of Afshar and his collaborators (Ch. 8.2). Concluding remarks are given (Ch. 8.3).

8.1 Description and results

The Afshar experiment was conceived in order to challenge the notion⁵⁵ that the wave- and particle-aspect of radiation are mutually incompatible, i.e. that it is impossible to simultaneously obtain in any single interferometry experiment a fully visible interference pattern (corresponding to the wavelike property) and a complete which-way (“welcher-Weg”) information (corresponding to the particlelike property). Thus, if we conduct a double-slit experiment with light it is possible to obtain a fully visible (in the sense of Eq. (171) below) interference pattern suggesting that the single photons have wave nature. However, if one chooses to place a detector behind one of the slits in order to obtain the information about which slit the photon “actually” went through, then the interference pattern will no longer be present. In some setups there is a possibility for obtaining a partial (i.e. not fully visible) interference pattern and partial (i.e. not completely certain) which-way information. In such situations it has been shown that the following inequality, called the Greenberger-Yasin inequality, must hold [124]:

$$V^2 + K^2 \leq 1, \tag{170}$$

⁵⁵This notion, firmly rooted in the standard interpretation of quantum mechanics, is due to Bohr and we will explore it in depth in Chapter 9.2. Another interpretation and its possible meaning for the duality problem will also be considered in that chapter.

where $V \in [0, 1]$ is the visibility of the interference pattern defined as:

$$V \equiv \frac{I_{\max} - I_{\min}}{I_{\max} + I_{\min}}, \quad (171)$$

with I_{\max} (I_{\min}) being the maximal (minimal) observed intensity in the interference fringes. On the other hand, $K \in [0, 1]$ quantifies the which-way information; $K = 1$ corresponds to full knowledge about which way the corpuscle went through, and $K = 0$ corresponds to no such knowledge at all. K is defined as:

$$K \equiv 2P - 1$$

where P is the probability that the light corpuscle went through a particular slit.

Although Eq. (170) was rigorously demonstrated in several ways (besides Greenberger and Yasin [124], see Jaeger, Shimony and Vaidman [125] and Englert [126]), its practical validity may be questioned, and we will come back to this issue in Chapter 8.3. For now we describe the Afshar experiment and explain its relation to Eq. (170).

The Afshar experiment has been described for the first time in 2005 [45], but in the following we will refer to the paper published in 2007 [46] in collaboration with Flores, McDonald and Knoesel where an improved version was presented. The experimental setup is shown in Fig. 52. Quasi-monochromatic diode laser light of wavelength $\lambda = 638$ nm from a diode laser with low photon flux passed through an aperture and was incident onto a pair of pinholes. Their diameters were 40 μm each, and their center-to-center separation was 250 μm . The two beams emerging from the pinholes overlapped in the far-field behind the pinhole screen, and produced an interference pattern consisting of light and dark fringes. At a distance 0.55 m behind the pinholes there were placed six thin wires of 127 μm diameter. The separation between two wires was approximately 1.3 mm. The locations of the wires corresponded to the locations of the minima of the interference pattern (with an accuracy of ± 10 μm).

The dual pinhole system was imaged by a lens system (placed behind the wires) onto two single-photon counting modules in such a way that pinhole A was imaged on detector 1, and pinhole B on detector 2. When the two pinholes were opened and the wire grid was removed, the peak photocount rate registered by each detector was approximately 10^4 C/s (see Fig. 52a). When the wire grid was inserted, the photocount rates were reduced only slightly: by 0.31% for detector 1 and by 1.13% by detector 2 (see Fig. 52b). It suggested the presence of a destructive interference pattern at the position of the wires, because otherwise (i.e. if no interference pattern were present) a larger fraction⁵⁶ of the incoming light should be scattered by the wires. This was demonstrated by blocking pinhole A or B, while the wire grid remained in place. When only one of the pinholes was opened, the peak photocount rate of the corresponding detector dropped to ca. 85% of the original value (i.e. the one from Fig. 52a), and the peak photocount rate of the second detector dropped to only 0.46% of the original value (see Fig. 52cd).

The authors concluded that in the case with both pinholes opened and the wire grid inserted, a destructive interference pattern was fully developed at the position of the wires, and at the same time one obtained a full which-way information about photons passing through apparatus. Besides, these photons had to be single, since with the low flux the average distance between successive photons (ca. 10 km) was much larger than both the dimension of the apparatus and than the coherence length of the laser light used (0.4 m).

In order to demonstrate a violation of the Greenberger-Yasin inequality (Eq. (170)) Afshar et al. estimated

⁵⁶The losses that were present were due to the finite thicknesses of the wires and imperfect alignment.

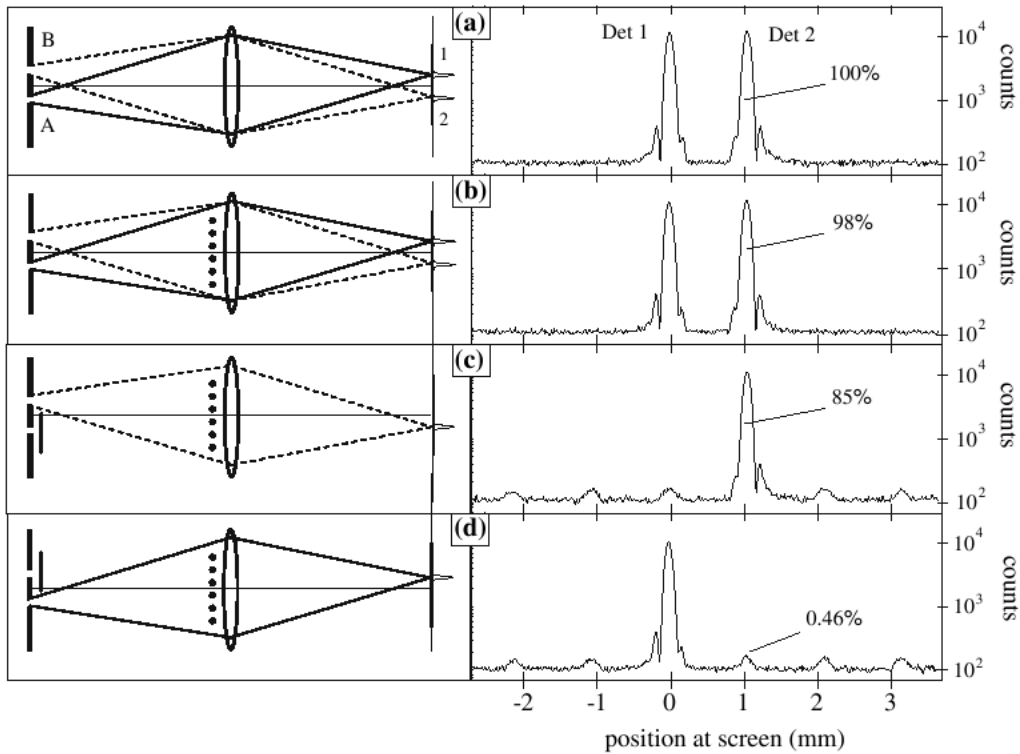


Figure 52: Results of the Afshar experiment presented as four intensity profiles for four different variations in the same experimental setup. In **a**) both pinholes are opened and the wire grid is removed, so light from pinhole A can reach (through lens imaging system) detector 1 uninhibited, just as light from pinhole B can reach detector 2. In **b**) the wire grid is inserted, but since the positions of the wires correspond to the positions of the destructive interference pattern, the intensity measured by the detectors is reduced only slightly. In **c**) and **d**) the wire grid remains, but only one pinhole is opened. The intensity at the respective detector drops to 85%, and the intensity at the second detector drops to the dark-count level. In addition the wire grid creates a diffraction pattern, because with only one pinhole opened there are no interference minima at the positions of the wires. *Source: Afshar et al. [46]*

the which-way information K directly and inferred the value of V by assuming a presence of an interference pattern with worst possible visibility, but compatible with their data. In their calculations $K \geq 0.97$ and $V \geq 0.64$, so $K^2 + V^2 \geq 1.35$ and the inequality was clearly violated. According to the authors, the outcome of the Afshar experiment indicates that the particlelike and the wavelike aspect of radiation may be present simultaneously in a single experimental setup, where the notion of simultaneity has been used in the sense given by the inequality. Taken the results to be correct, we will examine the implications of this simultaneity claim in Chapter 8.3. First, however, we review a critical response to the Afshar experiment which casts in doubt the validity of the results.

8.2 Criticism of the experiment

We stress that the results of the Afshar experiment did not offer (and did not aim at offering) any natural explanation to the wave-particle duality problem, but rather challenged the principle of complementarity associated with the duality. The principle of complementarity, due to Niels Bohr [127], represents the central feature of the standard (Copenhagen) interpretation of quantum mechanics. Both complementarity and the standard interpretation will be examined in detail in Ch. 9.2. For now, suffice it to say that complementarity implies the mutual exclusiveness of the corpuscular and the undulatory aspect of the nature of radiation in the double-slit (or double-pinhole) experiment. This exclusiveness is quantified by Eq. (170). Thus, by demonstrating the invalidity of Eq. (170) in their particular setup, Afshar et al. seemed to undermine the principle of complementarity itself.

Not surprisingly, the authors' analysis and interpretation of the experimental results were met with considerable amount of criticism. Kastner [128] pointed out that Afshar et al. had confused which-way information with which-slit information. This claim was later rebutted by Flores and Knoesel [129] who presented a modified, but equivalent version of the Afshar experiment, so the remarks of Kastner no longer applied. In another critical paper Drezet [130] concluded however that Afshar et al. had misused Eq. (52) by using one ensemble of photons for calculating V , and another ensemble for calculating K ; qualitatively such a conclusion condenses to the demand that the interference pattern cannot be simply inferred, but must be actually measured. According to Qureshi [131], however, the existence of interference pattern in the Afshar experiment is genuine and it can be inferred, but its presence destroys the which-way information, because measuring a photon by, say, detector 1 (see Fig. 52) does not longer guarantee that the photon originally emerged from pinhole A.

Qureshi's point has been pursued by Steuernagel [132] who presented a rather detailed quantitative analysis of the Afshar experiment in the framework of wave optics. On the basis of his calculations he could conclude that when the wire grid is inserted, the path detection becomes in fact less reliable. When the wires are positioned in the minima of the interference pattern, the direction of the first diffraction order for photons emerging from pinhole A (B) points towards the "wrong" detector, i.e. detector 2 (1). In fact the intensity profiles from Fig. 52, if properly interpreted, demonstrate this phenomenon. As we have already seen, when the wire grid is inserted and one of the pinholes, say pinhole A, is closed (Fig. 52c), the photocount rate of detector 2 is reduced to 85% of the original value, and the photocount rate of detector 1 is reduced to dark-count level. If we now open the pinhole A, it seems that the original (i.e. the one from Fig. 52a) intensity profile has been recovered, but the similarity of profiles from Fig. 52a and Fig. 52b is misleading.

As Steuernagel points out: “The increase of the count rates (...) is due to a partial compensation of the effects of the grid, but not their complete circumvention. This partial compensation arises at the expense of redirecting light to the “wrong” detector” (Steuernagel [132], p. 1378). So the fact that in Fig. 52b we again observe two distinct peaks with approximately the same height as in Fig. 52a does *not* mean that all photocounts of detector 1 (2) are caused by photons emerging from pinhole A (B), because now the wire grid causes diffraction and (partial) “mixing” of the path from pinhole 1 to detector A with the path from pinhole 2 to detector B.

Steuernagel proceeded to show that when this diffraction effect is taken into account, the which-way information K is accordingly reduced. The LHS of Eq. (170) becomes a function of wire thickness, but never exceeds one. In fact, the optimal situation with $V^2 + K^2 = 1$ is achieved only when the grid is completely absent, or when the wires are so thick that only very small slits remain open between them, and effectively instead of a wire grid we have a screen onto which the interference pattern is imaged. Steuernagel estimated that the correct value for the sum $V^2 + K^2$ in Afshar’s experiment is 0.813 at best. According to him, the error in the calculations of Afshar et. al was due to the fact that they determined V by considering the photons reflected by the wire grid, while K was determined by considering the photons transmitted to the detectors. This is emphatically not allowed, because these two photon ensembles are mutually exclusive, and the complementarity principle embodied in the Greenberger-Yasin inequality (Eq. (170)) must be applied to them separately.

Steuernagel’s comments were answered by Flores [133], one of the original authors, who highlighted an important feature of Afshar’s experiment. This feature had been apparently underestimated by Steuernagel and other critics. Flores recalled that the photon rate used in the experiment had been so low that the average separation between successive photons exceeded the size of the experimental apparatus by four orders of magnitude. Therefore it was reasonable to claim that at any given time there was only a single light particle (in the corpuscular model) present in the apparatus. Flores reasoned that in such circumstances separating these single photons into two mutually exclusive ensembles constituted an arbitrary division, because in the same spirit one could introduce an infinite number of mutually exclusive ensembles, one for each point of space where a photon could possibly be absorbed, thus rendering any analysis of visibility and which-way information impossible. What was of importance, according to Flores, was that each single photon entering the setup was subjected to the same experimental conditions. Flores argued further that Steuernagel in *his* quantitative analysis had used two different ensembles of photons when calculating the visibility, so that his criticism actually applied to his own approach. Flores, however, did not address explicitly the other problem pointed out by Steuernagel, i.e. the fact that the presence of the wire grid redirected light to the “wrong” detector.

8.3 Concluding remarks

Afshar’s experiment and the surrounding discussion motivates us in reassessing the wave-particle duality from a more general point of view. In the Introduction we have defined the wave-particle duality as the phenomenon where electromagnetic radiation and particles can exhibit either wavelike or particlelike behaviour, but not both. In the thesis the emphasis has been put on the problem of reconciling these two models and presenting the difficulties they both exhibit in theoretical frameworks and experimental setups. Afshar et al.

do not set out to propose and verify any alternative model of light; their goal is to examine the postulate that radiation cannot behave as waves and as particles simultaneously, and to eventually show that the inequality embodying this postulate, Eq. (170), is invalid, at least in the case of some non-perturbative measurement processes.

Such refutation (if unambiguous) would of course revolutionize quantum mechanics, because it would empirically rebut the principle of complementarity on which the standard interpretation of the theory rests (see Ch. 9.2). The rebuttal would then stimulate the interest in searching alternative models of matter and radiation. On the other hand it is rather striking that most of the parts involved in the analysis of Afshar’s experiment (i.e. Afshar et al. themselves, Steuernagel etc.) implicitly employ the customary approach to the nature of light: They switch arbitrarily between the undulatory and the corpuscular model, depending on which one is most suitable at any given moment in their treatments. For instance, Afshar et al. in their paper [46] resort exclusively to the corpuscular model and do not assign to the photons any wavelike properties. The question of how the single photons passing the apparatus actually interfered destructively with themselves at the wire grid, so they could proceed uninhibited to the respective detectors, was left out altogether. Steuernagel [132], however, makes heavily quantitative use of the wave model. Therefore Flores [133] is able to oppose his criticism by the simple remark about photons being present in the apparatus one at a time, but then again he subdues the undulatory aspect of the phenomena involved.

Of course, as long as the analysis of Eq. (170) proceeds in the usual framework of the wave-particle duality (where one sometimes employs the corpuscular view, and sometimes the undulatory view, depending on circumstances), such an inconsistent approach is per assumption allowed. However, one has to keep in mind that the equation has been derived for a very specific experimental situation, i.e. that of a double-slit (or double-pinhole) experiment without any wire grids or additional elements present in the setup, so the class of experiments that Eq. (170) applies to is rather narrow. Furthermore, it is not clear whether we are allowed to infer (or partially infer) visibility and / or which-way information as Afshar et. al did, and how “inference” and “actual measurement” should be defined⁵⁷. Preconceived judgments play some role in experiments of any kind (and in analysis of their results), so in the case of the wave-particle duality one should *a priori* and explicitly declare to which degree one will allow himself to be steered by them. Such a declaration is missing from both the paper of Afshar et al. [46] and from Steuernagel’s criticism [132].

Another crucial point, which has apparently been missed by most participants of the discussion, is that Afshar’s experiment could be explained in its entirety using only the undulatory model. Closer inspection shows that explicit introduction of corpuscle-like behaviour into the analysis is redundant, because, as we have seen in Section 5.1.2, the discreteness of the photodetection process can be easily accommodated by the semiclassical model. In such a situation the concept of which-way information becomes meaningless, and the parameter K from Eq. (170) disappears (or it could be reinterpreted as some kind of ratio between the intensity fluxes reaching the detectors, but in this version its significance is dubious). Steuernagel’s analysis lies rather close to the fully undulatory approach, but the concept of photon is nonetheless employed in connection with the detection process.

Thus it might be said that the conflict between the undulatory and the corpuscular view of light is not really present in Afshar’s experiment as it stands. It would be, however, interesting to consider for instance a combination of Afshar’s experiment and Grangier-Roger-Aspect experiment (see Ch. 3.5), because as we have noted before, it is the anticoincidence that serves to exhibit corpuscular properties more clearly. On its

⁵⁷We notice that any measurement is in fact an inference, because we use the experimentally obtained data to ascribe numerical values to physical quantities under examination.

own, Afshar's experiment embodies first and foremost a clever non-perturbative measurement scheme with possibly interesting further extensions, but its link to the essence of the wave-particle duality is not as direct as one could believe.

Even if we would manage to unambiguously demonstrate that Eq. (170) applies to the setup of Afshar's experiments, and even if we would agree on the fact that the data obtained breaks the inequality, the undulatory and corpuscular aspects of radiation would still remain complementary (in the usual, not Bohresque, sense of the word), because the experiment does not try to reduce them to any underlying physical theory⁵⁸. In order to reconcile the two models, one has to take a step back and either propose *a priori* an alternative physical model of light, or even try to explain the duality in the framework of an alternative interpretation of quantum mechanics. This will be done in the next chapter.

⁵⁸This is not an accusation – because Afshar et al. did not aim for such reduction – but only an observation regarding the meaning of the experiment.

9 Explaining the wave-particle duality

In the following chapter we will discuss how the wave-particle duality of light could be possibly expounded and its highly problematic nature elucidated. The word “expounding” is used here in the sense of giving such a picture of the physical world where both the corpuscular and the undulatory properties emerge from some underlying principle. This can be achieved in two distinct ways. Firstly, we could try to give an alternative model for the structure of light. In the long run such a model must be of course consistently incorporated into the more general framework of quantum mechanics, but to begin with it would be instructive to consider the model “on its own” and discuss its inherent assets, weaknesses and possible new predictions. Secondly, one could try to explain the wave-particle duality by modifying, or even replacing, the standard interpretation of quantum mechanics with which the duality is intimately connected.

The first approach will be presented in Chapter 9.1 where we examine the so-called “photon clump” model that aims at a direct elimination of the duality paradox of light. The role that the wave-particle duality plays in the standard interpretation of quantum mechanics is given in Chapter 9.2 which precedes examination of the radically different Bohmian interpretation in Chapter 9.3. We will see that while the standard interpretation deems questions about the wave-particle duality meaningless, the Bohmian interpretation manages to answer them directly.

We must, however, stress two things. First and foremost, the following chapter is much more speculative than the rest of the thesis. The author *does not* assume that the proposed explanations are correct; he simply intends to show how the wave-particle duality problem could be solved according to models and interpretations worked out by other physicists. Secondly, up until now the thesis has been concerned with the duality of light, but when examining different interpretations of quantum mechanics we will be forced to expand our perspective and include the duality of matter into the discussion (see Appendix C for general discussion of matter waves).

9.1 The “photon clump” model

9.1.1 Basic assumptions

In order to reconcile the undulatory and the corpuscular models of light, one could postulate that the pointlike particles of light – photons – travel through space in specific geometric arrangements which reflect their wavelike properties. We will in the following review the “photon clump” model proposed by Panarella [71] which rests on that notion and incorporates additional assumptions about the behaviour of such “photon

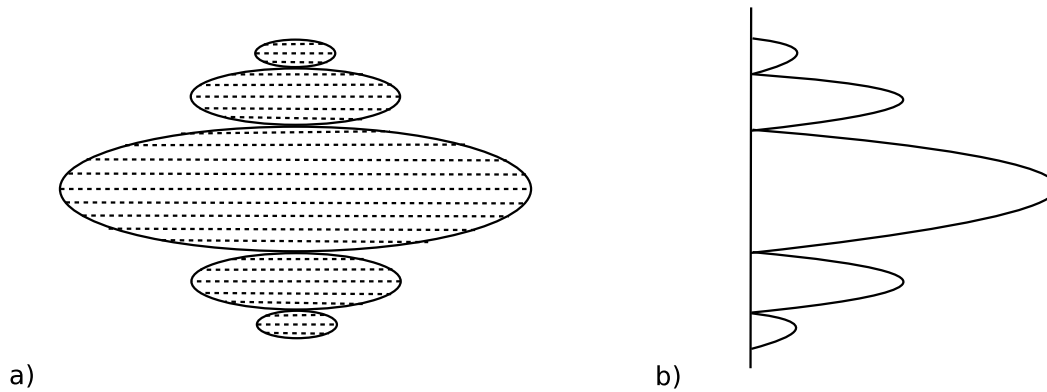


Figure 53: **a)** Two-dimensional slice through a photon clump emitted from a light source and moving horizontally (say, from left to right). Each point corresponds to a photon, and the envelope shows how the length of photon strings varies longitudinally. Only few of the strings are explicitly shown. **b)** If intensity of the clump were to be measured with sufficiently large spatial resolution, we would obtain the characteristic diffractive pattern. However, the spatial resolution of the real detecting devices is not large enough, so in order to observe diffraction photon clumps must be expanded by sending them through a narrow slit (see Sect. 9.1.2).

packets”. It should be stressed that “photon clumping” is different from “photon bunching” (see Ch. 4.3), because the latter is caused by the character of the radiation source and does not necessarily occur, while “clumping” is an inherent property of the radiation field.

The basic assumption is as following: Imagine a monochromatic⁵⁹ light source emitting a single outburst of radiation. In the corpuscular model this outburst would correspond to a single photon; in the undulatory model to an electromagnetic wave packet. Panarella’s model synthesizes both pictures: the single radiative outburst consists of several strings of point-like photons. Longitudinally (i.e. in the direction of the motion) the distance between two successive photons in one string equals the wavelength of the radiation. The length of the strings varies in such a way that the totality of the strings resembles a diffractive wave pattern with characteristic maxima and minima. This is shown in Fig. 53. The dimensions of the photon clump are finite.

We observe that the concept of coherence length is directly included in the photon clump model. The longitudinal coherence length of light in some spatial point must correspond to the length of the photon string passing through that point, and the transversal coherence length is simply the transversal size of the clump.

Since the clumping is an inherent property of the radiation field (to be examined in more detail in Sect. 9.1.2), the photon clumps retain their shape when interacting with typical elements of the optical setup like filters or beam splitters. Under transmission through a filter the total number of photons in a clump is decreased, because the filter absorbs some of them – however, it happens in such a way that the length of strings relatively to each other remains unchanged. Only if the filtering is very strong the short side strings will be absorbed altogether, and in the case of extremely strong filtering only few central strings will withstand the attenuation (but they will be strongly depleted of their photons as well). This indicates that – within the photon clump model – the longitudinal coherence length should decrease when the beam is very strongly attenuated (see also Sect. 9.1.3).

Under transmission through a beam splitter the original clump is split into two smaller clumps having

⁵⁹Panarella does not mention the frequency range to which his model could be applied, i.e. he does not explicitly state whether his model could be applied to the whole electromagnetic spectrum, or only to the region situated around visible light.

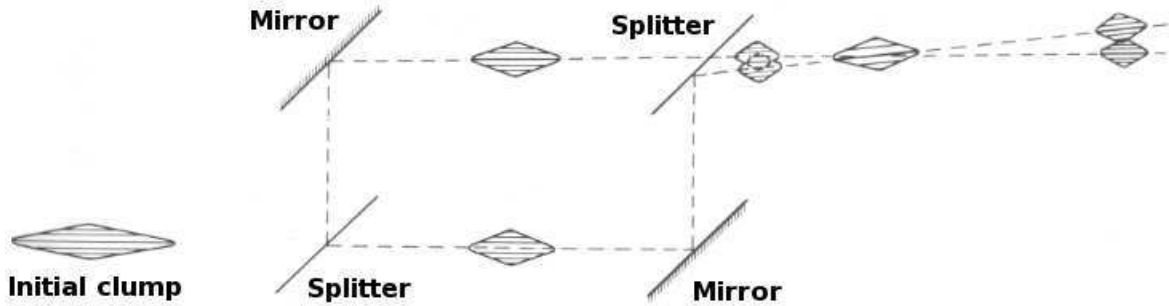


Figure 54: A pictorial description of Mach-Zender interferometry in the photon clump model. The fringes in the interference pattern correspond to the photon strings, but due to recombination of two clumps these strings are more widely separated and thus can be observed on screen. *Source: Panarella [71], p. 139*

the same structure as the original one. If another beam splitter is now used to recombine the two clumps, as in the case of Mach-Zender interferometer, Panarella postulates the two clumps will intersect at a very small angle and their associated photon strings will rearrange themselves in such a way that they will be more widely separated than in the original clump. The wide separation of the strings makes it possible to observe them on a screen as interference fringes (see Fig. 54).

Light in the photon clump model exhibits two other properties. Even if the source emits truly single photons (either because of the character of the emission process, or because the intensity is very low), after emission they will spontaneously tend to each other and form clumps. This process is presented in Fig. 55. The second property is that the transversal size of a photon clump may change when it propagates through space. This change could be then associated e.g. with evolution of the waist size of a Gaussian beam (see Sect. 5.3.2); also, the diffraction pattern obtained after light has passed a pinhole could be explained by a rapid expansion of the photon clump due to the interaction with the pinhole.

9.1.2 Quantitative considerations

The above presentation of the photon clump model is so far purely qualitative, but Panarella [71] tried to put it on a theoretical footing by assuming that Heisenberg's principle, when applied to photons, does not describe inherent position-momentum uncertainty of any single photon, but rather predicts how momentum will be transferred between *interacting* photons. Consider a standard diffraction experiment when light is sent through a slit of width Δx . When two photons pass through the slit at the same time, Heisenberg's principle (in Panarella's interpretation) tells us simply that the photons will repel each other in such a way that the momentum transferred from one photon to the other will be:

$$\Delta p_x = \frac{h}{\Delta x}.$$

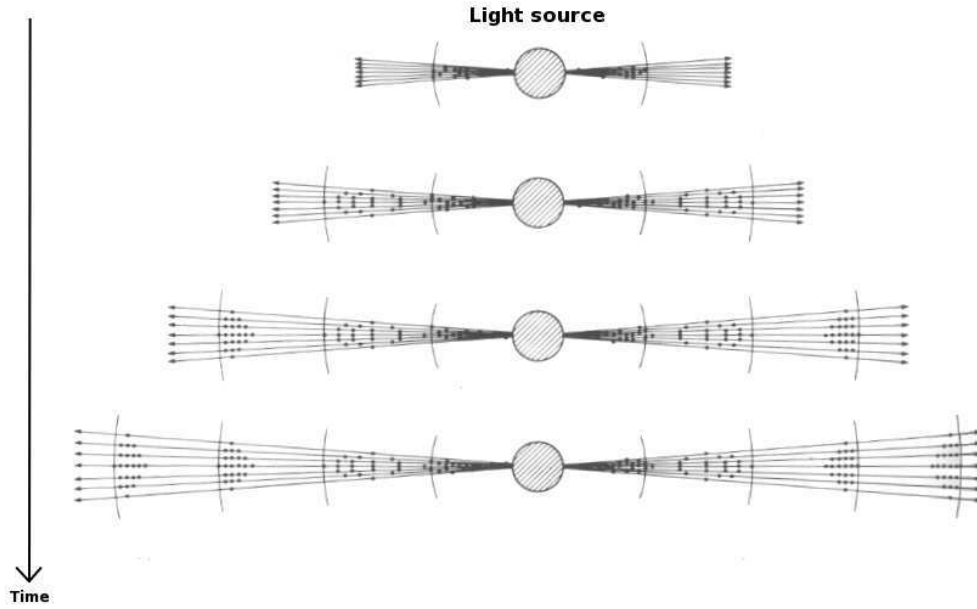


Figure 55: A pictorial description of the formation of photon clumps in space. The clumps are formed from single photons emitted by a source, because the single photons tend to attain a specific geometric arrangement in space. *Source: Panarella [71], p. 140*

This can be generalized to any two photons separated in space by distance r :

$$\mathbf{p} = \frac{h}{r} \mathbf{e}_r$$

where \mathbf{p} is the momentum transferred from photon 1 to photon 2 with \mathbf{e}_r being the unit vector pointing from photon 1 to photon 2. Derivation with respect to time yields the interaction force \mathbf{F} between photons:

$$\mathbf{F} = \frac{d\mathbf{p}}{dt} = -\frac{h}{r^2} \frac{dr}{dt} \mathbf{e}_r. \quad (172)$$

Thus the postulated interaction force between photons is inversely proportional to the square of the distance r between them, and proportional to their relative velocity $\frac{dr}{dt}$ (measured in the laboratory reference frame). If the photons move away from each other, the force is attractive; if they move towards each other, the force is repulsive.

It should be immediately noted that Panarella does not address the relativity issues. It seems that in his model the photons are allowed to propagate through (empty) space with speeds different from c (as measured in the laboratory reference frame). The “standard” speed of light c enters into the model only as the propagation speed of the interaction between photons. Nonetheless, it would be interesting to try to put the photon clump model in the relativistic framework and see whether it is possible to obtain a relativistically invariant form of Eq. (172).

Another complication introduced by the photon clump model is that it postulates an existence of a new type of interaction force between photons. The exact character of this interaction and the manner in which

it should be mediated is completely unknown, and it seems that there is no experimental evidence indicating that such an interaction exists⁶⁰. The ratios between the postulated interaction force F_I and the electrostatic and gravitational forces, respectively denoted by F_E and F_G , are:

$$\frac{F_I}{F_E} \approx 10^{-6} \times \left(\frac{dr}{dt} \right)$$

$$\frac{F_I}{F_G} \approx 10^{37} \times \left(\frac{dr}{dt} \right).$$

Despite the difficulties mentioned in the two previous paragraphs, Panarella continued his analysis by deriving Kirchhoff's theorem using the concept of interacting photons. Kirchhoff's theorem (see Born and Wolf [134], p. 378) may be taken as the starting point for classical diffraction theory, so other results associated with diffraction phenomena will follow from it. In Panarella's approach, however, the theorem no longer applies to the amplitudes of the electromagnetic waves, but to a type of optical disturbance which is related to the total momentum transfer between photons. By deriving Kirchhoff's theorem Panarella claimed that Eq. (172) is able to quantitatively explain the diffraction phenomena. Furthermore he showed that when a collection of propagating photons enters equilibrium, the distance between successive photons equals wavelength of the (monochromatic) radiation involved. Here, however, he had to refer to de Broglie's relation $\lambda = \frac{h}{p}$ (see Appendix C).

9.1.3 Concluding remarks

The photon clump model represents a possibility of reconciling the wave and the corpuscular models of radiation. Even if the model were to be refuted by empirical observations, it illustrates nonetheless how an alternative model of light, aiming at explaining the wave-particle duality and building on a rather simple idea, necessitates rather bold claims about the physical reality. On one hand, the basic assumption of the photon clump model is hardly innovative: it simply states that the collective behaviour of light corpuscles gives rise to undulatory behaviour of these. On the other hand, we see that the model, taken only a few steps further, exhibits a strongly speculative character, since it postulates existence of a new interaction force. But as the history of physics has taught us, speculations are always necessary in order to resolve problems concerning the nature of reality.

It seems that the idea that the collective behaviour of light corpuscles is responsible for the observed undulatory effects was already refuted by interference and coincidence experiments performed at intensities so low that the claim of one photon being present in the apparatus at any given time was fully justified. However, Panarella argues that the outcomes of such experiments (as the Jánossy experiment, see Ch. 3.2, or the Grangier-Roger-Aspect experiment, see Ch. 3.5) are not unambiguous: In the case of the Jánossy experiment, the one-photon-at-any-time claim was presented *a priori* and not verified in any way, and in the case of the Grangier-Roger-Aspect experiment, the limited quantum efficiency of the detectors made the authors unable to recognize photon clumps if they indeed had been present. These reservations were already mentioned when discussing the two experiments.

Panarella's theory, as any new physical model, should be judged by accordance of its predictions with the

⁶⁰Unless, of course, we take the problematic wave-particle duality phenomena to be the required indication.

empirical results. The photon clump model gives several predictions. First, in order to obtain with certainty single photons from a clump, one should break it up both transversally (e.g. using a very small pinhole) and longitudinally (e.g. using some kind of chopper). The single photons should then be devoid of any wavelike properties. If one employs very strong filtering instead, it is possible that some clumps after transmission will partially retain their original structures, and so they will still exhibit undulatory behaviour.

Secondly, we have already commented that the concept of photon clumps may be made consistent with the notion of coherence, and that the length of photon strings in a clump may be related to the longitudinal coherence length of light. Since filtering (at least when its very strong) reduces the string length considerably, it should also directly influence coherence properties of light. This prediction is not to be found in the classical theory of coherence (see Ch. 4) according to which the coherence length is not intensity-dependent. On the other hand, although it seems that this prediction has never been checked explicitly in the laboratory⁶¹, there are no empirical indications that it could be correct.

Finally, the quantitative part of the photon clump model predicts that the equilibrium separation between neighbouring photons in a clump equals the wavelength λ of the radiation field. When photon number density (i.e. intensity) of a laser beam is so high that each photon must occupy volume smaller than λ^3 , the theory implies that the radiation frequency increases in order to accommodate the “cramping” of the photons. Panarella gives a numerical example: for a 500 nm laser beam the threshold photon number density allowed by the photon clump model is 1.52×10^{13} photons per cm^3 which corresponds to intensity of $1.81 \times 10^5 \text{ W/cm}^2$. If the intensity is increased further, an increase of frequency should result. Such an increase of frequency could be used in order to explain anomalous photo-ionization of gases and anomalous photoelectric effects that were observed before (see Panarella [71], p. 165). The anomalous character of these effects consists of the fact that photo-ionization or photoelectrons are observed, even though the single photon energy is lower than, respectively, the ionization potential or the work function. However, there exist another, better developed explanation of these phenomena involving multi-photon scattering (see Girardeau-Montaut and Girardeau-Montaut [135]).

It remains to be seen whether the photon clump model will be developed further and whether experimentalists will be able to substantiate or refute it. Even if Panarella’s model will be dismissed, it will serve to show why it is very difficult (or impossible) to explain the wave-particle duality by assuming that corpuscular photons move through space in geometrical, wavelike patterns.

9.2 Complementarity of the Copenhagen interpretation

The core of every well-developed physical theory is a mathematical apparatus that serves to define and relate different quantities and notions. However, without a proper interpretation that provides a link between this apparatus and the physical world, the theory would remain only a purely mathematical and abstract tool. It is the interpretation that enunciates correspondence between the mathematical framework and the physical reality. It tells us how the mathematical methods are to be used in order to explain the nature of the world and in order to predict outcomes of diverse experiments (or, more generally: how to quantify natural phenomena using the given mathematical machinery).

The interpretations of physical theories have always been an important subject for the philosophy of sci-

⁶¹In scientific databases there are in fact no articles referring to Panarella’s paper [71].

ence. Up until the first half of the twentieth century the interpretations had been rather straight-forwardly associated with different branches of physical sciences, as Newtonian mechanics, ray optics or thermodynamics, to name a few examples. Even though these interpretations had played a crucial role in shaping of the human view of the physical world⁶², in the long run they never presented grave conceptual problems, because “common sense” was always able to accommodate them.

The situation changed with the arrival of quantum mechanics and its notorious standard interpretation (also called Copenhagen interpretation) which was developed mainly by Niels Bohr and Werner Heisenberg⁶³ [137]. The standard interpretation emphasized and cemented very peculiar features of the new theory that early research had already suggested. What was more important, however, was that the interpretation denied the quantum mechanical formalism any pictorial role in describing the physical world. Bohr claimed⁶⁴ that on the atomic level one should never speak of properties inherently attributed to material objects, but always consider them in the framework of experimental setup that is used to examine and measure them. In other words, “reality” should not be considered apart from “experiment” (in the sense of an observation), because it is the “experiment” that determines the nature of “reality”. The answers given by Nature lack epistemological value, unless they are appreciated together with the questions that observers have posed.

There are many concepts and ideas that constitute the standard interpretation of quantum mechanics⁶⁵; in fact, there is no agreement among contemporary scientists regarding how the standard interpretation should be precisely defined [140]. It is out of the scope of this chapter to give a detailed discussion about how the standard interpretation emerged historically, how it relates to philosophical issues or what is its exact meaning for the quantum-mechanical formalism. Among the different elements of the interpretation we will focus on only one: The notion of complementarity which Bohr employed to explain the wave-particle duality problem, and which was built around Heisenberg’s uncertainty principle.

The complementarity principle played a rather fundamental role in Bohr’s reasoning and therefore has been often identified with the Copenhagen interpretation. Complementarity is generally defined as:

[The natural principle according to which] it is not possible to describe atomic phenomena in as complete a manner as classical ones, since the pairs of conjugate variable that must be known for an exact description in the latter case are mutually exclusive in the former. From an experimental point of view there are therefore mutually exclusive descriptions of an atomic system which are complementary to each other. [141]

Thus, Bohr’s complementarity states that a physical object, examined on the microscopic or atomic level, may exhibit two contradictory properties, and these properties *in principle* cannot be reduced to some underlying physical model of reality. They should be treated, to use a simple metaphor, as opposite sides of one coin. It is the experimental setup that decides which property of the object will emerge in practice, in the same way as turning the coin around decides which side of it we look upon.

⁶²One of the earliest modern examples is Newton’s realization that an object moving in some reference frame, not subjected to any forces, will never stop. This opposed the old Aristotelian view according to which any motion must be sustained, or it would cease otherwise.

⁶³However, Bohr and Heisenberg never fully agreed how the mathematical formalism should be related to the physical world, and none of them ever used the term “the Copenhagen interpretation”. It was conceived by physicists who were opposing their view [136].

⁶⁴At least that was his more mature view, because Bohr’s opinion on the subject evolved with time. For instance, Bohr opposed the light-quantum hypothesis longer than most physicists of his time (Murdoch [138], p. 22).

⁶⁵For the summary of Bohr’s own thoughts, see Bohr [139].

The complementarity (pushed to the extreme⁶⁶) embodies the inherent conflict between two fundamental physical notions: that of space-time localization and that of causality (see Selleri [137], p. 101). If the causality is analyzed in terms of the conservation of energy and momentum when these are exchanged between systems, then measuring causality with infinitely large precision implies that the uncertainty in measured energy E and momentum \mathbf{p} is zero, $\Delta E = \Delta \mathbf{p} = 0$. But then, according to Heisenbergs' uncertainty principle (see Appendix A), the measurement has to disturb the space-time localizations (\mathbf{r}, t) of the measured objects, and the disturbance is maximal in the sense that $\Delta \mathbf{r} = \Delta t = \infty$. Since, as remarked above, it is the observation that determines the nature of reality, we see that space and time in the above scheme cease to exist, which is the price that we have to pay for establishing full causality.

On the other hand, if we try to measure space-time localization of a microscopic object without any uncertainty, so that $\Delta \mathbf{r} = \Delta t = 0$, the transfer of energy and momentum between the object and the measuring apparatus must be characterized by complete uncertainty, whence $\Delta E = \Delta \mathbf{p} = \infty$. Under such conditions verification of the energy-momentum conservation laws is obviously impossible, and thus the notion of causality has to be given up, because we are unable to speak about it in physical terms. We infer that (infinitely precise) observation of space and time is incompatible with (infinitely precise) observation of causality, and thus these two notions mutually exclude each other.

The complementarity principle as applied to space, time and causality may now be translated to the wave-particle duality problem. If we wish to analyze the interaction of radiation and matter in causal terms, we have to resort to the corpuscular view, because the conservation of energy and momentum is adequately expressed using the photonic view of radiation and the particle view of matter. In this scheme, however, we are unable to pinpoint space-time localizations of the corpuscles involved. If we rather want to do that, then the undulatory picture of radiation and matter must be employed, because squared modula of wave functions give us probabilistic prediction for finding the physical objects at different points. The fact that this prediction is essentially stochastic is of course another basic feature of the quantum theory.

Thus we see that radiation and matter pass through space-time in the form of probabilistic waves, and to describe this propagation the undulatory picture is appropriate. But in their interaction with another objects the causal considerations are crucial, and then the corpuscular behaviour is exhibited. The standard interpretation of quantum mechanics answers the question about the nature of light and matter by claiming that they are neither particles or waves until some specific experimental setup is employed in order to observe the system. Then the character of the observation forces the system to behave either in a particlelike or in a wavelike manner.

Within the framework of the standard interpretation the outcome of the double-slit experiment with single photons (i.e. conducted in the very low intensity regime) can be now explained. A source emits a very weak outburst of radiation with frequency f . The energy of the outburst is minimal in the sense that it corresponds to a single quantum of energy $E = hf$. The quantum propagates through space as a probabilistic wave which is diffracted by the double-slit screen. If we now let the radiation impinge on the second screen, and if we repeat the experiment many times, a corresponding diffraction pattern will eventually emerge. However, if we place a (perfect) detector closely behind, say, the upper slit, we will effectively ask about the space-time localization of the radiation before it has reached the second screen. Then we will either find out that the light quantum passed through the upper slit, interacted with the detector and transferred its momentum and energy in a corpuscle-like manner; or that it passed through the lower slit and impinged on the second screen

⁶⁶There are many versions of complementarity and it is somewhat unclear whether Bohr himself was among advocates of the strongest form of the principle. As noticed in two previous footnotes, his views evolved with time.

– but now no diffraction pattern is present, because the probabilistic wave could not be diffracted due to the detector covering one of the slits.

Such an explanation of the wave-particle duality is in some sense unsatisfactory, because instead of giving a tangible answer to the question about the “true” nature of light, it simply states that this “true” nature is dual and depends on our measuring instruments. The wavelike property and the particlelike property are complementary aspects of reality which cannot, in principle, be reduced to any common denominator.

It is interesting to note that Bohr himself did not necessarily treat particle and wave aspects on completely equal footing. As far as electromagnetic radiation was concerned, Bohr seemed to believe that the undulatory properties are in an ontological sense superior to the corpuscular properties [137] [138]. His attitude was most probably due to macroscopic observations of radiation confirming its classical undulatory descriptions. (But then it should be paralleled by the fact that in the classical limit matter behaves in a corpuscular fashion while the wave aspect is only an auxiliary concept.)

The Soviet physicist Vladimir Fock developed further the complementary explanation of duality (see Selleri [137], pp. 103-107). He stressed the claim that considering complementary properties (in their pure forms) simultaneously is meaningless, because the nature of reality is relative with respect to the means of observation. These means must be considered in classical terms, but the quantum-mechanical uncertainty relations still have to be taken into account. In the double-slit experiment any effort to measure a fully visible diffraction pattern excludes possibility of obtaining information about which slit the light quantum has travelled through. The means of observation are incompatible, and thus the wavelike and the particlelike properties are (according to Fock) incompatible also.

In Chapter 8, however, we have investigated whether these properties can be observed simultaneously in the sense of violating the Greenberger-Yasin inequality (Eq. (170) on p. 135), and we have seen that the results of Afshar experiment are inconclusive. Even if future research establishes with certainty that the experiment does not violate the equation, and that the equation indeed cannot be violated, it would still allow us to observe partially visible interference pattern and to obtain partial which-way information (Wootters and Zurek, [143]). Thus Bohr’s complementarity, strictly speaking, applies only to the pure forms of the undulatory or corpuscular behaviour. Furthermore, we have to remember that the key point of Bohr’s reasoning is the *assumption* that if two properties cannot be observed simultaneously, then they cannot be both real independently of experiment. But this assumption is philosophical rather than physical which encourages us to question it and seek other interpretations of quantum mechanics that do manage to reduce the undulatory and corpuscular properties to a single underlying model. Probably the most important of these alternative interpretations will be presented in the following section.

9.3 The Bohmian interpretation of quantum mechanics

An alternative interpretation of the quantum-mechanical formalism was proposed in 1952 by David Bohm [144] [145]. During the second half of the 20th century it has evolved through several stages. The evolution is reflected in its different names: Originally it was called “an interpretation in terms of ‘hidden’ variables”, but later renamed to “causal interpretation”, and finally to “ontological interpretation”. Sometimes it was also called de Broglie-Bohm theory in order to emphasize the similarities between Bohm’s and de Broglie’s approach to quantum mechanics [39]. For simplicity, in the following we will simply call it “the Bohmian

interpretation”.

Bohm opposed the Copenhagen interpretation by claiming that quantum mechanics should be ontologically applied to our understanding of Nature, instead of being merely treated as an epistemological tool. Thus, the Bohmian interpretation ascribes physical reality to microscopic phenomena in the same manner as classical physics ascribes reality to macroscopic phenomena. In the framework of the Bohmian interpretation the formalism of quantum mechanics does not only predict the results of measurements in an algorithmic manner – the Bohmian interpretation is causal, because it claims that all relevant variables (like position of an electron or strength of an electric field) are well-defined at any time, independently of measurement. The interpretation is also explicitly nonlocal⁶⁷, and it deals mainly with nonrelativistic phenomena – however, relativistic extensions are apparently possible (Bohm and Hiley [39], Chapter 12).

The Bohmian interpretation has never gained a broad appreciation among physicists, although it has been developed to a great degree by the author himself and his collaborators (especially Hiley). The following presentation will be heavily abbreviated, because many aspects must be omitted. We will explain the basic postulates of the interpretation (Section 9.3.1) and discuss how they serve to explain the wave-particle duality both in the case of matter (Section 9.3.2) and in the case of radiation (Section 9.3.3). The presentation is based on Bohm [144] [145], Bohm and Hiley [39] (especially Chapters 3 and 11) and Selleri [137] (Chapter 4). Concluding remarks are given in Section 9.3.4.

9.3.1 Reformulating the Schrödinger equation

In the Bohmian approach one starts by reformulating and reinterpreting the Schrödinger equation. As mentioned in Appendix A, the general form of Schrödinger equation is:

$$i\hbar \frac{d|\Psi(t)\rangle}{dt} = \hat{H} |\Psi(t)\rangle.$$

If we apply it to a single massive particle with mass m moving under an influence of external potential $V(\mathbf{r})$, and if we use the position representation of the quantum vector state $|\Psi(t)\rangle$, Schrödinger equation yields:

$$i\hbar \frac{\partial \psi(\mathbf{r}, t)}{\partial t} = -\frac{\hbar^2}{2m} \nabla^2 \psi(\mathbf{r}, t) + V(\mathbf{r})\psi(\mathbf{r}, t), \quad (173)$$

where $\psi(\mathbf{r}, t)$ is the position-dependent wave function of the particle. This is still the standard form of the equation. We can, without any loss of generality, write the wave function in the polar form:

$$\psi(\mathbf{r}, t) = R(\mathbf{r}, t)e^{iS(\mathbf{r}, t)/\hbar} \quad (174)$$

⁶⁷In the sense that objects may influence each other immediately, even though they are spatially separated. A detailed discussion of quantum nonlocality should occur in connection with Bell’s theorem, but, as remarked in Introduction, this lies outside the scope of this thesis.

where $R(\mathbf{r}, t)$ and $S(\mathbf{r}, t)$ are real and determine the amplitude and the phase of the wave function. Inserting Eq. (174) back into Eq. (173) gives:

$$\begin{aligned} \left(i\hbar \frac{\partial R}{\partial t} - \frac{\partial S}{\partial t} R \right) e^{iS/\hbar} &= \frac{-\hbar^2}{2m} \left[(\nabla^2 R) + \frac{2i}{\hbar} (\nabla R) \cdot (\nabla S) + \frac{i}{\hbar} R (\nabla^2 S) - \frac{1}{\hbar^2} R (\nabla S)^2 \right] e^{iS/\hbar} + V R e^{iS/\hbar} \\ i\hbar \frac{\partial R}{\partial t} - \frac{\partial S}{\partial t} R &= \frac{-\hbar^2}{2m} \left[(\nabla^2 R) + \frac{2i}{\hbar} (\nabla R) \cdot (\nabla S) + \frac{i}{\hbar} R (\nabla^2 S) - \frac{1}{\hbar^2} R (\nabla S)^2 \right] + V R \end{aligned}$$

By equating the real and the imaginary part of the above expression we obtain two equations. The first one is:

$$\frac{\partial S}{\partial t} + \frac{1}{2m} (\nabla S)^2 + V - \frac{\hbar^2}{2m} \frac{(\nabla^2 R)}{R} = 0,$$

and the second one is:

$$\frac{\partial R}{\partial t} + \frac{1}{m} (\nabla R) \cdot (\nabla S) - \frac{1}{2m} R (\nabla^2 S) = 0.$$

The last equation is equivalent to:

$$\begin{aligned} \frac{\partial R^2}{\partial t} + \frac{1}{m} (\nabla R^2) \cdot (\nabla S) - \frac{1}{m} R^2 (\nabla^2 S) &= 0 \\ \frac{\partial R^2}{\partial t} + \nabla \cdot \left(\frac{R^2 \nabla S}{m} \right) &= 0. \end{aligned}$$

(We observe immediately that $R^2 = |\psi(\mathbf{r}, t)|^2 \equiv \rho$ which in the standard interpretation gives probability density for finding particle in a given place at a given time.) The two equations resulting from the Schrödinger equation are thus:

$$\begin{aligned} \frac{\partial \rho}{\partial t} + \nabla \cdot \left(\frac{\rho (\nabla S)}{m} \right) &= 0 \\ \frac{\partial S}{\partial t} + \frac{1}{2m} (\nabla S)^2 + V - \frac{\hbar^2}{2m} \frac{(\nabla^2 R)}{R} &= 0. \end{aligned}$$

The Planck constant appears in only one term, and this motivates the definition of quantum potential Q :

$$Q \equiv \frac{-\hbar^2}{2m} \frac{(\nabla^2 R)}{R} = \frac{-\hbar^2}{2m} \left[\frac{\nabla^2 \rho}{2\rho} - \left(\frac{\nabla \rho}{2\rho} \right)^2 \right]. \quad (175)$$

The final form of the two equations is:

$$\frac{\partial \rho}{\partial t} + \nabla \cdot \left(\frac{\rho (\nabla S)}{m} \right) = 0 \quad (176)$$

$$\frac{\partial S}{\partial t} + \frac{1}{2m} (\nabla S)^2 + V + Q = 0. \quad (177)$$

These two equations follow directly from the Schrödinger equation (Eq. (173)) and their physical meaning is easy to comprehend. First, we notice that in the classical limit where $\hbar \rightarrow 0$, quantum potential Q can be neglected and Eq. (177) becomes simply:

$$\frac{\partial S}{\partial t} + \frac{1}{2m} (\nabla S)^2 + V = 0 \quad (178)$$

which is the Hamilton-Jacobi equation describing movement of a massive particle under influence of an external potential V . Bohm [144] quotes a theorem from classical mechanics that says that if trajectory of the particle is normal to any given surface of constant S , then it is normal to all surfaces of constant S . Furthermore, $\frac{\nabla S(\mathbf{r}, t)}{m}$ will equal velocity $\mathbf{v}(\mathbf{r}, t)$ of the particle, so Eq. (176) may be written as:

$$\frac{\partial \rho}{\partial t} + \nabla \cdot (\rho \mathbf{v}) = 0,$$

and it simply becomes the conservation law for the current represented by $\rho \mathbf{v}$. However, we will see below that this current is not the probabilistic current in the sense of the standard interpretation⁶⁸.

In the quantum limit, where $\hbar \neq 0$, quantum potential cannot be neglected, but its mathematical role is very simple: It serves to increase or decrease the classical potential of the system, so that the total potential is no longer given as V , but rather as $V + Q$. The presence of quantum potential gives a simple explanation to many peculiar phenomena associated with the quantum world. For instance, we can examine barrier penetration or tunnelling where a particle crosses potential that is classically forbidden, because the particle does not have sufficient energy to transfer through it. According to the standard interpretation, before a measurement of the particle position is made, it is meaningless to speak about the particle being located somewhere in the system, and one should consider only the probability distribution of the position. Since this probability is (usually) small, but non-vanishing on the “forbidden” side of the potential barrier, sometimes the measuring apparatus will locate the particle just there. In the Bohmian interpretation, however, the particle actually has a well-defined position at any time, but the quantum potential Q fluctuates in such a way that occasionally it becomes negative enough to decrease the classical potential sufficiently for the particle to pass through the barrier.

The quantum potential is calculated from $R(\mathbf{r}, t)$ (Eq. (175)) which is the modulus of the wave function $\psi(\mathbf{r}, t)$ written in polar form (Eq. (174)). Thus the wave function plays an essential role also in the Bohmian interpretation, but here its physical meaning is very different. In the standard interpretation the wave function represents probability amplitude of the system; in the Bohmian interpretation the wave function is a quantum field (or a quantum wave) that any material particle is embedded within. Both the material particle and its quantum field are physically real entities: the quantum field guides the particle according to the almost-classical equation of motion:

$$m\dot{\mathbf{v}} = -\nabla V - \nabla Q. \tag{179}$$

The wave-particle duality of matter can now be easily explained. We consider a double-slit experiment with electrons. A single electron is approaching the double-slit screen. Its position is well-defined at any time and can be causally determined with Eq. (179). The quantum field that the electron is embedded within is originally a plane wave:

$$\psi(\mathbf{r}, t) = R_0 e^{i(\mathbf{k}\cdot\mathbf{r} - \omega t)}$$

where R_0 is the constant amplitude, and \mathbf{k} and ω are, respectively, wave vector and angular velocity calculated from the de Broglie relations and related to the momentum and the energy of the electron in the ordinary way. Since R_0 is constant, Q is obviously zero, so (in absence of external classical potential) we deduce from Eq. (179) that the only possible trajectory for the electron is a straight line. The electron then passes

⁶⁸It should be noted that the Hamilton-Jacobi equation itself, Eq. (178), does not play a fundamental role in the Bohmian interpretation, but rather serves as a guideline for deducing the modified equation of motion, Eq. (179) (see below). This point has been stressed by Bohm [146] when responding to criticism by Halpern [147].

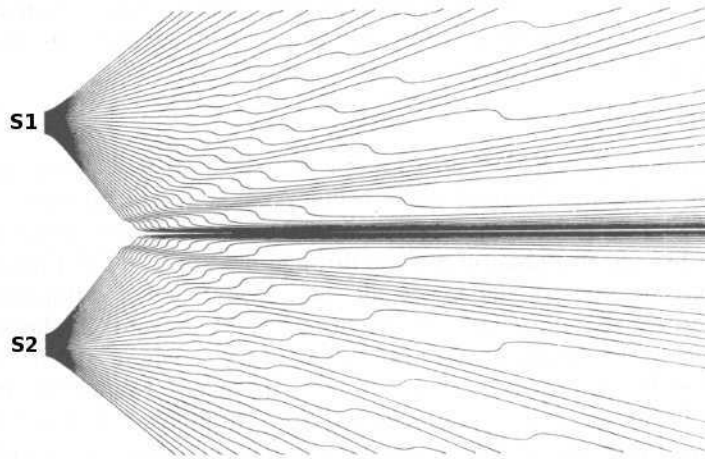


Figure 56: In the Bohmian interpretation of the double-slit experiment with electrons, every electron moves along a well-defined trajectory, but is influenced by the quantum potential determined from the quantum field associated with the electron. The quantum field is diffracted by the double-slit system, and the quantum potential is shaped in such a way that the electron is repelled from some regions in space, but attracted to others. The figure shows an ensemble of electron trajectories calculated in this model. Each electron emerge from one of the slits labeled as S1 and S2. The “kinks” in the trajectories coincide with the “troughs” in the quantum potential, because an electron entering the region of a trough is influenced by a repelling force due to the varying quantum potential. We see that statistically the trajectories reproduce the characteristic pattern of bright and dark fringes on the screen. *Source: Philippidis, Dewdney and Hiley [148] (modified)*

one of the slits⁶⁹, but its accompanying quantum field ψ passes through *both* of them and is diffracted (in the usual manner described by wave optics formalism). Thus on the other side of the double-slit screen the quantum field is no longer a plane wave and its amplitude R is no longer constant. Therefore Q and ∇Q are no longer zero. From Eq. (175) we see that in positions where R tends to zero, but $\nabla^2 R$ does not, Q tends to $-\infty$ which corresponds to infinite repulsion of the particle. The particle will then never be found at these positions, and thus we recover familiar destructive interference minima. The constructive interference maxima are present in the theory in a similar way. When the double-slit experiment is repeated many times, the ensemble of different electron trajectories will give rise to the familiar diffraction pattern on the second screen.

The above model was analyzed in detail by Philippidis, Dewdney and Hiley [148]. Their calculations show quantitatively that the distribution of different electron trajectories (different in the sense of starting positions, i.e. exact slit positions from which electron emerge) corresponds to the distribution of interference maxima and minima in the diffractive pattern (Fig. 56). In this way quantum probabilities are seen to arise from an ensemble average of individual processes, each of which can be causally described using Eq. (179). Dewdney and Hiley [149] showed also that scattering of particles by a square potential barrier and a square well may also be examined in the similar spirit and that the results are in accordance with the predictions of the standard interpretation (and thus with empirical facts).

We will now present a summary of the Bohmian interpretation as applied to material particles (after Bohm and Hiley [39], p. 29):

⁶⁹Often it would miss them and hit the screen instead, but we examine a situation where the electron actually passes through one of the slits.

1. The massive microscopic particles are corpuscles with well-defined positions. These positions vary continuously and can be causally determined.
2. Each particle is always accompanied by a new type of quantum field that fundamentally affects it. This field is described by real variables $R(\mathbf{r}, t)$ and $S(\mathbf{r}, t)$ satisfying Eq. (176) and (177), or alternatively by the wave function $\psi = Re^{iS/\hbar}$ satisfying the Schrödinger equation, Eq. (173). Thus the field also changes continuously and can be causally determined.
3. The particle has an equation of motion given by Eq. (179). The two forces acting on it is the classical force $-\nabla V$ (derived from the classical potential V) and the quantum force $-\nabla Q$ (derived from the quantum potential Q which depends on R and is given by Eq. (175)). In the classical limit where $\hbar \rightarrow 0$ quantum potential may be neglected and we recover the classical equation of motion.
4. The particle momentum is given as $\mathbf{p}(\mathbf{r}, t) = \nabla S(\mathbf{r}, t)$. Since the quantum field ψ is single valued, it can be shown that the following condition applies:

$$\oint \nabla S \, d\mathbf{r} = \oint \mathbf{p} \, d\mathbf{r} = nh,$$

where the integration is conducted along any closed curve in space, and $n \in \mathbb{N}$.

5. In a statistical ensemble of particles, selected so that all are characterized by the same quantum field ψ , the probability density for finding a single particle at a given position and at a given time is $\rho(\mathbf{r}, t) = R^2(\mathbf{r}, t)$. It should be stressed that the theory is *not* essentially probabilistic (as in the standard interpretation), because the statistics merely apply to an ensemble of *causally determined* particle trajectories.

9.3.2 The nature of the quantum field

As far as the wave-particle duality problem is concerned, the crucial point of the Bohmian interpretation is that the movement of massive particles in space is guided by the associated quantum field ψ . While the particles exhibit solely corpuscular behaviour, the quantum field is responsible for any undulatory (diffractive) effects that may arise. The main peculiar feature of the quantum field is that its influence depends only on the form of the field, and not on its amplitude (this is seen directly from the definition of the quantum potential, Eq. (175), where the amplitude part R of ψ is present both in the numerator and the denominator). Bohm and Hiley [39] emphasize that the effect of the quantum potential should not be understood mechanically and that ψ must be interpreted as a kind of information field that steers the movement of an electron. Furthermore, this steering is of a nonlocal character.

A direct detection of the quantum field proposed by Bohm would of course serve to strengthen his interpretation considerably, but it is actually debatable whether the quantum field possess any energy-momentum content. If it does, the content is so little that it has so far escaped attention of the experimentalists; if it does not, the quantum field are impossible to measure directly⁷⁰. It has been proposed that these waves could give rise to stimulated emission. Selleri [137] (Chapter 4.3) discussed different experiments aimed at

⁷⁰Although the lack of any energy content whatsoever would apparently contradict the postulate that the field has information content.

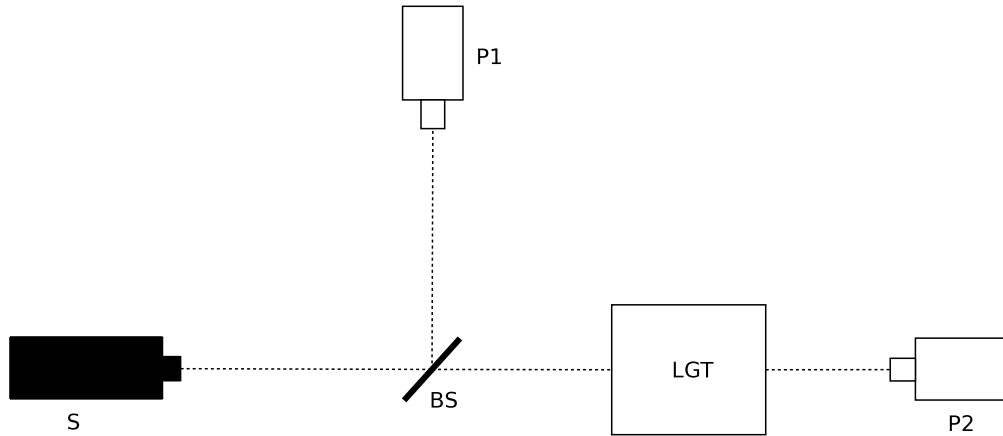


Figure 57: Experiment proposed by Selleri aiming at detection of an empty quantum wave. Source S emits single photons which, per assumption, are accompanied by quantum waves. In a situation where beam splitter BS sends the photon to photodetector P1, a part of the quantum wave is still transmitted in the direction of photodetector P2 through laser gain tube LGT. The quantum wave can stimulate emissions in LGT, and the emitted photons can be registered by P2.

proving this hypothesis. However, they are all flawed in the sense that they employ radiation quantum fields, not matter quantum fields, as the stimulating agent. This would not be problematic if Bohm’s reasoning regarding particles and their associated quantum fields could be extended directly to radiation. However, as we will see in the next section, in the case of radiation another approach must be used, so we are *not* allowed to think of light in terms of corpuscular photons guided by their quantum fields.

Let us nevertheless present the basic experimental setup proposed by Selleri in order to illustrate his idea (Fig. 57). A source S emits quasi-monochromatic radiation of central frequency f . The intensity is so low that we can safely assume that only one quantum of energy ($E = hf$) is present in the apparatus at any time. This photon reaches beam splitter BS and is sent either to phototube P1 or through a laser gain tube LGT to phototube P2. Selleri reasons in the following way: If the photon were a real corpuscular entity accompanied by quantum field, then only the quantum field would be divided by the beam splitter. Consider a situation where the photon is sent to P1, while (a part of) the quantum field moves through LGT in the direction of P2. Given that the quantum field is able to stimulate emissions in LGT, and that the photons emitted from LGT can be registered by P2, it follows that we can expect P1-P2 coincidences above the casual background. This would empirically demonstrate that some undulatory phenomenon is transmitted by BS in the direction of P2 even if the actual photon is sent to P1.

A more detailed statistical analysis of the experiment is given by Selleri [137] (Chapter 4.4). We note again that, according to Bohm himself [39], the idea of particles guided by associated quantum fields should be applied only to matter, and not to radiation, so Selleri built his reasoning on a wrong assumption. However, the proposed scheme could be in principle emulated with electrons, but practically it would present large difficulties, concerning both the process of “splitting” electrons and employing appropriate emitting medium that can be stimulated. We note also that it is unclear what would happen with the split quantum field in the moment of the absorption of the associated electron.

9.3.3 Interpretation of electromagnetic field

We have seen how the dual nature of material particles can be explained by the Bohmian interpretation using the idea of real corpuscles being guided by associated quantum fields (or waves). It is tempting to apply this explanation directly to the case of radiation, i.e. postulate existence of real massless light corpuscles (photons) influenced by quantum fields as well. However, Bohm and Hiley [39] (Chapter 11) presented several reasons that this approach cannot be carried out consistently. Their discussion involves elements of quantum field theory and we feel that it would be outside of the scope of our text to consider their arguments in detail. The main difficulty stems from the fact that, using the Klein-Gordon equation as the starting point, it is difficult, or maybe even impossible, to propose consistent guiding relation which would causally relate movement of photons to the scalar quantum field.

Bohm and Hiley proposed instead that in electromagnetism the only real physical objects are fields distributed continuously in space-time. No corpuscular photons actually exist, and any particlelike manifestations of these fields must be understood as a result of their nonlocal and nonlinear dynamics. Both nonlinearity and nonlocality are associated with the so-called super-quantum potential of the field which becomes negligible in the classical limit (in the similar way as quantum potential from Eq. (175)) where the fields again obey the classical wave equation.

If we restrict the model to the non-relativistic regime, the mathematical analysis⁷¹ is similar to the one conducted in Section 9.3.1. We introduce wave functional $\Psi = \Psi[\{\phi(x^\mu)\}]$ which is dependent on the set of all field variables $\{\phi(x^\mu)\}$ and where we write $\phi(x^\mu)$ instead of $\phi(\mathbf{r}, t)$. This wave functional can be also written as:

$$\Psi = R[\{\phi(x^\mu)\}]e^{iS[\{\phi(x^\mu)\}]}.$$

From the general form of Schrödinger equation it can be shown that every field variable, say ϕ_1 , must obey a modified wave equation:

$$\frac{\partial^2 \phi_1}{\partial t^2} = \nabla^2 \phi_1 - \frac{\delta Q}{\delta \phi_1}, \quad (180)$$

where $\frac{\delta}{\delta \phi_1}$ is the functional derivative with respect to ϕ_1 , and Q is the super-quantum potential defined as:

$$Q = -\frac{1}{2} \int \frac{\delta^2 R}{\delta \phi_1^2} R dV,$$

where the integration is performed over the whole space.

Bohm and Hiley claimed (without giving any rigorous proof) that it is the presence of the extra term $-\frac{\delta Q}{\delta \phi_1}$ that introduces nonlinear behaviour to the system, but that this term would disappear in the classical limit where the ordinary wave equation will be recovered. The nonlocality aspect, however, is involved in the transfer of energy between radiation and matter. For instance, when a wave packet of radiation excites an atom, energy is “swept in” from the entire wave packet at once as a single quantum of energy.

Thus in the Bohmian interpretation the wave-particle duality of light is no longer paradoxical. Any interference phenomena can be explained straight-forwardly, since the nature of radiation is *de facto* completely undulatory. At the same time any particlelike features are to be understood as the interaction between the electromagnetic field and matter, and the interaction might be both nonlinear and nonlocal (in the sense given above). We note that this approach is similar to the semiclassical model of radiation (see Sect. 5.1.2).

⁷¹We will use natural constants with $\hbar = c = 1$.

We have seen, however, that the semiclassical model of radiation has problems with accomodating results of some experiments concerned with photocount statistics. In Section 5.1.4 we have discussed the possibility of introducing effects of perhaps nonlinear character into the semiclassical model. Therefore it would be very interesting to examine quantitatively whether the model could be improved using the super-quantum potential idea from the Bohmian interpretation.

9.3.4 Concluding remarks

Two main arguments used by the opponents of the Bohmian interpretation is that it is nonlocal and that it does not give any new experimental predictions. The nonlocality makes it then untenable on the grounds of conflict with the relativity theory, while lack of new experimental predictions makes it worthless as a scientific theory. However, the Bohmian interpretation may be still defended.

It is true that the Bohmian interpretation is explicitly nonlocal, but elements of nonlocality are present in *any* present interpretation of the quantum theory, the standard interpretation included. Nonlocality emerges especially in connection with the EPR paradox and the collapse of the wave function. Other interpretations are today not able to give a fully local and satisfactory explanation of these phenomena – they are simply less “frank” about nonlocality than the Bohmian interpretation is. Bohm points out that consistent application of the nonlocal aspect in his interpretation leads “neither to internal logical contradiction nor to disagreement with any facts” (Bohm and Hiley [39], p. 157). Furthermore, nonlocal effects become insignificant in the macroscopic regime, so the explicit nonlocality does not imply presence of any nonlocal effects that are not confirmed experimentally. The Bohmian interpretation neither violates special relativity, because its quantum nonlocality does not allow a signal to be transmitted faster than light.

The second accusation, saying that the Bohmian interpretation does not give any new predictions and thus cannot be empirically verified, is even more extraneous, because interpretations do not need to give empirically verifiable predictions. They rather serve to highlight or question some elements of the formalism, and thus show a possible direction of future research. Strictly speaking, it is the formalism that serves to predict experimental results, not the interpretation. Both the Copenhagen and the Bohmian approaches have been showed to give a coherent qualitative description of the quantum-mechanical formalism and its results. Are there any reasons to favour one of them over the other? The standard interpretation is certainly much better established today than the Bohmian interpretation, but the reasons are mainly historical, psychological and sociological. The standard interpretation has been always supported by Niels Bohr’s enormous authority, while Bohm, during the time when his original papers were published, became somewhat of a scientific outcast due to political reasons⁷². However, modern science should show repugnance for the issues of personal authority, and any interpretation of a physical theory (if several interpretations of the same theory are possible, as in the case of quantum mechanics) should be judged by its elegance⁷³ and consistence, not by names attached to it.

⁷²In 1949 Bohm was called upon to testify before the House Committee on Un-American Activities because of his suspected ties to Communists. He was subsequently arrested and later acquitted, but in the meantime Princeton University had suspended him as an assistant professor and after the acquittal the university authorities did not want to renew his contract. Bohm left for Brasil, then moved to Israel and finally settled in England. He never returned to United States [150].

⁷³In the sense that as few *a priori* assumptions should enter it as possible. This is the principle commonly known as Occam’s razor.

In the recent times ideas of Bohm have been receiving renewed attention⁷⁴. Probably it has come together with the growing realization that the fundamental postulate of the standard interpretation – the denial of physical reality *per se* – is a blind alley which suffocates further inquiry into the nature of the physical world by claiming many interesting questions completely meaningless. On the other hand, the Bohmian interpretation strives to give a clear intuitive framework within which quantum-mechanical formalism can be analyzed and further developed. In this task it has already succeeded to some degree. It is most clearly seen in the case of the wave-particle duality which the interpretation elegantly explains by reducing the corpuscular and the undulatory behaviour to a common physical principle. It remains to be seen whether the Bohmian interpretation can be fully extended to the relativistic domain and whether its application will lead to new formal results that *can* be confirmed experimentally. If this will happen, the paradigm of quantum mechanics will doubtlessly change.

⁷⁴According to the online database at <http://prola.aps.org> more than 350 scientific papers have referred to Bohm's original article [144] in the course of last 10 years.

10 Conclusion

10.1 Summary and outlooks

In the course of the thesis we have discussed several aspects, both theoretical and experimental, of the wave-particle duality of light. As remarked already in the Introduction, the duality can be considered from several angles and thus offers a lot of opportunities for scientific inquiry. Therefore our review had to be limited – some elements of the problem were discussed in depth, some only mentioned, and some omitted altogether. However, our presentation of the subject shows clearly that the wave-particle duality can be considered on three levels.

First and foremost, the duality can be approached directly, as in Chapters 1-3, where we asked how our perception of light has changed through the last four centuries, what present physical theories support the undulatory and the corpuscular view, and what experimental evidence supports in turn these different theories. We have seen that *the historical development encourages us to question the contemporary perception of light*. The previous prevailing theories were either overthrown (as Newton’s corpuscular model) or heavily extended and modified by classical electromagnetism and quantum mechanics (as the Young-Fresnel wave theory) (Ch. 1). There is no reason to believe that the present paradigm will not change. Multiple questions regarding the relation between the wavelike and the particlelike behaviour rather suggest that a further development is inevitable.

From the theoretical point of view there are two main models which encapsulate the undulatory and the corpuscular view of light. These are, respectively, Maxwell’s electromagnetism (Ch. 2.1) and quantum mechanics applied to electromagnetic radiation (Ch. 2.3-2.4). While the first one describes light waves in a very elegant and concise manner, the second one does not manage to do the same for light corpuscles, because any attempts to localize single photons in space encounter fundamental difficulties (Sect. 2.3.4). Furthermore, since the radiation field is treated holistically, the distinction between photons and quantized energy content of the field is rather unclear. These two facts indicate that *our present corpuscular theory of light says more about the interaction between light and matter than about light itself*. This is not a disadvantage *per se*, but in the context of the wave-particle duality and discussions of “light corpuscles” one should keep this reservation in mind.

Any physical model should be of course judged by comparing its quantitative predictions with experimental results, and both theories have had many successes in this respect. The diverse interference phenomena are most elegantly explained using the undulatory model (Ch. 3.2). Also, contrary to the widespread belief, *the*

undulatory model is able to account for both photoelectric effect and Compton effect (Ch. 3.3-3.4). The basic features of these two effects must be therefore dismissed as conclusive empirical confirmation of the photon hypothesis. Instead of the photoelectric effect and the Compton effect, one should rather refer to correlation experiments of the type Grangier, Aspect and Roger conducted (Ch. 3.5), because anticoincidence effects seem to substantiate the corpuscular theory much better. However, we saw that their results could also be questioned due to the simplifying assumptions involved and the use of nonclassical cascading light source (see below).

More detailed analysis of the correlation experiments allows us to consider the wave-particle duality on another level, namely in the context of the photodetection processes and two competing models of photodetection – the semiclassical one and the fully quantized one (Ch. 5.1). Obviously, the photodetection process plays a fundamental role in any situation where the light beam is measured directly. Unfortunately, as far as statistical properties of light are concerned, *the quantum behaviour of classical light cannot be demonstrated in a satisfying way*. We illustrated this fact experimentally and numerically in Chapter 7.1 in the case of coherent radiation. We saw that it is necessary to employ nonclassical sources of light (i.e. not thermal and not coherent) in order to obtain experimental results that the semiclassical model cannot account for. But as we pointed out in Section 5.1.4, the model is somewhat limited by the stationarity condition, so here lies certain room for its further development.

The semiclassical model could be also improved by putting larger emphasis on *fluctuations inherent to the detectors* and through *careful analysis of the interactions between light and detectors*, especially in the very low intensity regime (Sect. 5.1.4). The issue of fluctuations was also raised in connection with beam splitter (Ch. 5.2) during the discussion of the *shortcomings of the existing beam splitter models* (Sect. 5.2.3). One should keep in mind that beam splitter is a crucial element of any optical setup aiming at measuring correlations, so if any hitherto undiscovered effects are present here, they would be able to considerably influence experimental results.

The theory of coherence presents us with another important aspect of the wave-particle duality. The concepts of coherence length and coherence time may be easily pictured and comprehended in the high intensity regime using the language of classical electromagnetism. They play a central role in the mathematical description of fluctuations of chaotic and partially coherent radiation, and they help to explain the emergence of interference fringes in e.g. double-slit experiments (Ch. 4). However, at very low intensity level it is unclear how the concept of coherence should be related to the notion of photon. One could for instance assume that photons are spatially extended and that their size in one way or another corresponds to coherence length, but then we are effectively replacing light corpuscles with wave packets. On the other hand *the notion of coherence length cannot be dismissed altogether at very low intensity level, because the interference phenomena still occurs* (Ch. 7.2). It seems that during a further investigation of wave-particle duality one should aim at establishing an accurate relation between coherence length and the concept of photon (perceived either as a corpuscle or as an energy quantum of the radiation field).

Finally, there is the third level on which the wave-particle duality can be considered. On this level *one seeks radically new models of light (as Panarella's photon clump model) or radically new interpretations of present theories (as Bohm's interpretation of quantum mechanics) in order to directly reconcile the undulatory and the corpuscular aspect* (Ch. 9). However, this approach requires caution due to its highly speculative character. We have seen that Panarella's model implies far-fetched (but nonetheless empirically verifiable) assumptions about the physical world (Ch. 9.1), while Bohm's interpretation per definition does not yield

any immediate new predictions, although it may stimulate the development of the formalism in some fruitful direction (Ch. 9.3). At the same time Bohm's interpretation suggests presence of a nonlinear term in the wave equation, and such nonlinearity may represent another possibility for improvement of the semiclassical model.

It is also conceivable that some new experimental setup will challenge the wave-particle duality in its present form by producing results which none of the present theories is able to account for. We have argued that *Afshar's experiment does not necessarily produce such results*, both because it can be described using the semiclassical model and because the application of the Greenberger-Yasin inequality (Eq. (170) on p. 135) to the analysis may be questioned (Ch. 8). Nonetheless, Afshar's experiment remains a very clever nonperturbative measurement scheme with possible future applications.

It is rather obvious that our whole discussion of the wave-particle duality has been slanted towards the undulatory view of light. This is not due to any prejudice present from the outset, but rather from the fact that the particlelike properties, after closer inspection, seem much more elusive than the wavelike properties. We notice that while *nonclassical sources of light are needed in order for radiation to exhibit corpuscular behaviour (in the sense of photocount statistics as discussed above), the undulatory behaviour is present for both classical and nonclassical sources at any level of intensity*, also in the very low intensity regime usually interpreted as "the single photon level". It seems therefore that *if* one of the models might be made redundant, the corpuscular properties could be embedded into the wave theory, but not the other way around. In the author's opinion future inquiries into the wave-particle duality problem should be connected with attempts to extend the semiclassical model beyond its present boundaries, both through a closer examination of the stationarity condition and through introducing additional (possibly nonlinear) effects into the semiclassical theory of photodetection.

On the basis of his work the author would now like to propose the following prospects:

- More detailed theoretical analysis of the difficulties that arise when we try to describe photon localization using wave function formalism. We touched briefly upon this subject in Sect. 2.3.4, but it deserves surely further examination.
- Closer analysis of the notion of coherence in the very low intensity regime. Especially one could try to construct models which associate coherence directly with the photonic entity and which perhaps predict that coherence length is dependent in a specific way on the number density of photons in the beam. Such predictions could be then tested experimentally.
- Conduct of a photomeasuring experiment with a classic light source which yields statistical results conflicting the predictions of the semiclassical model in its standard form. Such an experiment has been proposed in Sect. 5.1.4. The semiclassical model could then be appropriately extended in order to account for the results, and this extension could be in turn applied to nonclassical sources in order to see whether their emission can be described without referring to the fully quantized model.
- Development of new beam splitter models along the lines proposed in Sect. 5.2.3.
- Further development of the numerical routine presented in Appendix D which can be employed to simulate correlation measurements. More complex beam splitter and photodetection models could be incorporated into the routine and simulations based on diverse assumptions could be then performed,

both in order to gain better insight into different possibilities, and in order to test different hypotheses and compare their predictions with experimental results.

- Combining Afshar's experiment with Grangier, Roger and Aspect's correlation experiment in order to create an experimental setup where both the nonperturbative measurement of interference pattern and the anticoincidence effect observed by Grangier et al. are present at the same time.
- Explicit testing of the predictions given by Panarella's photon clump model.
- Theoretical development of Bohm's idea regarding the possible presence of nonlinear terms in equations governing the undulations of electromagnetic field. This nonlinearity could be used in order to extend the semiclassical model.

10.2 Closing words

Does the wave-particle duality deserves an explanation? Or, more precisely, should physicists seek a more general model of light from which the undulatory properties and the corpuscular properties emerge naturally? Or should we rather develop further the existing, mutually exclusive models, and do not attempt to build a bridge between them, unless future research will suggest in a direct way how such a connection could be constructed? The answers to these questions are heavily conditioned by one's approach to the science of physics in general. There are two main motivations for studying, doing and applying physics to the broad array of natural phenomena. In most cases these motivations are "superposed", but sometimes one dominates over the other, so it is easy to distill them in their pure forms.

The first motivation stems from our will to comprehend the world and the observable processes *ontologically*, through establishing as close correspondence as possible between our physical models and different aspects of reality. The correspondence can be never made complete, so there may easily occur a situation where the same aspect of reality is described by different models yielding correct quantitative predictions. However, one should then endeavor to attain a maximal degree of consistency between models in order to create as coherent *picture* of reality as possible. In this approach the qualitative plane seems superior to the quantitative one. Of course, the mathematical apparatus is indispensable as a methodological tool that makes us capable of verifying individual models by confronting their predictions with experimental results, but the ability to perform correct calculations and to quantitatively anticipate phenomena does not have any particular significance *on its own*.

With this approach to physics the need for an unambiguous clarification of the wave-particle duality is obvious. We want "only" to answer precisely the question about the nature of electromagnetic radiation without making use of the complementarity notion, because the claim that light sometimes behaves as a wave, and sometimes as a corpuscle, and that there is no deeper level of reality on which these two manifestations could be merged – such claim seems very unsatisfying. Of course, "unsatisfying" does not imply "untrue", but the history of physics has showed us so far that there are answers for almost any question, even though these answers eventually lead to new questions.

The second motivation for working with physics is of a calculational character. Physicists impelled by it want primarily to apply mathematical tools to natural phenomena in order to model them *quantitatively*,

and questions about the nature of reality (in the sense of looking for concise and fully consistent *qualitative* descriptions) are for them of secondary importance. Thus, this doctrine is rather *phenomenological* or *epistemological* than ontological. According to it the aim of physical models is to *simulate* natural phenomena. Any ambitions of *emulating* the reality must be given up. This simulative and more reserved approach was succinctly (and probably half-jokingly) expressed by David Mermin in his oft-quoted declaration: "If I were forced to sum up in one sentence what the Copenhagen interpretation says to me, it would be 'Shut up and calculate!'" [151]. The calculational attitude suggests that deliberation on the "true" meaning of theories and search for new interpretations of prevailing formalisms at some point should be simply ceased, and thereafter the only thing that counts is the ability to perform precise, empirically confirmed calculations.

Within this strategy the need for explaining the wave-particle duality is much less obvious. The calculational approach suggests that instead of struggling with the question on the nature of light, a physicist should focus his or her efforts on mathematical descriptions of phenomena in which light is involved. If results were to suggest an unequivocal qualitative interpretation, one should of course embrace it, but if no such interpretation were to appear, one should not consider it as a problem that physics must overcome. After all, employing several different models of electromagnetic radiation is not troubling from the calculational point of view, as long as each of these models yields correct results within its applicability range, and as long as no new phenomena are discovered that none of the models is able to explain.

Let us, however, notice two things. First of all, attempts at unificating different models have been one of the main drives for the development of physics, since new theories often are born on boundaries between the old ones. The phenomena of electricity and magnetism were fused by Maxwell's electromagnetism; when trying to explain inconsistencies between electromagnetism and classical mechanics Einstein worked out the special theory of relativity; and then, while incorporating Newton's theory of gravity into the latter, Einstein developed the general theory of relativity. Thus we see that in any situation where several competing physical models are present, there lies a possibility for unification, and unifications always lead to new and sometimes astonishing results.

Secondly, even if we are impelled by the first (emulative) motivation when searching for a new model, we will be guided by the methodology intimately connected with the second (simulative) motivation – which confronts predictions of temporary hypotheses with experimental results. In other words, if we at some time in the future achieve our goal and find a model that elegantly answers our qualitative questions about natural phenomena, the model will necessarily be correct from the empirical point of view (because otherwise it would be scientifically worthless), and thus can be employed in a purely quantitative manner. Therefore the advocates of the calculational approach will also greatly benefit from it, especially if the model makes use of more elegant and sharper mathematical methods.

We stress again that in practice both motivations are usually blended, as in the case of the author when working with the above thesis. Investigating the problem of the wave-particle duality presents us with an excellent opportunity for asking many exciting questions regarding the nature of the light, our way of perceiving and measuring it, the limits of our current models and our interpretations of physical theories. On the other hand, this type of inquiry serves at the very least to clarify the existing models – but possibly may also lead to development of new and fruitful ones.

As a final side note, we notice an interesting parallel. When modern physics was born in the 17th century, two crucial questions were posed regarding the nature of the world: "What is gravity?" and "What is light?". Newton admitted that he was not able to explain how physical bodies influence each other through vast

cosmic distances. The "essence" of gravitational interactions remained a mystery for several centuries, until Einstein presented his very elegant theory which interpreted gravitation as space-time curvature. The general theory of relativity led to many new questions within the cosmological framework, but today the geometrical view of gravity itself stands very strongly.

The question about the nature of light, however, led rather quickly to two conflicting answers, and this conflict has survived to the present day. The opposing views of light have gone far along their respective paths, but they have not been reconciled by any conceptual breakthrough comparable to that associated with Einstein's relativity. In the recent years it seems that these two paths finally started to converge, due to technological progress represented by laser, nonclassical sources of light and modern detectors, and due to new physical theories as quantum optics and quantum electrodynamics. It is the author's hope that the near future will show whether the convergence can be made complete and whether the notion of wave-particle duality will become as anachronistic as that of luminiferous aether that light had once been believed to propagate through.

Borys Jagielski
Oslo, 28.05.2009

A The formalism of quantum mechanics

The wave-particle duality is deeply rooted in the quantum mechanics. In the author's opinion, however, it would be exorbitant to dedicate a separate chapter to the basic notions of the quantum-mechanical formalism, since they are assumed to be well-known to the reader. Nonetheless, throughout the thesis, we refer to some particular (although still fundamental) relations incorporated in the theory. Therefore, for the sake of completeness, we present here in a highly abbreviated form the basic formalism of the quantum mechanics. Our focus is on the postulates, on the essential results related to the measurement theory and on Heisenberg's uncertainty principle (the full proof of which is included). For a more detailed and very readable formal introduction to quantum mechanics (which does not refrain from discussing several subtle points usually omitted by other authors) we refer to Isham [152]. A standard modern reference to the subject is Shankar [51].

The mathematical apparatus of quantum mechanics and its linkage to the physical world rest on the four following postulates:

1. Each physical state is represented by a (normalized) time-dependent vector $|\Psi\rangle$ belonging to a complex Hilbert space⁷⁵ \mathcal{H} . The complex Hilbert space forms the state space of the physical system.
2. Each measurable physical quantity A , called an observable, is represented by a self-adjoint⁷⁶ (i.e. Hermitian) operator \hat{A} acting on the vectors in the complex Hilbert space.
3. Given an ensemble of identical physical states, each represented by a normalized vector $|\Psi\rangle \in \mathcal{H}$, the mean measured value of A is the scalar product of $|\Psi\rangle$ with $\hat{A}|\Psi\rangle$. Using Dirac's notation⁷⁷ we write

$$\langle A \rangle = \langle \Psi | \hat{A} | \Psi \rangle. \quad (181)$$

4. The time evolution of any closed (isolated) system is described by a differential equation called Schrödinger's equation:

$$i\hbar \frac{d|\Psi(t)\rangle}{dt} = \hat{H} |\Psi(t)\rangle, \quad (182)$$

⁷⁵A complex Hilbert space is a complex inner product space that is complete under the norm defined by the inner product. Completeness means that every Cauchy sequence of vectors in the space has a limit that also belongs to the space.

⁷⁶Self-adjointness of an operator \hat{A} means that the operator is equal to its conjugate transpose, $\hat{A}^\dagger = \hat{A}$.

⁷⁷In this notation the scalar product of a vector $|x\rangle$ with a vector $|y\rangle$ is written as $\langle x|y\rangle = \langle y|x\rangle^*$.

where \hbar is Planck's constant divided by 2π , and \hat{H} is the Hamiltonian operator, an operator formed from the classical Hamiltonian of the system. Here we have written $|\Psi(t)\rangle$ instead of $|\Psi\rangle$ in order to stress the time-dependency of the vector.

It can be shown that all eigenvalues of any Hermitian operator \hat{A} are real, and that the eigenvectors $\{|\phi_i\rangle\}$ belonging⁷⁸ to these eigenvalues form an orthogonal and complete⁷⁹ set. Orthogonality implies $\langle\phi_i|\phi_j\rangle = 0$ if $i \neq j$, and because of the completeness any vector $|\Psi\rangle$ belonging to a finite-dimensional \mathcal{H} can be expressed as a linear combination of the orthonormalized eigenvectors of any Hermitian operator \hat{A} :

$$|\Psi\rangle = \sum_{i=1}^N c_i |\phi'_i\rangle,$$

where N is the total number of eigenvectors (or, equivalently, the dimensionality of the Hilbert space involved), c_i is a complex coefficient calculated from $c_i = \langle\phi_i|\Psi\rangle$ (this relation follows from the orthogonality of the eigenvectors), and $|\phi'_i\rangle$ is the normalized $|\phi_i\rangle$:

$$|\phi'_i\rangle = \frac{|\phi_i\rangle}{\sqrt{\langle\phi_i|\phi_i\rangle}}.$$

A crucial result can be derived from Rule 3. If, given a physical state described by $|\Psi\rangle$, we perform a measurement of an observable A , the measurement will always⁸⁰ yield one of the eigenvalues of \hat{A} . The probability of the measurement resulting in some non-degenerate eigenvalue is simply $|c_i|^2 = |\langle\phi_i|\Psi\rangle|^2$ where $|\phi_i\rangle$ is the associated eigenvector. If, however, the asked-for eigenvalue is degenerate, we have to sum $|\langle\phi_i|\Psi\rangle|^2$ over all associated eigenvectors $|\phi_i\rangle$.

The above result is fundamental for the quantum-mechanical measurement theory, and it shows how the probabilistic nature of the theory comes about. We emphasize that it is not an additional postulate, but it follows from Rule 3; alternatively, Rule 3 can be derived from it, so this result is sometimes presented as its equivalent version. However, both possible forms of Rule 3 have to be supplied by another (experimentally verifiable) postulate: The act of measurement leads to an instantaneous change of the quantum state from $|\Psi\rangle$ to $|\phi_i\rangle$, where $|\phi_i\rangle$ is the eigenvector associated with the eigenvalue which the measurement has yielded. This phenomenon is called the collapse of the wave function⁸¹.

We notice that the possibility of the collapse is altogether absent from Schrödinger's equation, Eq. (182). The equation describes the deterministic time evolution of $|\Psi\rangle$ until a measurement is made. Then the evolved state collapses to one of the eigenvectors of the operator associated with the measured observable, and the time evolution continues, again in accordance with Schrödinger's equation, until the next measurement is made, and so on. In other words, the time evolution of a quantum state consists of two parts: the deterministic and continuous part described fully by Schrödinger's equation, and the probabilistic and non-continuous part

⁷⁸The number of distinct eigenvalues may be smaller than the number of distinct (i.e. linearly independent) eigenvectors. In such a situation at least two distinct eigenvectors share the same eigenvalue, and we say that the (eigen)spectrum of the operator is degenerate.

⁷⁹The completeness of the eigenvectors is not to be confused with the completeness of the Hilbert space. Furthermore we implicitly assume that the considered is finite-dimensional. The argument can be extended to infinite-dimensional vector spaces as well, but then some additional aspects of the formalism must be discussed. The original reference is Dirac [153].

⁸⁰Given the measurement is ideal, i.e. as precise as theoretically possible.

⁸¹If the eigenvalue is degenerate, the vector collapses to a superposition of the associated eigenvectors. The eigenvectors in the superposition are weighted as in the original vector.

associated with the act of measurement.

We notice that Eq. (182), as written above, is formally problematic, because it is not clear what one means with the time derivative of a vector. We should rather express it as:

$$i\hbar \frac{\partial \psi(q, t)}{\partial t} = \langle q | \hat{H} | \Psi(t) \rangle, \quad (183)$$

where $\psi(q, t) \equiv \langle q | \Psi(t) \rangle$ is the coordinate representation of $|\Psi(t)\rangle$, and $|q\rangle$ is an eigenvector associated with an eigenvalue q of the coordinate observable \hat{q} . The most usual coordinate representations are those given by position x or momentum p . Their eigenspectra are continuous. If we work in the position representation, the position variable x is represented simply as x , but according to the standard prescription the momentum variable is represented as a differential operator, $p \rightarrow -i\hbar \frac{\partial}{\partial x}$. Thus the Hamiltonian for a free particle, $H = \frac{p^2}{2m} + V(x)$ (with m being the mass of the particle and V the position-dependent potential), becomes in the position representation the operator $\hat{H} = \frac{-\hbar^2}{2m} \left(\frac{\partial}{\partial x}\right)^2 + V(x)$. Schrödinger's equation for such a particle yields:

$$i\hbar \frac{\partial \psi(x, t)}{\partial t} = \frac{-\hbar^2}{2m} \frac{\partial^2 \psi(x, t)}{\partial x^2} + V(x) \psi(x, t).$$

Since the proper form of Schrödinger's equation, Eq. (183), is valid in any coordinate representation, it is justifiable to use the more compact version given by Eq. (182).

A central axiom of the quantum theory is that the position and momentum operators do not commute:

$$\hat{x} \hat{p}_x - \hat{p}_x \hat{x} \equiv [\hat{x}, \hat{p}_x] = i\hbar, \quad (184)$$

with the lower index x standing for the x-component of the momentum. In three dimensions we have:

$$[\hat{r}_i, \hat{p}_j] = i\hbar \delta_{ij}, \quad i, j = x, y, z. \quad (185)$$

One can prove that two Hermitian operators have the same set of eigenfunctions if and only if they commute. In physical terms this is interpreted as the claim that we are principally unable to measure simultaneously two non-commuting observables of a physical system with an arbitrarily large precision. One of the measurements will inevitably disturb the physical system and influence the outcome of the second measurement. If the first observable is measured with full precision, the disturbance of the value of the second observable will be maximal in the sense that uncertainty in the second measurement will be infinitely large.

It should be stressed that the last two sentences of the previous paragraph take for granted the realistic stance. By using the phrase “the disturbance of the value of the second observable” we have assumed that the formalism of quantum mechanics describes a physical reality, and that a quantity associated with a physical system has some value even before the actual measurement of that value is being made. Such a realistic approach is intuitively obvious, but in fact it is denied by the Copenhagen interpretation of quantum mechanics. We have elaborated on this point in Chapter 9.2.

Apart from the problem of choosing an appropriate interpretation, the uncertainty associated with measuring two non-commuting observables is quantified by the ubiquitous Heisenberg's principle. We end this appendix by demonstrating its generalized version. We follow the proof given by Griffiths [154] (pp. 110-111).

Rule 3 gives the formula for calculating the mean value of an observable A given a system described by $|\Psi\rangle$:

$$\langle A \rangle = \langle \Psi | \hat{A} | \Psi \rangle \equiv \mu_A.$$

The variance σ_A^2 (the spread of the results about $\langle A \rangle$) is:

$$\sigma_A^2 \equiv \langle (A - \mu_A)^2 \rangle = \langle \Psi | (\hat{A} - \mu_A)^2 | \Psi \rangle = \langle \Psi | (\hat{A} - \mu)^{\dagger} (\hat{A} - \mu_A) | \Psi \rangle, \quad (186)$$

where the last equality is allowed because \hat{A} (and thus $\hat{A} - \mu$, since μ is a real scalar) is Hermitian. We define a new vector state:

$$|\alpha\rangle \equiv (\hat{A} - \mu_A) | \Psi \rangle,$$

and so:

$$\sigma_A^2 = \langle \alpha | \alpha \rangle.$$

For any other observable B we thus have:

$$\sigma_B^2 = \langle \beta | \beta \rangle,$$

with $|\beta\rangle \equiv (\hat{B} - \mu_B) | \Psi \rangle$ and $\mu_B \equiv \langle \Psi | \hat{B} | \Psi \rangle$. Now, from the Schwarz inequality [155] it follows that:

$$\sigma_A^2 \sigma_B^2 = \langle \alpha | \alpha \rangle \langle \beta | \beta \rangle \geq |\langle \alpha | \beta \rangle|^2,$$

which is valid for any two observables A and B . Since the scalar product $\langle \alpha | \beta \rangle$ is a complex number z , and since for any complex number it is true that:

$$|z|^2 = \Re(z)^2 + \Im(z)^2 \geq \Im(z)^2 = \left[\frac{1}{2i} (z - z^*) \right]^2,$$

we have:

$$\sigma_A^2 \sigma_B^2 \geq \left[\frac{1}{2i} (\langle \alpha | \beta \rangle - \langle \beta | \alpha \rangle) \right]^2. \quad (187)$$

Now we calculate $\langle \alpha | \beta \rangle$ explicitly:

$$\begin{aligned} \langle \alpha | \beta \rangle &= \langle \Psi | (\hat{A} - \mu_A)^{\dagger} (\hat{B} - \mu_B) | \Psi \rangle = \langle \Psi | (\hat{A} - \mu_A) (\hat{B} - \mu_B) | \Psi \rangle = \\ &= \langle \Psi | \hat{A} \hat{B} | \Psi \rangle - \mu_B \langle \Psi | \hat{A} | \Psi \rangle - \mu_A \langle \Psi | \hat{B} | \Psi \rangle + \mu_A \mu_B \langle \Psi | \Psi \rangle = \\ &= \langle \Psi | \hat{A} \hat{B} | \Psi \rangle - \mu_B \mu_A - \mu_A \mu_B + \mu_A \mu_B = \langle AB \rangle - \mu_A \mu_B \equiv \mu_{AB} - \mu_A \mu_B, \end{aligned}$$

where $\mu_{AB} \equiv \langle AB \rangle$. Similarly we get $\langle \beta | \alpha \rangle = \mu_{BA} - \mu_A \mu_B$ with $\mu_{BA} \equiv \langle BA \rangle$. Thus:

$$\langle \alpha | \beta \rangle - \langle \beta | \alpha \rangle = \mu_{AB} - \mu_{BA} = \langle \Psi | (\hat{A} \hat{B} - \hat{B} \hat{A}) | \Psi \rangle = \langle \Psi | [\hat{A}, \hat{B}] | \Psi \rangle = \left\langle [\hat{A}, \hat{B}] \right\rangle.$$

If we insert the above result back into Eq. (187), we get the generalized uncertainty principle which gives us the lower bound for the product of two variances of two observables:

$$\sigma_A^2 \sigma_B^2 \geq \left[\frac{1}{2i} \left\langle [\hat{A}, \hat{B}] \right\rangle \right]^2. \quad (188)$$

It follows that if the operators associated with the two observables commute, then the lower bound is zero. If the two observables, however, are position x and the x -component of momentum p_x , Eq. (188) yields (with

the help of the canonical commutation relation, Eq. (184):

$$\sigma_x^2 \sigma_{p_x}^2 \geq \left[\frac{1}{2i} \langle [\hat{x}, \hat{p}_x] \rangle \right]^2 = \left[\frac{1}{2i} \langle i\hbar \rangle \right]^2 = \frac{\hbar^2}{4},$$

so:

$$\sigma_x \sigma_{p_x} \equiv (\Delta x) (\Delta p_x) \geq \frac{\hbar}{2}.$$

Using Eq. (185) we readily obtain a three-dimensional generalization:

$$(\Delta x)(\Delta y)(\Delta z) (\Delta p_x) (\Delta p_y) (\Delta p_z) \geq \frac{\hbar^3}{8} \approx \hbar^3. \quad (189)$$

B Demonstration of properties of the coherent states

In the following we will prove the properties of the coherent states listed in Chapter 2.4. Our treatment is guided by Leinaas [156] (Chapter 1) and Mandel and Wolf [55] (Chapter 11).

B.1 The minimal uncertainty

We are going to prove that the coherent states $|z\rangle$ are the minimal uncertainty states, i.e. that for all z Heisenberg's uncertainty principle becomes an equality:

$$\sqrt{\langle z | (\Delta\hat{q})^2 | z \rangle} \sqrt{\langle z | (\Delta\hat{p})^2 | z \rangle} = \frac{\hbar}{2}. \quad (190)$$

Here $(\Delta\hat{q})^2$ is the dispersion operator for the coordinate operator \hat{q} . The dispersion operator is defined as:

$$(\Delta\hat{q})^2 \equiv (\hat{q} - \mu_q)^2, \quad (191)$$

with:

$$\mu_q \equiv \langle z | \hat{q} | z \rangle \quad (192)$$

being the mean value of the coordinate q . Similarly, $(\Delta\hat{p})^2$ is the dispersion operator for the conjugate momentum operator \hat{p} . As noticed in Appendix A, the mean dispersion is simply the variance of the related observable (cf. Eq. (186)).

From Eqs. (191)-(192) we see that:

$$\langle z | (\Delta\hat{q})^2 | z \rangle = \langle z | \hat{q}^2 | z \rangle - \langle z | \hat{q} | z \rangle^2. \quad (193)$$

A similar relation holds for $\langle z | (\Delta\hat{p})^2 | z \rangle$. Furthermore, in Eqs. (17)-(18) in Chapter 2.2 we have seen how the annihilation and creation operators (then called the lowering and the raising operators) are defined in the case of a massive harmonic oscillator. In the case of electromagnetic field these definitions are almost identical, but since the photons are massless the mass is absent. Thus we have:

$$\begin{aligned} \hat{a} &\equiv \sqrt{\frac{\omega}{2\hbar}} \left(\hat{q} + \frac{i}{m\omega} \hat{p} \right) \\ \hat{a}^\dagger &= \sqrt{\frac{\omega}{2\hbar}} \left(\hat{q} - \frac{i}{m\omega} \hat{p} \right), \end{aligned}$$

where ω is the angular mode frequency. It follows that:

$$\begin{aligned}\hat{q} &= \sqrt{\frac{\hbar}{2\omega}} (\hat{a}^\dagger + \hat{a}) \\ \hat{p} &= i\sqrt{\frac{\hbar\omega}{2}} (\hat{a}^\dagger - \hat{a}).\end{aligned}$$

The formula for \hat{q} gives us:

$$\hat{q}^2 = \frac{\hbar}{2\omega} (\hat{a}^{\dagger 2} + \hat{a}^2 + \hat{a}^\dagger \hat{a} + \hat{a} \hat{a}^\dagger) = \frac{\hbar}{2\omega} (\hat{a}^{\dagger 2} + \hat{a}^2 + 2\hat{a}^\dagger \hat{a} + 1)$$

where we have used the commutation relation from Eq. (41) (Ch. 2.3.3) Using the above expression together with the defining eigenvalue relation for the coherent states (Eq. (52), Ch. 2.4), Eq. (193) readily yields:

$$\langle z | (\Delta\hat{q})^2 | z \rangle = \frac{\hbar}{2\omega} (z^{*2} + z^2 + 2z^*z + 1) - \frac{\hbar}{2\omega} (z^{*2} + z^2 + 2z^*z) = \frac{\hbar}{2\omega}.$$

Along the same lines one could show that:

$$\langle z | (\Delta\hat{p})^2 | z \rangle = \frac{\hbar\omega}{2}.$$

The minimal uncertainty relation that we have set out to prove, Eq. (190), follows at once.

B.2 The time evolution of a coherent state

We examine how an arbitrary coherent state $|z\rangle$ evolves in time. We choose to work in the Heisenberg picture, so let us equip the annihilation operator \hat{a} with time-dependency according to the standard quantum mechanical formula:

$$\hat{a}(t) = \hat{U}(t)^\dagger \hat{a} \hat{U}(t), \quad (194)$$

where $\hat{U}(t)$ is the time operator:

$$\hat{U}(t) = e^{-\frac{i}{\hbar} \hat{H} t},$$

with \hat{H} being the Hamilton operator. Thus, using Eq. (23) (Ch. 2.2) we see that $\hat{U}(t) = e^{-i\omega(\hat{a}^\dagger \hat{a} + \frac{1}{2})t}$ and from Eq. (194) we get

$$\hat{a}(t) = e^{i\omega t \hat{a}^\dagger \hat{a}} \hat{a} e^{-i\omega t \hat{a}^\dagger \hat{a}} \quad (195)$$

after the $\frac{1}{2}$ -factors have been cancelled. Now, the operator expansion theorem states that for any two operators \hat{A} and \hat{B} [157]:

$$e^{x\hat{A}} \hat{B} e^{-x\hat{A}} = \hat{B} + x[\hat{A}, \hat{B}] + \frac{x^2}{2!} [\hat{A}, [\hat{A}, \hat{B}]] + \dots$$

An important lemma follows immediately:

$$e^{\hat{A}} \hat{B} e^{-\hat{A}} = \hat{B} + [\hat{A}, \hat{B}] + \frac{1}{2!} [\hat{A}, [\hat{A}, \hat{B}]] + \dots \quad (196)$$

With its help Eq. (195) can be simplified to:

$$\hat{a}(t) = e^{-i\omega t} \hat{a}.$$

Now let us apply the time evolution operator to a coherent state $|z\rangle$ and operate with \hat{a} on top of that.

$$\begin{aligned} \hat{a}(\hat{U}(t)|z\rangle) &= \hat{U}(t)(\hat{U}(t)^\dagger \hat{a} \hat{U}(t))|z\rangle = \hat{U}(t)\hat{a}(t)|z\rangle = \hat{U}(t)(e^{-i\omega t} \hat{a})|z\rangle = \\ &= \hat{U}(t)(e^{-i\omega t} z)|z\rangle = e^{-i\omega t} z(\hat{U}(t)|z\rangle) \end{aligned}$$

If we define $|z(t)\rangle \equiv \hat{U}(t)|z\rangle$, we see that $\hat{a}|z(t)\rangle = z(t)|z(t)\rangle$ with $z(t) = e^{-i\omega t} z$. The coherent state evolves with time into other coherent states, and the original eigenvalue z simply gets a revolving phase factor $e^{-i\omega t}$. Thus the time evolution is periodic with period $\frac{2\pi}{\omega}$. It follows that the uncertainty examined in the previous section is always minimal.

B.3 The coherent states as a basis

We demonstrate now that the coherent states form a basis for the representation of arbitrary quantum states, but a basis that is non-orthogonal and over-complete (in the sense soon to be explained). We begin the proof with introducing the displacement (shift) operator $\hat{D}(z)$ which may be used to generate an arbitrary coherent state from the ground state $|0\rangle$. It is defined as:

$$\hat{D}(z) = e^{z\hat{a}^\dagger - z^*\hat{a}}, \quad (197)$$

so that:

$$\hat{D}^\dagger(z) = e^{z^*\hat{a} - z\hat{a}^\dagger}.$$

From the algebraic formula [157]:

$$e^{\hat{A}}e^{\hat{B}} = e^{\hat{B}}e^{\hat{A}}e^{[\hat{A}, \hat{B}]}, \quad \text{if } [\hat{A}, [\hat{A}, \hat{B}]] = [\hat{B}, [\hat{A}, \hat{B}]] \quad (198)$$

and from the commutation relation Eq. (19) (Ch. 2.2) it follows that $\hat{D}(z)\hat{D}^\dagger(z) = \hat{1}$, so the displacement operator is unitary.

Now use the displacement operator to unitary transform the annihilation and creation operator:

$$\begin{aligned} \hat{D}^\dagger(z)\hat{a}\hat{D}(z) &= e^{z^*\hat{a} - z\hat{a}^\dagger} \hat{a} e^{z\hat{a}^\dagger - z^*\hat{a}} = \hat{a} + z\hat{1} \\ \hat{D}^\dagger(z)\hat{a}^\dagger\hat{D}(z) &= e^{z^*\hat{a} - z\hat{a}^\dagger} \hat{a}^\dagger e^{z\hat{a}^\dagger - z^*\hat{a}} = \hat{a}^\dagger + z^*\hat{1}. \end{aligned}$$

The lemma from Eq. (196) has been employed. We see now that $\hat{D}(z)$ is effectively able to shift the ground state to an arbitrary coherent state:

$$\begin{aligned} \hat{a}(\hat{D}(z)|0\rangle) &= (\hat{D}(z)\hat{D}^\dagger(z))\hat{a}(\hat{D}(z)|0\rangle) = \hat{D}(z)(\hat{D}^\dagger(z)\hat{a}\hat{D}(z))|0\rangle = \\ &= \hat{D}(z)(\hat{a} + z\hat{1})|0\rangle = z\hat{D}(z)|0\rangle, \end{aligned}$$

Thus we obtain the following expression for an arbitrary coherent state $|z\rangle$:

$$|z\rangle = \hat{D}(z)|0\rangle.$$

We now have to examine the wave function of a number state in the coherent state representation, $\varphi_n(z) \equiv \langle z|n\rangle = \langle n|z\rangle^*$. First we state the Campbell-Baker-Hausdorff formula which is again valid for any two operators \hat{A} and \hat{B} whose commutator $[\hat{A}, \hat{B}]$ commutes with both \hat{A} and \hat{B} [157]:

$$e^{x(\hat{A}+\hat{B})} = e^{x\hat{A}}e^{x\hat{B}}e^{-x^2[\hat{A}, \hat{B}]/2} = e^{x\hat{B}}e^{x\hat{A}}e^{x^2[\hat{A}, \hat{B}]/2}. \quad (199)$$

Now we are in position to calculate $\langle n|z\rangle$:

$$\begin{aligned} \langle n|z\rangle &= \langle n|\hat{D}(z)|0\rangle = \langle n|e^{z\hat{a}^\dagger - z^*\hat{a}}|0\rangle = \langle n|e^{-\frac{1}{2}|z|^2}e^{z\hat{a}^\dagger}e^{-z^*\hat{a}}|0\rangle = \\ &e^{-\frac{1}{2}|z|^2}\langle n|\sum_{j=0}^{\infty}\frac{z^j}{j!}(\hat{a}^\dagger)^j\sum_{k=0}^{\infty}\frac{(-z^*)^k}{k!}\hat{a}^k|0\rangle = e^{-\frac{1}{2}|z|^2}\langle n|\sum_{j=0}^{\infty}\frac{z^j}{j!}(\hat{a}^\dagger)^j|0\rangle = e^{-\frac{1}{2}|z|^2}\frac{z^n}{\sqrt{n!}}. \end{aligned} \quad (200)$$

Here we have made use of, respectively, Eq. (199), the fact that $\hat{a}|0\rangle = 0$, and Eq. (20). Thus we have:

$$\varphi_n(z) \equiv \langle z|n\rangle = \langle n|z\rangle^* = e^{-\frac{1}{2}|z|^2}\frac{(z^*)^n}{\sqrt{n!}} \quad (201)$$

The probability distribution for having n photons in the coherent state as a function of the complex variable z is given by the absolute square of $\varphi_n(z)$:

$$|\varphi_n(z)|^2 = e^{-|z|^2}\frac{|z|^{2n}}{n!}.$$

Since the expectation value of the number of photons in the coherent state $|z\rangle$ is simply:

$$\langle n\rangle = \langle z|\hat{n}|z\rangle = \langle z|\hat{a}^\dagger\hat{a}|z\rangle = |z|^2,$$

we observe that the probability distribution for having n photons in the coherent state is Poissonian:

$$\mathcal{P}_{|z\rangle}(n) = e^{-\langle n\rangle}\frac{\langle n\rangle^n}{n!} \quad (202)$$

Let us also notice that the alternative definition of the coherent states, Eq. (51) (Ch. 2.4), follows easily from Eq. (200) supplemented by Eq. (21) (Ch. 2.2):

$$|z\rangle = \sum_{n=0}^{\infty}|n\rangle\langle n|z\rangle = \sum_{n=0}^{\infty}e^{-\frac{1}{2}|z|^2}\frac{z^n}{\sqrt{n!}}|n\rangle.$$

We are now ready to complete the proof and show that the coherent states form a non-orthogonal and over-complete basis. We are going to use the completeness of the number states (Eq. (21)) and Eq. (201).

We consider the scalar product of two different coherent states called $|z\rangle$ and $|z_0\rangle$:

$$\begin{aligned}\langle z|z_0\rangle &= \sum_n \langle z|n\rangle \langle n|z_0\rangle = \sum_n e^{-\frac{1}{2}|z|^2} \frac{(z^*)^n}{\sqrt{n!}} e^{-\frac{1}{2}|z_0|^2} \frac{(z_0)^n}{\sqrt{n!}} = \\ &= e^{-\frac{1}{2}(|z|^2+|z_0|^2)} \sum_n \frac{(z^*z_0)^n}{n!} = e^{-\frac{1}{2}(|z|^2+|z_0|^2+z^*z_0)}.\end{aligned}\quad (203)$$

Absolute squaring gives

$$|\langle z|z_0\rangle|^2 = e^{-|z-z_0|^2}.$$

Thus we see that the two different coherent states are not orthogonal. However, the modulus of their inner product converges quickly to zero if the difference between z and z_0 is significant.

We finally show that the coherent states form an over-complete basis. We do it by verifying the completeness relation directly. Since z is a continuous variable, the summation from Eq. (21) has to be replaced by integration over all possible z :

$$\int d^2z |z\rangle \langle z| = \int d^2z \sum_{m,n} |m\rangle \langle m|z\rangle \langle z|n\rangle \langle n| = \int d^2z \sum_{m,n} |m\rangle e^{-|z|^2} \frac{z^m (z^*)^n}{\sqrt{m!n!}} \langle n|$$

We have employed Eq. (201). Now, by switching to polar coordinates and utilizing the fact that $z^m = r^m e^{im\theta}$ where $r \equiv |z|$ and $\theta = \arg(z)$, we obtain

$$\begin{aligned}\int d^2z |z\rangle \langle z| &= \sum_{m,n} \frac{|m\rangle \langle n|}{\sqrt{m!n!}} \int_0^\infty dr r^{m+n+1} e^{-r^2} \int_0^{2\pi} d\theta e^{i(m-n)\theta} = \\ &= \sum_{m,n} \frac{|m\rangle \langle n|}{\sqrt{m!n!}} \int_0^\infty dr r^{m+n+1} e^{-r^2} 2\pi \delta_{mn} = \\ &= 2\pi \sum_n \frac{|n\rangle \langle n|}{n!} \int_0^\infty dr r^{2n+1} e^{-r^2} = 2\pi \sum_n \frac{|n\rangle \langle n|}{n!} \frac{1}{2} n! = \pi \hat{1}\end{aligned}$$

where we have used the definition of the Γ -function and its relation to the factorial:

$$\begin{aligned}\Gamma(s) &= \int_0^\infty r^{s-1} e^{-r} dr \\ \Gamma(s) &= (s-1)!, \quad \text{when } s \in \mathbb{N}\end{aligned}$$

Thus we conclude that the coherent states fulfill the relation:

$$\frac{1}{\pi} \int d^2z |z\rangle \langle z| = \hat{1}.\quad (204)$$

We have shown that the coherent states form a non-orthogonal and over-complete basis. Over-completeness implies that any coherent state can be expressed in terms of other coherent states. Using Eqs. (203) and (204) we immediately obtain for an arbitrary coherent state $|z\rangle$:

$$|z\rangle = \hat{1} |z\rangle = \frac{1}{\pi} \int |z'\rangle \langle z'|z\rangle d^2z' = \frac{1}{\pi} \int e^{-\frac{1}{2}(|z|^2+|z'|^2+z'^*z)} |z'\rangle d^2z'.$$

It was demonstrated by Cahill [158] that the set of coherent states cannot be made exactly complete by subtracting from it a countable number of elements. On the other hand, the over-completeness of the coherent states is mathematically a very desirable property, because a coherent-state representation of an arbitrary quantum state $|\Psi\rangle$ is completely determined by coefficients $\langle z|\Psi\rangle$ within some arbitrarily (but not infinitesimally) small range of z . Furthermore, a coherent-state representation of any traceable, positive definite Hermitian operator \hat{A} is completely determined by its diagonal matrix elements $\langle z|\hat{A}|z\rangle$ again within some arbitrarily (but not infinitesimally) small range of z . These two properties are proved and discussed at length in Mandel and Wolf [55] (Chapters 11.6-11.7).

C Matter waves

As explained in Introduction, the wave-particle duality is commonly associated with both light and matter, but in the thesis our attention has been restricted to light only. However, in several places (Chapter 3.4 and Chapter 9.3) we are nonetheless forced to refer to the duality of matter. Therefore, for the sake of completeness, in the following appendix we give a strongly abbreviated presentation of the subject, both from the theoretical and from the experimental side.

It was the French physicist and nobleman Louis de Broglie who in his doctoral thesis in 1924 presented the revolutionary idea that all matter had a wavelike nature. This conceptual breakthrough, confirmed in an electron diffraction experiment due to Lester Germer and Clinton Davisson three years later, paved way for the further development of quantum mechanics in the late 20s and the 30s. The so-called de Broglie relations, put in a very simple but strictly mathematical form, assign to every physical particle (like an electron) a wavelength and a frequency. These parameters can then be used to anticipate and describe the diffractive behaviour of the particles.

The basic postulate is this: Given a physical object with momentum \mathbf{p} and total energy E , we relate to it a wavelength λ and a frequency f given by the formulas [36]:

$$\lambda = \frac{h}{p} \tag{205}$$

$$f = \frac{E}{h}. \tag{206}$$

The relativistic effects could be taken into account by introducing the Lorentz factor, $\gamma = 1/\sqrt{1 - \frac{v^2}{c^2}}$, and setting $p = \gamma mv$ and $E = \gamma mc^2$.

It is not immediately clear what is meant by “relating wavelength and frequency to a physical object”. We have seen in Chapter 9.2 that within the Copenhagen interpretation of quantum mechanics one simply perceives physical objects themselves as undulatory phenomena (in specific experimental circumstances), while Bohm’s interpretation (see Ch. 9.3) claims that particles are always accompanied by quantum fields responsible for their undulatory behaviour.

It is instructive to consider a simple numerical example. An electron with mass $m_e = 9.11 \times 10^{-31}$ kg and moving with 10% of the speed of light, $v = 0.1c$, has wavelength $\lambda = 2.4 \times 10^{-11}$ m which is comparable with the size of an atom ($\approx 10^{-10}$ m). Thus, a slowly moving electron will be able to show a diffractive behaviour while interacting with matter. On the other hand a car with mass, say, $m = 1000$ kg and moving with speed $v = 100$ km/h ≈ 28 m/s has wavelength $\lambda = 2.4 \times 10^{-38}$ m which is three orders of magnitude smaller than

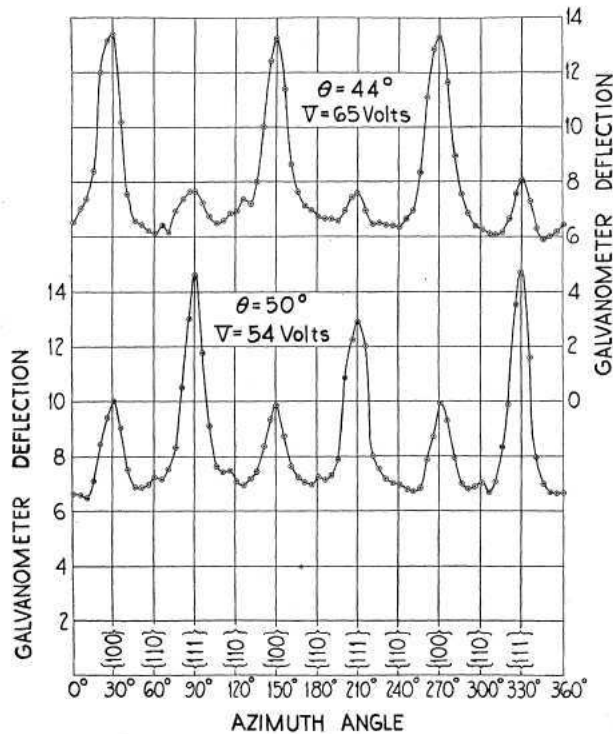


Figure 58: Results of the Davisson-Germer experiment where a block of nickel crystal was bombarded with thermally excited electrons. The crystal scattered the electrons and the authors measured the distribution of the electron intensity behind the target to be periodically dependent on the azimuth angle ϕ . The diagram shows the measured intensity of the scattered electrons as a function of the angle. Two data series are shown. They differ in the accelerating potential V (which determines the speed of the incident electrons) and the co-latitude of the beam θ . The oscillating pattern, suggesting an interference of some kind, is easily seen. Source: Davisson and Germer [159]

the Planck length $\ell_P \approx 1.6 \times 10^{-35}$ m. The undulatory aspect of the macroscopic physical objects is therefore unobservable and in the everyday life our senses perceive them just as large “corpuscles”.

De Broglie’s theoretical suggestion that matter in motion could be perceived as a wave with a well-defined wavelength was confirmed experimentally in 1928 by Davisson and Germer [37] [159], and, independently, by Thomson and Reid [160]. The experiments involved scattering narrow electron beams (cathode rays) from a nickel crystal (Davisson and Germer) and a thin celluloid film (Thomson and Reid). The diffraction pattern obtained in both cases (see Fig. 58 for the results of Davisson and Germer) could be easily explained under the assumption that electrons behaved like waves with wavelength given by Eq. (205), and that these waves interfered during their propagation through material just as an ordinary electromagnetic radiation would do. However, the occurrence of these patterns were not predicted by standard corpuscular model combined with knowledge about the atomic structure inside the target.

For some time afterwards it was not known whether the analogous diffraction phenomena occur with other elementary particles like neutrons and protons, or even with much larger atoms and molecules. The second question was settled already in 1930 by Immanuel Estermann and Otto Stern who diffracted a beam of hydrogen and helium atoms using a lithium fluoride crystal [38]. The validity of Eq. (205) was again confirmed. In 1945 Ernest Wollan and R. B. Sawyer carried out the first neutron diffraction experiments using a beam of “monochromatic” neutrons obtained from an atomic reactor [161]. Soon neutron diffraction

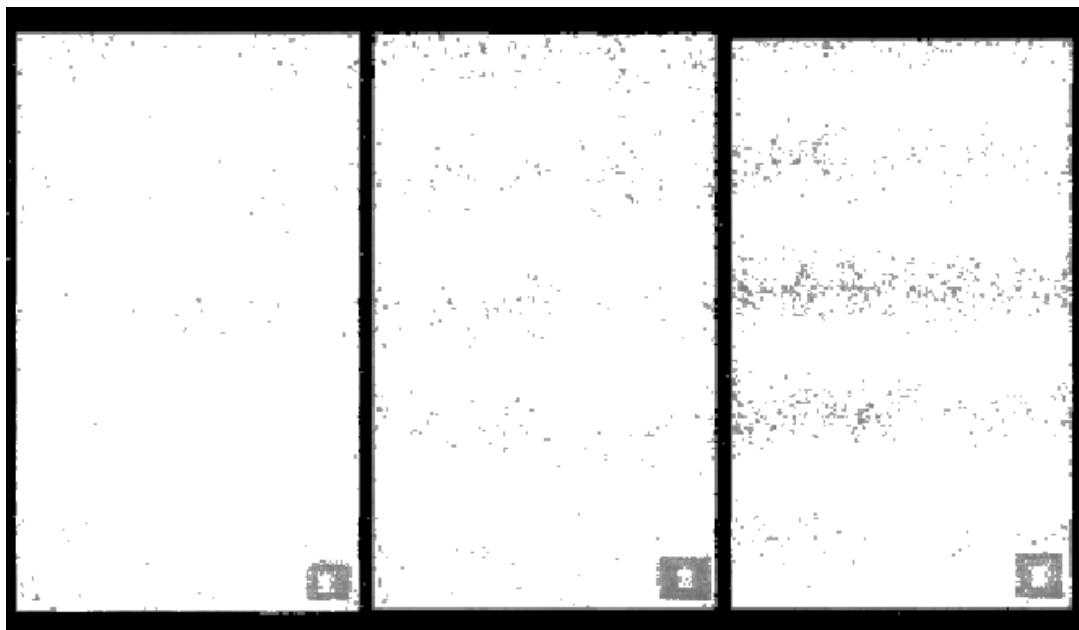


Figure 59: The statistical build-up of an interference pattern in the single-electron diffraction experiment due to Tonomura et al. Only the central part of the whole field of view of the detector is shown. The interference fringes are more distinct as the number of single electrons that have hit the detector increases. From left to right, there are respectively 3000, 20000 and 70000 electron hits. This is a negative of the original picture with increased contrast. *Source: Tonomura et al. [5]*

proved itself to be a fruitful crystallographic technique for the determination of the structure of various materials.

A loophole, however, had existed in the matter diffraction experiments so far. In each of them a continuous flow of particles was considered, and one had to ask whether the diffraction pattern could be explained in terms of some collective behaviour of these particles (see the argument from Ch. 3.2 about the corpuscular photons scattering from each other) instead of employing de Broglie waves. The ambiguity would be resolved by performing a diffraction experiment where particles (like an electron or a neutron) travel through the apparatus one by one. If the diffraction pattern would eventually occur, then the case for a matter wave associated with a *single* particle would be made much stronger.

It was A. Tonomura and his team that in 1989 successfully performed the first precise diffraction experiment with single electrons⁸² [5]. Moreover, the experiment was also the first exact realization of the famous thought experiment with a single electron passing a double slit (see Introduction) [162]. Tonomura et al. employed an electron microscope equipped with an electron biprism as an equivalent to the double slit, and a position-sensitive electron-counting system as an equivalent to the screen on which the interference pattern could be formed. Fig. 59 presents the pattern they obtained. Their results unambiguously implied that it was a single electron that was able to interfere in a wavelike fashion with itself, and that the phenomenon must not be ascribed to a collective behaviour of a large number of electrons propagating together through system.

So far the largest material objects that has been shown to exhibit interferential behaviour are fullerene C₆₀-molecules. A research team led by Zeilinger obtained in 1999 a diffraction pattern by sending a beam of

⁸²Earlier experiments of these kind were conducted by Claus Jönsson in 1961 [163] and P. G. Merli, G. F. Missiroli and G. Pozzi in 1974 [164], but they were less exact and used less sophisticated apparatus.

C_{60} -molecules through a diffraction grating consisting of nominally 50 nm wide slits with a 100 nm period [44]. The velocity distribution of the molecules was measured and fitted; the most probable velocity corresponded to a de Broglie wavelength of 2.5 pm which is approximately 400 smaller than the diameter of C_{60} . It should be stressed the total mass M of one molecule was used in calculating the de Broglie wavelength, i.e. it was assumed that each interfering de Broglie wave corresponded to a single undivided particle of mass M . Furthermore, the observations supported the view that each C_{60} -molecule interferes with itself alone, even though they did not propagate singly through the apparatus.

Many different experiments confirmed the validity of de Broglie's relation between momentum and wavelength of material objects. Although the relation does not make any explicit distinction between the macroscopic and the microscopic level, it has been verified only in the case of the latter. It remains to be seen if analogous results will be obtained for still larger and more complicated molecules. If not, it will be very interesting to see if it is the size, mass or rather the structure of the physical object under examination that decides when the diffractive behaviour ceases to occur. It is also conceivable that the diffractive behaviour of matter will persist, but that the simple de Broglie relation, Eq. (205), will have to be replaced by some other formula which maybe will give us a better physical insight into the nature of the phenomenon.

Aside from looking for the upper spatial bound, there is another crucial question that could be answered empirically. Imagine that an experiment similar to that of Zeilinger et al. is performed, but with slits in the diffraction grating being considerably smaller than the size of the material object we wish to diffract. Will the diffractive pattern still be obtained? If no, it would imply that there is something intrinsically solid about the matter (in addition to the de Broglie waves) that does not allow a material object to propagate through a slit which is smaller than the object itself (the size of the object being determined with help of some different means). The persistence of the diffractive pattern, however, would suggest that – at least at the microscopic level and under particular circumstances – the structure of matter is completely undulatory.

D Numerical routines

We include the source code of Matlab programs used to simulate **a)** thermal emission of light for the purpose of illustrating coherence (Chapter 4.2); and **b)** coincidence measurements (Chapter 8.1).

D.1 Simulation of thermal emission

```
function [ el_field_array ] = coherence
%COHERENCE Summary of this function goes here
% Generation of a chaotic radiative field by
% superposing randomly generated wave packets (WP)

total_t = 1e5;           % time steps
emission_prob = 0.05;   % probability of WP per time step
amplitude_var = 0.1;    % WP amplitude variation
damping = 0.01*total_t; % WP damping time
damping_var = 0.1*damping; % variation of damping time
ang_freq = 2*pi/100;    % WP basic ang. frequency
ang_freq_var = 0;       % variation of ang. frequency

time_token_array = zeros(1,total_t);
packets_number = 0;

'number of wave packets'
for i=1:total_t-damping           % random emission of WP
    if rand <= emission_prob
        time_token_array(i) = 1;
        packets_number = packets_number + 1;
    end
end

time_positions = find(time_token_array);
rand_param_matrix = zeros(packets_number,4);

'random parameters'
for i=1:packets_number           % stochastic variations of WP
    rand_param_matrix(i,1) = 2*pi*rand;
    rand_param_matrix(i,2) = 1+(rand-0.5)*amplitude_var;
    rand_param_matrix(i,3) = damping+(rand-0.5)*damping_var;
    rand_param_matrix(i,4) = ang_freq+(rand-0.5)*ang_freq_var;
end

el_field_array = zeros(1,total_t);
int_array = zeros(1,total_t);

'generating packets'
for i=1:packets_number           % generating WP
    t = 0:1:total_t-time_positions(i);
    packet_main = cos(rand_param_matrix(i,4)*t+rand_param_matrix(i,1));
    packet_damp = exp(-t./rand_param_matrix(i,3));
    packet = rand_param_matrix(i,2)*packet_main.*packet_damp;
    for j=time_positions(i):1:total_t % superposing WP
        el_field_array(j) = el_field_array(j)+packet(j-time_positions(i)+1);
    end
end

'intensity'
```

```

for i=1:total_t           % calculate field intensity
    int_array(i) = el_field_array(i)*el_field_array(i);
%end

packets_number

```

D.2 Simulation of coincidence measurements

```

function [ timedelay ] = coinc_sim()
%COINC_SIM Simulation of coincidence measurements
% We simulate the coincidence measurements in order to
% examine the corpuscular hypothesis of light.
% The simulation has segmental structure with
% segments corresponding to:
% 1) emission of photons from a source (possibly attenuated)
% 2) beam splitting
% 3) detection of photons (i.e. conversion of actual photons
% to photocounts)
% 4) triggering
%
% The output argument gives time differences between the
% triggering photocount in one detector and all photocounts
% registered in one sweep by the second photodetector.

L1 = 3.125e5; % length of each simulation in pts, 1 pt <=> 4 ns (usually, but
            % depends on resolution)
midpoint = ceil(L1/2);
prob_array = 0.0002*ones(1,L1); % emission probability estimated
                                % from the intensity, 0.0002 <=> 50e3
                                % photons/sec

trigger_flag = 0;

% Loop continued until trigger is found,
% usually it will happen after a single run
while trigger_flag == 0;

    photons = zeros(1,L1); % photons emitted
    photons1 = zeros(1,L1); % photons to det. 1
    photons2 = zeros(1,L1); % photons to det. 2
    photocounts1 = zeros(1,L1); % photocounts detected by det. 1
    photocounts2 = zeros(1,L1); % photocounts detected by det. 2

    % Emission segment. Choose one of the models
    % 1) Poissonian process
    for i=1:L1
        if rand<prob_array(i)
            photons(i) = 1;
        end
    end

    % 2) Regular intervals between photons
    % for i=1:62.5
    % photons(i*5000) = 1;
    % end

    % 3) Bunching or antibunching
    % bunch_time = 1000;
    % bunch_strength = 0.00015
    % for i=1:L1
    % if rand<prob_array(i)
    % photons(i) = 1;
    % a1 = i+1;
    % a2 = i+1001;
    % for j=1:1000
    % if (i+j) <= L1
    % prob_array(i+j)=prob_array(i+j)-bunch_strength*(bunch_time+1-j)/bunch_time;
    % end
    % end
    % end

    % 4) Continuous, "coherent" radiation
    % x=1:L1;
    % coherence_length = 750;
    % k = 2*pi/coherence_length;

```

```

% rand_phase = 2*pi*rand;
% photons=0.5e-4*cos(k*x+rand_phase).^2+2.0e-4;

% 5) Continuous, "random" radiation
% x = 1:L1;
% random_variation = 0.5e-4*(rand(1,L1)-0.5);
% photons = 2.0e-4+random_variation;

% Localize photons
where_phot = find(photons);
numb_phot = length(where_phot);

% =====
%
% Beam splitter segment
% Assume 53:47 splitting
% 1) Indivisible photons
% for i=1:numb_phot
%     if rand<0.53
%         photons1(where_phot(i)) = 1;
%     else
%         photons2(where_phot(i)) = 1;
%     end
% end

% 2) Divisible photons
% for i=1:numb_phot
%     dir_factor = 0.53+(rand-0.5)/5;
%     photons1(where_phot(i)) = dir_factor;
%     photons2(where_phot(i)) = 1-dir_factor;
% end

% 3) Continuous radiation
photons1 = 0.53*photons;
photons2 = 0.47*photons;

% =====
%
% Detection segment

prob_array_det1 = zeros(1,(L1+15));
prob_array_det2 = zeros(1,(L1+15));

i = 1;
while i<=L1
    if rand<(0.962*photons1(i))
        photocounts1(i) = 1;
        for j=1:15
            prob_array_det1(i+j)=prob_array_det1(i+j)+0.0005*(16-j)/15; %afterpulsing probability
        end
        i = i+6;
    elseif rand<prob_array_det1(i)
        photocounts1(i) = 1;
        for j=1:15
            prob_array_det1(i+j)=prob_array_det1(i+j)+0.0005*(16-j)/15;
        end
        i = i+6;
    elseif rand<4.432e-6
        photocounts1(i) = 1;
        for j=1:15
            prob_array_det1(i+j)=prob_array_det1(i+j)+0.0005*(16-j)/15;
        end
        i = i+6;
    else
        i = i+1;
    end
end

i = 1;
while i<=L1
    if rand<(0.681*photons1(i))
        photocounts2(i) = 1;
        for j=1:15
            prob_array_det2(i+j)=prob_array_det2(i+j)+0.0005*(16-j)/15;
        end
        i = i+6;
    end
end

```

```

elseif rand<prob_array_det2(i)
    photocounts1(i) = 1;
    for j=1:15
        prob_array_det2(i+j)=prob_array_det2(i+j)+0.0005*(16-j)/15;
    end
    i = i+6;
elseif rand<8.92e-7
    photocounts2(i) = 1;
    for j=1:15
        prob_array_det2(i+j)=prob_array_det2(i+j)+0.0005*(16-j)/15;
    end
    i = i+6;
else
    i = i+1;
end
end

% =====
%
% Triggering segment
poss_trigger = 0;

% Triggering with det. 2
for i=1:ceil(L1/10);
    poss_trigger = midpoint+i;
    if photocounts2(poss_trigger)==1
        trigger_flag = 1;
        break
    end
    poss_trigger = midpoint-i;
    if photocounts2(poss_trigger)==1
        trigger_flag = 1;
        break
    end
end

end

% Choosing the time window centered about trigger
halfL2 = floor(L1/2)-ceil(L1/10);
lowerbound = poss_trigger-halfL2+1;
upperbound = poss_trigger+halfL2-1;
photons_meas = photocounts1(lowerbound:upperbound);
L2 = length(photons_meas);

% Calculate time delays
where_phot = find(photons_meas);
numb_phot = length(where_phot);
timedelay = zeros(1, numb_phot);

for i=1:numb_phot
    timedelay(i) = where_phot(i)-halfL2;
end

function [ tot_timedelay ] = iterate_coinc(thous_repetitions)
%ITERATE_COINC Iteration of coinc_sim
% This function simply iterates coincidence measurements
% X thousand times where X is the argument of the function.
% The time differences from all iterations are stored in the output
% argument which can then be used in order to plot histogram,
% e.g. hist(tot_timedelay,1000).

index=1;
tot_timedelay_temp = zeros(1,thous_repetitions*1000*50); % temporary array,
% assume on average less than 50 events per iteration

numb_phot = 0;

for i=1:thous_repetitions;
    for j=1:1000;
        timedelay = coinc_sim;
        for k=1:length(timedelay)
            tot_timedelay_temp(index) = timedelay(k);
            index = index + 1;
        end
    end
end

```

```
    end
  i
end
tot_timedelay = tot_timedelay_temp(1:index-1);
```


References

- [1] Roger Penrose, *The Large, the Small and the Human Mind*, Cambridge University Press, 2000
- [2] *The Cambridge Dictionary of Philosophy*, edited by Robert Audi, Cambridge University Press, Second Edition, 1999
- [3] *Dictionary of Physics*, edited by H.J. Gray and Alan Isaacs, Longman, 1990
- [4] Richard P. Feynman, Robert B. Leighton, Matthew Sands, *The Feynman Lectures on Physics*, Second Edition, vol. 3, Addison Wesley, 2005
- [5] A. Tonomura, J. Endo, T. Matsuda, T. Kawasaki, H. Ezawa, *Demonstration of single-electron buildup of an interference pattern*, *American Journal of Physics* **57** (1989), pp. 117-120
- [6] Martio Bertolotti, *The History of the Laser*, Taylor & Francis, 2004
- [7] http://india_resource.tripod.com/physics.htm, retrieved on 9.09.2008
- [8] Euclides, *Optics*, translated to English by Harry E. Burton, *Journal of the Optical Society of America* **35** (1945), pp. 357-372
- [9] Arne Næss, *Filosofiens historie*, Universitetsforlaget, 2001 (in Norwegian)
- [10] <http://muslimmedianetwork.com/mmn/?p=1886>, retrieved on 9.09.2008
- [11] George Sarton, *Introduction to the history of science*, Baltimore, 1927
- [12] René Descartes, *Optics (La dioptrique)*, from *The Philosophical Writings of Descartes*, translated by John Cottingham, Robert Stoothoff and Dugald Murdoch, Cambridge University Press, 1985
- [13] René Descartes, *Principles of Philosophy (Principia philosophiae)*, from *The Philosophical Writings of Descartes*, translated by John Cottingham, Robert Stoothoff and Dugald Murdoch, Cambridge University Press, 1985
- [14] Andrzej Kajetan Wróblewski, *Historia fizyki*, Wydawnictwo Naukowe PWN, 2007 (in Polish)
- [15] Edmé Mariotte, *De la nature des couleurs*, as quoted by [14]
- [16] Christiaan Huygens, *Treatise on light*, translated by Silvanus P. Thompson, University of Chicago Press, www.gutenberg.org, retrieved on 9.09.2008
- [17] Isaac Newton, *The history of the Royal Society of London*, vol. 3, p. 249, edited by T. Birch
- [18] Isaac Newton, *Answer to some Considerations upon his Doctrine of Light and Colors*, *Philosophical Transactions* **88**, pp. 5084-5103
- [19] *The history of the Royal Society of London*, vol. 3, pp. 247-305, edited by T. Birch
- [20] Isaac Newton, *Opticks*, Dover Publications, 1979
- [21] I. Bernard Cohen, Preface to [20]
- [22] Thomas Young, *Bakerian Lecture on the Theory of Light and Colour*, from *Abstracts of the Papers Printed in the Philosophical Transactions of the Royal Society of London*, vol. 1, (1800 - 1814), pp. 63-67
- [23] Thomas Young, *The Bakerian Lecture: Experiments and Calculations Relative to Physical Optics*, *Philosophical Transactions* **94**, pp. 1-16

- [24] J. J. O'Connor, E. F. Robertson, *Augustin Jean Fresnel*, <http://www-history.mcs.st-andrews.ac.uk/Biographies/Fresnel.html>, retrieved on 30.09.2008
- [25] James Clerk Maxwell, *A Treatise on Electricity and Magnetism*, Clarendon Press, Oxford, 1873, vol. 2, p. 383
- [26] <http://scienceworld.wolfram.com/biography/Michelson.html>, retrieved on 9.09.2008
- [27] Otto Lummer, Ernst Pringsheim, *Die Vertheilung der Energie im Spectrum des Körpers*, Verhandlungen der Deutschen Physikalischen Gesellschaft **1**, pp. 23-41 (1899)
- [28] Helge Kragh, *Max Planck: the reluctant revolutionary*, Physics World, December 2000
- [29] Helge Kragh, *Quantum Generations: A History of Physics in the Twentieth Century*, Princeton University Press, 1999
- [30] Britannica Online Encyclopedia, www.britannica.com, PHOTOELECTRIC EFFECT, retrieved on 9.09.2008
- [31] Albert Einstein, *Über einen die Erzeugung und Verwandlung des Lichtes betreffenden heuristischen Gesichtspunkt*, Annalen der Physik **322**, pp. 132-148 (1905); as translated by D. Ter Haar, http://lorentz.phl.jhu.edu/AnnusMirabilis/AeReserveArticles/eins_lq.pdf, retrieved on 25.11.2008
- [32] Owen W. Richardson, *The theory of photoelectric action*, Philosophical Magazine **24**, pp. 570-574 (1912)
- [33] Arthur H. Compton, *A Quantum Theory of the Scattering of X-Rays by Light Elements*, Physical Review **21**, pp. 483-502 (1923)
- [34] Niels Bohr, Hendrik Kramers, John Slater, *The quantum theory of radiation*, Philosophical Magazine **47**, 785-802 (1924)
- [35] Jagdish Mehra, Helmut Rechenberg, *The historical development of quantum theory*, Springer-Verlag, 1982, Vol. 1, Part 2, pp. 532-554
- [36] Louis de Broglie, *Recherches sur la théorie des quanta*, doctoral thesis, Paris, 1924; as translated by A. F. Kracklauer, http://www.enscm.fr/aflb/LDB-oeuvres/De_Broglie_Kracklauer.pdf, retrieved on 15.09.2008
- [37] Clinton Davisson, Lester Germer, *Reflection of electrons by a crystal of nickel*, Nature **119**, pp. 558-560 (1927)
- [38] Immanuel Estermann, Otto Stern, *Beugung von Molekularstrahlen*, Zeitschrift für Physik **61**, pp. 95-125 (1930)
- [39] David Bohm, B. J. Hiley, *The Undivided Universe: An ontological interpretation of quantum theory*, Routledge, 1995
- [40] Edwin Jaynes, Leonard Mandel, *Survey of the present status of neoclassical radiation theory*, in: *Proceedings of the Third Rochester Conference on Coherence and Quantum Optics*, Plenum Press, 1973, pp. 35-81
- [41] R. Hanbury Brown, R. Q. Twiss, *A Test of a New Type of Stellar Interferometer on Sirius*, Nature **177**, p. 27 (1956)
- [42] P. W. Milonni, *Wave-Particle Duality of Light: A Current Perspective*, in: *The Wave-Particle Dualism*, pp. 27-67, Springer, 1983
- [43] Roy J. Glauber, *The Quantum Theory of Optical Coherence*, Physical Review **130**, pp. 2529-2539 (1963)

- [44] M. Arndt, O. Nairz, J. Vos-Andreae, C. Keller, G. van der Zouw, A. Zeilinger, *Wave-particle duality of C_{60} molecules*, Nature **401**, pp. 680-682 (1999)
- [45] Shahriar Afshar, *Sharp complementary wave and particle behaviours in the same “welcher Weg” experiment*, Proceedings of SPIE **5866**, pp. 229-244 (2005)
- [46] Shahriar Afshar, Eduardo Flores, Keith McDonald, Ernst Knoesel, *Paradox in Wave-Particle Duality*, Foundation of Physics **37**, pp. 295-305 (2007)
- [47] Nannapaneni Narayana Rao, *Elements of Engineering Electromagnetics*, 6th Edition, Prentice Hall, 2004
- [48] Bahaa E. A. Saleh, Malvin Carl Teich, *Fundamentals of Photonics*, Second Edition, Wiley, 2007
- [49] John D. Jackson, *Classical Electrodynamics*, Third Edition, Wiley, 1998
- [50] <http://electricz.blogspot.com/2007/05/let-there-be-light-as-hertz-proved.html>, retrieved on 16.09.2008
- [51] Ramamurti Shankar, *Principles of Quantum Mechanics*, Second Edition, Springer, 1994
- [52] Rodney Loudon, *The Quantum Theory of Light*, Third Edition, Oxford University Press, 2000
- [53] Julian Schwinger, Lester L. Deraad, Kimball A. Milton, Wu-yang Tsai, Joyce Norton, *Classical Electrodynamics*, Westview Press, 1998
- [54] E. A. Power, *Introductory Quantum Electrodynamics*, Longmans, 1964
- [55] Leonard Mandel, Emil Wolf, *Optical Coherence and Quantum Optics*, Cambridge University Press, 1995
- [56] D. F. Walls, G. J. Milburn, *Quantum Optics*, Springer-Verlag, 1994
- [57] Mark Fox, *Quantum Optics: An Introduction*, Oxford University Press, 2006
- [58] David Chandler, *Introduction to Modern Statistical Mechanics*, Oxford University Press, 1987
- [59] Max Planck, *Über das Gesetz der Energieverteilung im Normalspectrum*, Annalen der Physik **309**, pp. 553-563 (1901); translation retrieved from <http://bourabai.narod.ru/articles/planck/planck1901.pdf> on 21.01.2009
- [60] H. Rubens, F. Kurlbaum, *Proceedings of the Imperial Academy of Science*, Berlin, 25.10.1900, p. 929
- [61] H. Beckmann, Inaugural dissertation, Tübingen 1898. See also: H. Rubens, Weid. Ann. **69**, p. 582 (1899)
- [62] Martin White, *Anisotropies in the CMB*, <http://arxiv.org/abs/astro-ph/9903232v1>, retrieved on 21.01.2009
- [63] *Dictionary of Pure and Applied Physics*, edited by Dipak Basu, CRC, 2000
- [64] George S. Monk, *Light: Principles and Experiments, First Edition*, McGraw-Hill Book Company, 1937
- [65] *A Dictionary of Physics*, edited by John Daintith, Oxford University Press, 2005
- [66] Britannica Online Encyclopedia, www.britannica.com, OPTICAL INTERFEROMETER, retrieved on 19.11.2008
- [67] R. W. Ditchburn, *Light*, Academic Press, 1976

- [68] A. A. Michelson, *Inteference Phenomena in a New Form of Refractometer*, Philosophical Magazine **13**, pp. 236-242 (1882)
- [69] Richard Feynman, *QED: The Strange Theory of Light and Matter*, Princeton University Press, 2006
- [70] F. Selleri, “*Gespensterfelder*”, in: *The Wave-Particle Dualism*, pp. 101-128, Springer, 1983
- [71] E. Panarella, *Nonlinear behaviour of light at very low intensities: The “photon clump” model*, in: *Quantum Uncertainties*, Plenum Press, 1986, pp. 105-167
- [72] L. János, Zs. Náray, *Investigation into interference phenomena at extremely low light intensities by means of a large Michelson interferometer*, Il Nuovo Cimento **9** (Supplement **2**), pp. 588-598 (1958)
- [73] John F. Clauser, *Experimental distinction between the quantum and classical field-theoretic predictions for the photoelectric effect*, Physical Review D **9**, pp. 853-860 (1974)
- [74] Philipp Lenard, *Über die lichtelektrische Wirkung*, Annalen der Physik **313**, pp. 149-198 (1902)
- [75] O. W. Richardson, K. T. Compton, *The Photoelectric Effect*, Philosophical Magazine **24**, pp. 575-594 (1912)
- [76] P. W. Milonni, *Answer to Question #45*, Questions and Answers, American Journal of Physics **64**, pp. 11-12 (1997)
- [77] O. W. Richardson, *Some Applications of the Electron Theory of Matter*, Philosophical Magazine **23**, pp. 594-627 (1912)
- [78] Charles Erwin Tyler, *The Element of Time in the Photoelectric Effect*, 1969, Ph.D. thesis, Washington University
- [79] W. Davis, L. Mandel, *Time Delay Statistics of Photoelectric Emissions: An Experimental Test of Classical Radiation Theory*, in: *Proceedings of the Third Rochester Conference on Coherence and Quantum Optics*, Plenum Press, 1973, pp. 113-119
- [80] Leonard Mandel, *The Case for and against Semiclassical Radiation Theory*, Progress in Optics **13**, pp. 27-68, North-Holland (1976)
- [81] Frank C. Jones, *Calculated Spectrum of Inverse-Compton-Scattered Photons*, Physical Review **167**, pp. 1159-1169 (1968)
- [82] Peter Debye, *Zerstreuung von Rontgenstrahlen und Quantentheorie*, Physikalische Zeitschrift **24** 8, pp. 161-166 (1923)
- [83] R. E. Bell, R. L. Graham, *Measurement of a Second Half-Life in Yb^{170}* , Physical Review **78**, pp. 490-491 (1950)
- [84] Chandrasekhara Venkata Raman, *A Classical Derivation of the Compton Effect*, Indian Journal of Physics **3**, pp. 357-369 (1928)
- [85] Richard Kidd, James Ardini, Anatol Anton, *Compton effect as a double Doppler shift*, American Journal of Physics **53**, pp. 641-644 (1985)
- [86] Walter Roy Mellen, *Compton effect from a center-of-momentum system*, American Journal of Physics **49**, pp. 505-506 (1981)

- [87] Malcom J. Cooper, *Compton scattering and electron momentum determination*, Reports on Progress in Physics **48**, pp. 415-481 (1985)
- [88] J. N. Dodd, *The scattering of electromagnetic radiation by a free electron*, Journal of Physics B **8**, pp. 157-164 (1975)
- [89] Philippe Grangier, Gerard Roger, Alain Aspect, *Experimental Evidence for a Photon Anticorrelation Effect on a Beam Splitter: A New Light on Single-Photon Interference*, Europhysics Letters **1**, pp. 173-179 (1986)
- [90] Alain Aspect, Philippe Grangier, Gerard Roger, *Experimental Tests of Realistic Local Theories via Bell's Theorem*, Physical Review Letter **47**, pp. 460-463 (1981)
- [91] J. Dugundji, *Envelopes and pre-envelopes of real waveforms*, IRE Transactions on Information Theory, 1958
- [92] Marian O. Scully, Murray Sargent III, *The Concept of the Photon*, Physics Today, March 1972
- [93] Michael G. Raymer, *Observations of the modern photon*, Letter to the Editor, American Journal of Physics **58**, p. 11 (1990)
- [94] Leonard Mandel, Emil Wolf, *The Measures of Bandwidth and Coherence Time in Optics*, Proceedings of the Physical Society **80**, pp. 894-897 (1962)
- [95] Emil Wolf, *Reciprocity Inequalities, Coherence Time and Bandwidth in Signal Analysis and Optics*, Proceedings of the Physical Society **71**, pp. 257-269 (1958)
- [96] Leonard Mandel, *Fluctuations of Photon Beams: The Distribution of the Photo-Electrons*, Proceedings of the Physical Society **74**, pp. 233-243 (1959)
- [97] R. Hanbury Brown, R. Q. Twiss, *Interferometry of the Intensity Fluctuations in Light. I. Basic Theory: The Correlation between Photons in Coherent Beams of Radiation*, Proceedings of the Royal Society A **242**, pp. 300-324 (1957)
- [98] R. Hanbury Brown, R. Q. Twiss, *Interferometry of the Intensity Fluctuations in Light II. An Experimental Test of the Theory for Partially Coherent Light*, Proceedings of the Royal Society A **243**, pp. 291-319 (1958)
- [99] Rodney Loudon, *Non-classical effects in the statistical properties of light*, Reports on Progress in Physics **43**, pp. 913-949 (1980)
- [100] Peter W. Milonni, Joseph H. Eberly, *Lasers*, First Edition, Wiley-Interscience, 1988
- [101] A. E. Siegman, *Lasers*, University Science, 1986
- [102] K. F. Riley, M. P. Hobson, S. J. Bence, *Mathematical Methods for Physics and Engineering*, Second Edition, Cambridge University Press
- [103] P. L. Kelley, W. H. Kleiner, *Theory of electromagnetic field measurement and photoelectron counting*, Physical Review **136**, pp. A316-A334 (1964)

- [104] A. C. Funk, M. Beck, *Sub-Poissonian photocurrent statistics: Theory and undergraduate experiment*, American Journal of Physics **65**, pp. 492-500 (1997)
- [105] X. T. Zou, L. Mandel, *Photon-antibunching and sub-Poissonian photon statistics*, Physical Review A **41**, pp. 475-476 (1990)
- [106] R. Short, L. Mandel, *Observation of Sub-Poissonian photon statistics*, Physical Review Letters **51**, pp. 384-387 (1983)
- [107] M. C. Teich, B. E. A. Saleh, *Observation of sub-Poisson Franck-Hertz light at 253.7 nm*, Journal of the Optical Society of America B **2**, pp. 275-282 (1985)
- [108] P. R. Tapster, J. G. Rarity, J. S. Satchell, Use of parametric down-conversion to generate sub-Poissonian light, Physical Review A **37**, pp. 2963-2967 (1988)
- [109] H. J. Kimble, M. Dagenais, L. Mandel, *Photon Antibunching in Resonance Fluorescence*, Physical Review Letters **39**, pp. 691-695 (1977)
- [110] Ch. Kurtsiefer, S. Mayer, P. Zarda, H. Weinfurter, *Stable Solid-State Source of Single Photons*, Physical Review Letters **85**, pp. 290-293 (2000)
- [111] Ch. Santori, M. Pelton, G. Solomon, Y. Dale, Y. Yamamoto, *Triggered Single Photons from a Quantum Dot*, Physical Review Letters **86**, pp. 1502-1505 (2001)
- [112] Hans-A. Bachor, Timothy C. Ralph, *A Guide to Experiments in Quantum Optics*, Wiley, Second Edition, 2004
- [113] A. Gerrard, J. M. Burch, *Introduction to Matrix Methods in Optics*, Dover Publications, 1994
- [114] <http://optoelectronics.perkinelmer.com/catalog/Product.aspx?ProductID=SPCM-AQRH-16>, retrieved on 22.02.2009
- [115] http://optoelectronics.perkinelmer.com/content/Datasheets/DTS_SPCMAQRH.pdf, retrieved on 22.02.2009
- [116] Newport, <http://search.newport.com/?sku=05BC16PC.4>, retrieved on 6.04.2009
- [117] Thorlabs, <http://www.thorlabs.com/thorProduct.cfm?partNumber=WPH05M-633>, retrieved on 6.04.2009
- [118] Thorlabs, http://www.thorlabs.com/NewGroupPage9.cfm?ObjectGroup_ID=266, retrieved on 6.04.2009
- [119] <http://www.newport.com/Laser-Line-Non-Polarizing-Cube-Beamsplitters/141121/1033/catalog.aspx>, retrieved on 20.02.2009
- [120] Thorlabs, <http://www.thorlabs.com/Thorcat/12100/12109-S01.PDF>, retrieved on 12.12.2008
- [121] Thorlabs, <http://www.thorlabs.com/thorProduct.cfm?partNumber=ES120>, retrieved on 6.04.2009
- [122] Thorlabs, <http://www.thorlabs.com/catalogPages/951.pdf>, retrieved on 6.04.2009
- [123] LeCroy, <http://www.lecroy.com/tm/products/scopes/specs.asp?mseries=25>, retrieved on 6.04.2009

- [124] Daniel M. Greenberger, Allaine Yasin, *Simultaneous Wave and Particle Knowledge in a Neutron Interferometer*, Physics Letters A **128**, pp. 391-394 (1988)
- [125] Gregg Jaeger, Abner Shimony, Lev Vaidman, *Two interferometric complementarities*, Physical Review A **51**, pp. 54-67 (1995)
- [126] Berthold-Georg Englert, *Fringe Visibility and Which-Way Information: An Inequality*, Physical Review Letters **77**, pp. 2154-2157 (1996)
- [127] Niels Bohr, *The Quantum Postulate and the Recent Development of Atomic Theory*, Nature **121**, pp. 580-590 (1928)
- [128] R. E. Kastner, *Why the Afshar Experiment Does Not Refute Complementarity*, <http://arxiv.org/abs/quant-ph/0502021>, retrieved on 24.04.2009
- [129] Eduardo Flores, Ernst Knoesel, *Why Kastner analysis does not apply to a modified Afshar experiment*, <http://arxiv.org/abs/quant-ph/0702210>, retrieved on 24.04.2009
- [130] Aurelien Drezet, *Complementarity and Afshar's experiment*, <http://arxiv.org/abs/quant-ph/0508091>, retrieved on 24.04.2009
- [131] Tabish Qureshi, *Complementarity and the Afshar Experiment*, <http://arxiv.org/abs/quant-ph/0701109>, retrieved on 24.04.2009
- [132] Ole Steuernagel, *Afshar's Experiment Does Not Show a Violation of Complementarity*, Foundations of Physics **37**, pp. 1370-1385 (2007)
- [133] Eduardo Flores, Reply to Comments of Steuernagel on the Afshar's Experiment, Foundation of Physics **38**, pp. 778-781 (2008)
- [134] Max Born, Emil Wolf, Principles of Optics, Second Edition, Pergamon Press, 1964
- [135] J. P. Girardeau-Montaut, C. Girardeau-Montaut, *Theory of ultrashort nonlinear multiphoton photoelectric emission from metals*, Physical Review B **51**, pp. 13560-13567 (1995)
- [136] Stanford Encyclopedia of Philosophy, Copenhagen Interpretation of Quantum Mechanics, <http://plato.stanford.edu/entries/qm-copenhagen/>, retrieved on 2.05.2009
- [137] Franco Selleri, *Quantum Paradoxes and Physical Reality*, Kluwer Academic Publishers, 1990
- [138] Dugald Murdoch, *Niels Bohr's Philosophy of Physics*, Cambridge University Press, 1989
- [139] Niels Bohr, The Quantum Postulate and the Recent Development of Atomic Theory, Nature **121**, pp. 580-590 (1928)
- [140] Asher Peres, *Carl Popper and the Copenhagen Interpretation*, Studies In History and Philosophy of Science Part B: Studies In History and Philosophy of Modern Physics **33**, pp. 23-34 (2002), preprint available at <http://arxiv.org/abs/quant-ph/9910078m>, retrieved on 3.05.2009
- [141] *Encyclopaedic Dictionary of Physics*, vol. 2, editor-in-chief: J. Thewlis, Pergamon Press, 1961
- [142] Leon Rosenfeld, *The Wave-Particle Dilemma*, in: *The Physicist's Conception of Nature*, edited by Jagdish Mehra, Springer, 2007, available on <http://books.google.no>, retrieved on 3.05.2009

- [143] William K. Wootters, Wojciech H. Zurek, *Complementarity in the double-slit experiment: Quantum nonseparability and a quantitative statement of Bohr's principle*, Physical Review **D19**, pp. 473-484 (1979)
- [144] D. Bohm, *A Suggested Interpretation of the Quantum Theory in terms of "Hidden" Variables I*, Physical Review **85**, pp. 166-179 (1952)
- [145] D. Bohm, *A Suggested Interpretation of the Quantum Theory in Terms of "Hidden" Variables II*, Physical Review **85**, pp. 180-193 (1952)
- [146] David Bohm, *Reply to a Criticism of a Causal Re-Interpretation of the Quantum Theory*, Physical Review **57**, pp. 389-390 (1952)
- [147] Otto Halpern, *A Proposed Re-Interpretation of Quantum Mechanics*, Physical Review **57**, p. 389 (1952)
- [148] C. Philippidis, C. Dewdney, B. J. Hiley, *Quantum interference and the quantum potential*, Il Nuovo Cimento **B52**, pp. 15-28 (1979)
- [149] C. Dewdney, B. J. Hiley, *A Quantum Potential Description of One-Dimensional Time-Dependent Scattering From Square Barriers and Square Wells*, Foundation of Physics **12**, pp. 27-48 (1982)
- [150] Will Keepin, *Lifework of David Bohm – River of Truth*, http://www.vision.net.au/~apaterson/science/david_bohm.htm, retrieved on 7.05.2009
- [151] N. David Mermin, *What's Wrong with this Pillow?*, Physics Today, April 1989, p. 9
- [152] Chris J. Isham, *Lectures on Quantum Theory: Mathematical and Structural Foundations*, World Scientific Publishing Company, 1995
- [153] P. A. M. Dirac, *Lectures on Quantum Mechanics*, Dover Publications, 2001
- [154] David J. Griffiths, *Introduction to Quantum Mechanics*, Second Edition, Prentice Hall, 2005
- [155] F. Riesz, B. Sz.-Nagy, *Functional Analysis*, Section 21, Unger, 1955
- [156] Jon Magne Leinaas, *Non-Relativistic Quantum Mechanics*, lecture notes, University of Oslo, 2008, <http://www.uio.no/studier/emner/matnat/fys/FYS4110/h08/undervisningsmateriale/LectureNotes2008.pdf>, retrieved on 10.10.2008
- [157] William H. Louisell, *Quantum Statistical Properties of Radiation*, Chapter 3, Wiley, 1990
- [158] Kevin E. Cahill, *Coherent-State Representations for the Photon Density Operator*, Physical Review **138**, p. B1566 (1965)
- [159] Clinton Davisson, Lester Germer, *Diffraction of Electrons by a Crystal of Nickel*, Physical Review **30**, pp. 705-740 (1927)
- [160] George P. Thomson, Andrew Reid, *Diffraction of Cathode Rays by a Thin Film*, Nature **119**, p. 890 (1927)
- [161] Ernest O. Wollan, C. G. Shull, *The Diffraction of Neutrons by Crystalline Powders*, Physical Review **73**, pp. 830-841 (1948)

- [162] Peter Rodgers, *The double-slit experiment*, Physics World, <http://physicsworld.com/cws/article/print/9745>, retrieved on 4.12.2008
- [163] Claus Jönsson, *Electron Diffraction at Multiple Slits*, American Journal of Physics **42**, pp. 4-11 (1974); translation of a paper which originally appeared in: Zeitschrift für Physik **161**, p. 454 (1961)
- [164] P. G. Merli, G. F. Missiroli, G. Pozzi, *On the statistical aspect of electron interference phenomena*, American Journal of Physics **44**, pp. 306-307 (1976)